In Vitro Selection of New DNAzymes as Metal Biosensors

by

Po-Jung Jimmy Huang

A thesis
presented to the University of Waterloo
in fulfilment of the
thesis requirement for the degree of
Doctor of Philosophy
in
Chemistry

Waterloo, Ontario, Canada, 2015

© Po-Jung Jimmy Huang 2015

Author's Declaration

This thesis consists of material all of which I authored or co-authored: see Statement of Contributions included in the thesis. This is a true copy of the thesis, including any required final revisions, as accepted by my examiners.

I understand that my thesis may be made electronically available to the public.

Statement of Contributions

The work presented in this thesis is the result of work performed by the author and several scientific collaborations. Contributions from each scientist and the resulting publications are listed in detail below.

The work in Chapter 2 has been accepted as: Huang, P. J.; Lin, J.; Cao, J.; Vazin, M.; Liu, J. Ultrasensitive DNAzyme Beacon for Lanthanides and Metal Speciation. *Anal. Chem.* **2014**, 86, 1816-1821. Jenny Lin and Jing Co provided assistance on gel electrophoresis in the *in vitro* selection. pH-dependent enzyme activity was performed by Mahsa Vazin. All other works in this chapter were performed by the author.

The work in Chapter 3 has been accepted as: Huang, P. J.;Vazin, M.; Liu, J. *In Vitro* Selection of a New Lanthanide-Dependent DNAzyme for Rtiometric Sensing Lanthanides. *Anal. Chem.* **2014**, 86, 9993-9999. Mahsa Vazin performed the *in vitro* selection using lutetium salt with N35 DNA library. Other works presented in this chapter were performed by the author.

The work in Chapter 4 has been accepted as: Huang, P. J.;Vazin, M.; Matuszek, Z.; Liu, J. A New Heavy Lanthanide-Dependent DNAzyme Displaying Strong Metal Cooperativity and Urescuable Phosphorothioate Effect. *Nucleic Acids Res.* **2015**, 43, 461-469. pH-rate profile of Tm7 DNAzyme was performed by both Mahsa Vazin and Źaneta Matuszek. The author performed all other works in this chapter.

The work in Chapter 6 has been accepted as: Huang, P. J.; Liu, J. Sensing Parts-per-Trillion Cd^{2+}, Hg^{2+}, and Pb^{2+} Collectively and Individually Using Phosphorothioate DNAzymes. *Anal. Chem*. **2014**, 86, 5999-6005.

Abstract

In vitro selection of metal-specific DNAzymes has been shown to be a powerful method to obtain biosensors for metal ion detection. Most previously reported DNAzymes employed divalent metal ions as cofactors. In this thesis, two types of selection experiments are described. First, five representative DNAzymes with distinct activity patterns across the trivalent lanthanide series were isolated from 14 independent *in vitro* selection experiments using each of the lanthanides (except the radioactive promethium) as the metal cofactor. Based on my understanding attained from the lanthanides selections, a modified *in vitro* DNAzyme selection protocol was developed for thiophilic metal ions. A highly sensitive and exceptionally selective Cd^{2+}-dependent DNAzyme was isolated. Each of these DNAzymes was studied extensively and the results are presented in each chapter.

In Chapter 2, a new DNAzyme named Ce13d with a bulged hairpin structure was isolated after six rounds of *in vitro* selection. Although the selection was performed using a Ce^{4+} salt as the intended target metal, Ce13d has almost no activity with Ce^{4+}. However, this DNAzyme is highly active with all the trivalent lanthanides, Y^{3+}, and Pb^{2+}. With the addition of thiol containing reagents, the Ce13d can serve as a general probe for rare earth metals with a detection limit down to ~1 nM. In addition, this DNAzyme demonstrated the capability of distinguishing the different oxidation states of the cerium ion.

In Chapter 3, another representative DNAzymes named Lu12 was studied in detail. The study revealed that this DNAzyme has smaller conserved sequences in the unstructured catalytic core. Unlike Ce13d, Lu12 is more active with smaller lanthanides and has the lowest activity with the largest lanthanide, Lu^{3+}. The study showed that this DNAzyme is able to achieve a rate

of 0.12 min^{-1} in the presence of 10 μM Nd^{3+} at pH 6.0. Although both Ce13d and Lu12 showed cleavage with two non-lanthanide ions: Y^{3+} and Pb^{2+}, the two DNAzymes displayed two different lanthanides affinity patterns. By combining only the Ce13d and the Lu12 DNAzymes, a few large lanthanides were identified with a ratiometric assay.

In Chapter 4, a new family of DNAzymes is described with a simple loop structure that was identified from 3 independent selections from which Tm7 was chosen as a representative DNAzyme for evaluation. Interestingly, Tm7 is active only with the seven large lanthanides. In fact, Tm7 exhibits a cleavage rate of 1.6 min^{-1} at pH 7.8 with 10 μM Er^{3+}. In addition, unlike the Ce13d and Lu12, only Y^{3+} induced cleavage among the tested non-lanthanide ions. The lanthanides binding study also revealed that 3 metal ions are involved in the catalytic step for Tm7. When the non-bridging oxygen at the cleavage junction was substituted with a phosphorothioate bond, the enzymatic activity was completely abolished and could not be rescued. This result suggested that two interacting metal ions are involved in direct bonding to both non-bridging oxygen atoms. Based on these findings, a new model involving three lanthanide ions was proposed.

In Chapter 5, two more lanthanide-dependent DNAzymes (Dy10a and Gd2b) with distinct activity patterns were isolated and studied. By labeling with fluorophore/quencher pairs, 5 DNAzyme beacon sensors were prepared. Each of these DNAzymes can detect down to low nM lanthanide concentrations with minimal interference from other metals. A sensor array was prepared to achieve pattern-recognition-based detection using linear discriminant analysis (LDA), where separation was achieved between lanthanides and other metals, light and heavy lanthanides, and for the most part, each lanthanide.

In Chapter 6, the Ce13d DNAzyme with phosphorothioate (PS) modifications was studied. With just a single PS at the substrate cleavage site, the enzymatic activity of the Ce13d DNAzyme drastically shifts from lanthanide ions dependent to soft thiophilic metal ion-dependent. By incorporating the PS modification to a few other DNAzymes, a sensor array with PO- and PS-DNAzymes was prepared to detect each metal. This study provides a new route to obtain metal-specific DNAzymes by atomic replacement and also offers important mechanistic insights into metal binding and DNAzyme catalysis.

In Chapter 7, I demonstrated the feasibility of using a DNA library with a single phosphorothioate (PS) modification for *in vitro* DNAzyme selection. This simple modification not only increases the functionality of the DNA but also boosts its affinity for thiophilic metals without complicating the selection process. For this particular study, Cd^{2+} was used as the intended target. After using a blocking DNA and negative selections to rationally direct the library outcome, a highly specific DNAzyme with only 12 nucleotides in the catalytic loop is isolated. Remarkably, the DNAzyme is capable of detecting Cd^{2+} down to 1.1 nM. In addition, the DNAzyme is most active with Cd^{2+} and its selectivity against Zn^{2+} is over 100,000-fold. Finally, its application in detecting Cd^{2+} in rice is also demonstrated.

Acknowledgements

I would like to express my deepest and sincere gratitude to my Ph.D. supervisor, Dr. Juewen Liu, for his continual encouragement and guidance. The time spent under his supervision has made research in his laboratory both a rewarding and enjoyable experience. I would also like to express great appreciation to my committee members: Dr. Gary Dmitrienko, Dr. Thorsten Dieckmann, and Dr. Richard Manderville for their advice and time given to evaluate my research project. In addition, I would like to thank my external examiner, Dr. Yingfu Li, for taking the time to attend my examination. In addition, I would also like to extend my deepest thanks to Dr. Dmitrienko, Dr. Dieckmann and their respective research groups for use of their equipment and space during my studies. Also, I would like to acknowledge the following people for their support and guidance: Cathy van Esch, Marguerite Greavette, and Dr. Steven Forsey.

I would also like to thank my colleagues in the Liu lab, both past and the present, for making the working environment so friendly and enjoyable: Dr. Neeshma Dave, Dr. Xu Zhang, Imran Khimji, Alex Ip, Dr. Feng Wang, Jing Cao, Biwu Liu, Wenhu Zhou, Zijie Zhang, Ziyi Sun, Mahsa Vazin, Runjhun Saran, Howard Tsai, Michael Hoang, and Qingyun Chen. I also take this opportunity to thank undergraduate volunteers and co-op researchers who worked with me: Rachel Pautler, Żaneta Matuszek, Jenny Lin, Wei Ting David Lin, Erin Kelly, Courtney Van Ballegooie, and Jenitta Shanmu.

Special thanks go to my friends and family especially my parents and my sister for believing in me and for their unconditional support and love. In addition, financial support from the University of Waterloo, the Natural Sciences and Engineering Research Council (NSERC) of Canada, and Canadian Institutes of Health Research (CIHR) through a Canada-UK team grant

are greatly appreciated. Last but not least, I would use this opportunity to show my gratitude to University of Waterloo, the Department of Chemistry for financial support and for providing access to research facilities.

Dedication

I would like to dedicate this thesis to my family for their encouragement and support.

Table of Contents

List of Figures

List of Tables

List of Schemes

List of Abbreviations

A	adenine
AAS	atomic absorption spectrometry
ABTS	2,2'-azino-bis(3-ethylbenzothiazoline-6-sulphonic acid)
AES	atomic emission spectrometry
ASV	anodic stripping voltammetry
AuNPs	gold nanoparticles
bp	base pairs
C	cytosine
CE	capillary electrophoresis
cDNA	complementary DNA
DNA	deoxyribonucleic acid
dPAGE	denaturing polyacrylamide gel electrophoresis
dsDNA	double-stranded DNA
EPA	Environmental Protection Agency
FAM	fluorescein amidite
FRET	fluorescence resonance energy transfer
G	guanine
G-quartet	guanine quartet
HDV	hepatitis delta virus
HEPES	4-(2-Hydroxyethyl)piperazine-1-ethanesulfonic acid
ICP-MS	inductively coupled plasma mass spectroscopy

k_{cat}	turnover number
K_d	dissociation constant
K_m	Michaelis constant
LDA	linear discriminant analysis
Ln^{3+}	lanthanides ions
MCL	maximum contaminant level
MCH	mercaptohexanol
MES	2-(N-morpholio)ethanesulfonic acid
µl	micro-liter
ml	milliliter
µm	micrometer
µM	micro-molar
MOPS	3-(N-morpholino)propanesulfonic acid
MRI	magnetic resonance imaging
MS	mass spectrometry
nM	nano-molar
nmol	nano-mole
NMR	nuclear magnetic resonance
n.r.	not reported
PCS	pseudo-contact shift
PEG	polyethylene glycol
PO	phosphodiester
ppb	parts-per-billion

ppm	parts-per-million
ppt	parts-per-trillion
PS	phosphorothioate
Q	fluorescence quencher
RFU	relative fluorescence units
rA	ribo-adenosine
RNA	ribonucleic acid
rt-PCR	real-time polymerase chain reaction
SELEX	systematic evolution of ligands by exponential enrichment
SPR	surface plasmon resonance spectroscopy
ssDNA	single-stranded DNA
Tris	tris(hydroxymethyl)aminomethane
PCR	polymerase chain reaction
pmol	pico-mole
T	thymine
T_m	melting temperature
TMB	3,3',5,5'-tetramethylbenzidine
U	uracil
VS	Varkud satellite
WHO	World Health Organization
XRF	X-ray fluorescence spectrometry
Zn-DIGP	tetrakis-(diisopropyl-guanidino) zinc phthalocyanine

Chapter 1. Introduction to Functional Nucleic acids

The four major classes of macromolecules found in biological systems are carbohydrates, lipids, nucleic acids and proteins. Together, these organic molecules are responsible for all of the most sophisticated functions of living cells. Nucleic acids such as deoxyribonucleic acid (DNA) and ribonucleic acid (RNA) function to preserve, store and transfer genetic information. While nucleic acids carry the genetic information of the cell, the primary responsibility of proteins is to execute the instructions that are encoded in the DNA. The potential of nucleic acids to behave as functional molecules had not attracted much interest due to the classical notion that proteins are functional molecules playing an important role in the body, whereas DNA is a blueprint of proteins and RNA is a mediator.

1.1 Chemical structure of nucleic acids

Nucleic acids are essential biological molecules that are found in all forms of life. There are two types of nucleic acids: RNA and DNA. Both RNA and DNA are linear polymers made from monomers called nucleotides. Each nucleotide consists of three parts (Figure 1.1): a) a nitrogenous base; b) a five-membered pentose sugar ring; c) a phosphate group at the 5′-carbon. The nitrogenous bases are further sub-categorized into pyrimidine and purine. Each base is attached to the 1′-carbon of the sugar ring via a *N*-glycosidic bond. The molecule without the phosphate group is called a nucleoside. In a polynucleotide, the phosphate group links successive nucleotides together linearly through the 3′-hydroxyl group of one nucleotide and 5′-phosphate group of another nucleotide.

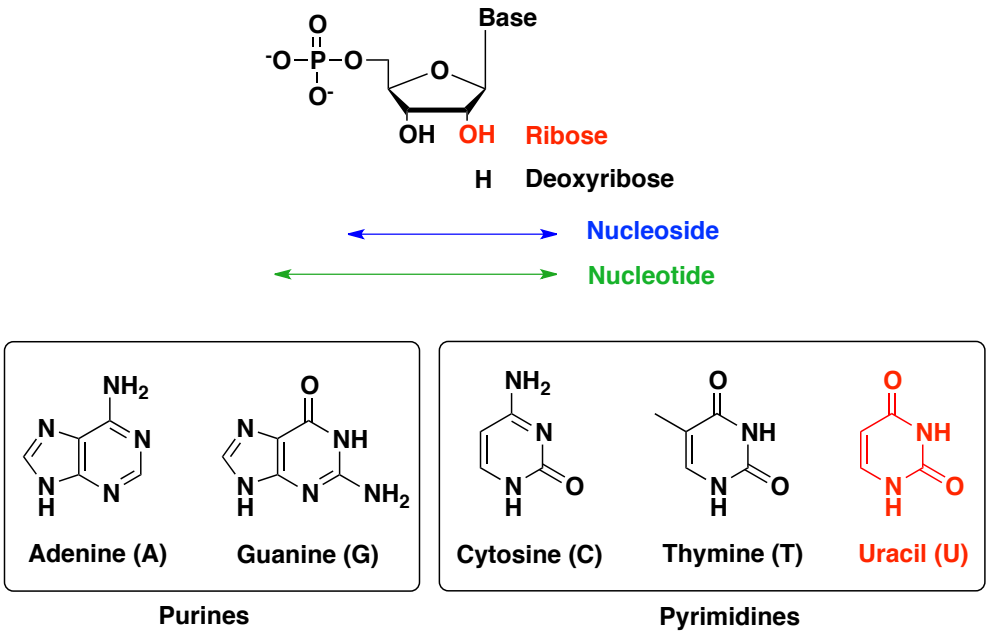

Figure 1.1 The chemical structure of nucleobases, nucleosides, and nucleotides.

This bond is usually referred as phosphodiester linkage. The hydrophilic backbone phosphates, with a pK_a value near 1, are completely ionized and negatively charged at pH 7. These negatively charges are largely neutralized by ionic interactions with positive charges on metal ions. There are two structural differences between RNA and DNA nucleotides: RNA has a hydroxyl group instead of a hydrogen at the 2′-position of the pentose. Secondly, RNA has slightly different base pairing than DNA. For both nucleic acids, guanine (G) binds with cytosine (C). However, in RNA, adenine (A) pairs with uracil (U) instead of thymine (T). These base interactions are referred as Watson-Crick base pairing (Figure 1.2). In fact, a few other forms of base pairing also exist. Hoogsteen base pairing is found in triple helices while wobble base pairing is more common in RNA (Figure 1.3).

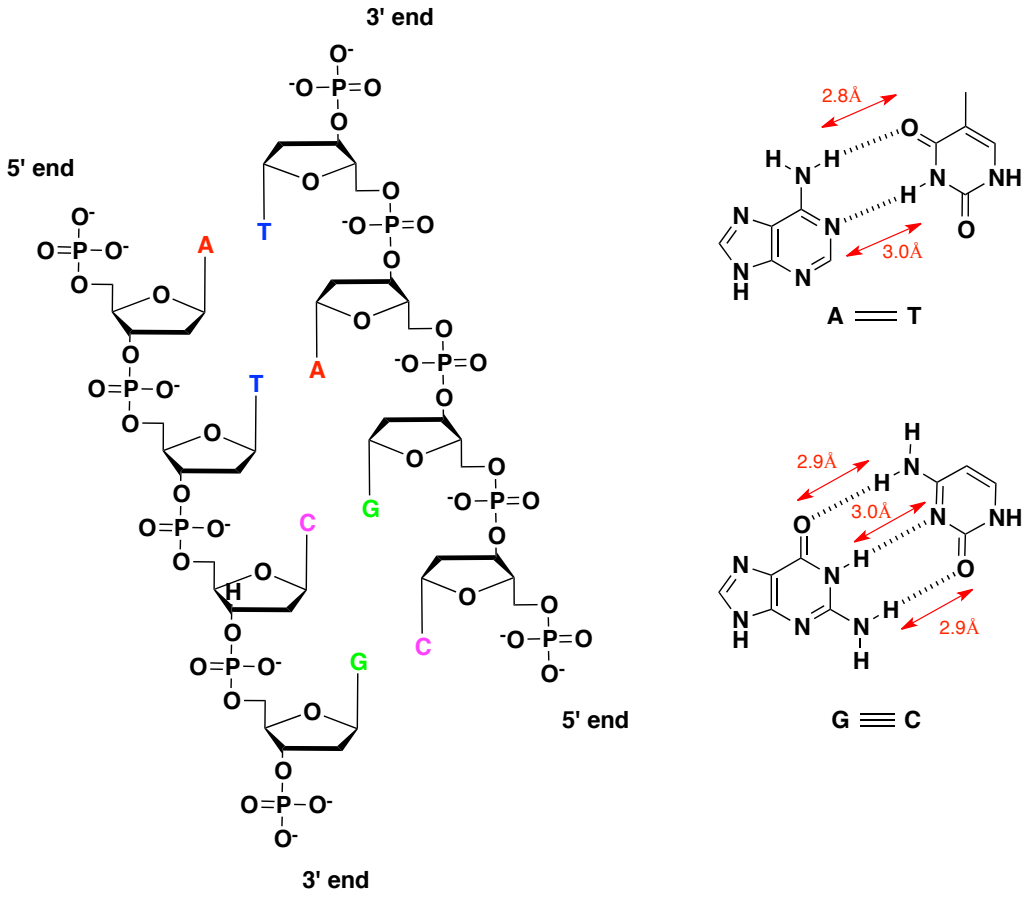

Figure 1.2 Phosphodiester linkage backbone and Watson-Crick base pairing of DNA.

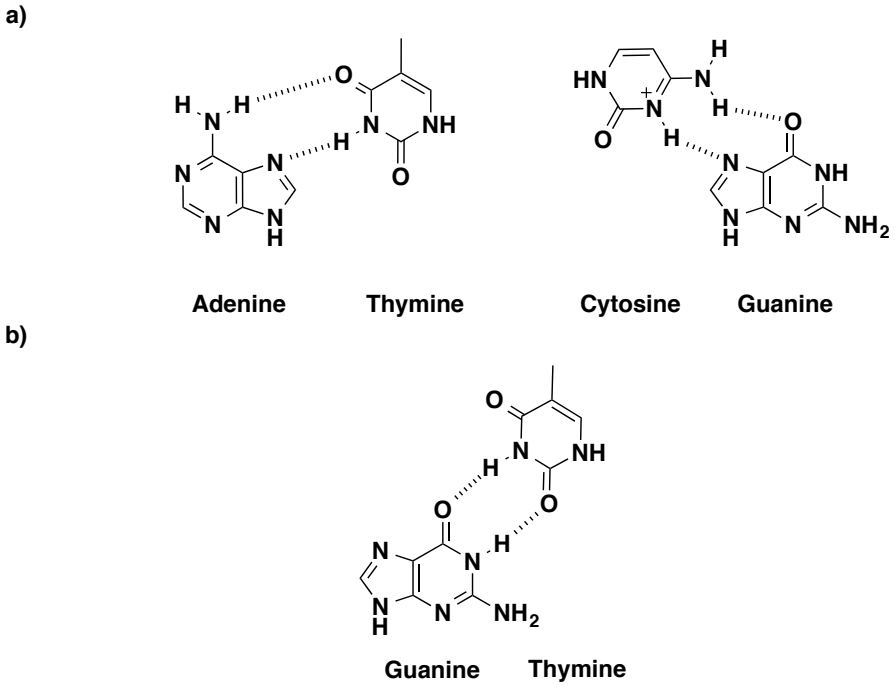

Figure 1.3 Types of DNA base pairing. a) A-T and C^{+}-G Hoogsteen base pairing b) Wobble base pairing.

1.2 Naturally occurring catalytic RNAs: ribozymes

Enzymes are essential biomolecules in living systems that catalyze biochemical reactions with extraordinary speed and precision. While enzymes made of protein are the dominant form of biocatalyst in modern cells, there are some natural RNA-based enzymes (or ribozymes) that are capable of catalyzing fundamental biological reactions.[1,2] For instance, ribosome for protein translation[3] and the spliceosome for RNA splicing[4] are two well studied ribozymes. These catalytic RNAs are usually classified into two main categories: small self-cleaving ribozymes and large ribozymes.[5] For example, the small ribozymes include the hammerhead, hairpin, hepatitis delta virus (HDV), Varkud satellite (VS), and *glmS* ribozymes.[6] These ribozymes are usually 50-150 nucleotides in length and they catalyze sequence-specific intramolecular cleavage of RNA. The large ribozymes include the group I[7] and II[8] introns and the RNA component of RNase P.[9] Just like protein enzymes, ribozymes also require rigorous geometrical positioning of the catalytic site with respect to the substrate for the reaction to occur. Unlike proteins contain versatile functional groups, natural occurring ribozymes require divalent metal ions (mostly Mg^{2+}) as cofactor for the activity under physiological conditions.[10,11]

1.3 Interaction between nucleic acids and metal ions

Metal ions play an important role in structure and function[12,13] of nucleic acids. Under physiological pH, the phosphate backbone of single-stranded DNA (ssDNA) is highly negatively charged. Thus, the inorganic cations have a strong influence on the tertiary structure of ssDNA. Bringing the two complementary strands into close proximity requires overcoming an electrostatic energy barrier. In general, the presence of counter ions can reduce the long-range electrostatic repulsion. It is known that metal ions are necessary for stabilizing the dsDNA structure by binding to the phosphate backbones.[14] In fact, divalent and trivalent metal ions bind

more tightly than monovalent ions as a result of greater charge density. However, metal ions can also interact with nucleobases via Lewis acid-base reactions. The amino and keto tautomeric forms of the nucleobases are obvious metal binding sites due to their available lone pair electrons on the unprotonated endocyclic N-atoms and exocyclic carbonyl O-atoms (Figure 1.4).

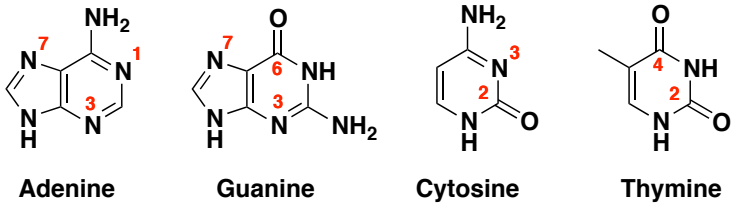

Figure 1.4 Possible metal binding sites for the nucleobases.

These sites include N3, N7, and O6 in guanine; N3 and O2 in cytosine; N1, N3, and N7 in adenine and O2 and O4 in thymine. It has been shown that N7 sites of purines are excellent metal binding sites as a result of exposure. Even though there is a lone pair on the exocyclic amino group, the delocalization of the lone pair into the heterocyclic ring leads to very low basicity.[15] Thus, it makes it a less favorable metal binding site. Sometimes the interaction between the metal ions and nucleobases leads to distinct structural pattern or structures with higher order such as DNA triple helices, G-quadruplex, and helical junctions. [16]

Since many metal ions are able to bind to both phosphate and nucleobases, the relative affinity of the metal ion toward the two binding sites will determined the effect on DNA. Eichhorn and Shin demonstrated that initial increase in concentration of Mn^{2+}, Zn^{2+}, Cd^{2+}, and Cu^{2+} helps increase the melting temperature (T_m) of dsDNA due to phosphate binding.[17] However, a further increase in metal concentration has an adverse effect. In this case, base binding disrupts the hydrogen bonding of the double helix that leads to destabilization of dsDNA. Difference in T_m at the same concentration of metal ions also indicated that every metal ion has different interaction with DNA. Moreover, it has been shown that metal ions can be used

to promote formation of non-Watson-Crick base pairing via metal coordination. A guanine quartet (G-quartet) is composed of four guanines that are hold together by eight hydrogen bonds via Hoogsteen pairing. The metal ion is located at the centre and coordinates with O6 atom on each of the guanine bases via electrostatic interactions. The stability of the quartet is strongly dependent on the presence of alkali metal ions (Figure 1.5a).

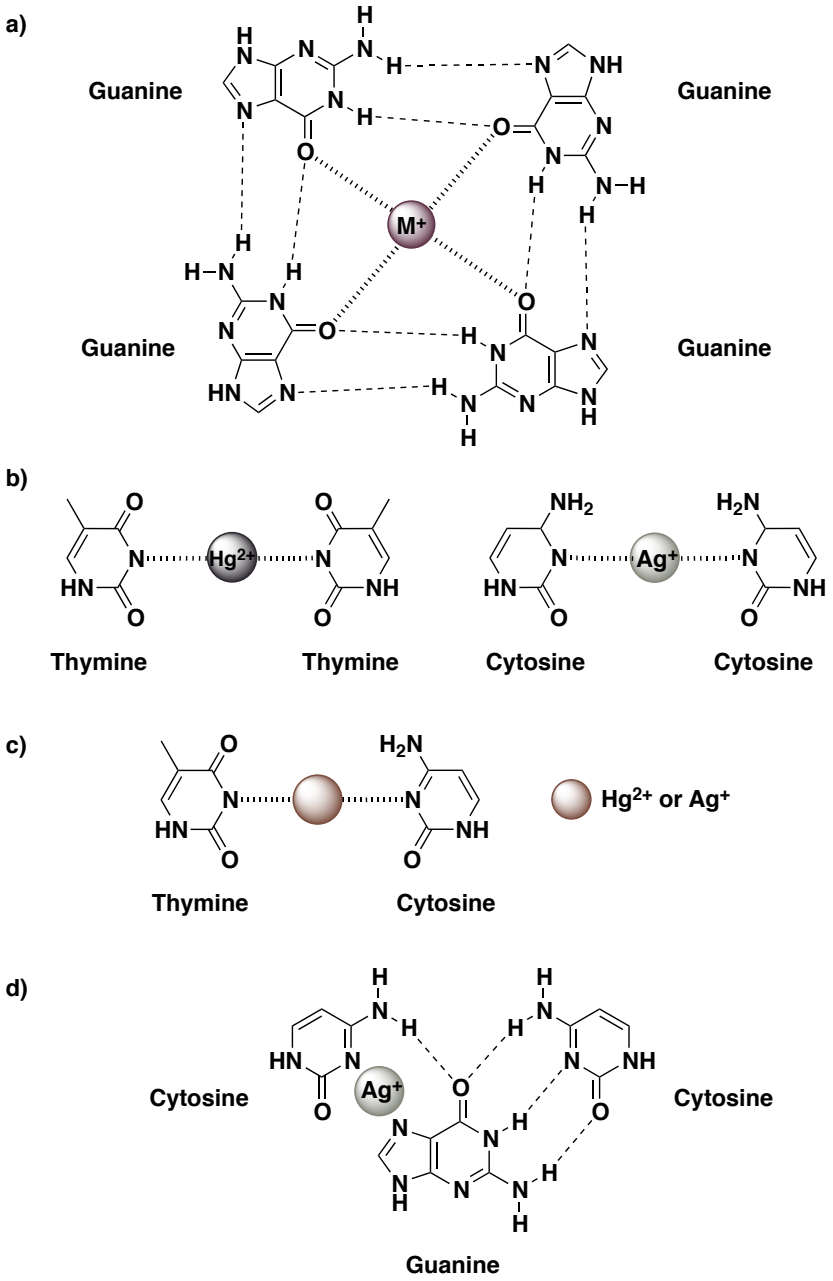

Figure 1.5 Illustration of metal ion mediated base pairing. a) G-quartets b)T-Hg^{2+}-T and C-Ag^{+}-C pairings c)T-Hg^{2+}-C or T-Ag^{+}-C pairing d) C-Ag^{+}-GC triplex.

On the other hand, it has been reported that some metal ions exhibit specific binding toward specific base pairs such as thymine-Hg^{2+}-thymine and cytosine-Ag^{+}-cytosine (Figure 1.6b).[18,19] Other heavy metal ions such as Cu^{2+}, Ni^{2+}, Pd^{2+}, CO^{2+}, Mn^{2+}, Zn^{2+}, Pb^{2+}, Cd^{2+}, Mg^{2+}, Ca^{2+}, Fe^{2+}, Fe^{3+}, and Ru^{2+} cannot induce the pairing. [20] Recently, two groups also discovered that Ag^{+} and Hg^{2+} can moderately stabilize T-C mismatched base pair in dsDNA (Figure 1.6c).[21,22] Ihara et al. reported that Ag^{+} ion can also mediate the formation of CG·CAg^{+} triplex (Figure 1.6d).[23] With the specific interaction between the metal ions and the nucleobases, metal ions mediated base pairing had been utilized for metal ion detection.

1.4 Importance of metal ions detection

Metal ions are ubiquitous in biological system and in the environment. It is known that metal ions play critical roles in important cellular processes. While some metal ions in a certain concentration range are essential for health, many others are considered very toxic. For instance, accumulation of cadmium (Cd^{2+}), mercury (Hg^{2+}), arsenic (As^{3+}) or lead (Pb^{2+}) in the body can cause severe health risks such as neurological diseases and organ damage.[24] As a result, detection of metal ions and especially heavy metal ions is a priority concern from environmental and the biological aspects. It is known that toxic levels for some of these metals ions exist just above the background concentrations naturally found in the environment or food chain. Therefore, it is important to monitor the concentrations of these contaminants and take protective measures against excessive exposure. In the United States, Environmental Protection Agency (EPA) set the maximum contaminant level (MCL) drinking water for heavy metals to ensure that their concentration falls below the safe limit (Table 1.1).

Table 1.1 List of drinking water contaminants and MCLs.

Contaminant	MCL (mg/L)	Potential health risk	Source of contaminant in drinking water
Arsenic	0.01	Skin damage, circulatory system problems, cancer risk	Erosion of natural deposits; runoff from orchards and glass/electronics production wastes
Cadmium	0.005	Kidney damage	Corrosion of galvanized pipes; erosion of natural deposits; discharge from metal refineries; runoff from waste batteries/paints
Chromium (total)	0.1	Allergic dermatitis	Discharge from steel/pulp mills; erosion of natural deposits
Copper	1.3 (Action level)	Gastrointestinal distress, liver/kidney damage	Corrosion of household plumbing systems; erosion of natural deposits
Lead	0.015 (Action level)	Physical/mental development delay, kidney damange, high blood pressure	Corrosion of household plumbing systems; erosion of natural deposits
Mercury (inorganic)	0.002	Kidney damage	Erosion of natural deposits; discharge from refineries and factories; runoff from landfills and croplands
Selenium	0.05	Hair/finger nail loss, circulatory system problems	Discharge from petroleum refineries; erosion of natural deposits; discharge from mines
Thallium	0.002	Hair loss, kidney/intestine/liver problems	Leaching from ore-processing sites; discharge from electronics/glass/drug factories

Source: U.S. Environmental Protection Agency. Ground Water and Drinking Water.

1.5 Common methods for metal ion detection

Currently, heavy metal ion analysis relies on instrumental techniques, such as atomic absorption spectrometry (AAS),[25-27] atomic emission spectrometry (AES),[28] inductively coupled plasma mass spectroscopy (ICP-MS),[29,30] anodic stripping voltammetry (ASV),[31-33] surface plasmon resonance spectroscopy (SPR),[34] and X-ray fluorescence spectrometry (XRF).[35-38] All of these techniques are based on intrinsic physical properties of the element. Although these instrumental techniques can easily achieve highly sensitive detection (often down to low parts-per-billion level), they require sophisticated instrumentation and trained operators.[39,40] Many of these methods also require complicated, multi-step sample pretreatment. In addition, the analysis is carried out in a centralized laboratory. Therefore, on-site and real-time monitoring is difficult to achieve. All these drawbacks have motivated the development of alternative detection methods for metal ions.

1.6 Biosensors

Unlike instrumentation techniques, biosensors show both fast analysis and high sensitivity. A biosensor contains two main components: target recognition and signal transduction. Signal transduction elements are the components for converting molecular recognition events into physically detectable signals. These signals can be generated either from fluorescence,[41,42] color,[43,44] or electrochemical signals.[45-49] Moreover, the availability of a large selection of fluorophores and quenchers makes it a popular choice.[50]

The target recognition element can be either chemical or biological entities such as small organic molecules, peptides, proteins, nucleic acids, carbohydrates, or even whole cells. Ideally, the recognition element should have high affinity, high specificity, wide dynamic range, fast response time, long shelf life, and good generality for detecting a broad range of analytes. With various combinations of 20 amino acids, the possibility of forming a large array of protein-based sensor on its chemical functionalities is endless. Thus, antibodies are usually the first choice of biomolecule as a building block for developing a biosensor. However, problems associated with enzyme or antibody immobilization and their relatively high cost and low stability have limited their applications.[51]

There are several advantages to the use of DNA over other biomolecules, which could be leveraged toward the sensor development. First of all, DNA is more stable to use than RNA and protein. The absence of a 2'-OH group at the sugar ring makes DNA 100,000-fold more resistant to hydrolysis than RNA under physiological conditions.[52] In addition, the phosphodiester bonds are also 1000-fold more resistant to hydrolytic degradation than are peptide bonds.[53] Secondly, DNA is less expensive and can be easily synthesized. Moreover, it can be readily chemically modified to increase stability or provide extra functional groups. These properties can generally

make DNA more versatile and convenient to use. Since its discovery, aptamers and DNAzymes have emerged as a promising alternative method for metal ions detection.

1.7 Aptamer

The term "aptamer" derives from the Latin *aptus*, which means "to fit." Aptamers are single-stranded nucleic acids with 15-100 bases that can fold into a well-defined three-dimensional structure to form selective binding pockets. Aptamers can be either RNA or DNA molecules that bind molecular targets. Nature developed RNA aptamers long before scientists did. The first RNA aptamers were reported by two different group around the same time in 1990. Ellington and Szostak identified RNAs that bind to small organic dyes, whereas Tuerk and Gold found RNAs that bind to T4 DNA polymerase. Since then, most aptamers are isolated through a technique called systematic evolution of ligands by exponential enrichment (SELEX).[54-56]

1.7.1 SELEX for aptamer

In a typical *in vitro* selection (Scheme 1.1), target molecules are first immobilized on a column. The immobilized targets are then incubated with a pool of ssDNA. For each ssDNA, a region that contains 20-60 nucleotides with randomizes sequence flanked by two primer binding regions. Thus, the pool contains a total of ~10^{16} possible sequences. After an incubation period, the column is washed extensively to remove any unbound ssDNA before bounded sequence were collected. Elution of binding sequences with free target ensures that the resulting aptamers can also bind to untethered target as well. After several rounds of selection, an aptamer sequence is identified.

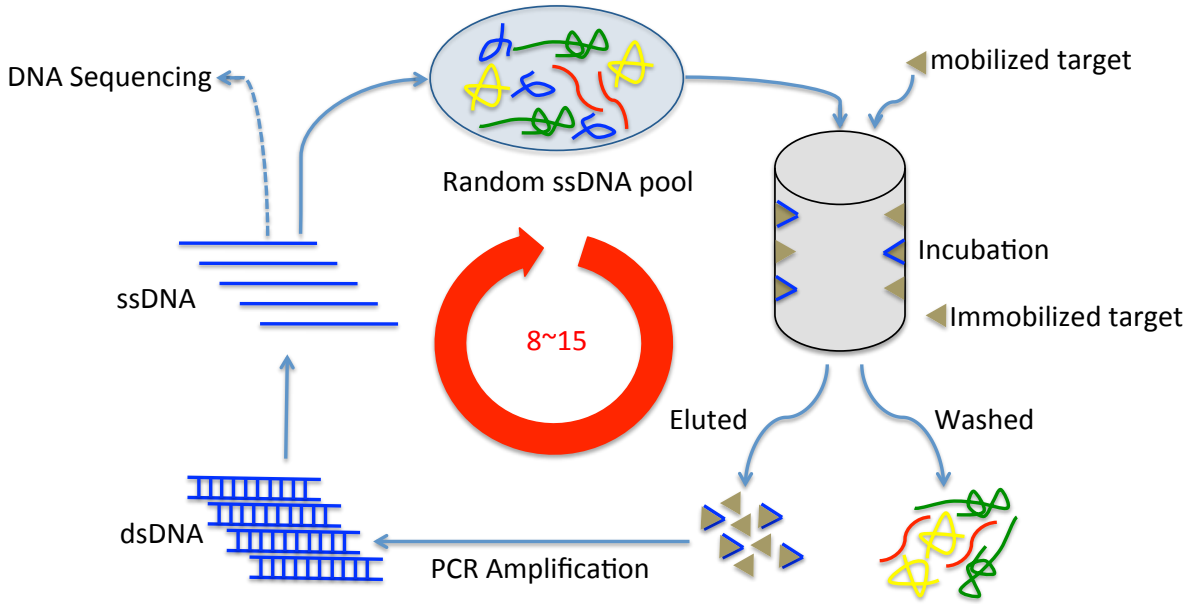

Scheme 1.1 Schematic of a traditional *in vitro* selection.

During the selection process, it is necessary to separate ssDNA from its complement after polymerase chain reaction (PCR) between each round of selection. The separation can be achieved by using a modified primer. For instance, inserting a moiety such as a polyethylene glycol (PEG) spacer in one of the two PCR primers will result in termination of extension. This is due to the fact that the Taq polymerase cannot extend past the spacer within the template strand. Therefore, two complementary strands of PCR product have unequal lengths and can be easily separated by denaturing polyacrylamide gel electrophoresis (dPAGE).

1.7.2 Examples of known metal binding DNAs

1.7.2.1 G-quadruplexes

The most well known higher-order DNA structure is the G-quadruplexes. With consecutive guanine nucleotides in oligonucleotides, these planar G-quartets stack together in a helical fashion to form a G-quadruplex structure. G-quadruplexes are stabilized by hydrogen bonds and by the alkali metal ions that are located between two G-quartets (Scheme 1.2). Since

G-quadruplexes are highly polymorphic, the structure depend on the composition and length of the DNA and the nature of the cations.[57]

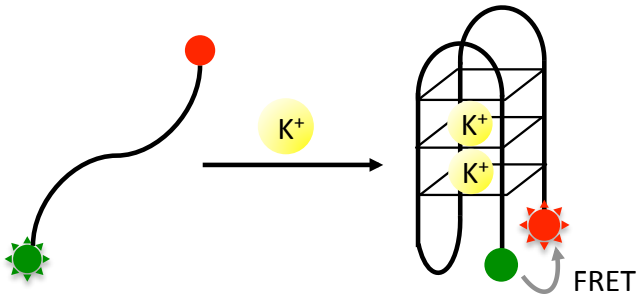

Scheme 1.2 Schematic representation of G-quadruplex stabilized by the presence of K^+ ions. The formation of the G-quadruplex brings the fluorophores closer which leads to FRET.

Throughout the years, many groups combined different methods with guanine rich DNA probes for metal ion detection. Even though the results showed good sensitivity, there is a major draw back due to the interaction of G-quadruplexes with many metal ions (Table 1.2).

Table 1.2 G-quadruplex based biosensor for metal ion detection.

Analyte	Detection method	Detection Limit	Reference
K^+	Fluorescence (FRET)	n.r.	58
	Fluorescence (crystal violet dye)	1 mM	59
	Fluorescence (berberine dye)	2 μM & 31nM	60,61
	Fluorescence (Zn-DIGP dye)	800 nM	62
	Colorimetric (ABTS)	0.1uM	62,63
	Colorimetric (TMB dye)	2 μM	64
Ag^+	Colorimetric (ABTS)	6.3 nM & 64 nM	65,66
Cu^{2+}	Fluorescence	3 nM	67
Hg^{2+}	Colorimetric (ABTS)	9.2nM & 50nM	68,69
Pb^{2+}	Colorimetric (ABTS)	32nM	70
	Luminescence (luminol)	1nM	70

n.r. = not reported

1.7.2.2 Hg^{2+} binding DNA

Although G-quadruplex based sensors show low detection limit of Hg^{2+} ion, another Hg^{2+} aptamer design takes advantage of the ability of Hg^{2+} ion to bind specifically to the T-T bases mismatch in DNA. In 2004, Ono et al. was the first group to report using dual-labeled thymine rich ssDNA to detect Hg^{2+} ion.[20] In this design (Scheme 1.3a), a fluorophore (fluorescein) and a quencher (dabcyl) are labeled on each end of terminal. In the absence of Hg^{2+} ion, ssDNA exist in random coil structure. Thus, a fluorescence signal was detected. Upon binding with Hg^{2+} ions, the ssDNA folded into a hairpin structure that forces the fluorophore and the quencher into close proximity. The short distance between the two moieties leads to enhancement of fluorescence resonance energy transfer (FRET). As a result, a significant decrease in fluorescence signal is observed. Even though it is a "turn-off" design, the sensor is able to achieve 40 nM detection limits.

Another common technique to generate an aptamer fluorescence signal with any fluorophore labeling is to use a duplex binding dye (Scheme 1.3b). The dye is generally used in real-time polymerase chain reaction (RT-PCR) for monitoring DNA amplification. The free dye exhibits low background fluorescence in solution but the fluorescence increase up to 1,000 fold when the dye was bound to dsDNA. SYBR Green I dye is one of the most sensitive fluorescent stains available for detecting dsDNA. By incorporating SYBR Green dye with non-label mercury specific DNA, Wang and Liu were able to detect as low as 1.33 nM Hg^{2+} in water.[71]

Gold nanoparticles (AuNPs) exhibit unique optical properties. When AuNPs are aggregated, the surface plasmon resonance (SPR) band shifts and the colloidal solution changes from red to blue (Scheme 1.3c). Combining these two properties, Lee et al. were able to design a colorimetric Hg^{2+} sensor that can detect Hg^{2+} in aqueous media down to 100 nM.[72]

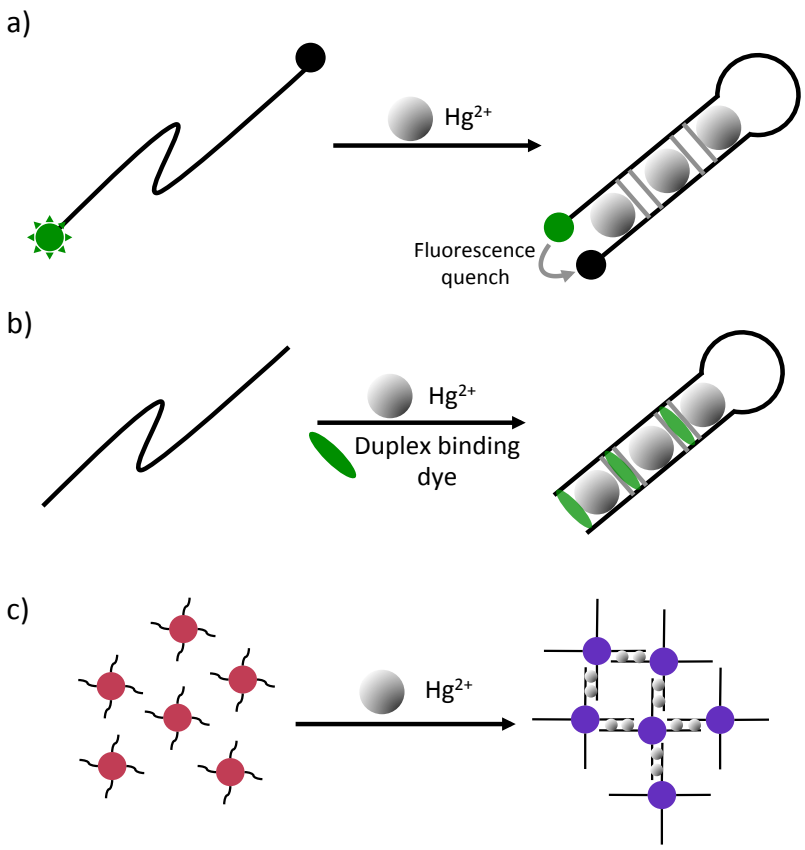

Scheme 1.3 Schematic representation of the double-stranded hairpin structure stabilized by the formation of T-Hg^{2+}-T mismatches. Sensor design based on a) fluorescence quenching (turn-off). b) Intercalation of the duplex binding dye (turn on). c) Colorimetric changes due to AuNPs aggregations.

1.7.2.3 Ag^{+} binding DNA

Just like Hg^{2+} detection, similar approaches have been done to develop Ag^{+} sensor. With a FRET design, Ono et al. demonstrated that the sensor can detect 10 nM of Ag^{+} ions.[19] Lin and Tseng reported that a detection limit of 32 nM was achieved with non-labeled probe.[73] With a colorimetric method, 0.59 nM of Ag^{+} ion can be detected.[74]

1.7.2.4 Zn^{2+} binding DNA

So far, the above examples of metal ion binding DNA were due to the intrinsic properties of the nucleotides. Since metal ions especially divalent metal ions are important for functional nucleic acids to fold and function properly,[75] Rajendran and Ellington employed SELEX method

to obtain a Zn^{2+} binding aptamer, Zn-6m2 (Figure 1.6).[76] With the fluorescence turn-on design, the aptamer beacon demonstrated detection limit of 5 μM Zn^{2+}. Although Cd^{2+} also induced significant fluorescence enhancement, Zn^{2+} produced much faster kinetics response than Cd^{2+}.

Figure 1.6 Sequences and predicted structures of Zn-6m2 aptamer beacon.

1.7.3 *In vitro* Selection for DNAzymes

Although DNAzyme selections follow the similar protocol as aptamer selection, there are several differences. For example, immobilization of the DNA library or target is usually not necessary. Unlike aptamer selection, the actual progression can be observed directly. When the DNAzyme cleaves its RNA-containing substrates, it generates two strands with different lengths. Thus, its activity can be easily monitored by dPAGE (Scheme 1.4).

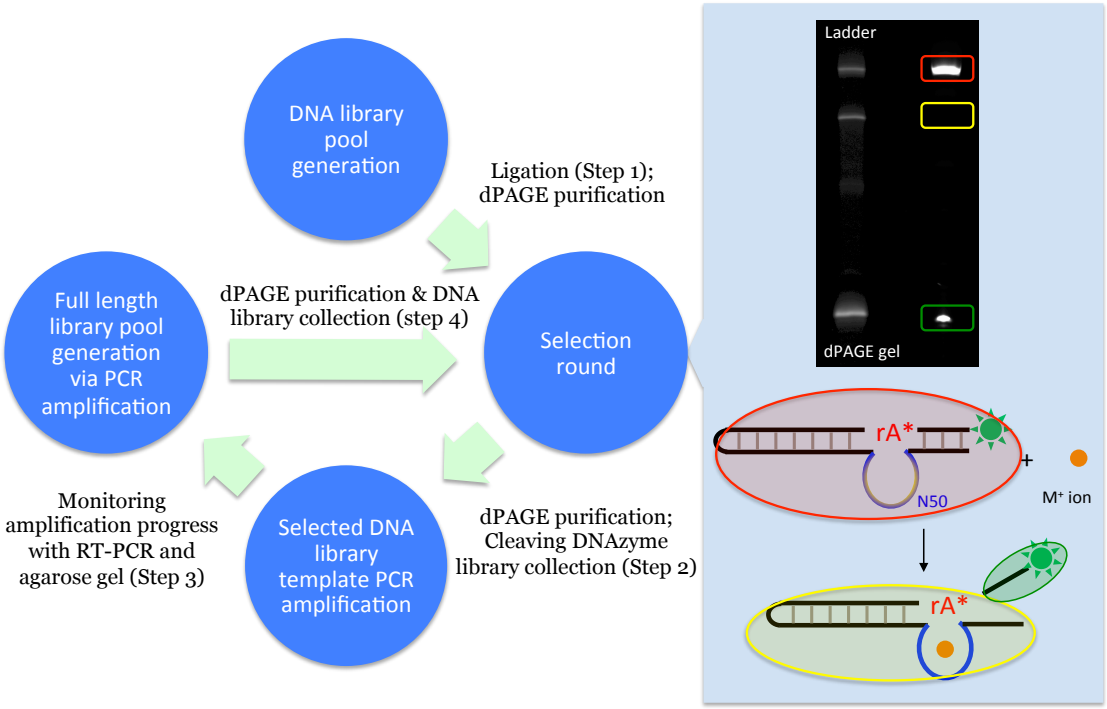

Scheme 1.4 Schematic of DNAzyme selection.

1.8 Role of metal ions in DNAzyme catalysis

Metal ion coordination to the non-bridging oxygen not only increases the elecrophilicity of the phosphorus centre but also stabilizes the charged trigonal-bipyramidal during the transition step. The possible catalytic functions of metal ions can be summarized in Figure 1.7.[77] First, metal-coordinated hydroxide can act as a general base to deprotonate the 2′-hydroxy group and make oxygen a good nucleophile. Alternatively, metal-bound water can act as a general acid to stabilize the developing negative change on 5′-oxygen leaving group. Metal ions can also directly coordinate to the 2′-OH and facilitate deprotonation.

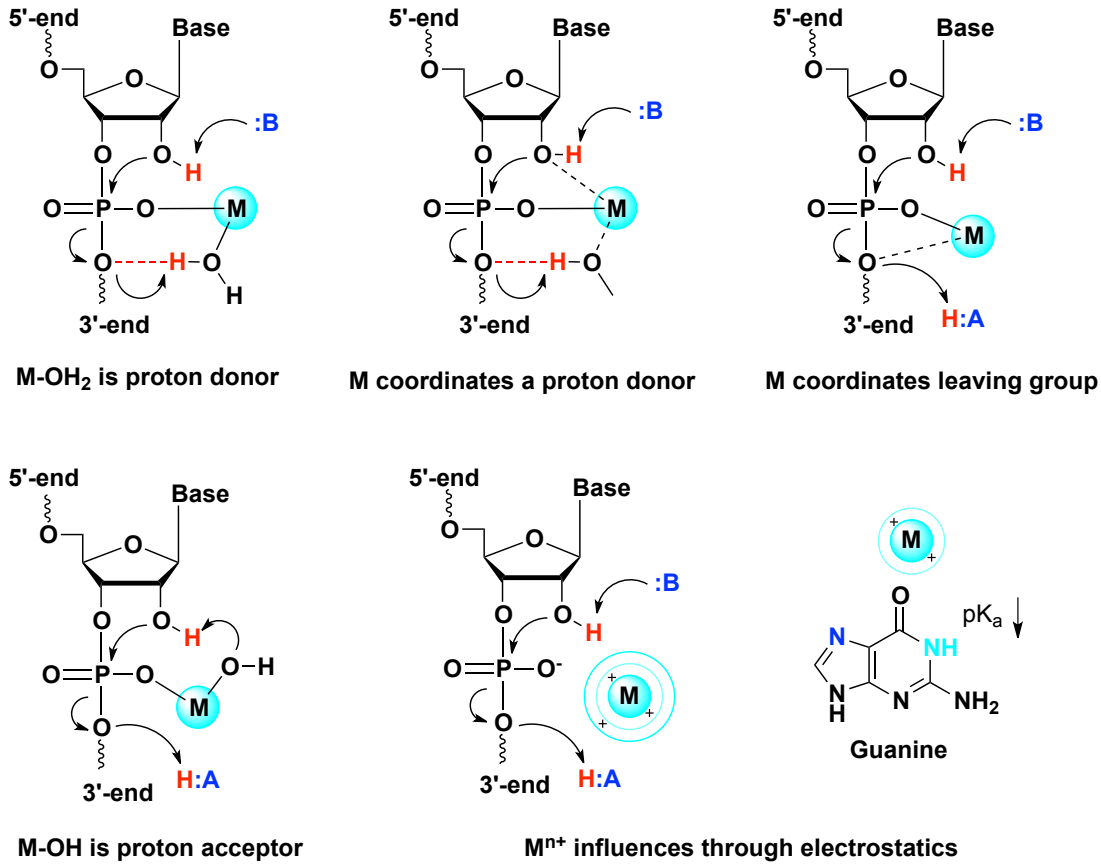

Figure 1.7 Potential roles for metal ions in RNA hydrolysis. Adopted from ref 76. Copyright © 2014 American Chemical Society

Metal ions can also affect the hydrolysis without direct coordination. The long-range electrostatics effects near the active site can change the nearby electrostatic environment to induce the reaction.

1.9 DNAzymes and their catalysis

Due to the structural similarities between RNA and DNA, it is reasonable to consider the possibility of catalytic DNA existence. Just like ssRNA, ssDNA has conformational flexibility that could permit intricate three-dimensional shapes and consequently catalytic activity. DNAzymes, also known as deoxyribozymes or DNA enzymes, refer to single-stranded DNA molecules with catalytic capabilities. Because most DNA in biological systems exists primarily in double-stranded form, it lacks the necessary structural intricacy to act as a catalyst. Thus, no naturally occurring enzymes have been found to be composed of DNA. So far, they have been created in the laboratory. In 1994, the first DNAzyme was discovered and isolated by *in vitro* selection[78] and since that time an increasing variety of DNA catalysts has been isolated (Table 1.3). Although there are only four nucleobases, these different DNAzymes demonstrated that DNA can facilitate many different type of reactions: cleavage of RNA, DNA or the phosphoramidate bond, the ligation of DNA or RNA, the formation of an RNA branch or lariat, the formation of nucleopeptide bond, phosphorylation, adenylation, and depurination, Diels-Alder reaction, and porphyrin metallation of DNA. In fact, each of the catalysis required specific metal cofactors. In other words, each of these DNAzymes showed high specificity towards different metal ions.

Table 1.3 Different types of reactions catalyzed by DNAzymes.

Type of Reaction	Metal cofactor	Reference
RNA cleavage	Pb^{2+}, Zn^{2+}, Mg^{2+}, Ca^{2+}, Mn^{2+}, UO_2^{2+}, or Ln^{3+}	78-87
DNA cleavage (oxidative)	Cu^{2+}	88-90
DNA cleavage (hydrolytic)	Zn^{2+} or Mn^{2+}	91-93
Phosphoramidate bond cleavage	Mg^{2+}	94
RNA ligation	Zn^{2+} or Mg^{2+}	95-98
RNA branching	Mn^{2+} or Mg^{2+}	99-102
RNA lariat formation	Mn^{2+}	103,104
DNA ligation	Cu^{2+} or Zn^{2+}, Mn^{2+}	105,106
Nucleopeptide linkage formation	Mn^{2+} or Mg^{2+}	107
DNA phosphorylation	Mn^{2+}	108
DNA adenylation	Mg^{2+} & Cu^{2+}	109
DNA deglycosylation	Ca^{2+}	110
Diels-Alder reaction	Ca^{2+}	111
Porphyrin metalation	Cu^{2+} or Zn^{2+}	112,113

These DNAzyme catalysis can exhibit the same efficiency and selectivity as protein enzymes. For instance, these DNAzymes showed high rate enhancements, high specificity, and in some, but not all cases, the ability to perform multiple substrate turnovers.

1.10 Representative examples of RNA-cleaving DNAzymes

Many DNAzymes have been isolated by *in vitro* selection. While DNAzymes with other functionalities have also been isolated, most of the DNAzymes selected to date are either cleave or ligate the phosphodiester bond. DNAzymes that catalyze the cleavage of RNA are by far the largest class of catalytic DNA molecules.[114] This section summarizes biochemical and biophysical studies on three of the most characterized RNA-cleaving DNAzymes and their sensing applications.

1.10.1 The GR-5 DNAzyme

Breaker and Joyce were the first researchers to obtain an artificial DNAzyme via *in vitro* selection in 1994.[78] This DNAzyme showed Pb^{2+} dependence with single site RNA-cleaving

capability. It has a catalytic core composed of 15 nucleotides flanked by two base-pairing regions (Figure1.8).

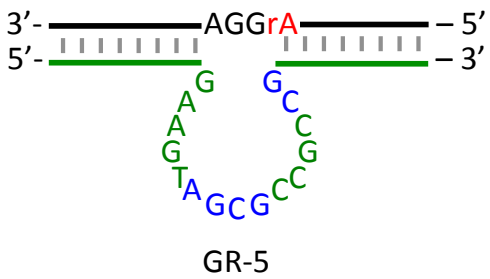

Figure 1.8 Secondary structure of the Pb^{2+}-dependent GR-5 DNAzyme.

Two conserved sequences lie within this domain. One sequence is 5′-AGCG-3′ and the other is 5′-CG(A)-3′. The substrate strand contains a single RNA base within the DNA strand. Also, it required a short stretch of unpaired nucleotides, in this case 3'-GGA-5', between the two regions that are involved in base pairing. Surprisingly, GR-5 DNAzyme was not able to hydrolyze an all-RNA strand under the same conditions. In fact, the target riboadenylate was especially stable. Although the selection buffer contained 50 mM $MgCl_2$, it appeared that the DNAzyme was still very active in the absence of Mg^{2+}. The DNAzyme exhibits Michaelis-Menten kinetics with k_{cat} = 1 min^{-1} and K_m = 2 μM. This rate is about 10^5 fold faster than the uncatalyzed reaction. In the subsequent study, it was reported that this DNAzyme is about 40,000-fold more active with Pb^{2+} than with other competing metal ions.[115] This unique DNAzyme became a model compound for exploring the structural and enzymatic properties of DNA. While GR-5 is a highly efficient DNAzyme, it cannot cleave full RNA substrates and it works only with Pb^{2+}. Therefore, it cannot be applied as an anti-viral agent. For this reason, subsequent selections were carried out with physiological metal ions such as Mg^{2+}.

1.10.2 The 10-23 DNAzyme

It was remarkable that GR-5 DNAzyme demonstrated DNA can have catalytic activity. Unfortunately, unlike naturally occurring ribozymes, the DNAzymes have little utility for biological application. By trying to develop a general purpose RNA-cleaving DNAzyme, Santoro and Joyce carried out an *in vitro* selection under simulated biological conditions (150 mM KCl, 2 mM $MgCl_2$, 50 mM Tris buffer, pH 7.5, 37°C).[79] After multiple rounds of stringent selection and enzyme engineering, two most promising DNAzymes were isolated. One of the two DNAzymes is referred to as the 10-23 DNAzyme (Figure 1.9).

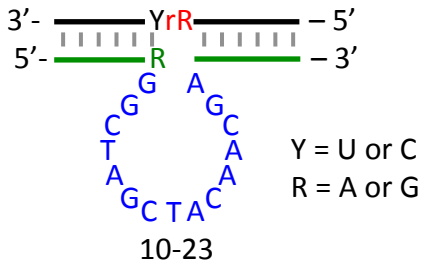

Figure 1.9 Secondary structure of the Mg^{2+}-dependent 10-23 DNAzyme.

Just like GR-5 DNAzyme, 10-23 DNAzyme also contained an unstructured catalytic loop composed of 15 nucleotides that are flanked by two substrate-recognition binding arms. The initial study revealed that the core was almost completely intolerant of variation. 10-23 DNAzyme interacted with the substrate entirely though standard Watson-Crick pairing. Cleavage occurred on the 3′ side of a single unpaired nucleotide, preferable at a purine that was followed by a paired pyrimidine. The 10-23 DNAzyme can be made to cleave almost any target RNA that contains a purine-pyrimidine junction. Target sites surrounded by A and U were cleaved most efficiently, with a catalytic rate of ~0.1 min^{-1} under simulated physiological conditions.[79] However, it was found that its catalytic activity is dependent on the presence of Mg^{2+}. A mutagenesis study showed that changes at the borders of the catalytic domain cause dramatic

loss of enzymatic activity, while changes in nucleotides in between have minimal effects.[116] A deletion study carried out by the same group showed later that the deletion of a C or T base located at the bottom of the core did not affect the activity. [117] However, deleting both C and T bases caused a 10-fold decrease in the catalytic rate. Another deletion study on 10-23 DNAzyme conducted by revealed a novel DNAzyme that is 10-fold more active in the presence of Ca^{2+} than Mg^{2+} and Mn^{2+}.[118]

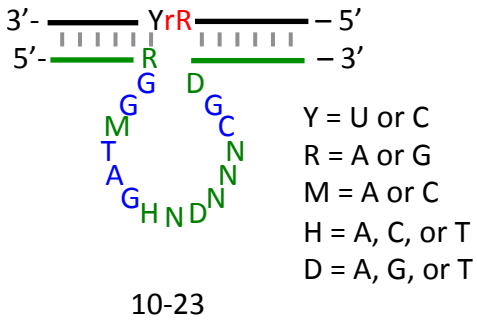

Figure 1.10 Sequence of the10-23 DNAzyme conserved region.

Since the sequence of the substrate-recognition binding arms can be changed, the DNAzyme can be made to target different RNA substrates. For instance, the first report demonstrated that 10-23 DNAzyme could be used to cleave a variety of biologically relevant RNAs.[79] It showed that 10-23 DNAzyme can cleave the translation initiation region of various types of HIV-1 mRNA with a k_{cat} range from 0.03 min^{-1} to 0.1 min^{-1}. Since then, the 10-23 DNAzyme has been widely used as a therapeutic agent for suppressing RNA levels in various systems[119,120] and for degrading viral RNA.[121-123]

1.10.3 The 8-17 DNAzyme

8-17 DNAzyme is the other RNA-cleaving enzyme that was discovered at the same time as 10-23 DNAzyme. It was also named by the round and clone number in its selection. This enzyme and its variants are likely one of the most thoroughly investigated DNAzymes. Based on

the small population of clones, it was originally thought that 8-17 catalytic core is composed of a three base pair stem-loop and a 4 to 5 nucleotides loop.[79] In fact, it was thought that at least two of base pairs on the stem were GC pairs with an AGC tri-nucleotides loop. The other unpaired region have a quite conserved sequence, it can either be 5′-WCGR-3′ or 5′-WCGRA-3′ (W = A or T and R = A or G) with 5′-TCGAA-3′exhibited the highest catalytic activity (Figure 1.11). In addition, just like the 10-23 DNAzyme, most of the sequence of the substrate could be changed without loss of catalytic activity as long as the substrate-binding arms of the enzyme were also changed to complementary the substrate strand. However, the initial report suggested that the 8-17 enzyme required a special G·T ‘‘wobble’’ pair located immediately downstream from the cleavage site. Replace this pair with a Watson-Crick pair at this position eliminated catalytic activity.[79]

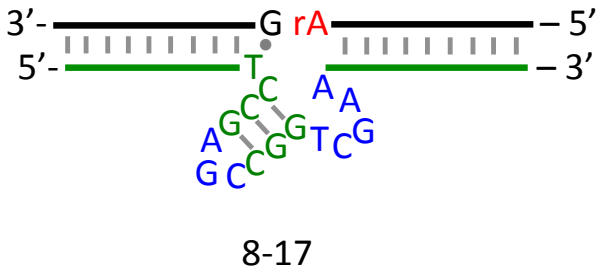

8-17

Figure 1.11 Secondary structure of the Pb^{2+}-dependent 8-17 DNAzyme.

Later, more extensive mutagenesis studies have suggested that only four nucleotides, which are A, G in the stem loop and C, G in the unpaired region, are conserved (Figure 1.12). [124] With a closer comparison between the 8-17 and 10-23 DNAzymes, the positions and neighboring nucleotides of those four nucleotides are remarkable similar. The mutation result also indicated a stable stem is crucial but not sufficient for optimal activity, which agreed partially with the original study. Although an early report suggested that only a 5′-AG-3′ junction can be cleaved by 8-17 DNAzyme, more recent studies demonstrated that this DNAzyme can actually cleave all

sixteen possible dinucleotide junctions at different rates.[81,85,125,126]

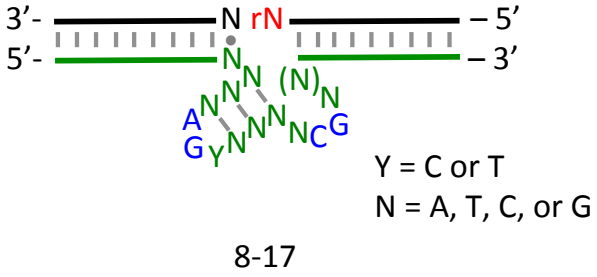

Figure 1.12 Sequence of the 8-17 DNAzyme conserved region.

Over the years, 8-17 DNAzyme has been obtained numerous times through *in vitro* selection by several groups under different conditions.[81,83,85,126-128] This suggested that this DNAzyme is a small, efficient sequence that occurs very frequently during the selections. Even though the same 8–17 DNAzyme was selected against different metal ions such as Mg^{2+}, Zn^{2+}, and Ca^{2+}, the metal ion-selectivity analysis showed that the 8–17 DNAzyme displayed substantially higher activity in the presence of Pb^{2+} than any other metal ion. Although it is selective for Pb^{2+}, the 8–17 DNAzyme is still active in the presence of other metal ions, such as Mg^{2+}, Zn^{2+}, Mn^{2+}, Co^{2+} and Ca^{2+}. With various biochemical and biophysical studies, a lock-and-key mechanism typically seen in protein enzymes has been found to be accountable for the high selectivity for Pb^{2+}.[85,124-126,129-134]

Since its discovery, the 8-17 DNAzyme was used in various applications. It has been utilized in nucleic acid detection,[135,136] metal ion sensing, [137-139] and DNA computing. [140-145]

1.10.4 The 39E DNAzyme

In 2007, Liu et al. reported a novel DNAzyme that can detect UO_2^{2+} down to 45 pM with >1 million-fold selective over other competing metal ions (Figure 1.13).[86] Subsequently, A biochemical study revealed the bulge region has conserved sequences that are likely responsible

for the uranyl binding and enzymatic activity.[146] Furthermore, a fluorescence resonance energy transfer study provided a closer look the global folding of 39E DNAzyme in the presence of various divalent metal ions.[147] The study suggested that 39E also operates in a lock-and key mechanism. Recently, the result from a uranyl photocleavage study pinpointed the exact nucleobases that binding directly with uranyl ion (in blue).[148] AuNPs (13 nm) were functionalized with 39E DNAzyme for intracellular uranyl ion detection.[149]

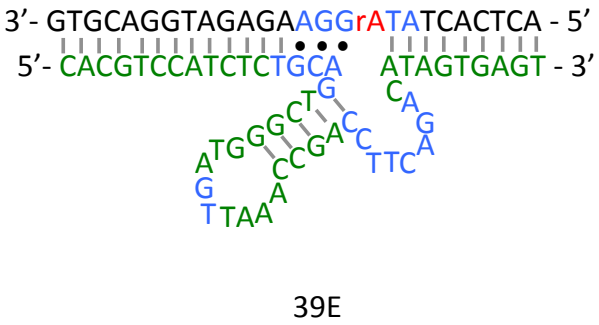

Figure 1.13 Secondary structure and the conserved sequence of the $UO2^{2+}$-dependent 39E DNAzyme.

1.10.5 Comparison of GR-5, 8-17, 10-23, and 39E catalytic efficiency in the presence of different metal ions

Table 1.4 Catalytic efficiency of the GR-5, 8-17, 10-23, and 39E DNAzymes in the presence of different metal ions.

Name of DNAzyme	Metal cofactor	k_{obs} (min^{-1})	k_{cat}/K_m (min^{-1} M^{-1})	Reference
GR-5	1 mM Pb^{2+}	1	5 x 10^5	78
	50 mM Mg^{2+}	3.4	4.5 x 10^9	79
	25 mM Mn^{2+}	1.19	7.0 x 10^7	
	25 mM Ca^{2+}	0.863	1.4 x 10^7	118
	25 mM Mg^{2+}	0.961	2.2 x 10^7	
	25 mM Ba^{2+}	0.101	0.26 x 10^7	
10-23	10 mM Mn^{2+}	>4		
	10 mM Ca^{2+}	0.12		
	10 mM Mg^{2+}	0.28	n.r.	118,150
	10 mM Ba^{2+}	0.015		
	10 mM Sr^{2+}	0.026		
	2 mM Mg^{2+}	~0.01		79
	0.2 mM Pb^{2+}	0.47		125
	5 mM Zn^{2+}	0.12		
8-17	3 mM Mn^{2+}	~0.1	n.r.	
	3 mM Mg^{2+}	~0.002		127
	3 mM Ca^{2+}	~0.02		
	0.1 mM Pb^{2+}	5.75		
	10 mM Zn^{2+}	1.35		
17E (8-17 variant)	10 mM Mn^{2+}	0.24	n.r.	125
	10 mM Mg^{2+}	0.017		
	10 mM Ca^{2+}	0.015		
	0.2 mM Pb^{2+}	2.1		125
	5 mM Zn^{2+}	0.74		
Mg5 (8-17 variant)	3 mM Mg^{2+}	>3	n.r.	
	3 mM Mg^{2+}	0.06		125
	3 mM Ca^{2+}	1		
39E	400 nM	1		86

n.r. = not reported

1.11 Lanthanide ions

The lanthanides are comprised of fifteen elements in the first row of the *f*-block in the periodic table. All of these elements have very similar chemical and physical properties. Most of lanthanides exist in the 3+ oxidation state, although several of them can also form stable 2+ and 4+ ions.[151] Owing to their unique electronic, optical, magnetic and catalytic properties, the demand for lanthanides has grown dramatically over the past few decades. Lanthanides are currently indispensable for modern technological applications such as lasers, superconductors, catalysts, luminescent labels, and imaging contrast agents. Lanthanides can be used either as

solid materials (e.g. oxides), ions or metal complexes (e.g. for MRI imaging). Because of their high positive charge density, lanthanides are good Lewis acids. In addition, they are known to bind tightly to biological molecules. Some lanthanides were shown to have effects in plant metabolism.[152,153] Yet, their exact role in the mechanism is still to be determined.[154] Due to the low bioavailability of lanthanides, it was believed the circumstance prevent any existence of lanthanide variants of metallo-enzymes.[155] Recently, it was reported that that lanthanides were essential cofactor for *Methylacidiphilum fumariolicum* SoIV to sustain growth. [156] This discovery was the first example of organism using a lanthanide in biological processes. Beyond their critical role in modern technologies, lanthanides are also widely utilized in biological probing.[157-159] In particular, they have been extensively used to study the structure and function of nucleic acids due to some of their intrinsic properties.

It is known that lanthanides and their complexes can efficiently cleave nucleic acids. [160] For example, Komiyama et al. demonstrated that Ce^{4+}/EDTA complex acts as catalytic scissors for specific DNA cleaving.[161] In addition, a number of *in vitro* selection experiments were carried out using lanthanides as metal cofactors to obtain DNAzymes[79,162-165] for RNA or DNA cleavage.[166,167]

Besides its catalytic properties, lanthanides like Eu^{3+} and Tb^{3+} also display excellent luminescence characteristics. Since lanthanides show strong binding with nucleic acids,[168] this is useful for probing metal binding sites[169] and for developing biosensors.[170] For example, Fu and Turro[171] used Tb^{3+} as a probe to study the binding of the ions to the bases and nucleotides. In addition, it showed the difference luminescent enhancement between each pair of mismatch bases where GG > CA > GA > CC > TT = TG. Since only ssDNA but not dsDNA can greatly enhance the Tb^{3+} emission, it can be used to detect single mismatches in DNA duplexes.

In addition to luminescence properties, the paramagnetic properties of the lanthanides are useful in probing metal ion binding sites in nucleic acids.[172] Although each lanthanide has similar chemical properties, they all exhibits different magnetic strength. The lanthanide ions binding can be studied with nuclear magnetic resonance (NMR). When the lanthanide ions and the nucleotide protons are in close proximity, those protons will undergo effective line broadening due to the paramagnetic. With a series of titrations, binding sites are identified by following the protons that are influenced by the lanthanide pseudo-contact shift (PCS).[173] For instance, Morrow et al. solved the DNA and RNA structure of lanthanide ion binding sites by combining luminescent and NMR data.[174]

Due to its size, lanthanides can compete with other metal ions in enzymes and act as enzyme inhibitors. For example, Walter et al. used Tb^{3+} as a probe for studying ribozyme structure.[175] The study showed that a deprotonated Tb^{3+} complex acts as competitive inhibitor by competing to a crucial, but non-selective cation binding site in the ribozyme. In addition, both the 17E DNAzyme and the hammerhead ribozyme are also inhibited by lanthanides.[130,169] On the other hand, the Leadzyme (a small ribozyme) and a DNA-based ligase are accelerated by lanthanides.[99,176-178] All these examples suggest strong interactions between lanthanides and nucleic acids. Finally, nucleotides and lanthanides can form coordination complexes with useful luminescence and DNA binding properties.[179-182]

1.12 Research focus

Although a few monovalent-dependent DNAzymes were reported,[82,183] they appear to have poor metal selectivity or catalytic rate. Throughout the years, more divalent metal-dependent DNAzymes were selected successfully. Interestingly, most of these divalent metal-

dependent DNAzymes have better catalytic efficiency when comparing with those monovalent metal-dependent DNAzymes. Thus, it is logical to think that using higher valent metal ions for selection might result in even more efficient DNAzymes. However, no selection was carried with just using trivalent or tetravalent metal ions. The main research reported in this thesis was aimed at expanding the diversity of RNA-cleaving DNAzymes by using a series of lanthanide ions as the cofactor. Trivalent lanthanides were chosen due to their high positive charge density and high affinity toward the nucleotides and phosphate groups. In addition, lanthanides are known to cleave RNA quite efficiently. Combination of all of these facts suggests a possibility for selecting more efficient DNAzymes. Phosphorothioate (PS) modification is known to be a useful method to probe metal binding sites in nucleic acid enzymes. Since lanthanides are hard Lewis acids, the effect of the modification on the DNAzymes will be extensively studied. It is known to be difficult to obtain highly active and selective DNAzymes that bind with thiophilic metal ions with just four natural bases. Although a few thiophilic metal ion-dependent DNAzymes have been successfully selected, they were often based on nucleobase modifications that are not commercially available. By combining the PS modification and our newly developed selection method, the possibility of isolating a cadmium-specific DNAzyme, which has never been achieved before was pursued. These selected new DNAzymes were to be extensively studied to characterize several critical properties, including the nature of their metal binding sites, their exact catalytic mechanisms, and most importantly, their active structures. To demonstrate their practical application on metal ion detection, fluorescence DNAzymes were developed and their performances are highlighted throughout the chapters.

Chapter 2. *In Vitro* Selection of a General Lanthanide-Dependent DNAzyme[a]

2.1 Introduction

The combination of catalytic, magnetic, optical, and electronic properties[158,159] makes lanthanides indispensable materials for modern technologies. It has been estimated that about 100,000 metric tons of lanthanides were consumed globally per year.[184] However, their widespread applications and increasing demand also raised the concern about lanthanide pollution and depletion. Those issues have prompted scientists to develop new analytical tools for environmental monitoring, electronic recycling, and finding new mineral sources.

Currently, trace analysis relies primary on instrumentation methods such as inductively coupled plasma mass spectrometry (ICP-MS) and capillary electrophoresis (CE). [185] Although these methods can analyse a few metals simultaneously with excellent sensitivity, this expensive analysis requires timely sample preparation and can only be performed in a laboratory. In this regard, developing portable and easy-to-use sensors becomes an attractive solution for real-time and on-site detection. Several sensors based on ion selective electrodes and fluorescent/colorimetic chelators for lanthanides have been reported in recent years.[186,187] However, most of these small organic molecule-based probes not only required organic solvents but also demonstrated poor sensitivity. Most importantly, the current sensors are not capable of discriminating among the individual lanthanide.

While lanthanide complexes have been used as markers for bioanalyses and imaging, [188] using the biosensor strategy for their detection has yet to be investigated. Out of the many

[a] This chapter is the basis for a published manuscript: Huang, P. J.; Lin, J.; Cao, J.; Vazin, M.; Liu, J. Ultrasensitive DNAzyme Beacon for Lanthanides and Metal Speciation. *Anal. Chem.* **2014***, 86*, 1816-1821.

biomolecules, DNAzymes have emerged as unique platforms for designing metal biosensors. A number of divalent metal-specific DNAzymes have been isolated successfully and many of these DNAzymes have been engineered into metal biosensors.[164] However, using DNAzymes for detecting trivalent and tetravalent metals has yet to be explored.

Lanthanides might be a good choice for RNA/DNA cleavage since many lanthanide complexes are efficient catalysts for non-specific nucleic acid hydrolysis.[160,189] In fact, catalysis by several DNAzymes have been shown to involve lanthanides although the effects on catalysis vary depended on the DNAzyme. For example, lanthanides were shown to accelerate RNA ligation and hydrolysis that were catalyzed by Mg^{2+}-dependent DNAzyme and Pb^{2+}-dependent ribozyme respectively.[176-178] Even though GR5, the first DNAzyme discovered,[78] is active with lanthanides alone, the rate was very slow (<0.02 min^{-1}) when comparing with Pb^{2+} activity.[167] In addition, it was reported that Tb^{3+} inhibited the 8-17 DNAzyme and hammerhead ribozyme.[130] Recently, a few DNA-cleaving DNAzymes were selected in the presence of Ce^{3+}, Eu^{3+} or Yb^{3+} together with Zn^{2+}.[166] That study showed that these lanthanides were critical for the enzyme activity. However, this type of co-addition system actually complicates the downstream analytical applications. To date, no selection was carried out using lanthanides as the sole metal cofactor to obtain RNA-cleaving DNAzymes.

In this chapter, the selection of an RNA-cleaving DNAzyme using tetravalent lanthanide as the intended metal cofactor is presented. Ce^{4+} was chosen because it is highly efficient in assisting cleavage of the phosphodiester bond bond.[161] Interestingly, a new DNAzyme that is active only with Ce^{3+} and other trivalent lanthanides was obtained. The conversion between these two oxidation states of cerium was also monitored, showing the feasibility of metal speciation analysis.

2.2 Results and Discussions

2.2.1 DNAzyme Selection

A DNA library containing a 50-nucleotide randomized region (N_{50}) as shown in Figure 2.1A (blue region) was used for *in vitro* selection. This initial library is estimated to contain ~10^{14} random DNA sequences. The randomized region is flanked by two short base paired duplexes, holding the single ribo-adenosine (rA) in its proximity. This rA linkage serves as the putative cleavage site, since RNA is about one million fold more susceptible to hydrolysis than DNA.[52] $(NH_4)_2Ce(NO_3)_6$ was used as the Ce^{4+} source owing to its excellent solubility and stability. After incubating the library with the salt, the cleaved sequences were separated and isolated using gel electrophoresis since they were 28-nucleotide shorter than the original full-length library. Two rounds of polymerase chain reactions (PCR) were carried out to amplify the cleaved DNA. In PCR1, a full-length library was regenerated and was used as a template for PCR2. In PCR2, two special modified primers were used. P3 has a FAM label on its 5′-end terminus and a rA base on its 3′-end terminus. P4 has a polymer spacer that can stop the polymerase reaction. As a result, PCR2 produced two strands with unequal length that can be separated easily by gel electrophoresis. The isolated positive strand containing rA and FAM was seeded for the subsequent round of selection. The selection was stopped at round 6, when the library was cloned and sequenced. Table 2.1 listed the detail of the selection conditions and progress.

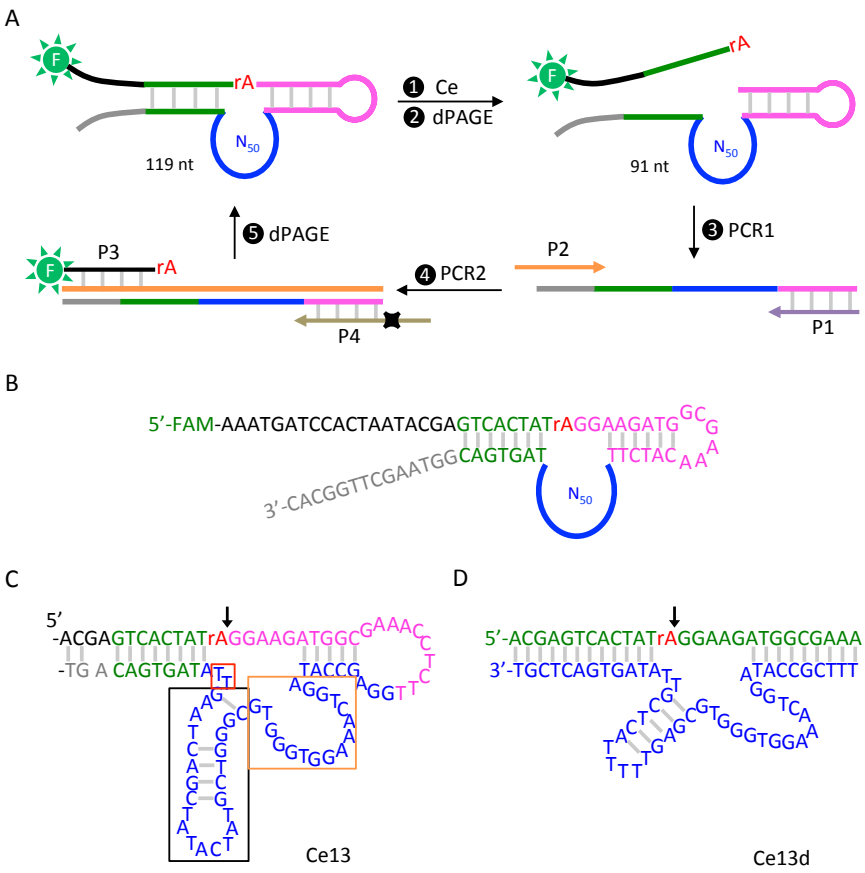

Figure 2.1 A design scheme for the Ce^{4+} DNAzyme selection. A) The initial library contains N_{50} randomized region and a single RNA linkage (rA) as the cleavage site. Cleaved sequences in the presence of Ce (step 1) are isolated using gel electrophoresis (dPAGE, step 2). Two rounds of PCR are carried out followed by another dPAGE to re-generate the full-length single-stranded library. B) The sequence of the library prior to the cleavage step. C) The secondary structure of the original Ce13 DNAzyme with the N_{50} region in blue. Three regions of this enzyme (in the boxes) are assayed. D) An optimized and truncated trans-cleaving DNAzyme, Ce13d.

Table 2.1 Ce^{4+} selection conditions and progress.

Round #	[Ce(IV)] (μM)	Incubation time (min)	Cleavage (%)
1	500	60	1.1
2	500	60	7.4
3	500	60	12.7
4	500	40	34.4
5	50	40	53.5
6	50	40	56.2

2.2.1 DNAzyme secondary structure analysis

Nineteen clones with the correct DNA insertion were obtained and their exact sequences are listed in Table 2.2. The alignment shows that half of the populations have almost identical

sequences. One of the representative clones, named Ce13, folds into the structure shown in Figure 2.1C. The core of the Ce13 contains a hairpin-like structure (black box) and a loop (orange box). The result from mutation studies (Figure 2.2) indicated that this hairpin plays only a structural role. Thus, an optimized and truncated trans-cleaving version of the enzyme named Ce13d was designed and used for further analysis (Figure 2.1D).

Table 2.2 Sequence alignment of the selected Ce^{4+} DNA.

Clone#	Sequences	
20	CTGCAGAATTCTAATACGAGTCACTATAGGAAGAT----GGCGAAACATTT--GGAG---	51
22	CTGCAGAATTCTAATACGAGTCACTATAGGAAGAT----GGCGAAACATT---GGAG---	50
6	CTGCAGAATTCTAATACGAGTCACTATAGGAAGAT----GGCGAAACAT----GGAG---	49
4	CTGCAGAATTCTAATACGAGTCACTATAGGAAGAT----GGCGAAACATCTT-GGAG---	52
34	CTGCAGAATTCTAA-ACGAGTCACTATAGGAAGAT----GGCGAAACATCCT-GGAG---	51
13	CTGCAGAATTCTAATACGAGTCACTATAGGAAGAT----GGCGAAACATCTT-GGAG---	52
9	CTGCAGAATTCTAATACGAGTCACTATAGGAAGAT----GGCGAAACATCTT-GGAG---	52
3	CTGCAGAATTCTAATACGAGTCACTATAGGAAGAT----GGCGAAACATCTT-GGAG---	52
11	CTGCAGAATTCTAATACGAGTCACTATAGGAAGAT----GGCGAAACATCTT-GGAG---	52
15	CTGCAGAATTCTAATACGAGTCACTATAGGAAGAT----GGCGAAACATCTT-TA-----	50
5	CTGCAGAATTCTAATACGAGTCACTATAGGAAGAT----GGCGAAACATCTT-TA-----	50
2	CTGCAGAATTCTAATACGAGTCACTATAGGAAGAT----GGCGAAACATCTT-TACG---	52
16	CTGCAGAATTCTAATACGAGTCACTATAGGAAGAT----GGCGAAACATCTT-TACG---	52
12	CTGCAGAATTCTAATACGAGTCACTATAGGAAGAT----GGCGAAACATCTT-AACG---	52
23	CTGCAGAATTCTAATACGAGTCACTATAGGAAGAT----GGCGAAACATCTT-AACG---	52
10	CTGCAGAATTCTAATACGAGTCACTATAGGAAGAT----GGCGAAACATCTT-TACG---	52
14	CTGCAGAATTCTAATACGAGTCACTATAGGAAGAT----GGCGAAACATCTT-T----TA	51
32	CTGCAGAATTCTAATACGAGTCACTATAGGAAGAT----GGCGAAACATCTT-TACGACA	55
7	CTGCAGAATTCTAATACGAGTCACTATAGGAAGAT----GGCGAAACATCTCACAAG---	53
20	-CCATAGGTCAAAGGTGGGTGCGTGTC----GTATC-ATATCG-ACTAA----------	93
22	-CCATAGGTCAAAGGTAGGTGCG-GTC----GTATC-ATATCG-ACTAA----------	91
6	-CCATAGGTCAAAGGTAGGTGCGAGTC----GTATC-ATATCG-ACTAA----------	91
4	-CCATAGGTCAAAGGTAGGTGCGGGTC----GTATC-ATATCG-ACTAA----------	94
34	-CCATAGGTCAAAGGTAGGTGCGGGTC----GTATC-ATATCG-ACTA-----------	92
13	-CCATAGGTCAAAGGTAGGTGCGGGTC----GTATC-ATATCG-ACTA-----------	93
9	-CCATAGGTCAAAGGTAGGTGCGGGTC----GTATC-ATATCG-ACYA-----------	93
3	-CCATAGGTCAAAGGTAGGTGCGGGTC----GTATC-ATATCG-ACCA-----------	93
11	-CCATAGGTCAAAGGTWGGTGCKGGYS----KWWYM-WWWYCR-MYWA-----------	93
15	--CAAGGAACAATAATGGGGTCGGGT-------ATA-TTGTCGTACCG-----------	88
5	-CGAACGGTTAAGAAAAGTGACTTATC----CAGTGGTTATCTGACTA-----------	93
2	-----A-CGTCA----TCCCAAACAGG-CCATTAAA--AAAAGGATATAAG--------G	91
16	-----A-CGTCA----TCCTAAACAGG-CCATTAAA--AAAAGGATATAAG--------G	91
12	-----AGTGTAGAATCTCCCTGAAAGG-C-AGAATG--CAAAGTACAC----------G	92
23	-----AGTGTAGAATCTCCCTGAAAGG-C-AGAATG--CAAAGTACAC----------G	92
10	-----AGAGTAG----TCATTTAAA-------TTAA--CAAAGTACACTGACGCAAAACG	94
14	TC----GCGTAAATGACCGTATTCATG-C--GAATA--GGACATACG----------G	90
32	TCCGGGGCATGAACCACGATGGCCAT-------ATA--TAACGAATG----------G	94
7	---GGGGTGTATTAT-TCACGCGGATAACGTTAATA--CATGGTAC----------G	94

Table 2.2 Sequence alignment of the selected Ce^{3+}/Ce^{4+} DNA. (Continued)

Clone#	Sequences	
20	GTTATAGTGACG-GTA----AGCTTGGCAC	118
22	GTTATAGTGACG-GTA----AGCTTGGCAC	116
6	GTTATAGTGACG-GTA----AGCTTGGCAC	116
4	GTTATAGTGACG-GTA----AGCTTGGCAC	119
34	GTTATAGTGACG-GTA----AGCTTGGCAC	117
13	GTTATAGTGACG-GTA----AGCTTGGCAC	118
9	GTTATAGWGACG-GTA----AGCTTGGCAC	118
3	GTTATAGTGACG-GTA----AGCTTGGCAC	118
11	GTTATAGTGACG-GTA----AGCTTGGCAC	118
15	GTTATAGTGACG-GTA----AGCTTGGCAC	113
5	GTGTTAGTGACG-GTA----AGCTTGGCAC	118
2	GTTATAGTGACG-GTA----AGCTTGGCAC	116
16	GTTATAGTGACG-GTA----AGCTTGGCAC	116
12	GTTATAGTGACG-GTA----AGCTTGGCAC	117
23	GTTATAGTGACG-GTA----AGCTTGGCAC	117
10	GTTATAGTGACG-GTA----AGCTTGGCAC	119
14	---ATAGTGACG-GTA----AGCTTGGCAC	112
32	GTTATAGTGACG-GTA----AGCTTGGCAC	119
7	GTTATAGTGACG-GTA----AGCTTGGCAC	119

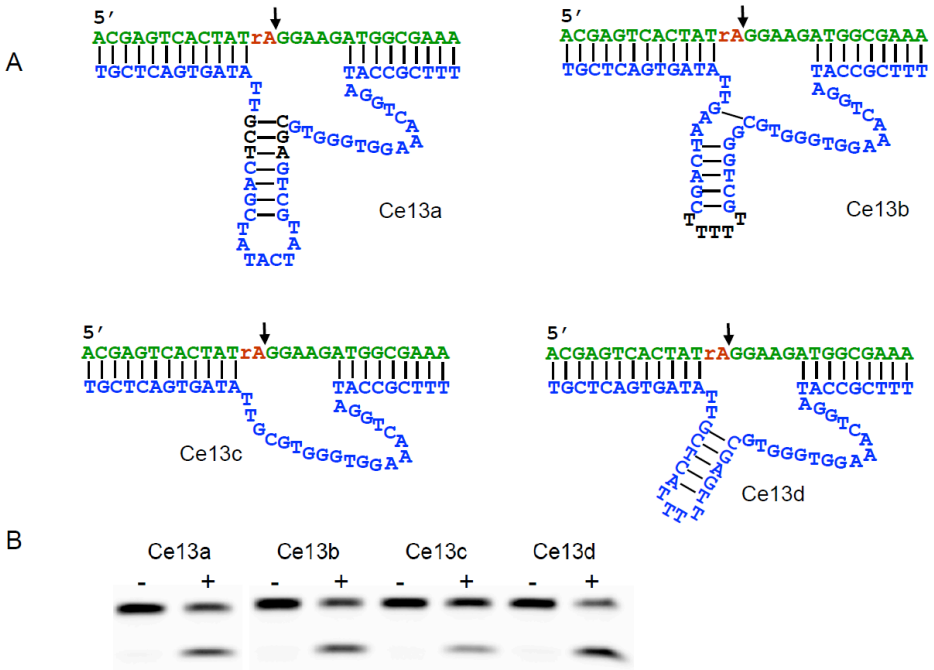

Figure 2.2 Secondary structure of the Ce13a-d mutants. A) Design of mutation studies to confirm the hairpin structure and its optimization for the Ce13 DNAzyme. B) Activity assays of these mutants.

To further understand this enzyme, additional mutants were tested. There is a TT sequence right next to the enzyme hairpin (red box in Figure 2.1C). Deleting one or both of the thymines only slightly decreased the activity (see Figure 2.3). On the other hand, deleting any of

the GG di-nucleotides in the orange box resulted in completely disappearance of the activity. Therefore, these nucleotides appeared to be critical for the catalysis.

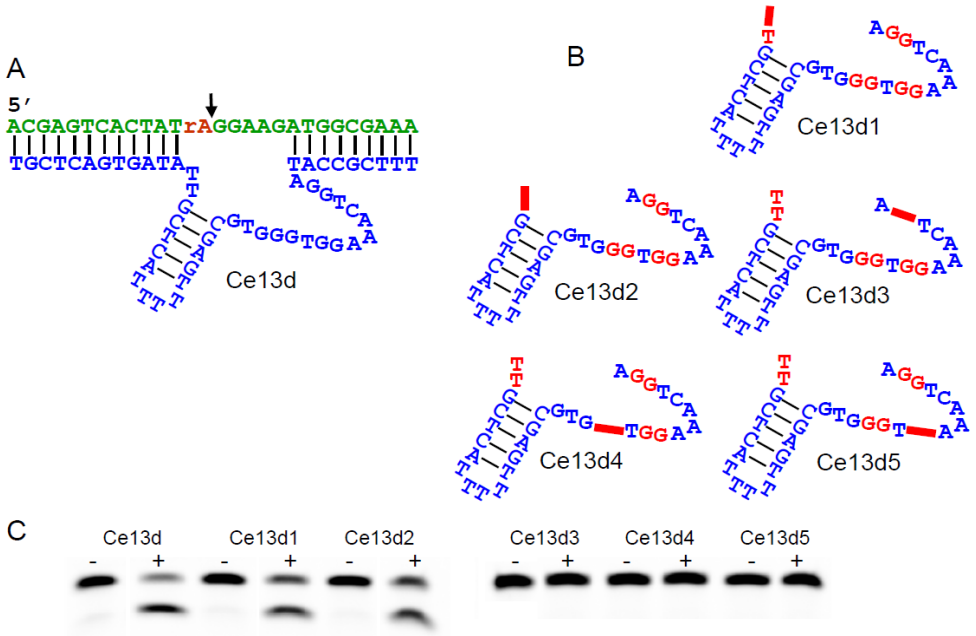

Figure 2.3 Secondary structure of the Ce13d1-5 mutants. A) The secondary of the truncated trans-cleaving form Ce13d. B) Nucleotide deletions; deleted nucleotides are represented by the thick red lines. C) Gel assay of the mutants in B); the plus and minus signs denote for with and without the metal cofactor respectively.

While using mfold[190] software for secondary structure prediction, a second small hairpin that contains two Watson-Crick base pairs and a G•T wobble pair was also shown in the loop region of the Ce13 DNAzyme (Figure 2.4A, Ce13a). However, the prediction was made under the impression that 1 M NaCl was used. Since the selection buffer contained only ~50 mM Na^+, it was not clear whether this is an actual structure that was important for the enzymatic activity. To verify this, we either deleted the stem-loop entirely (Ce13a1) or extended it gradually (Ce13a2 and Ce13a3). In all the cases, the mutants were inactive (Figure 2.4B). Therefore, the result indicated that the hairpin is unlikely to be present for the active enzyme. This was also consistent with the deletion studies in Figure 2.3, where changes to the loop region often eliminate the enzyme activity.

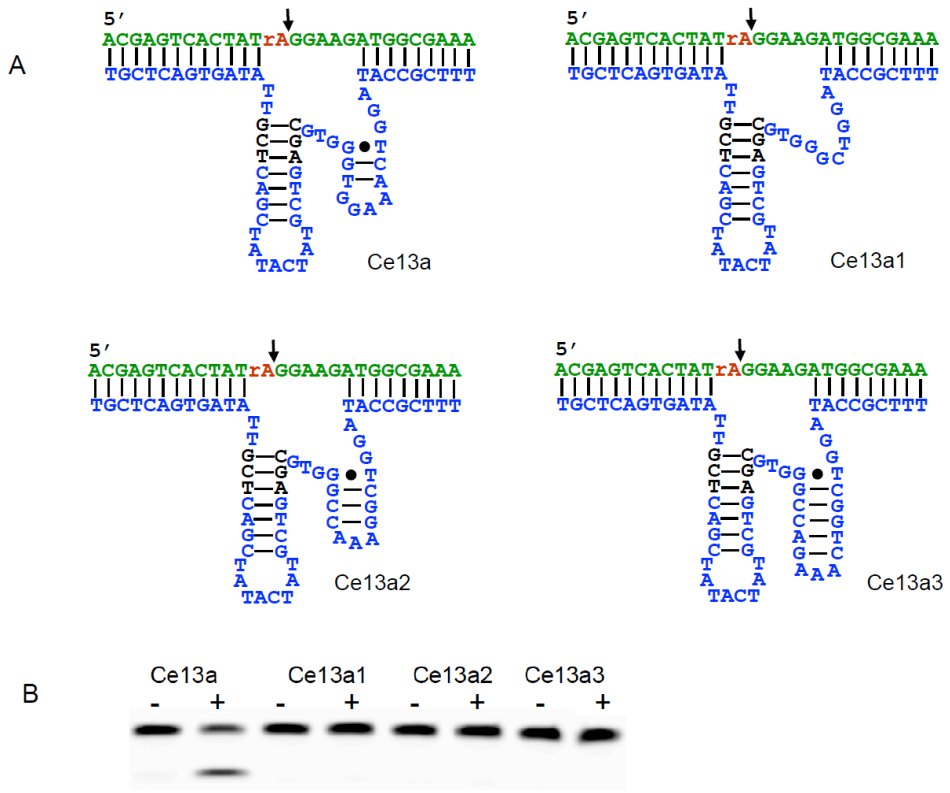

Figure 2.4 Secondary structure of the Ce13a and Ce13a1-3 mutants. A) Design of mutation studies to disprove the second hairpin structure for the Ce13 DNAzyme. B) Activity assays of these mutants.

This DNAzyme was also unique in terms of the bases that located next to the rA cleavage site. More specifically, the five unpaired nucleotides GGAAG. As shown in Figure 2.5, the activity dropped considerably after the base pairing with the substrate strand was gradually extended. However, the enzyme was still active. Consequently, the original unpaired Ce13d was still the optimal construct for subsequent studies.

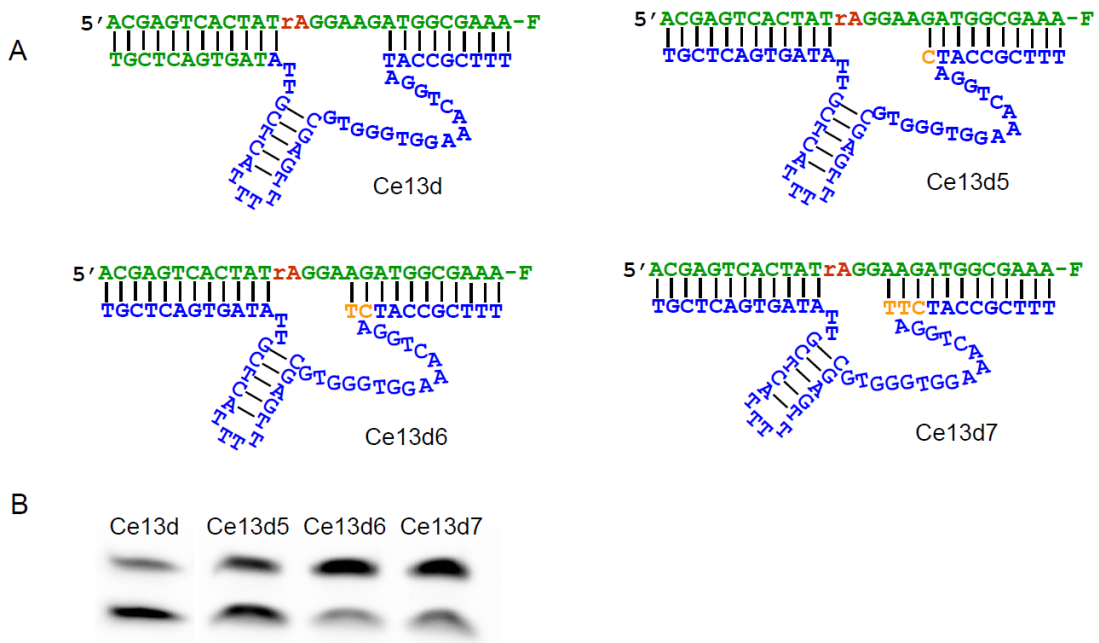

Figure 2.5 Secondary structure of the Ce13d and Ce13d5-7 mutants. A) Design of mutation studies to understand the unpaired nucleotides of the substrate strand of the Ce13 DNAzyme. B) Activity assays of these mutants.

2.2.3 Activity with Ce^{3+} vs. activity with Ce^{4+}

Although the sensitivity and specificity of the divalent metal ions dependent DNAzymes have been well documented, the DNAzyme activity with metals of different oxidation states have yet been investigated. Since both Ce^{3+} and Ce^{4+} are stable, this DNAzyme activity can be studied in both oxidation states. An assay was performed as a function of Ce^{3+} and Ce^{4+} concentration and was plotted in Figure 2.6A. With increasing Ce^{3+} concentration, the cleavage product initially increased followed by an inhibition effect. The optimal activity was observed at 10 μM Ce^{3+} (Figure 2.6C, black dots). Surprisingly, little activity was observed in the presence of Ce^{4+}. Even though Ce^{4+} was used as the intended metal cofactor, only a small amount of cleavage (~10%) was observed with ~100 μM Ce^{4+} (Figure 2.6B and Figure 2.6C, red dots). Ce13d shows a cleavage rate of 0.25 min^{-1} with 10 μM Ce^{3+} (Figure 2.6D). This rate is comparable with many divalent metal-dependent DNAzymes that are selected or assayed at pH ~6.[86,191]

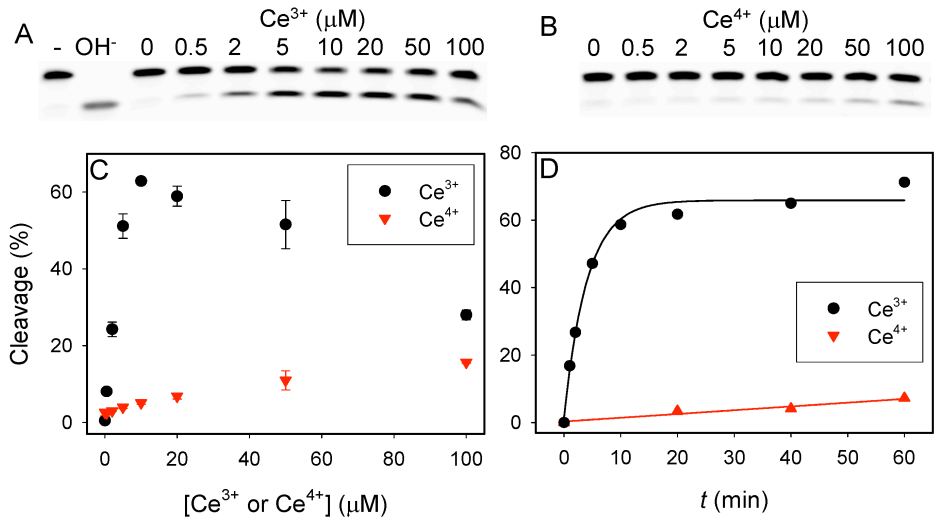

Figure 2.6 Sensitivity and kinetic studies of the Ce13d DNAzyme. Gel image of Ce13d assay after incubating with various concentrations of Ce^{3+} A) or Ce^{4+} B) for 1 h. In A), the first lane is the substrate alone (no Ce13d, negative control); the second lane is the substrate treated with NaOH (positive control). C) Quantification of the gel data in A) and B). D) Kinetics of Ce13d cleavage with 10 μM Ce^{3+} or Ce^{4+}.

2.2.4 Searching for possible explanations of low Ce^{4+} activity

Since the nitrate salt for Ce^{4+} and the chloride salt for Ce^{3+} were used, it is quite possible that the nitrate anions might inhibit the enzyme activity. To test whether the difference in activity was due to the different salt anions, the enzyme was assayed in the presence of $NaNO_3$. As shown in Figure 2.7, the presence of nitrate has little effect on the activity of the enzyme. Therefore, nitrate cannot explain the lack of Ce^{4+}-dependent activity.

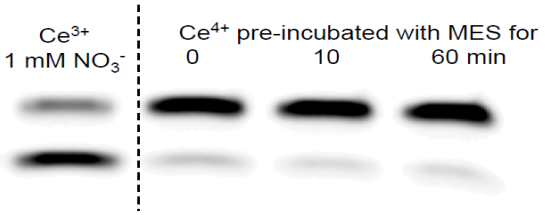

Figure 2.7 Gel analysis of Ce13d in the presence $NaNO_3$ buffer. Lane 1: Ce13d assay in the presence of 1 mM $NaNO_3$ to the reaction buffer. The Ce^{3+} concentration was 10 μM and the reaction time was 1 h. Lane 2-4: Ce^{4+} was pre-incubated with 50 mM MES (pH 6) for various time before adding to the enzyme.

Another possibility for the lack of Ce^{4+}-dependent activity is that the Ce^{4+} salt is an inhibitor for such DNAzyme-based catalysis. To test whether or not the Ce^{4+} salt was the cause

of inhibition, the mixture of the Ce^{3+}/Ce^{4+} salts was used. First, 10 μM Ce^{3+} was mixed with various concentrations of Ce^{4+} range from 0 to 1 mM. Complete inhibition was observed only with 1 mM Ce^{4+} (Figure 2.8). It should be noted that only 10 to 100 μM Ce^{4+} was used for the selection and the assay. At such low concentrations, Ce^{4+} should not be an inhibitor. In addition, similar observations were made by fixing Ce^{4+} at 10 μM and varying the Ce^{3+} concentration. Based on the results, the reason for the lack of Ce^{4+}-dependent activity also cannot be attributed to the Ce^{4+} salt being a DNAzyme inhibitor.

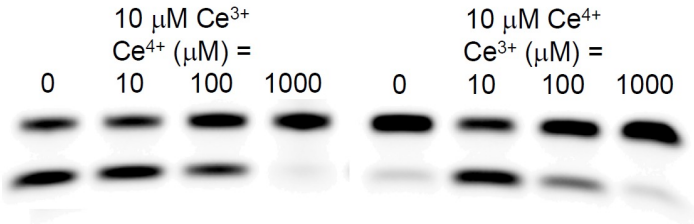

Figure 2.8 Ce13d assay with mixture of Ce^{3+}/Ce^{4+} salts.

Based on the data shown above, a more reasonable explanation is that there might be a small fraction of Ce^{3+} present in the Ce^{4+} salt. Ce^{4+} is a strong oxidant so it is possible that some Ce^{4+} could be converted into Ce^{3+}. If Ce^{4+} was completely inactive and all the activity observed in Ce^{4+} was from the Ce^{3+} impurity, the amount of Ce^{3+} was estimated to be ~1% in the Ce^{4+}. Since the Ce^{3+}-catalyzed reactions were faster than those by Ce^{4+}, the selection process was gradually guiding the library towards Ce^{3+}-dependent DNAzymes. Although the resulting DNAzyme reacted in an opposite way as originally intended, this enzyme can still distinguish between the two oxidation states of cerium.

2.2.4 pH-dependent assay

To further optimize the condition for Ce13d, a pH dependent assay was carried out. In this study, DNAzyme was mixed with 10 μM Ce^{3+} in various pH buffers for 10 min. All the buffer

concentration was 50 mM. As shown in Figure 2.9, the enzyme is inactive at pH 3.5 and has very low activity at pH 5. The highest activity was observed in between pH 6 and 7.5, where as at pH 8.5 the activity was lower. Therefore, the enzyme showed a bell-shaped pH-dependent activity and is suitable for detection in water samples.

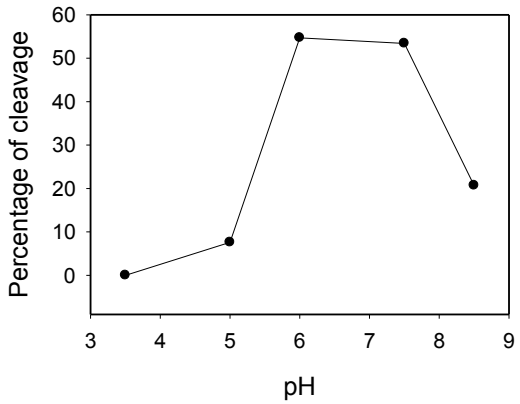

Figure 2.9 pH-dependent enzyme activity (10 min reaction time). The buffers are acetate (pH 3.5), MES (pH 5, 6), HEPES (pH 7.5) and Tris (pH 8.5).

2.2.5 Metal specificity

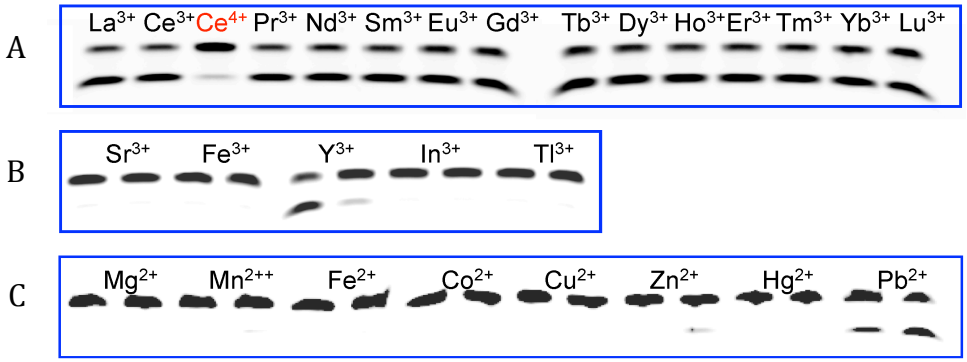

Figure 2.10 Selectivity of the Ce13d with various divalent and trivalent metal ions. Gel images with 10 μM various lanthanides A), with 10 and 100 μM trivalent metals B) or divalent metals (C). In B) & C) below each metal label, the left lane is 10 μM and the right lane is 100 μM of the metal. All assays are performed in 50 mM MES buffer (pH 6) with 25 mM NaCl.

Figure 2.10A showed that Ce13d can be cleaved by all the trivalent lanthanides with a similar activity, reaching ~70% cleavage in 1 h with 10 μM metal ions. Other trivalent metal ions were also tested (Figure 2.10B), including Fe^{3+}, Cr^{3+}, In^{3+}, Sc^{3+}, Y^{3+} and Tl^{3+}. Only Y^{3+} showed

cleavage activity; Y is known to be very similar to lanthanides (e.g. ionic radius similar to Ho^{3+}) and is also classified as one of the rare earth metals together with the lanthanides. Sc^{3+} showed no activity although it is in the same row, possibility due to its smaller size. None of the other trivalent metals showed activity, despite the fact that size of Tl^{3+} is also similar to that of Y^{3+}. Therefore, in addition to size and charge (see Table 2.3), metal coordination chemistry must also play an important role.

For divalent metal ions, Pb^{2+} is the only one that showed moderate activity at 10 μM concentration, while Zn^{2+} showed a very small amount of cleavage at 100 μM (Figure 2.10C). Based on the cleavage assay, the selectivity for lanthanides over Pb^{2+} is more than 20-fold and for other divalent ions is more than 500-fold. Since Pb^{2+} is a thiophilic soft cation while lanthanides are hard Lewis acids with low affinity toward thiol, interference from Pb^{2+} can be masked (*vide infra*). Overall, this enzyme may serve as a general probe for rare earth metals, which has not been achieved previously.

Table 2.3 Oxidation states, ionic radii and activity of selected metal ions.[192] In the first column, Ox means oxidation state, r denotes for ionic radii and A refers to activity (Y = active; N = inactive, M=moderate).

	Fe	In	Tl	Sc	Y	La	Ce	Ce	Pr	Nd	Sm	Eu	Gd	Tb	Dy	Ho	Er	Tm	Yb	Lu	Pb
Ox	3	3	3	3	3	3	3	4	3	3	3	3	3	3	3	3	3	3	3	3	2
R (pm)	65	80	89	75	90	103	101	87	99	98	96	95	94	92	91	90	89	88	87	86	119
Activity	N	N	N	N	Y	Y	Y	N	Y	Y	Y	Y	Y	Y	Y	Y	Y	Y	Y	Y	M

2.2.6 Kinetics of Ce13d DNAzyme with other lanthanides

So far, the majority of the lanthanide data presented only showed cleavage at 1 hr. To compare the actual rate of cleavage, a few lanthanides were chosen to measure the cleavage kinetics and the data were displayed Figure 2.11. The rates are 0.25 min^{-1} (Ce^{3+}), 0.17 min^{-1} (Sm^{3+}), 0.13 min^{-1} (Dy^{3+}) and 0.082 min^{-1} (Yb^{3+}). Therefore, the difference in rate among all lanthanides is within 3-fold.

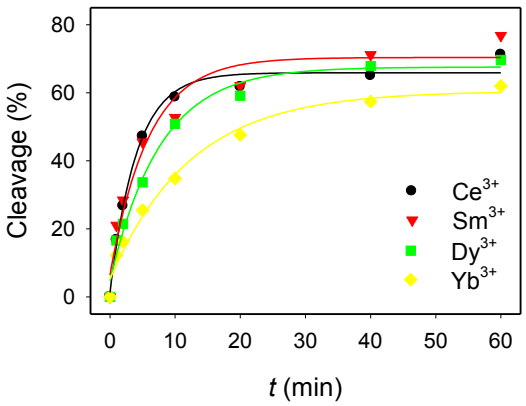

Figure 2.11 Ce13d cleavage kinetics in the presence of 10 μM lanthanides. The buffer contained 25 mM NaCl, 50 mM MES (pH 6.0) and the DNAzyme concentration was 1 μM.

Since divalent metal ions are much more efficient than monovalent ions for DNAzyme catalysis, one may deduce that higher valent metal ions might be even more efficient. From the inorganic chemistry standpoint, a higher oxidation state corresponds to a higher positive charge density and possibly different coordination geometry. The pK_a value of the bound water may also be affected, all of which are important parameters to influence DNA catalysis. However, despite that Ce^{4+} was initially used, the selected enzyme was more active with Ce^{3+}. In addition, the rate for this Ce^{3+}-dependent DNAzyme did not appear to be superior to other DNAzymes using divalent metal cofactors. One possible explanation is that with increasing positive charge density, higher valent cations display stronger non-specific interactions with DNA, making it more difficult to form efficient enzyme structures. Since combining divalent metals and lanthanides has been shown to accelerate DNAzyme catalysis,[166,176,177] further studies are needed to fully understand the use of lanthanide alone as the metal cofactor.

2.2.7 DNAzyme beacon sensor

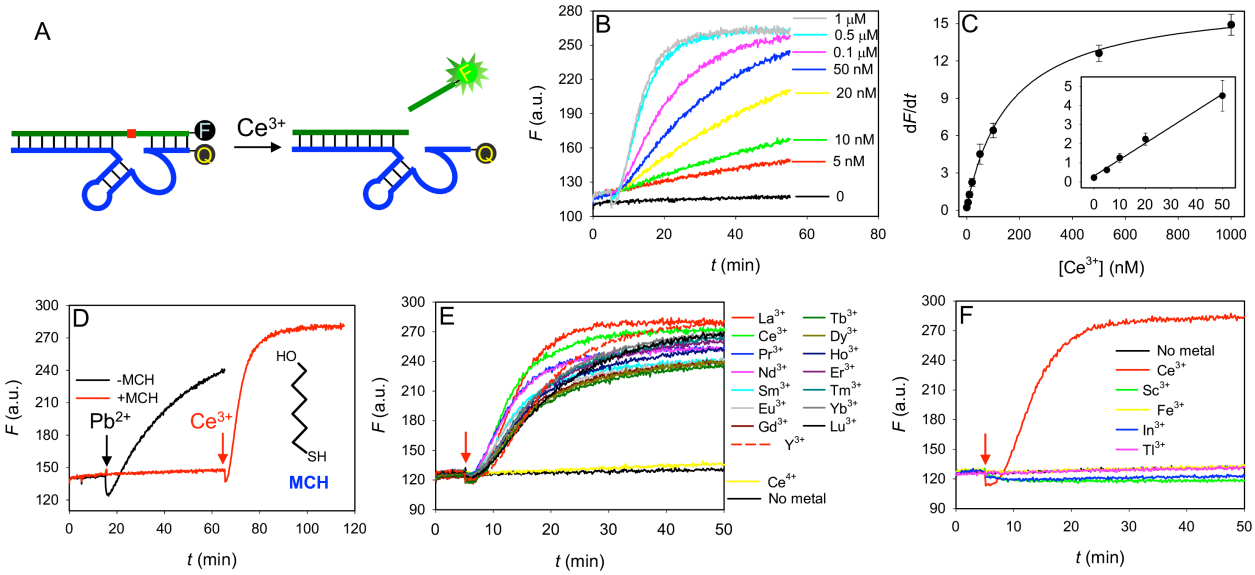

Figure 2.12 Kinetic study of the Ce13d DNAzyme beacon. A) Schematic representation of the DNAzyme beacon. B) Sensor signaling kinetics to various concentrations of Ce^{3+}. DNAzyme concentration = 50 nM in 50 mM HEPES buffer (pH 7.6). C) Quantification of Ce^{3+} based on the initial rate of fluorescence enhancement. Inset: the linear region at low Ce^{3+} concentrations. D) Masking the 10 μM Pb^{2+} response by 1 mM MCH. Sensor response to 1 μM various lanthanides and Y^{3+} E) and to other trivalent metal ions F).

A biosensor based on fluorescence "turn-on" DNAzyme was designed for real-time analysis (Figure 2.12A). In this design, the 5′-end of the substrate strand was extended by 3 nucleotides to form a 15-mer duplex with the enzyme. The 3′-end of the substrate was labeled with a FAM, and it still formed 9 base pairs to allow fluorophore to release after cleavage. The enzyme strand was labeled with a quencher on 5′-end. In the presence of Ce^{3+}, the cleavage reaction may facilitate the release of the FAM-labeled fragment to enhance fluorescence signal (Figure 2.12A).[193] To ensure that the fluorescence enhancement in the DNAzyme beacon setup was indeed due to the cleavage reaction, a gel electrophoresis experiment was performed. The detail of the design and the confirmation of the cleavage are shown in Figure 2.13. In Figure 2.13B, Lane 1 is the free FAM-labeled extended substrate and lane 2 is the substrate hydrolyzed with NaOH. Lane 3 is the substrate hybridized with the quencher-labeled enzyme after reacting

with Ce^{3+}. The substrate was effectively cleaved, confirming the fluorescence enhancement was due to cleavage.

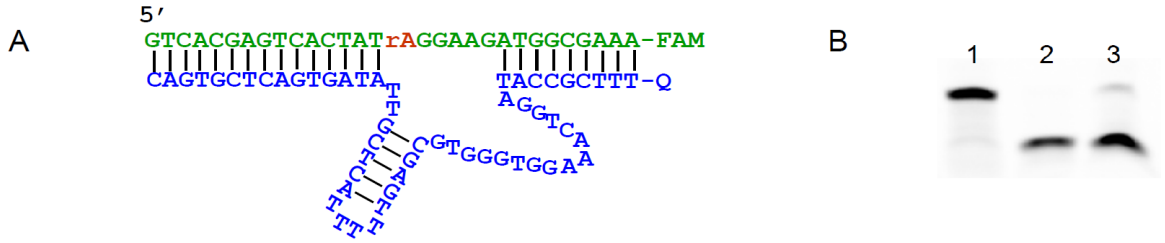

Figure 2.13 Design of the fluorescent Ce13d DNAzyme beacon. A) The sequence of the DNAzyme beacon. B) Confirmation of cleavage in the catalytic DNA beacon based sensor.

With 50 nM of the sensor complex, a steady fluorescence in the absence of Ce^{3+} was observed and the rate of fluorescence enhancement was progressively faster with increasing Ce^{3+} concentration (Figure 2.12B). The initial slopes of the fluorescence traces were plotted to quantify Ce^{3+} up to 500 nM (Figure 2.12C). A detection limit of 1.7 nM Ce^{3+} (240 parts-per-trillion) was obtained based on signal greater than 3 times of background variation (Figure 2.12C, inset). Just as in the case of the gel-based assays, the sensor showed similar sensitivity with all the lanthanides and Y^{3+} with slope difference smaller than 1-fold (Figure 2.12E). Therefore, the detection limits for all these elements are better than 4 nM. This represents the most sensitive biosensor for lanthanides. Note that this study does not include promethium (Pm^{3+}) since it is radioactive, but it is reasonable to believe that Pm^{3+} should also be active based on the chemical trend.

2.2.8 Masking Pb^{2+} interference

The previous gel-based assays indicated that Pb^{2+} might be the main interfering ion. Indeed, 10 μM Pb^{2+} produced a strong signal (Figure 2.12D, black trace). With 1 mM mercaptohexanol (MCH), the Pb^{2+} response was completely masked, while 1 μM Ce^{3+} still

produced a strong fluorescence increase (red trace). In addition, the sensor showed no response to other trivalent metal ions (Figure 2.12F) which was consistent with previous gel-based assays.

2.2.9 Ce^{4+}/Ce^{3+} conversion

To have a complete analysis of metal ions in the environment, it is important to have information not only on the total metal concentration but also about the metal speciation.[194,195] However, most analytical instruments such as ICP-MS measure only the total metal concentration. The DNAzyme platform might offer a solution to this problem as shown in Figure 2.14A.

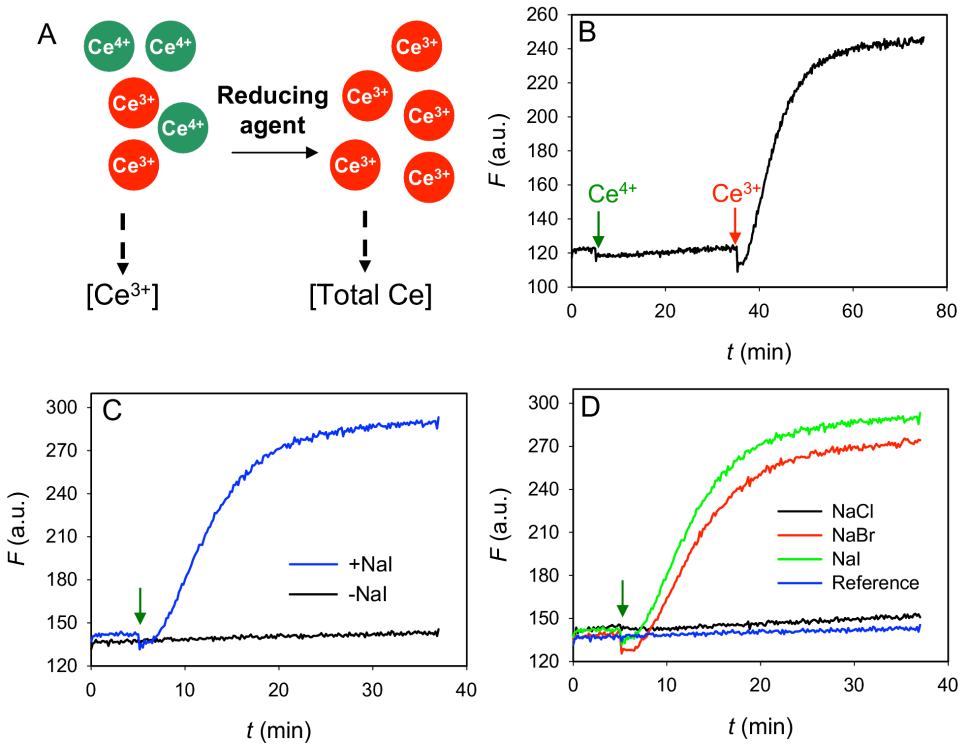

Figure 2.14 Cerium speciation analysis with the Ce13d DNAzyme beacon. A) A scheme illustrating the analysis of metal speciation using the DNAzyme sensor for different oxidation states. B) Sensor response to 1 μM Ce^{4+} and then 1 μM Ce^{3+}. C) Sensor response to Ce^{3+} generated by reacting Ce^{4+} with 50 mM NaI. D) Sensor response to Ce^{3+} generated by reacting Ce^{4+} with various halide salts, all at 50 mM concentration. The final Ce concentration in the sensor was 1 μM.

Although Ce^{4+} is insensitive to the sensor, its concentration can be indirectly obtained by measuring the Ce^{3+} concentration before and after a reducing reaction. To test this idea, the sensor was first exposed to 1 μM Ce^{4+} and the signal remained quite stable (Figure 2.14B). Addition of Ce^{3+} resulted in a quick fluorescence increase. This excellent selectivity between Ce^{3+} and Ce^{4+} makes it possible to monitor the conversion between these two species. Alkali halides are potential reducing agents. Thus, NaI can be used as the reducing agent to convert Ce^{4+}. The oxidized product can then be detected by DNAzyme sensor. Immediately, fluorescence enhancement was observed (Figure 2.14C), this suggested that Ce^{4+} was reduced to Ce^{3+}. Different halide anions with Ce^{4+} were further tested, where reaction with NaI was the fastest followed by NaBr, while NaCl had no reaction (Figure 4D). This is consistent with the redox trends of these anions, indicating that NaI is the most efficient reagent for the reduction. Aside from its environmental application, this work represents the first example of monitoring metal redox reaction using a DNAzyme. Previously, the conversion of protein enzyme catalyzed chemical transformation has been monitored using aptamers,[196,197] and this ability is useful for understanding reaction mechanisms and screening for reaction inhibitors.

2.3 Summary

In this chapter, *in vitro* selection of a general trivalent lanthanide-dependent DNAzyme is described. A number of important observations were made. First of all, a novel RNA-cleaving DNAzyme using a lanthanide ion as the sole metal cofactor was obtained. Secondly, the DNAzyme beacon has remarkable sensitivity and represents the first general probe for rare earth metals. This DNAzyme showed similar sensitive to all trivalent lanthanides plus Y^{3+} in the absence of any divalent metals. Last but not least, this is the first example of using DNAzymes to

distinguish the different oxidation states of the same metal ions and monitoring the conversion of oxidation states was further demonstrated. This work shows the possibility of using the DNAzyme technology to obtain metal speciation information, which is important for environmental and water quality monitoring.

2.4 Materials and Methods

2.4.1 Chemicals

The DNA library for *in vitro* selection, related primers, and fluorophore/quencher modified DNAs were purchased from Integrated DNA Technologies (IDT, Coralville, IA). The sequences of DNA used in this selection are listed in Table 2.4. The trans-cleaving enzyme strands and their mutants were from Eurofins (Huntsville, AL). The lanthanides that were used in the experiment include lanthanum nitrate hexahydrate, ammonium cerium nitrate, cerium chloride heptahydrate, praseodymium chloride hydrate, neodymium chloride hexahydrate, samarium chloride hexahydrate, europium chloride hexahydrate, gadolinium chloride hydrate, terbium chloride hexahydrate, dysprosium chloride hexahydrate, holmium chloride hexahydrate, erbium chloride hexahydrate, thulium chloride hexahydrate, ytterbium chloride hexahydrate, and lutetium chloride hexahydrate. Their solutions were made by directly dissolving their salts in water. Other metal ions that were used for analysis include magnesium sulfate, scandium chloride hydrate, manganese chloride tetrahydrate, iron chloride hexahydrate, iron chloride tetrahydrate, cobalt chloride hexahydrate, copper chloride dehydrate, zinc chloride, yttrium chloride hexahydrate, silver nitrate, indium chloride, mercury perchlorate, lead acetate. All these salts were purchased from Sigma-Aldrich except the iron and silver salts were purchased from Alfa Aesar. Tris(Hydroxymethyl)aminomethane (Tris), 2-(N-morpholino)ethanesulfonic acid

(MES) free acid monohydrate, 2-[4-(2-hydroxyethyl)piperazin-1-yl]ethanesulfonic acid (HEPES) sodium salt, HEPES free acid, EDTA disodium salt dehydrate, sodium chloride, sodium bromide, sodium iodide and ammonium acetate were purchased from Mandel Scientific Inc (Guelph, Ontario, Canada). Acrylamide/bisacrylamide 40% solution (29:1), urea, and 10x TBE solution were purchased from Bio Basic Inc. SsoFast EvaGreen supermix was purchased from Bio-Rad for real-time PCR analysis. T4-DNA ligase, deoxynucleotide (dNTP) solution mix, Taq DNA polymerase with ThermoPol buffer, and low molecular weight DNA ladder were purchased from New England Biolabs. All metal ions, buffer and gel stock solutions were prepared with Milli-Q water. The pH of the buffers was measured with Denver Instrument UltraBasic pH meter.

Table 2.4 DNA sequences design for *In vitro* selection.

DNA Name	Sequence and modifications
Lib-FAM	5′-GGCGAAACATCTT**N$_{50}$**TAGTGACGGTAAGCTTGGCAC-**FAM**
Lib-rA	5'-AATACGAGTCACTAT**rA**GGAAGAT
splint	5′-AAGATGTTTCGCCATCTTCCTATAGTCCACCACCA
P1 primer	5′-GTGCCAAGCTTACCG
P2 primer	5′-CTGCAGAATTCTAATACGAGTCACTATAGGAAGATGGCGAAACA
P3 primer	5′-**FAM**-AAATGATCCACTAATACGACTCACTAT**rA**GG
P4 primer	5′-AACAACAACAAC-**iSp18**-GTGCCAAGCTTACCG

2.4.2 *In vitro* selection

For this *in vitro* selection experiment, the initial DNA library was prepared by ligating two pieces of DNA (Lib-FAM and Lib-rA) with a splint DNA. Lib-FAM DNA (200 pmol) and Lib-rA DNA (300 pmol) were mixed with splint DNA (300 pmol) first in buffer A (50 mM pH 7.5 Tris-HCl, pH 7.5, 10 mM $MgCl_2$). The three strands of DNA were annealed at 95 °C for 1 min followed by slow cooling to room temperature. The T4 ligation protocol provided by New England Biolabs was followed for the ligation reaction. The ligated DNA product was purified with 10% denaturing polyacrylamide gel (dPAGE) at 650 V for 1 h and the DNA was extracted

from the gel with buffer B (1 mM EDTA, 10 mM Tris-HCl, pH 7.0). The extracted DNA library was further concentrated via ethanol precipitation and re-suspended in 60 μL of buffer C (50 mM MES, pH 6.0, 25 mM NaCl), which was the selection buffer. This DNA was used directly as the DNA library for the first round of selection. For each of the subsequent round, the library was generated from PCR. For the *In vitro* selection experiment, the random DNA pool was incubated with freshly prepared Ce^{4+} metal ion. After incubation, the reaction was quenched with 8 M urea and was purified in 10% dPAGE. A fraction of the selected DNA was extracted from the gel and further purified with a Sep-Pak C18 column (Waters). The purified selected DNA was then dried in an Eppendorf Vacufuge at 30 °C overnight. The dried DNA was re-suspended in 70 μL of 5 mM HEPES buffer (pH 7.5).

2.4.3 PCR

During the *In vitro* selection experiment, three PCR reactions were carried out for each round. After the cleavage reaction, a real-time PCR (rt-PCR) was carried out to quantify the amount of cleaved DNA that was extracted from the gel. The 20 μL reaction mixture contains 1 μL of purified DNA template, 400 nM primer (P1 and P2), and 10 μL of SsoFast EvaGreen Supermix (Bio-Rad). The thermocycling steps provided by vendor were followed (95 °C for 30s, 95 °C for 5s, and 55 °C for 5s). PCR1. A 50 μL PCR reaction mixture contained the following: 1 μL DNA template, 200 nM of each of P1 and P2, 200 μM dNTP mixture, 1× Taq buffer, and 1.25 units of Taq DNA polymerase. The reaction was carried out for 15-20 cycles. The DNA was amplified using the following cycling steps: 94 °C for 5 min; 94°C for 30 s, 55 °C for 30 s, and 72 °C 30 s. A gel/PCR DNA fragment extraction kit (IBI Scientific) was used to purify the PCR1 product. The purified product was used as template for PCR2. One-tenth of the purified

product was further amplified for 12 cycles using P3 and P4 as the primers. A 200 μL PCR reaction mixture contains 4 μL diluted template from PCR1, 250 nM each of P3 and P4, 200 μM dNTP mixture, 1× Taq buffer, and 5 units of Taq DNA polymerase. The thermocycling steps mentioned above were also used here. The final PCR2 product was again purified in 10% dPAGE. The single-stranded FAM-labeled DNA was excised from the gel, ethanol precipitated and used as the library pool for the subsequent round of selection.

2.4.4 Cloning and sequencing

The selection was stopped at round 6, where the PCR1 product was cloned using the TA-TOPO Cloning Kit (Invitrogen) and Subcloning Efficiency DH5α competent cells (Invitrogen). The protocol provided by vendor was followed. The plasmid DNA was extracted and purified by using DirectPrep 96 MiniPrep Kit (QIAGEN). The sample was then submitted to TCAG DNA Sequencing Facility (Toronto, ON) for analysis. The alignment was performed using ClustalW2.

2.4.5 Activity assays

For a typical gel-based activity assay, metal ions at a final concentration of 10 μM were incubated with 5 μL of 1 μM DNAzyme complex in buffer C for 1 h. The complex was formed by annealing the FAM-labeled substrate and the enzyme in buffer C. The samples were quenched with 8 M urea and run in 15% dPAGE at 120V for 80 min. The gel images were taken with Bio-Rad ChemiDoc MP imaging system.

2.4.6 Fluorophore/quencher-based assay

The kinetic studies were carried out in a 96 well plates using a Molecular Device SpectraMax M3 microplate reader. The complex was formed by annealing the FAM-labeled

substrate and the quencher-labeled enzyme in buffer C. 100 μL of 50 nM FAM-Q DNAzyme in 50 mM pH 7.5 HEPES (pH 7.5) was used for each well. 1 μL of target ions was added after 5 min of background reading. The samples were monitored continuously after addition for at least 30 min with a 10 s interval between measurements. For reactions between Ce^{4+} and NaI, the initial Ce^{4+} concentration was 10 mM and then diluted to 1 μM for detection and the NaI concentration was 50 mM.

Chapter 3. *In Vitro* Selection of a New Lanthanide-Dependent DNAzyme and Its Application for Ratiometric Sensing Lanthanides[b]

3.1 Introduction

DNAzymes are DNA-based catalysts, where metal ion cofactors are required for activity.[79,162-164,198,199] In the previous chapter, a DNAzyme named Ce13d was selected and its application as a biosensor for lanthanide detection was demonstrated.[87] Although the selection was initially performed with cerium (Ce^{4+}) as an intended target, this enzyme showed similarly active with all the trivalent lanthanides but had almost no activity with Ce^{4+}. Not only Ce^{4+} is a poor metal cofactor for cleaving RNA,[160] but also Ce^{4+} is a strong oxidant. Together, we reason that a small fraction (~1% by our estimation) of Ce^{4+} was reduced, which gradually guide the selection process toward the more active Ce^{3+}.

Ce13d provides a starting point for solving the lanthanide detection problem since it demonstrates excellent selectivity for lanthanides as a group. However, it cannot discriminate each lanthanide within the group based on the reaction rate. To achieve this, more selective lanthanide-dependent DNAzymes are needed. Towards this goal, I describe my effort using praseodymium (Pr^{3+}) as the intended target for new DNAzyme selection using the N50 library. At the same time, a colleague used the N35 library to select lutetium (Lu^{3+})-dependent DNAzymes. Interestingly, several Pr^{3+} sequences were also found to be present in the Lu sequences. To simplify the analysis, a Lu sequence was used for subsequent detail studies. In this chapter, a new DNAzyme named Lu12 that displays better lanthanide discrimination is studied.

[b] This chapter is the basis for a published manuscript: Huang, P. J.; Vazin, M.; Liu, J. *In Vitro* Selection of a New Lanthanide-Dependent DNAzyme for Ratiometric Sensing Lanthanides. *Anal. Chem.* **2014**, *86*, 9993-9999.

By combining Ce13d and Lu12 lanthanide-dependent DNAzymes, a ratiometric sensor was developed. Although the information provided by the two sensors is able to discriminate only a few large lanthanides, it presents the possibility of identify each individual lanthanide within the series when more DNAzymes become available.

3.2 Results and discussion

3.2.1 *In vitro* selection

The previous report demonstrated that high concentration (> 5 mM) of free lanthanide ions can cleave RNA efficiently, and the cleavage activity is directly proportional to the size of the lanthanides.[160] To obtain a lanthanide-dependent DNAzyme, a selection was carried out with an N50 library (e.g. 50 random nucleotides).[87] In that selection, a large fraction of the obtained sequences belong to the Ce13d (Figure 3.1E) family, which had similarly activity with all trivalent lanthanide, including Lu^{3+}. To discriminate different lanthanides, it is necessary to select a new DNAzyme with a different lanthanide. Since previous selection was using tetravalent lanthanide as a target, a trivalent lanthanide Pr^{3+} was chosen for this study.

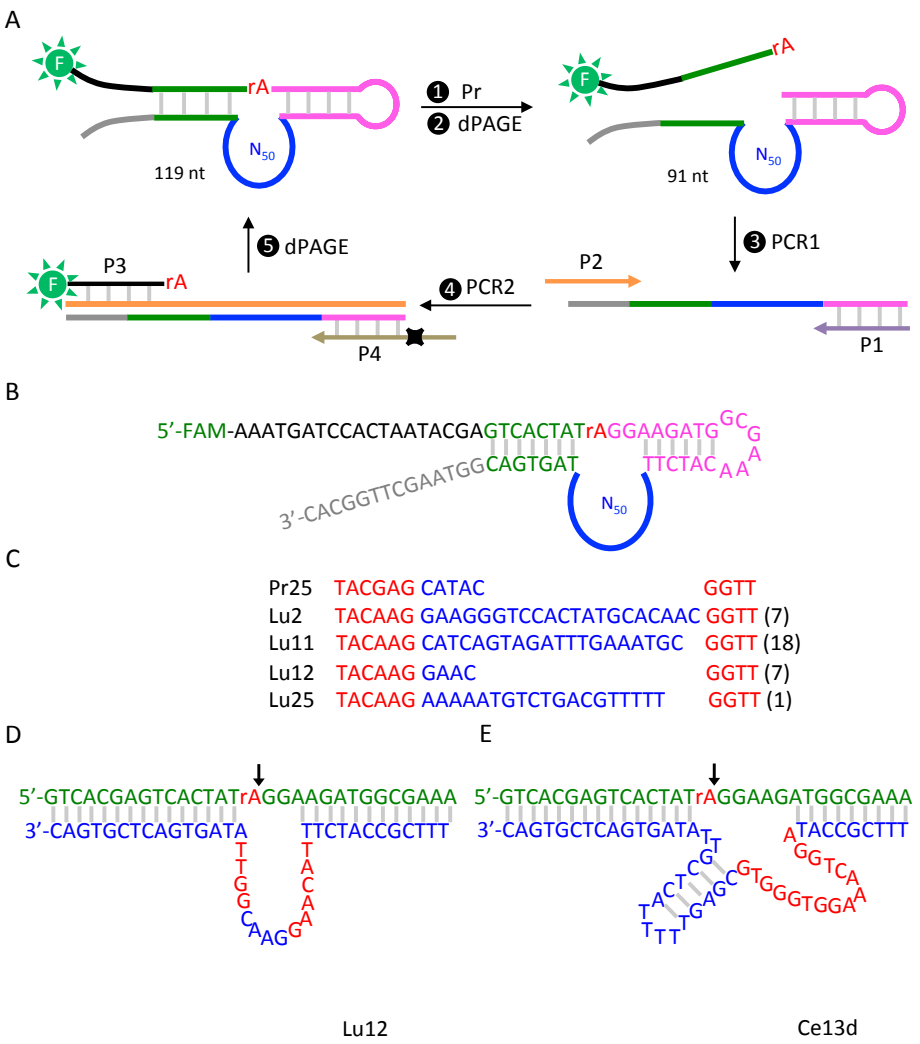

Figure 3.1 A design scheme for the Pr^{3+} DNAzyme selection. A) Scheme of *in vitro* DNAzyme selection in the presence of Pr^{3+}. The initial library contains an N50 randomized region and a single RNA linkage (rA) as the cleavage site. Cleaved sequences in the presence of Lu^{3+} (step 1) are harvested after gel electrophoresis (PAGE, step 2). After two rounds of PCR the full-length single-stranded library is re-generated and the positive strand is isolated after another PAGE step. B) The library sequence before the cleavage step. C) Sequence alignment from the start of the N50 region. The nucleotides in red are highly conserved. The numbers in the parenthesis are the number of identical or very similar sequences (differ by less than 2 nucleotides) as the listed. The secondary structure of the trans-cleaving Lu12 D) and Ce13d E) DNAzymes. Important nucleotides for catalysis are marked in red.

Just as in the previous selection, the initial library contained a sequence population of ~10^{14}. The randomized region (the blue loop in Figure 3.1A) joined the two short base-paired duplexes and held the single ribo-adenosine (rA) in its proximity. Since RNA is more susceptible to cleavage than DNA, the rA linkage served as the designated cleavage site.[52] The exact sequence of the library design is shown in Figure 3.1B. During the selection process, the library

was first incubated with Pr^{3+} for a period of time to induce cleavage (Figure 3.1A, step 1). After that, the shorter cleaved DNA strands were harvested using gel electrophoresis (step 2). Two rounds of polymerase chain reactions (PCR) were performed to bring the library back to the original length and amplify the cleaved DNA to seed the next round of selection. After five rounds of selection, cleavage reached 43%. At that point, the library was cloned and sequenced. The details of the selection conditions and progress are summarized in Table 3.1.

Table 3.1 *In vitro* selection conditions and progress for Pr^{3+}.

Round #	[Pr^{3+}] (μM)	Incubation time (min)	Cleavage (%)
1	50	60	0.2
2	50	60	0.8
3	50	80	6.5
4	20	120	46.9
5	20	120	42.8

While aligning the Pr sequences, it was found that about half of the clone sequences belong to one family. In addition, these sequences are also present in the Lu^{3+} selection that was conducted by a colleague. Since Ce13d structure is quite large, shorter N35 library was used to prevent re-selecting Ce13d sequence.

3.2.2 DNAzyme secondary structure analysis

Thirty-eight out of 40 clones were valid sequences and their full sequences are listed in Table 3.2. One of the representatives Pr sequence named Pr25 was also included in the alignment for comparison. Remarkably, none of the sequences were Ce13d related. In addition, all of the selected DNA can be aligned into a single sequence family. Some of the representative ones with sequences starting from the 5′-end of the random region were listed in Figure 3.1C. The first six nucleotides are highly conserved (TACAAAG, in red), followed by a highly variable region both in terms of sequence and length, and ended with another highly conserved tetra-nucleotide, GGTT.

Table 3.2 Alignment of Pr25 sequence with Lu^{3+} selection sequences.

Clone #	Sequence (from 5′-end)	
11	CTGCAGAATTCTAATACGAGTCACTATAGGAAGATGGCGAAACA----TCTTTACAAGCA	56
32	CTGTAGAATTCTAATACGAGTCACTATAGGAAGATGGCGAAACA----TCTTTACAAGCA	56
40	CTGCAGAATTCTAATACGAGTCACTATAGGAAGATGGCGAAACA----TCTTTACAAGCA	56
39	CTGCAGAATTCTAATACGAGTCACTATAGGAAGATGGCGAAACA----TCTTTACAAGCA	56
3	CTGCAGAATTCTAATACGAGTCACTATAGGAAGATGGCGAAACA----TCTTTACAAGCA	56
28	CTGCAGAATTCTAATACGAGTCACTATAGGAAGATGGCGAAACA----TCTTTACAAGCA	56
21	CTGCAGAATTCTAATACGAGTCACTATAGGAAGATGGCGAAACA----TCTTTACAAGCA	56
20	CTGCAGAATTCTAATACGAGTCACTATAGGAAGATGGCGAAACA----TCTTTACAAGCA	56
13	CTGCAGAATTCTAATACGAGTCACTATAGGAAGATGGCGAAACA----TCTTTACAAGCA	56
8	CTGCAGAATTCTAATACGAGTCACTATAGGAAGATGGCGAAACA----TCTTTACAAGCA	56
14	CTGCAGAATTCTAATACGAGTCACTATAGGAAGATGGCGAAACA----TCTTTACAAGCA	56
9	CTGCAGAATTCTAATACGAGTCACTATAGGAAGATGGCGAAACA----TCTTTACAAGCA	56
37	CTGCAGAATTCTAATACGAGTCACTATAGGAAGATGGCGAAACA----TCTTTACAAGCA	56
18	CTGCAGAATTCTAATACGAGTCACTATAGGAAGATGGCGAAACA----TCTCTACAAGCA	56
22	CTGCAGAATTCTAATACGAGTCACTATAGGAAGATGGCGAAACA----TCTTTACAAGCA	56
34	CTGCAGAATTCTAATACGAGTCACTATAGGAAGATGGCGAAACA----TCTTTACAAGCA	56
24	CTGCAGAATTCTAATACGAGTCACTATAGGAAGATGGCGAAACA----TCTTTACAAGCA	56
4	CTGCAGAATTCTAATACGAGTCACTATAGGAAGATGGCGAAACA----TCTTTACAAGCA	56
5	CTGCAGAATTCTAATACGAGTCACTATAGGAAGATGGCGAAACA----TCTTTACAAG--	54
36	CTGCAGAATTCTAATACGAGTCACTATAGGAAGATGGCGAAACA----TCTTTACAAGAA	56
2	CTGCAGAATTCTAATACGAGTCACTATAGGAAGATGGCGAAACA----TCTTTACAAGGA	56
7	CTGCAGAATTCTAATACGAGTCACTATAGGAAGATGGCGAAACA----TCTTCRCAAGGA	56
29	CTGCAGAATTCTAATACGAGTCACTATAGGAAGATGGCGAAACA----TCTTTACAAGGA	56
17	CTGCAGAATTCTAATACGAGTCACTATAGGAAGATGGCGAAACA----TCTTTACAAGGA	56
1	CTGCAGAATTCTAATACGAGTCACTATAGGAAGATGGCGAAACA----TCTTTACAAGGA	56
27	CTGCAGAATTCTAATACGAGTCACTATAGGAAGATGGCGAAACA----TCTTTACAAGGA	56
30	CTGCAGAATTCTAATACGAGTCACTATAGGAAGATGGCGAAACA----TCTTTACAAGGA	56
31	CTGCAGAATTCTAATACGAGTCACTATAGGAAGATGGCGAAACA----TCTTTACGAG-A	55
16	CTGCAGAATTCTAATACGAGTCACTATAGGAAGATGGCGAAACAAAAAATGTAGACAGCGA	60
23	CTGCAGAATTCTAATACGAGTCACTATAGGAAGATGGCGAAACAAAAAATGTAGACAGCGA	60
25	CTGCAGAATTCTAATACGAGTCACTATAGGAAGATGGCGAAACA----TCTTTACAAGAA	56
Pr25	CTGCAGAATTCTAATACGAGTCACTATAGGAAGATGGCGAAACA----TCTTTACGAGCA	56
33	CTGCAGAATTCTAATACGAGTCACTATAGGAAGATGGCGAAACA----TCTTTACAAGGA	56
12	CTGCAGAATTCTAATACGAGTCACTATAGGAAGATGGCGAAACA----TCTTTACAAGGA	56
38	CTGCAGAATTCTAATACGAGTCACTATAGGAAGATGGCGAAACA----TCTTTACAAGGA	56
15	CTGCAGAATTCTAATACGAGTCACTATAGGAAGATGGCGAAACA----TCTTTACAAGGA	56
6	CTGCAGAATTCTAATACGAGTCACTATAGGAAGATGGCGAAACA----TCTTTACAAGGA	56
26	CTGCAGAATTCTAATACGAGTCACTATAGGAAGATGGCGAAACA----TCTTTACAAGCG	56
10	CTGCAGAATTCTAATACGAGTCACTATAGGAAGATGGCGAAACA----TCTTTACAAGCG	56

Table 3.2 Alignment of Pr25 sequence Lu^{3+} selection sequences. (Continued)

Clone #	Sequence (from 5′-end)	
11	TCAGTAGATTTGAA----------AT-GCGGTTA-----TAGTGACGGTAAGCTT	95
32	TCAGTAGATTGGAA----------AT-GCGGTTA-----TAGTGACGGTAAGCTT	95
40	TCAGTAGATTGGAA----------AT-GCGGTTA-----TAGTGACGGTAAGCTT	95
39	TCAGTAGATTGGAA----------AT-GCGGTTA-----TAGTGACGGTAAGCTT	95
35	TCAGTAGATTGGAA----------AT-GCGGTTA-----TAGTGACGGTAAGCTT	95
28	TCAGTAGATTGGAA----------AT-GCGGTTA-----TAGTGACGGTAAGCTT	95
21	TCAGTAGATTGGAA----------AT-GCGGTTA-----TAGTGACGGTAAGCTT	95
20	TCAGTAGATTGGAA----------AT-GCGGTTA-----TAGTGACGGTAAGCTT	95
13	TCAGTAGATTGGAA----------AT-GCGGTTA-----TAGTGACGGTAAGCTT	95
8	TCAGTAGATTGGAA----------AT-GCGGTTA-----TAGTGACGGTAAGCTT	95
14	TCAGTAGATTGGAA----------T-GCGGTTA-----TAGTGACGGTAAGCTT	94
9	TCAGTGGATTGGAA----------AT-GCGGTTA-----TAGTGACGGTAAGCTT	95
37	TCGGTGGATTGGAA----------AT-GCGGTTA-----TAGTGACGGTAAGCTT	95
18	TCAGTTGATTGGAA----------AT-GCGGTTA-----TAGTGACGGTAAGCTT	95
22	TCAGTAGACTGGAA----------AT-GCGGTTA-----TAGTGACGGTAAGCTT	95
34	TCAGTAGACTGGAA----------AT-GCGGTTA-----TAGTGACGGTAAGCTT	95
24	TCAGTAGATCGGAA----------AT-GCGGTTA-----TAGTGACGGTAAGCTT	95
4	TCAGTAGGTTGCAA----------AT-GCGGTTA-----TAGTGACGGTAAGCTT	95
5	TTATATGGTAAGAAT----------ATAGCGGTTA-----TAGTGACGGTAAGCTT	95
36	TCCGACATTCAGGA----------T-TCGGTTA-----TAGTGACGGTAAGCTT	94
2	AGGGTCCACTATGC----------ACAACGGTTA-----TAGTGACGGTAAGCTT	96
7	AGGG-CCACTATGC----------ACAACGGTTA-----TAGTGACGGTAAGCTT	95
29	AGGGTCCACTATGC----------ACAACGGTTA-----TAGTGACGGTAAGCTT	96
17	AGGGTCCACTATGC----------ACAACGGTTA-----TAGTGACGGTAAGCTT	96
1	AGGG--TACTATGC----------ACAACGGTTA-----TAGTGACGGTAAGCTT	94
27	AGGGTCCACTATAC----------ACAACGGTTA-----TAGTGACGGTAAGCTT	96
30	AGGGTCCACTACAC----------ACAACGGTTA-----TAGTGACGGTAAGCTT	96
31	GGGAAATACAATGC----------CCTCGGTTA-----TAGTGACGGTAAGCTT	94
16	GCAT----TCCGAA----------TTAGGTTAA----TAGTGACGGTAAGCTT	95
23	GCAT----TCCGAA----------TTAGGTTAA----TAGTGACGGTAAGCTT	95
25	AAATG---TCTGACG----------TTTTTGGTTA-----TAGTGACGGTAAGCTT	94
Pr25	TA---CGGTTATAGGAGTCGGACTTACAGATTTAAGATACAGAGCTATGACGGTAAGCTT	113
33	-A---CGGTTATA---------CTGACGAG----GGATACTA----GTGACGGTAAGCTT	95
12	-A---CGGTTATAG---------TGAAAGG----AAACTCGTAGT-----CGGTAAGCTT	94
38	-A---CGGTTATAG---------TGAAAGG----AAACTCGTAGT-----CGGTAAGCTT	94
15	-A---CGGTTATAG---------TGAAAGG----AAACTCGTAGT-----CGGTAAGCTT	94
6	-A---CGGTTATAG---------TGAAAGG----AAACTRGTAGT-----CGGTAAGCTT	94
26	GAG--CGGTTATAGG---------AACGAGC----GATATAGT-------CGGTAAGCTT	94
10	AAG--CGGTTATGG----------GGACACGCACTGGTGACGGTAAGCTT	94

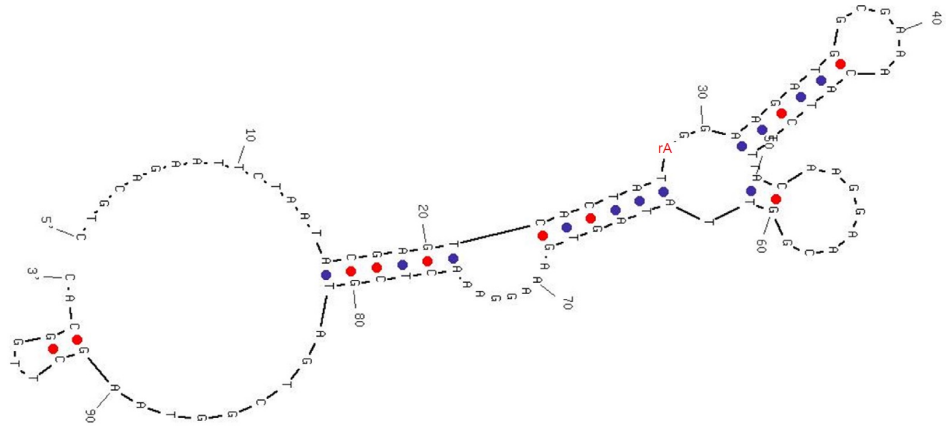

Figure 3.2 Secondary structure prediction of Lu12.

Since Lu12 has the shortest insertion between the two fixed regions, mfold was used for secondary structure predicaments (Figure 3.2).[190] The cleavage site is shown in the red rA. The thymine at position 48 is the starting of the N35 region. This is the cis-cleaving version of the DNAzyme since the system is self-cleaving. Aside from the 14 nucleotides in the small loop for catalysis, the other 21 nucleotides from the randomized regions formed base pairs or bulges. The secondary structure of the active region is quite straightforward to rationalize. Figure 3.1D showed the trans-cleaving version of the DNAzyme that was redesigned by cutting the loop nearby nucleotide number 40 and extending the two binding arms. The two conserved regions are located at the two sides of this enzyme (in red). For those DNAzymes with longer insertions, the inserted sequences either form a hairpin or a structureless loop, suggesting that they were less likely to participate in the catalytic reaction.

3.2.2 Metal specificity

When compared with Ce13d (Figure 3.1E), the structure of Lu12 looked very different and it could possibly pose a different activity trend cross the lanthanide series. For sensing applications, metal specificity is very important. Therefore, its activity against other divalent and

trivalent cations was first tested. In the presence of 10 μM metal ions (Figure 3.3A), only Y^{3+} showed substantial cleavage and Pb^{2+} displayed little cleavage. When the concentration was increased to 100 μM (Figure 2B), both Pb^{2+} and Y^{3+} showed a large fraction of cleavage. It should be noted that a smeared band was observed in the presence of Au^{3+}. This was likely due to DNA base binding but no cleavage was observed. It is commonly known that DNAzyme-based sensors suffer from Pb^{2+} interference. Fortunately, for lanthanide detection, the Pb^{2+} activity can be masked with the addition of thiol compounds such as mercaptohexanol (MCH). [87] However, Y^{3+} interfereence is more difficult to mask because of its similar size and charge to those of the lanthanides. Other divalent or trivalent metal ions did not produce significant cleavage at both concentrations, suggesting this DNAzyme is highly selective for lanthanides.

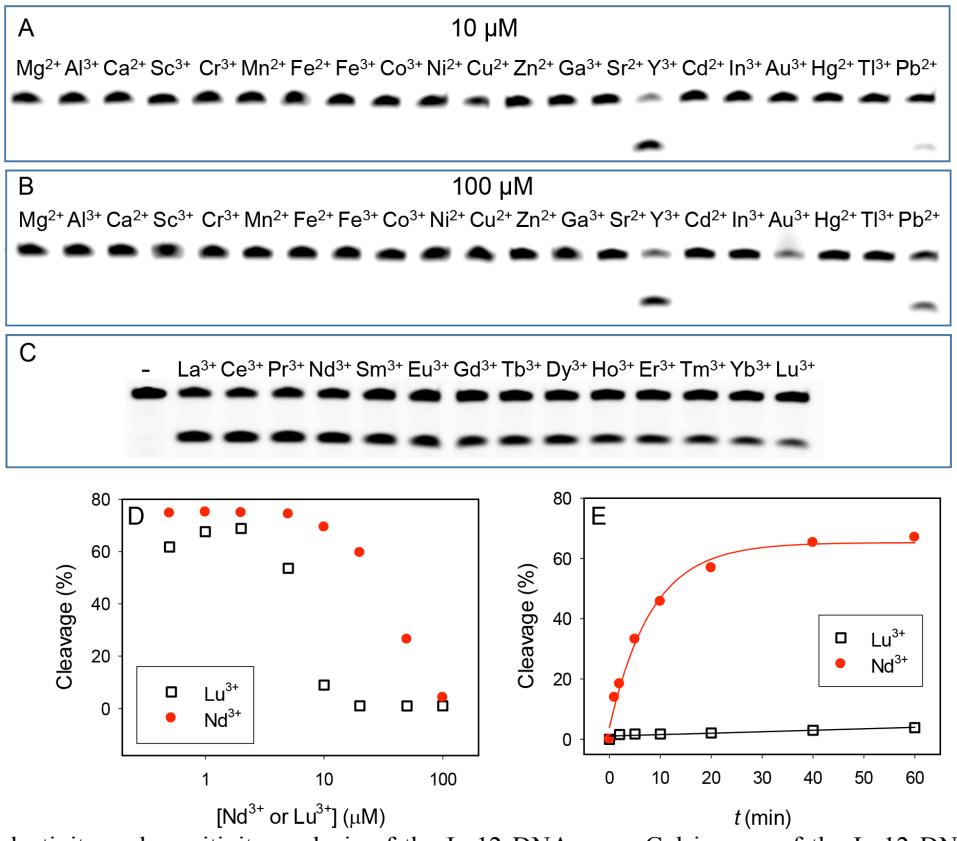

Figure 3.3 Selectivity and sensitivity analysis of the Lu12 DNAzyme. Gel images of the Lu12 DNAzyme assay with A) 10 μM and B) 100 μM metal ion for 1 h. C) Lu12 reacting with 1 μM lanthanides for 5 min. All assays are performed in 50 mM MES buffer (pH 6.0) with 25 mM NaCl. D) Fraction of cleavage as a function of Nd^{3+} or Lu^{3+} concentration after 1 h reaction time. E) Kinetics of Lu12 in the presence of 10 μM Nd^{3+} or Lu^{3+}.

For the lanthanide activity test, Lu12 was incubated with 1 μM of each individual lanthanide for 5 min. Just as in the case of Ce13d, cleavage was observed for all the lanthanides (Figure 3.3C). It fact, the lighter lanthanides from La^{3+} to Tb^{3+} showed a similarly high efficiency of cleavage. However, the efficiency gradually decayed for the last few heavier ones (Figure 3.3C). Next, the effect of the lanthanide concentration on enzyme activity was investigated (Figure 3.3D). Neodymium (Nd^{3+}) and Lu^{3+} were chosen to represent light and heavy lanthanides, respectively. In both cases, efficient cleavage was observed when the metal ion concentration was from 0.5 μM to a few μM and inhibition occurred at higher metal ion concentrations. Even though Nd^{3+} did not start to inhibit the activity until 10 μM, Lu^{3+} started to show inhibition around 2 μM. The inhibition was largely due to non-specifically interacting between lanthanides and the DNAzyme.

Once the condition was optimized, the cleavage rate of Lu12 was measured (Figure 3.3E). With 10 μM Nd^{3+}, a steady increase of the cleaved fraction was observed over time and the rate was estimated to be 0.12 min^{-1}. Within 1 hour, ~70% of the substrate was cleaved in the presence of Nd^{3+}. As a result of the inhibition effect at this concentration, Lu^{3+} barely induced any cleavage. To avoid artifacts associated with DNAzyme activity inhibition, low lanthanide concentrations should be used for sensing applications.

What made Lu12 interesting is that among all the tested lanthanides, Lu^{3+} gives the slowest activity. Matsumura and Komiyama reported that Lu^{3+} was among the most efficient lanthanides for cleaving a dinucleotide RNA while lighter lanthanides such as Nd^{3+} are almost inactive when 5 mM of lanthanides were used.[200] On the other hand, when Geyer and Sen tried to cleave a chimeric substrate alone with 60 μM lanthanides, they reported that Lu^{3+} displayed lowest activity (< 0.0012 h^{-1}). However, when the substrate was hybridized to the GR5

DNAzyme, Lu^{3+} induced the fastest cleavage.[167] Based on the previous studies, the assays conducted in this chapter were done at lower lanthanide concentrations (< 10 μM in most cases) and the results showed that Lu^{3+} was the least active.

It seems that lanthanide concentration, substrate length, and the presence of DNAzyme are all key factors to determine the activity trend. To further understand the effects of lanthanides on cleaving a chimeric substrate, a 30mer substrate strand alone was incubated with 2 mM of each lanthanide for 2.5 h (Figure 3.4A). Even with such high concentration of lanthanides, only ~4% cleavage was observed for all the samples and the difference across the series wass very small (Figure 3.4B). This lack of significant cleavage was probably due to the condensation of the substrate in the presence of high trivalent lanthanides concentration. Under such condition, RNA linkage was shielded from further attacks. As a result, assays had to be done at low lanthanide concentrations to avoid denaturation. The data also indicated that the intrinsic RNA-cleaving ability of lanthanides is very weak and the efficiency can be significantly enhanced in the presence of DNAzyme.

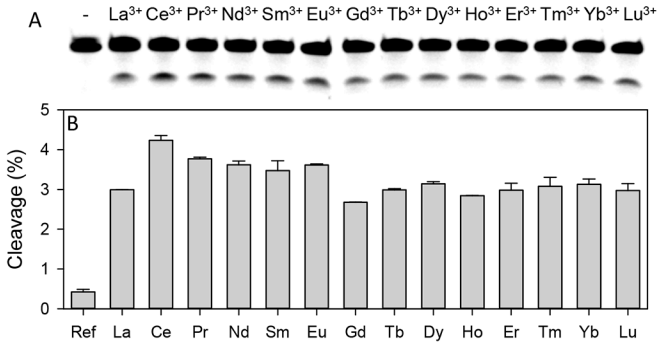

Figure 3.4 Lanthanides specificity of Lu12. Gel image A) and its quantification B) of the FAM-labeled substrate strand (no enzyme strand) cleavage by 2 mM lanthanides in MOPS buffer (pH 7.0, 50 mM), 25 mM NaCl for 2.5 h. The first lane of the gel is a reference without lanthanide.

RNA cleavage has been extensively studied and both nucleobases and metal ions can participate the critical catalytic step.[77] A generally proposed mechanism for catalysis involves

the metal ion acting as a general base to assist deprotonation of the 2′-OH on the ribose. The pK_a value of lanthanides bound water range from 8.2 to 9.4 and these values are inversely proportional to the size of lanthanide. Thus, the bound water on Lu^{3+} should be the best general base catalyst. Since this single mechanism does not explain our observation, lanthanides must play additional roles in this catalysis. For instance, lanthanides are known to neutralize the phosphate negative charges in the transition state, where the smaller lanthanides might be more effective. Detailed mechanistic studies will be a topic of follow-up research. Overall, Lu12 is a DNAzyme that is highly specific for lanthanides. Unlike previously selected Ce13d DNAzyme, Lu12 actually showed some lanthanide size-dependent activity that might be useful analytically.

3.2.3 Additional characterization of the DNAzyme catalytic core

Based on the mfold[190] prediction, one of the sequences named Lu1 has a very similar structure as that of Lu12. The main difference is that the loop size is much larger (Figure 3.5). In addition, it also displayed a similar active trend with various lanthanides (Figure 3.6). Since Lu1 has a very large loop and Lu12 has a much smaller loop, it was logical to systematically vary the loop size and tested their activity. Two new DNAzymes named Lu1a and Lu1b were introduced and their sequences are listed in Table 3.3 below. Even though all the DNAzymes were active, Lu12 seemed to be the most active one (Figure 3.7).

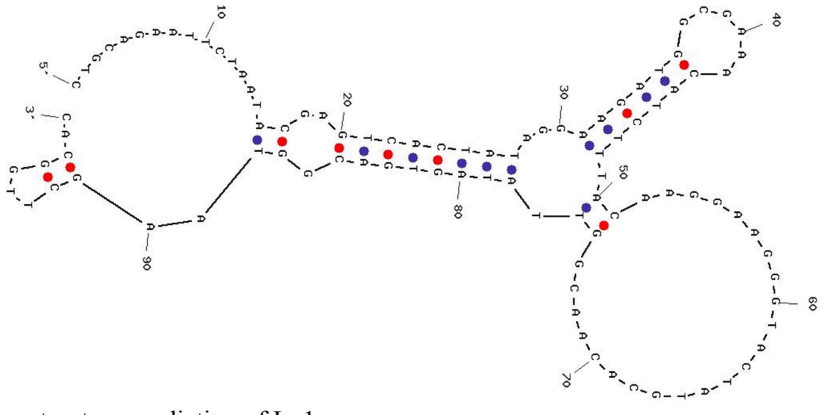

Figure 3.5 Secondary structure prediction of Lu1.

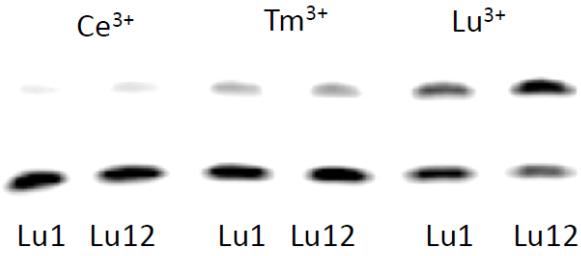

Figure 3.6. Cleavage activity of Lu1 and Lu12 (trans-cleaving) in the presence of various lanthanides (10 μM).

Table 3.3 Sequences comparison of the DNAzymes with various size loops.

DNAzyme	Sequence (from 5'-end)				
Lu1	TTTCGCCATCTT	TACAAG	GAAGGGTACTATGCACAAC	GGTT	ATAGTGACTCGTGAC
Lu1a	TTTCGCCATCTT	TACAAG	GAAGGATGCACAAC	GGTT	ATAGTGACTCGTGAC
Lu1b	TTTCGCCATCTT	TACAAG	GAACACAAC	GGTT	ATAGTGACTCGTGAC
Lu1c	TTTCGCCATCTT	TACAAG	AAAAAAAAAAAAA	CGGTT	ATAGTGACTCGTGAC
Lu1d	TTTCGCCATCTT	TACAAG	TTTTTTTTTTTTT	CGGTT	ATAGTGACTCGTGAC
Lu1e	TTTCGCCATCTT	TACAAG	CCCCCCCCCCCCC	CGGTT	ATAGTGACTCGTGAC
Lu12	TTTCGCCATCTT	TACAAG	GAAC	GGTT	ATAGTGACTCGTGAC

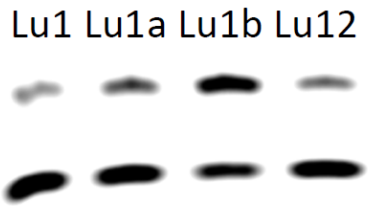

Figure 3.7 Cleavage activity of the trans-cleaving Lu1 mutants and Lu12 in the presence of various Ce^{3+} (10 μM).

To understand the effects of loop size further, a stretch of poly-A, poly-T or poly-C (Table 3.3) were inserted in the loop region of Lu12 and only the poly-C insertion inactivated the DNAzyme (Figure 3.8). These studies confirmed that as long as the conserved nucleotides are maintained, the DNAzyme is likely to remain active. The reason for Lu1e being inactive might be due to misfolding of the DNAzyme.

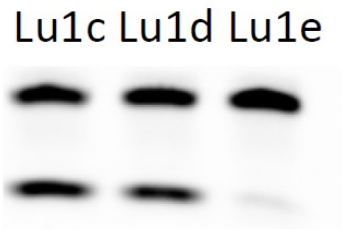

Figure 3.8 Cleavage activity of the Lu1 mutants that containing homopolymer insertions in the presence of various Ce^{3+} (10 µM).

3.2.4 Lanthanide sensing

The studies demonstrated that Lu12 DNAzyme has excellent lanthanide sensitivity. It would be interesting to see its performance as a biosensor. Just like Ce13d beacon design, the 3′-end of the substrate strand was labeled with a FAM and the 5′-end of the enzyme was labeled with a quencher (Figure 3.9).

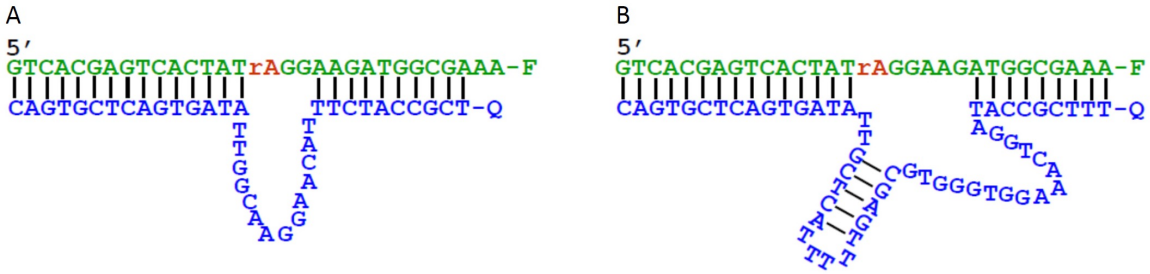

Figure 3.9 Design of the fluorescent Lu12 and Ce13d DNAzyme beacon. Catalytic beacon design of A) Lu12 and B) Ce13d. F = FAM. Q = Iowa Black® FQ dark quencher.

This complex was very stable in the absence of lanthanides and showed low background fluorescence due to the close proximity of the two dyes (Figure 3.10A). With increasing concentration of Nd^{3+}, the rate of fluorescence enhancement increased proportionately. When

Nd^{3+} concentration finally reached 1 μM, ~ 10-fold of fluorescence enhancement was observed. From these kinetic traces, the initial slope was plotted (Figure 3.10B). The Lu12 response can be fitted to binding to one Nd^{3+} ion with an apparent dissociation constant (K_d) of 38 nM. From the initial linear response (inset) data, the limit of detection was determined to be 0.4 nM Nd^{3+} (or 72 parts-per-trillion) based on signal greater than three times of background variation. The common metal ion-selectivity test was consistent with the results from gel analysis. The data showed that only Y^{3+} and Pb^{2+} produced responses besides Nd^{3+} (Figure 3.10C). Most importantly, Lu12 was able to display different responses toward each lanthanide more clearly than the gel analysis. In fact, the kinetic traces showed the catalytic rate is proportional to the size of lanthanides (Figure 3.10D).

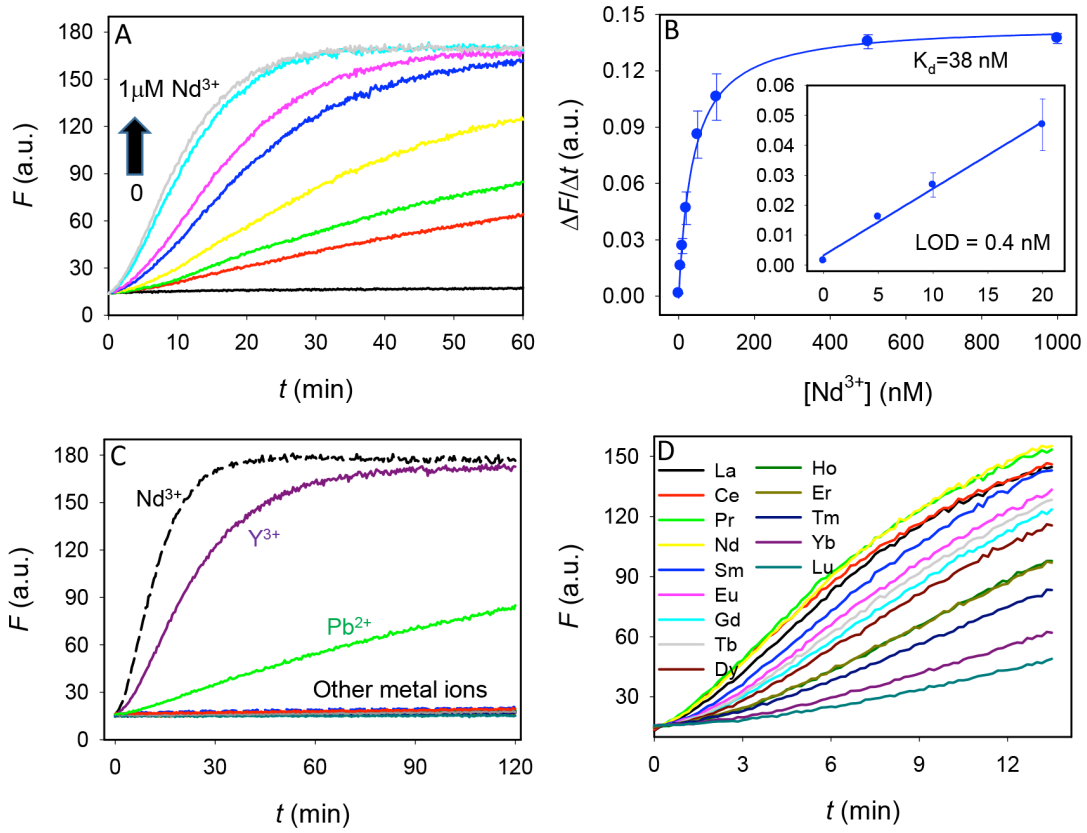

Figure 3.10 Kinetic study of the Lu12 DNAzyme beacon. A) Sensor signaling kinetics in the presence of various concentrations of Nd^{3+}. DNAzyme sensor concentration = 50 nM. B) Quantification of Nd^{3+} based on the initial rate of sensor fluorescence enhancement. Inset: the initial linear response at low Nd^{3+} concentrations. C) Sensor response to 0.5 μM of divalent and trivalent metal ions. The list of the other metal ions tested can be found in Figure 2B. D) Sensor response to 0.5 μM of various lanthanides.

3.2.5 Ratiometric sensing

So far, two lanthanide-dependent DNAzymes have been selected successfully (Figure 3.1D & E) and both displayed high specificity toward lanthanides as a group. However, none of them can identify each lanthanide individually. Since both DNAzymes showed different propensity toward some of the lanthanides, it is possible to extract more analytical information by combining the two DNAzymes (Figure 3.11A & B). First, the responses of each sensor to different lanthanides were first tested separately. For example, both DNAzymes were individually tested and both showed a similar rate of fluorescence change with Nd^{3+} (Figure 3.11C). On the other hand, Lu^{3+} produced a much slower response with Lu12 than with Ce13d (Figure 3.12D). The results were consistent with the previous gel-based assays. If these two sensors were combined, different lanthanides would produce different overall response patterns. As a result, these patterns might be used for their identification by applying the simplest mathematical treatment called ratiometric detection. The Lu12/Ce13d ratio of sensor signaling rate is plotted for all the lanthanides (Figure 3.11E). For lanthanides smaller than Tb^{3+}, the value of the ratio is closer to 1. For the larger lanthanides, the ratio shows a descending trend.

Ideally, each lanthanide should present a unique ratio. However, there are a total of 14 analytes and only two sensor probes are available. It is almost impossible to identify individual lanthanides with the current system. To fully identify each lanthanide, it is necessary that more sensor probes with unique patterns of response be discovered.

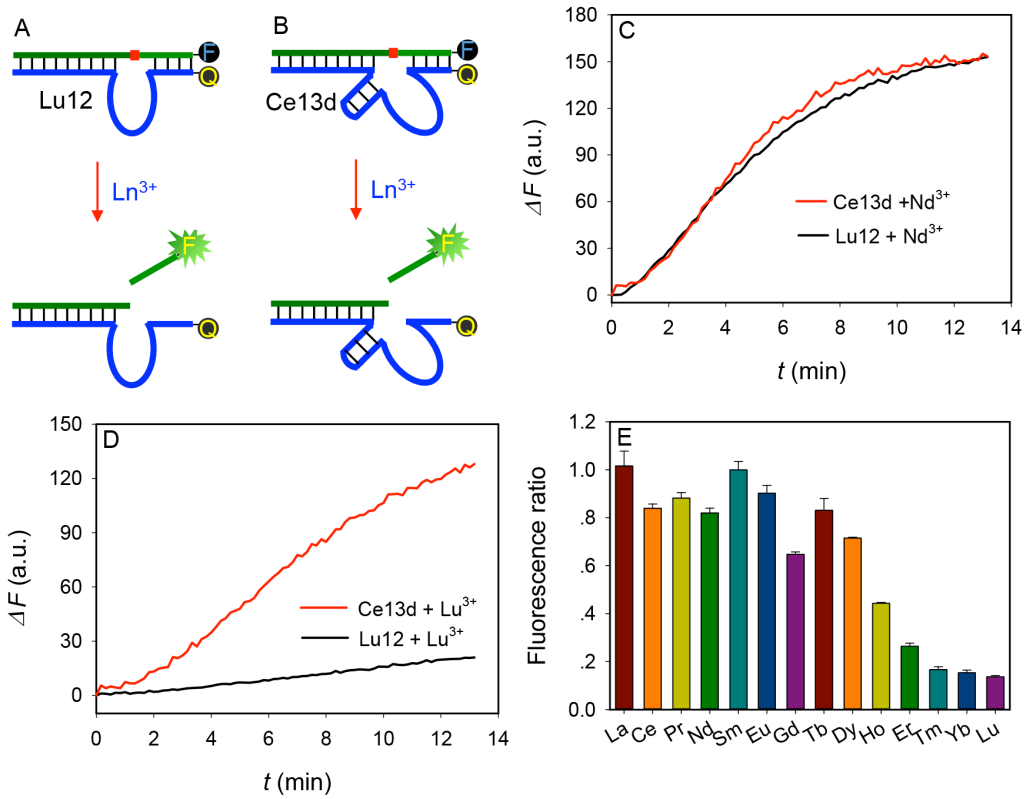

Figure 3.11 Ratiometric sensing of lanthanides with Lu12 and Ce13d DNAzyme becons. Schematics of detecting lanthanides using A) the Lu12 DNAzyme and B) the Ce13d DNAzyme based catalytic beacons. Sensor signal increase as a function of time for the two sensors in the presence of C) 500 nM Nd^{3+} or D) 500 nM Lu^{3+}. E) Ratio of fluorescence increase rate of the Lu12 over the Ce13d DNAzyme sensor.

3.3 Summary

In vitro selection was carried out with Pr^{3+}. Through sequence alignment, a representative sequence can be well-aligned with sequences from another selection carried out using Lu^{3+} by a colleague. Therefore, further studies were carried out using this sequence named Lu12. This DNAzyme is active with lanthanides alone without the need of divalent metal ions. Importantly, a lanthanide size dependent activity trend was observed. This enzyme also provided a scaffold to study lanthanide coordination to DNA. By combining two lanthanide-dependent DNAzyme-based sensors, we can partially discriminate a few large lanthanides via a ratiometric assay. With more unique DNA sequences obtained via *in vitro* selection, a larger sensor array might be formed to discriminate each lanthanide.

3.4 Materials and Methods

3.4.1 Chemicals

The lists of chemicals used in this chapter can be found in Chapter 2 section 2.4.1.

3.4.2 *In vitro* selection

The Selection and PCR conditions were the same as described in previous chapter. The incubation time and concentration of metal salts are in Table 3.1. For the last few rounds of selection, Pr^{3+} was added in 10 μM incremental with 1 h interval instead of all at once. This was to avoid its possible inhibition of DNAzyme activity at high concentration.

3.4.3 Activity assays

Gel-based activity assays were performed with a final concentration of 0.7 μM of the FAM-labeled substrate strand and 1.1 μM of the enzyme. The DNAzyme complexes were prepared by annealing them in buffer A (25 mM NaCl, 50 mM MES, pH 6) and a final of 10 μM lanthanide ions were added to initiate the cleavage reaction. The products were separated on a denaturing polyacrylamide gel and analyzed using a Bio-Rad ChemiDoc MP imaging system.

3.4.4 Sensing

The sensing kinetic studies were carried out using 96 well plates using a Molecular Device SpectraMax M3 microplate reader. The complex was formed by annealing the FAM-labeled substrate and the quencher-labeled enzyme in buffer A. 100 μL of 50 nM FAM-Q DNAzyme in 1 mM pH 7.5 HEPES (pH 7.5) was used for each well. 1 μL of target ions was added after 5 min of background reading. The samples were monitored continuously after addition with a 10 s intervals.

Chapter 4. A New Heavy Lanthanide-Dependent DNAzyme Displaying Strong Metal Cooperativity[c]

4.1 Introduction

Lanthanides and their complexes have been developed as artificial nucleases and chemical probes for nucleic acids.[130,169,201,202] In the previous chapters, two new RNA-cleaving DNAzymes that are highly specific for lanthanides were reported (Ce13d and Lu12). Detailed studies of each DNAzyme were carried out and their applications in sensing lanthanides were demonstrated using a catalytic beacon sensor design. Ce13d was selected in the presence of Ce^{3+}/Ce^{4+},[87] and Lu12 was selected in the presence of Lu^{3+}.[203] Ce13d showed similar activity throughout the entire lanthanide series while Lu12 appeared to have lower activity toward the last few heavy ones. Only based on the activity trend difference shown between the two DNAzyme, the last few heavy lanthanides could be discriminated. Ideally, 15 lanthanides might be discriminated if each selected DNAzyme active only with the target lanthanide. However, the results from previous studies suggested that this is difficult to achieve due to the physical similarity between the lanthanides. If a few DNAzyme probes with distinct activity patterns across the lanthanides series can be obtained, it may enable a sensor array to discriminate between each of the 15 lanthanide ions.[204,205] In an effort to isolate more lanthanide-dependent DNAzymes, three new selections were conducted using Ho^{3+}, Er^{3+} and Tm^{3+} respectively using our N35 library. Holmium has the largest magnetic strength among all the known elements. Thus, it is commonly used for making magnets. In addition, with its ability to strongly absorb

[c] This chapter is the basis for a published manuscript: Huang, P. J.; Vazin, M.; Matuszek, Z.; Liu, J. A New Heavy Lanthanide-Dependent DNAzyme Displaying Strong Metal Cooperativity and Unrescuable Phosphorothioate Effect. *Nucleic Acids Res.* **2015**, *43*, 461-9.

neutrons, it is also used in nuclear reactors. Erbium is mainly used for making lasers and thulium is used in X-ray devices.

In many aspects, a new class of DNAzymes from these selections was identified. Different from Ce13d or Lu12, they were only active with the seven heavy lanthanides. So far, all the reported DNAzymes catalysis were involved with single metal ion. This is the first RNA-cleaving DNAzyme showing metal cooperativity. The analysis suggested that multiple metal ions were involved in catalysis. In addition, phosphorothioate modification of the substrate strand has resulted in complete inactivation of the DNAzyme. Even with the addition of thiophilic metal ions, its activity cannot be rescued. Combined with all these results, a trinuclear lanthanide mechanism is proposed.

4.2 Results and Discussions

4.2.1 *In vitro* selection

It is known that high concentration of free lanthanide ions and some of their complexes can cleave RNA.[167,200] In the previous two chapters, DNA was used as a scaffold to greatly improve the RNA-cleaving efficiency of lanthanide ions. It was shown that the same reaction could take place at much lower lanthanide concentrations and at a designated position. To achieve the goal of discriminating each individual lanthanide from a mixture, more DNAzymes with unique activity patterns are needed. In this work, three separate selections were carried out using different lanthanides to increase sequence diversity. The design of the library is shown in Figure 4.1A. To track the selection progress easily and quantify the cleavage reaction, the library was labeled with a FAM fluorophore at the 5'-end terminal. The ribo-adenosine (rA) is the only RNA linkage in the entire sequence and the rAG (indicated by the arrowhead) is the designated

cleavage junction. Since RNA is about one million fold less stable compared to DNA, cleavage is most likely to take place at this junction. [52] When the library is properly folded into a pre-designed structure in the presence of lanthanides, the cleavage site is positioned in proximity to the randomized N35 loop (35 random nucleotides). If any sequence in this library can cleave the RNA linkage, a shorter 74 nucleotides DNA is generated from the full length 102 nucleotides DNA (Figure 4.1B). This shortened piece is isolated after gel electrophoresis and amplified by two PCR steps to seed the next round of selection.

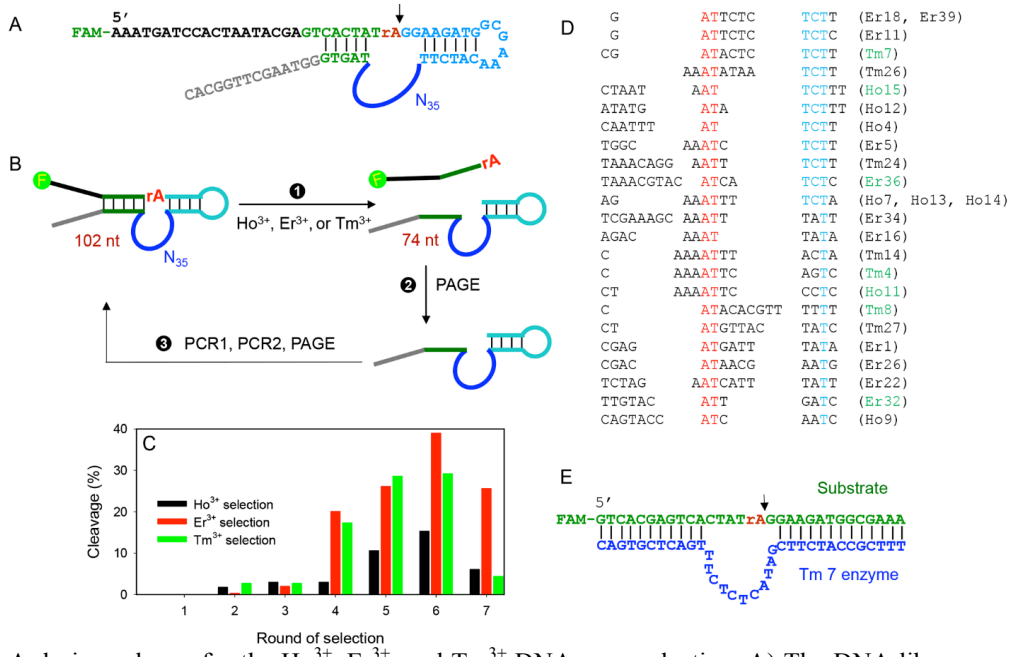

Figure 4.1 A design scheme for the Ho^{3+}, Er^{3+}, and Tm^{3+} DNAzyme selection. A) The DNA library sequence. The cleavage site is indicated by the arrowhead. B) A simplified scheme of the *in vitro* selection process. C) Selection progress and the round 6 library was sequenced. Lanthanides concentration was 50 µM for rounds 1-4 and 10 µM for rounds 5-7. Incubation time was maintained at 60 min. D) Sequence alignment in the enzyme loop region. E) The secondary structure of the trans-cleaving version of the Tm7 DNAzyme.

The progressions of three selections are presented in Figure 4.1C. For the first six rounds, all three selections experienced a steady improvement in cleavage yield. At round six, 15-38% cleavage was achieved. Since the activity of the round 7 libraries dropped noticeably, the round 6 libraries were used for sequencing.

4.2.2 DNAzyme characterization

A total of 60 sequences were obtained from all three selections. Alignments were performed altogether for a systematic comparison and can be found in Table 4.1. For clear identification, the DNAzymes were named by the lanthanide used in selection followed by the clone number for sequencing. Based on the Mfold[190] prediction, most of them can fold into a simple loop structure and the folding of Tm7 is shown in Figure 4.2 as a representation. To make the analysis more cost effective, a trans-cleaving version was designed for subsequent analysis (Figure 4.1E).

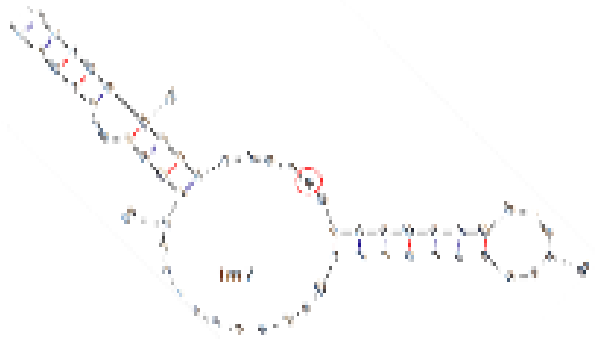

Figure 4.2 M-fold[190] predicted Tm7 secondary structure in the cis-cleaving form. The numbering starts from the 5′-end of the sequence. The cleavage site rA is marked in the red circle.

Searching for the repeating sequences within the region flanked by two base paired regions, only the sequences in the loop were re-aligned and presented in Figure 4.1D. Unfortunately, these sequences did not show a long stretch of conserved nucleotides. This situation is quite different from the two previously reported selections.[87,203] In those two cases, the conserved nucleotides were easily spotted. In Figure 4.1D, the sequences were aligned based on an AT dinucleotide and a thymine that were marked in red and blue respectively. About half of these sequences ended with TCTT (also marked in blue), and many contained a stretch of adenines right before the conserved AT dinucleotide. The sequences shown in Figure 4.1D represented about 50% of the library. For the rest, 16 of them (~27%) are belonged to the Lu12

family that were reported earlier.[203] It was not surprising that Lu12 was selected again since it is active with all these three lanthanide ions.

Table 4.1 Sequence alignment for the Ho^{3+}, Er^{3+}, and Tm^{3+} selection.

Clone #	Sequence (from 5'-end)	
Ho7	CTGCAG-AATTCTAATACGAGTCACTATAGGAAGATGGCGAAACATCT-----TAG--A-	51
Ho13	CTGCAG-AATTCTAATACGAGTCACTATAGGAAGATGGCGAAACATCT-----TAG--A-	51
Ho14	CTGCAG-AATTCTAATACGAGTCACTATAGGAAGATGGCGAAACATCT-----TAG--A-	51
Er5	CTGCAG-AATTCTAATACGAGTCACTATAGGAAGATGGCGAAACATCT-----TTGG-C-	52
Er1	CTGCAG-AATTCTAATACGAGTCACTATAGGAAGATGGCGAAACATCT-----TCGAGA-	53
Er16	CTGCAG-AATTCTAATACSAGTCACYMTAGGAAGATGGCGAAACATCT-----T--AGA-	51
Er18	CTGCAG-AATTCTAATACGAGTCACTATAGGAAGATGGCGAAACATCT-----TGA--T-	51
Er39	CTGCAG-AATTCTAATAC------CTATAGGAAGATGGCGAAACATCT-----TGA--T-	45
Er11	CTGCAG-AATTCTAATACGAGTCACTATAGGAAGATGGCGAAACATCT-----TGA--T-	51
Tm4	CTGCAG-AATTCTAATACGAGTCACTATAGGAAGATGGCGAAACATCT-----TCA--A-	51
Tm7	CTGCAG-AATTCTAATACGAGTCACTATAGGAAGATGGCGAAACATCT-----TCG--A-	51
Tm26	CTGCAG-AATTCTAATACGAGTCACTATAGGAAGATGGCGAAACATCT-----TAA--A-	51
Ho12	CTGCAG-AATTCTAATACGAGTCACTATAGGAAGATGGCGAAACATCT-----TATATG-	53
Tm27	CTGCAG-AATTCTAATACGAGTCACTATAGGAAGATGGCGAAACATCT-----TCTATG-	53
Ho9	CTGCAG-AATTCTAATACGAGTCACTATAGGAAGATGGCGAAACATCT-----TCAGTA-	53
Er34	CTGCAG-AATTCTAATACGAGTCACTATAGGAAGATGGCGAAACATCT-----TCGAAAG	54
Tm14	CTGCAG-AATTCTAATA-GAGTCACTAT-GGAAGATGGCGAAACATCT-----TCAAAA-	51
Ho2	CTGCAG-AATTCTAATACGAGTCACTATAGGAAGATGGCGAAACATCT-----TAGCTC-	53
Er22	CTGCAG-AATTCTAATACGAGTCACTATAGGAAGATGGCGAAACATCTTC---TAGAAT-	55
Ho6	CTGCAG-AATTCTAATACGAGTCACTATAGGAAGATGGCGAAACATCT-----TAATAA-	53
Er32	CTGCAG-AATTCTAATACGAGTCACTATAGGAAGATGGCGAAACATCT-----TTTGTA-	53
Er24	CTGCAG-AATTCTAATACGAGTCACTATAGGAAGATGGCGAAACATCT-----TTAAACA	54
Er30	CTGCAG-AATTCTAATACGAGTCACTATAGGAAGATGGCGAAACATCT-----TTAAA--	52
Ho4	CTGCAG-AATTCTAATACGAGTCACTATAGGAAGATGGCGAAACATCT-----TCAAT--	52
Ho11	CTGCAG-AATTCTAATACGAGTCACTATAGGAAGATGGCGAAACATCT-----TCTAA--	52
Er36	CTGCAG-AATTCTAATACGAGTCACTATAGGAAGATGGCGAAACATCT-----TTAAA--	52
Er4	CTGCAG-AATTCTAATACGAGTCACTATAGGAAGATGGCGAAACATCT-----TAGTA--	52
Tm16	CTGCAG-AATTCTAATACGAGTCACTATAGGAAGATGGCGAAACATCT-----TAAGA--	52
Tm32	CTGCAG-AATTCTAATACGAGTCACTATAGGAAGARGGCGAAACATCT-----TAAGA--	52
Er23	CTGCAG-AATTCTAATACGAGTCACTATAGGAAGATGGCGAAACATCC-----TCAAACT	54
Ho15	CTGCAG-AATTCTAATACGAGTCACTATAGGAAGATGGCGAAACATCT-----TCTAATA	54
Tm8	CTGCAG-AATTCTAATACGAGTCACTATAGGAAGATGGCGAAACATCT-----TCATACA	54
Ho1	CTGCAG-AATTCTAATACGAGTCACTATAGGAAGATGGCGAAACATCT-----TAGAGGT	54
Er6	CTGCAG-AATTCTAATACGAGTCACTATAGGAAGATGGCGAAACATCT-----TAGA---	51
Er13	CTGCAG-AATTCTAATACGAGTCACTATAGGAAGATGGCGAAACATCT-----TCGAAAA	54
Er31	CTGCAG-AATTCTAATACGAGTCACTATAGGAAGATGGCGAAACATCTT---ATAGGTAA	56
Er25	CTGCAG-AATTCTAATACGAGTCACTATAGGAAGATGGCGAAACATCT------TGGAGA	53
Er35	CTGCAG-AATTCTAATACGAGTCACTATAGGAAGATGGCGAAACATCTTAGGGGTAGTGC	59
Tm17	CTGCAG-AATTCTAATACGAGTCACTATAGGAAGATGGCGAAACATCTT--GAGAAGCAC	57
Er12	CTGCAG-AATTCTAATACGAGTCACTATAGGAAGATGGCGAAACATCTT----G--TATA	53
Er26	CTGCAG-AATT-TAATACGAGTCACTATAGGAAGATGGCGAAACATCTT----CGACATA	54
Er27	CTGCAG-AATTCTAATACGAGTCACTATAGGAAGATGGCGAAACATCTT----TTATAGA	55
Er33	CGCCCTTAATTCTAATACGAGTCACTATAGGAAGATGGCGAAACATCTT----TTATAGA	56
Tm1	CTGCAG-AATTCTAATACGAGTCACTATAGGAAGATGGCGAAACATCTTG---TACAAGA	56
Er9	CTGCAG-AATTCTAATACGAGTCACTATAGGAAGATGGCGAAACATCTT----TACAAGC	55
Er20	CTGCAG-AATTCTAATACGA-TCACTATAGGAAGATGGCGAAACATCTT----TACAAGC	54
Er10	CTGCAG-AATTCTAATACGAGTCACTATAGGAAGATGGCGAAACATCTT----TACAAGC	55
Tm3	CTGCAG-AATTCTAATACGAGTCACTATAGGAAGATGGCGAAACATCTT----TACAAGC	55
Tm22	CTGCAG-AATTCTAATACGAGTCACTATAGGAAGATGGCGAAACATCTT----TACAAGC	55
Er37	CTGCAG-AATTCTAATACGAGTCACTATAGGAAGATGGCGAAACATCTT----TACAAGC	55
Ho3	CTGCAG-AATTCTAATACGAGTCACTATAGGAAGATGGCGAAACATCTT----TACAAGC	55
Ho10	CTGCAG-AATTCTAATACGAGTCACTATAGGAAGATGGCGAAACATCTT----TACAAGC	55
Er2	CTGCAG-AATTCTAATACGAGTCACTATAGGAAGATGGCGAAACATCTT----TACAAGG	55
Er17	CTGCAG-AATTCTAATACGAGTCACTATAGGAAGATGGCGAAACATCTT----TACAAGG	55
Er28	CTGCAG-AATTCTAATACGAGTCACTATAGGAAGATGGCGAAACATCTT----TACAAGG	55
Ho8	CTGCAG-AATTCTAATACGAGTCACTATAGGAAGATGGCGAAACATCTT----TACAAGG	55
Er19	CTGCAG-AATTCTAATACGAGTCACTATAGGAAGATGGCGAAACATCTT----TACAAGG	55
Er38	CTGCAG-AATTCTAATACGAGTCACTATAGGAAGATGGCGAAACATCTT----TACAAGG	55
Ho5	CTGCAG-AATTCCAATACGAGTCACTATAGGAAGATGGCGAAACATCTT----TACGAGA	55
Er15	CTGCAG-AATTCTAATACGAGTCACTATAGGAAGATGGCGAAACATCTT----TGTATAC	55

Table 4.1 Sequence alignment for the Ho^{3+}, Er^{3+}, and Tm^{3+} selection. (Continued)

Clone #	Sequence (from 5'-end)	
Ho7	-AATTTTC---------TATAACGAGTTTGAT-CATGTACCGTTAGT--CGGTAAGCTTG	98
Ho13	-AATTTTC---------TATAACGAGTTTGAT-CATGTACCGTTAGT--CGGTAAGCTTG	98
Ho14	-AATTTTC---------TATAACGAGTTTGAT-CATGTACCGTTAGT--CGGTAAGCTTG	98
Er5	-AAATCTC---------TTTAACGAATTTAGT-AGTGTACCG-TAGT--CGGTAAGCTTG	98
Er1	-TGATTTA---------TATAACGAGTAAAGG-ACCGA--TTGTAGT--CGGTAAGCTTG	98
Er16	-CAAATTA---------TATAACGAGTATAGG-AGCGAGCACATAGT--CGGTAAGCTTG	98
Er18	-TCT-CTC---------TTTAACGAGTATCAGTGGCTRCAACGTAGT--CGGTAAGCTTG	98
Er39	-TCT-CTC---------TTTAACGAGTATCAGTGGCTCCAACGTAGT--CGGTAAGCTTG	92
Er11	-TCT-CTC---------TCTAACGAGTATCAGTGGCTCCACCGTAGT--CGGTAAGCTTG	98
Tm4	-AATTCAG---------TCTGACGCG-GTAGGTGGGTCCACCATAGT--CGGTAAGCTTG	98
Tm7	-TACTCTC---------TTTGACGTTCGTATAAACGAGACA-ATAGT--CGGTAAGCTTG	98
Tm26	-TATAATC---------TTTAACG--AGTAACCCAGACACATATAGT--CGGTAAGCTTG	97
Ho12	-ATATCT----------TTTAACGAGTATTAA--ACCATAAGATAGT--CGGTAAGCTTG	98
Tm27	-TTACTA----------TCTAACGAGAAGAGA--ACCATAA-CTAG---CGGTAAGCTTG	96
Ho9	-CCATCAA---------TCTAACGAGTGTTAG--AACGCAA-ATAGT--CGGTAAGCTTG	98
Er34	CAAATTTA---------TTTGACGAGAAT-----GCATACAAACAGT--CGGTAAGCTTG	98
Tm14	---TTTAC---------TATAACGAGTGTTTA--ACGTGGAAATTAG--CGGTAAGCTTG	95
Ho2	---AATCA--------GCACGCATGCGTGATT-ATAGTGAAG-TAGT--CGGTAAGCTTG	98
Er22	---CATTT--------ATTTGACCACG-GATT-GCAGATTA--TAG---CGGTAAGCTTG	97
Ho6	---CTTT---------ATCTAACGAAGTATTA-CTCAAAGAGGTAGT--CGGTAAGCTTG	98
Er32	---CATTG--------ATCTGACTCACTCATG-CT-GTGGACCTAGT--CGGTAAGCTTG	98
Er24	GGAATTTC---------TTTAACTCGCTGTAG-GTG-GACT---AGT--CGGTAAGCTTG	98
Er30	--ACTTTA---------TTTGACTCGGAGGAA-GAG-AATTGGTAGT--CGGTAAGCTTG	97
Ho4	--TTATTC---------TTTGATGAGAAAAAG-GTGGAACTATTAGT--CGGTAAGCTTG	98
Ho11	-AATTCC---------CTCTAACTCGTACAAT-GAC-CCTTGTTAGT--CGGTAAGCTTG	98
Er36	-CGTACAT-----CATCTCTAACTCGTTGATA-GAA-C----TTAGT--CGGTAAGCTTG	98
Er4	-CCCAAAGGGAGGATGTTATAACTCGTATCT------C-----TAGT--CGGTAAGCTTG	98
Tm16	GCCGTCAG--------GTATGCCCTGTCAAAA-ACT-CGT--ATAGT--CGGTAAGCTTG	98
Tm32	GCCGTCAG--------GTATGCCCTGTCAAAA-ACT-CGT--ATAGT--CGGTAAGCTTG	98
Er23	GATATCAG--------AAGATCAACTCCTATA-ACT-CG----TAGT--CGGTAAGCTTG	98
Ho15	A-TTCTTT----------TAACTCGATTATG-TAG-CGTATATAG---CGGTAAGCTTG	97
Tm8	CGTTTTTT----------TAACTCGCT-ATG-TAT-GGAAGGTAG---CGGTAAGCTTG	97
Ho1	ACGTATAG---------AGACGAG-GTGACGCAATT----GAGTAGT--CGGTAAGCTTG	98
Er6	---TATGG---------AAACGATTGTGAGGCTATATGACGAGGTAG--CGGTAAGCTTG	97
Er13	AGGTATCT---------GAGTTTATTTGATTCGTTG----AT-TAGT--CGGTAAGCTTG	98
Er31	TGGAAACT---------AA---TATTTGACTCGCTG----ATATAGT--CGGTAAGCTTG	98
Er25	GAGAAACT---------CAATTTATTTGACTCAATG----GGTTAGT--CGGTAAGCTTG	98
Er35	GTAGGACG---------AGATTTATTTGGCTCGTAG------------CGGTAAGCTTG	97
Tm17	GAAGTGC----------AGGTTTATTTGACAAATAAT-------AGT--CGGTAAGCTTG	98
Er12	ACTTAAGT---------AGGTTATTTTAACGAGTATT----ATTAGT--CGGTAAGCTTG	98
Er26	ACGAATGT---------TACCCCCTTTAACGAGTA------ATTAGC--CGGTAAGCTTG	97
Er27	TCGATAGA---------GGATTTATTTGACAGGTAT------TTAGT--CGGTAAGCTTG	98
Er33	TCGATAGA---------GGATTTATTTGACAGGTAT------T-AGT--CGGTAAGCTTG	98
Tm1	ACGGGAGA---------GGGTATATTTAAATCGTAG------T--AG--CGGTAAGCTTG	97
Er9	ATCAGTAG----------ATTGGAAATGCGGTT------ATAGTGACGGTAAGCTTG	96
Er20	ATCAGTAG----------ATTGGAAATGCGGTT------ATAGTGACGGTAAGCTTG	95
Er10	ATCAGTAG----------ATTGGAAATGCGGTT------ATAGTGACGGTAAGCTTG	96
Tm3	ATCAGTAG----------ATTGGAAATGCGGTT------ATAGTGACGGTAAGCTTG	96
Tm22	ATCAGTAG----------ATTGGAAATGCGGTT------ATAGTGACGGTAAGCTTG	96
Er37	ATCAGTAG----------ATTGGAGATGCGGTT------ATAGTGACGGTAAGCTTG	96
Ho3	ACAAATAG----------ATTGGAAATGCGGTT------ATAGTGACGGTAAGCTTG	96
Ho10	ACCGGACA---------AACTATGGGAGGAGCGGTT------ATAGT--CGGTAAGCTTG	98
Er2	AAGGGTCC---------A---CTATGCACAACGGTT------ATAGTGACGGTAAGCTTG	97
Er17	AAGGGTCC---------A---CTATGCACAACGGTT------ATAGTGACGGTAAGCTTG	97
Er28	AAGGGTCC---------A---CTATGCACAACGGTT------ACAGTGACGGTAAGCTTG	97
Ho8	AAGGGTCC---------A---CTATGCACAACGGTT------GTAGTGACGGTAAGCTTG	97
Er19	AAGGGTCC---------A---CTATGCACAACGGTT------ATAGTGGCGGTAAGCTTG	97
Er38	AAGTGTCC---------A---CTATGCACAACGGTT------ATAGTGACGGTAAGCTTG	97
Ho5	TAGAATGT---------TG--TACAGTCTAGCGGTT------ATAGT--CGGTAAGCTTG	96
Er15	CGGAAAGG---------TAAAATTAATTTAACGAGA------GTAGT--CGGTAAGCTTG	98

Note: The bold A in red is the cleavage site. The bases in blue are conserved for Lu12. The green T denotes for the starting of the sequence alignment in the randomized region.

4.2.3 Lanthanide selectivity

Since the sequences of this new DNAzyme family were quite diverse, it was difficult to predict rationally the most optimal sequence. Therefore, seven representative ones were picked for further assay (those marked in green in Figure 4.1D). Six of these DNAzyme secondary structures are shown in Figure 4.3A (substrate binding arms are denoted by the bars). It should be noted that all these DNAzymes contained a stretch of four unpaired nucleotides in the substrate strand at the right of the cleavage junction.

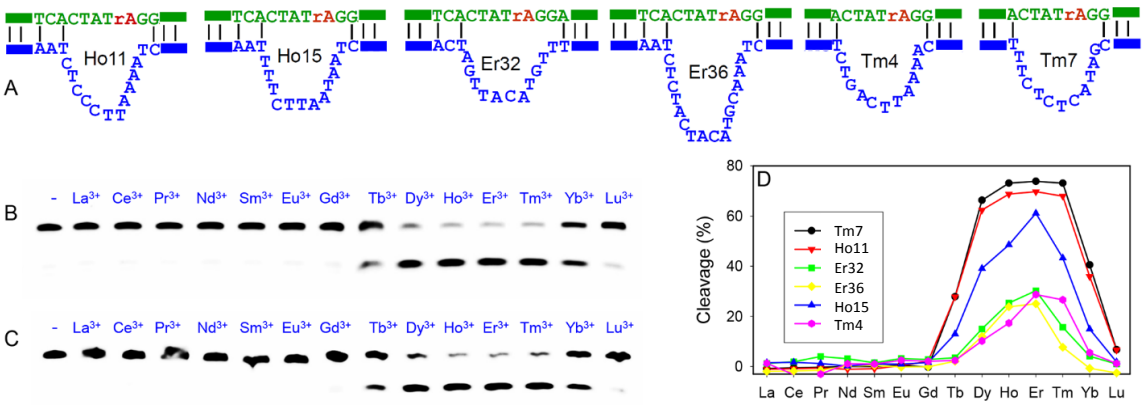

Figure 4.3 Lanthanides selectivity of the six active DNAzymes from Ho^{3+}, Er^{3+}, and Tm^{3+} selection. A) Secondary structures of the six DNAzymes in this study. Gel images showing cleavage activity of B) Tm7 and C) Ho11 with different lanthanide ions (10 μM) after 1 h reaction. D) Quantification of the cleavage results of the six DNAzymes by lanthanides.

The enzyme activities of these six DNAzymes were tested against all 14 lanthanides with 1 h incubation time. The activity trend for the Tm7 and Ho11 DNAzymes were shown in Figure 4.3B and 4.3C respectively. Surprisingly, barely any cleavage was observed with the first seven lighter ions (radioactive Pm^{3+} was excluded) and only moderate cleavage was observed with Tb^{3+}. Efficient cleavage occurred from Dy^{3+} to Tm^{3+}, and then the cleaved product decreased rapidly with Yb^{3+} and Lu^{3+}. All six tested DNAzymes followed exactly the same trend with slightly different efficiency and their activities are quantified in Figure 4.3D. Based on this study, we reason that these DNAzymes belong to the same family even though they did not share

any common stretch of nucleotides. In fact, they seem to be quite tolerant to mutations and insertions when looking at the sequence diversity shown in Figure 4.1D.

In Figure 4.3D, Tm7, Ho11 and Ho15 are the three fastest DNAzymes among the six. They all have a stretch of pyrimidines at the 3′-end followed by a few purines in the loop. The other three DNAzymes are slower and their base contents in the loop region are more disorganized, especially on the pyrimidine side. One thing that stood out when comparing the three most active sequences was that only Tm7 has a single guanine in the loop, while Ho11 and Ho15 do not contain any guanines. Among the four nucleobases, guanine is the most efficient ligand for lanthanide-binding.[171,206-209] In fact, many guanine nucleotides can be found in the conserved sequences of the two reported lanthanide-dependent DNAzymes.[87,203] This might be a reasonable explanation for these new DNAzymes to display a much narrower activity window across the lanthanide series than the previous examples.

The ionic radii of lanthanides decrease gradually and steadily from 1.17 Å to 1.0 Å, while the pK_a values of their bound water decrease from 9.3 to 8.2 from La^{3+} to Lu^{3+}. Given the abrupt change of the cleavage activity from Gd^{3+} to Tb^{3+}, it is unlikely for either the size or pK_a to be the main factor. However, the 'gadolinium break' in Figure 4.3D may be attributed to the change of coordination number. As the lanthanide atomic number increases, the coordinated water decreases from 9 to 8 due to lanthanide contraction and steric effects.[209] This transition takes place around Gd^{3+} for a water ligand. It might be that the low coordination number allows better metal binding and catalysis in this DNAzyme.

The gadolinium break was reported previously with cleavage of a dinucleotide in the presence of 5 mM lanthanide,[87] and with the GR5 DNAzyme in the presence of 60 μM lanthanides.[167] In both examples, Lu^{3+} was among the most active ions. However, Tm7 has

almost no activity with Lu^{3+}. Therefore, Tm7 likely has different catalytic mechanism. Since Tm7 has the highest efficiency among all the tested sequences and it has a small enzyme loop containing only 11 nucleotides, it was chosen for subsequent studies.

4.2.4 Biochemical characterization of Tm7

To explore the activity of this new DNAzyme even further, metal selectivity for non-lanthanide ions was tested. A gel image of Tm7 reacted with 10 μM other metal ions is shown in the inset of Figure 4.4A. Besides Er^{3+} (used as a representative lanthanide) and Y^{3+} produced cleavage, all the other metals were inactive. The chemical and physical properties of Y^{3+} are between Ho^{3+} and Er^{3+}. As a result, similar cleavage was observed in the presence of Y^{3+}. When the metal ion concentration was increased to 100 (the red bars in Figure 4.4A), still only Y^{3+} showed moderate cleavage. It shoud be noted that 100 μM Er^{3+} inhibited the activity so even higher concentration was not tested. It is important to note that Pb^{2+} was not active at any given concentration. Almost all the previously reported DNAzymes are active with Pb^{2+}.[81,87,125,203] This is a rare example where Pb^{2+} failed to show activity. The high selectivity displayed by Tm7 made it another useful probe for lanthanides, especially for the heavy ones.

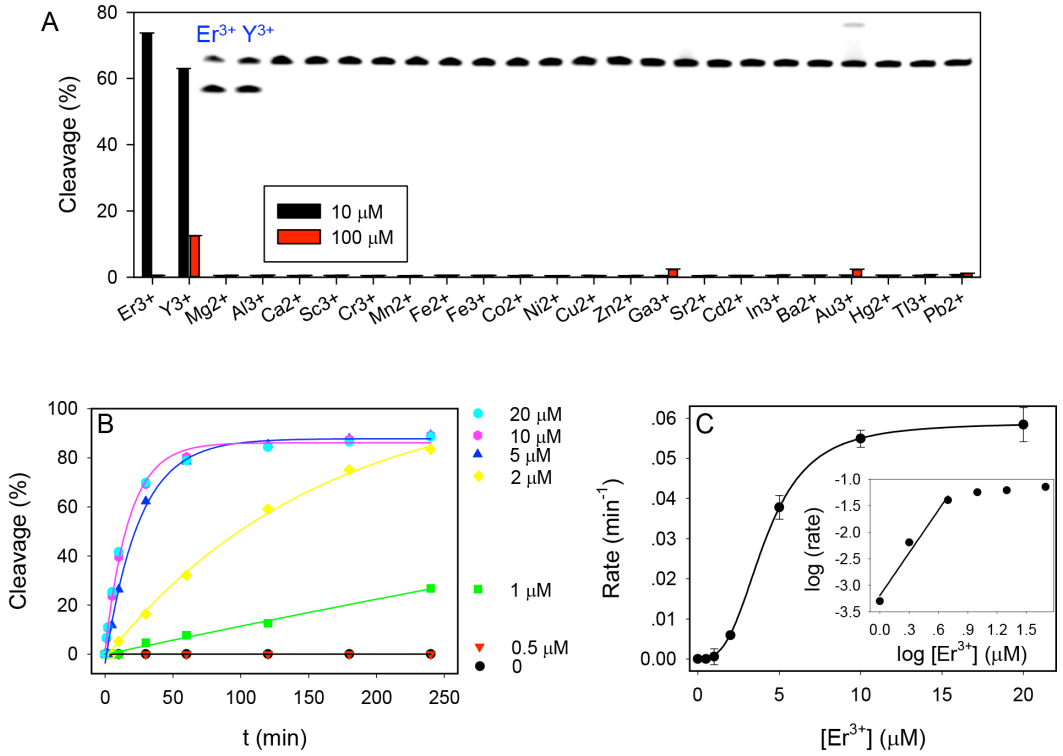

Figure 4.4 Selectivity and sensitivity analysis of the Tm7 DNAzyme. A) Percentage of substrate cleavage by the Tm7 DNAzyme using 10 μM or 100 μM metal ions. Inset: gel image of cleavage in the presence of 10 μM metal ions. The lanes correspond to the metal ions in the *x*-axis. Only Au^{3+} produced streaking and Er^{3+} and Y^{3+} produced cleavage. B) Kinetics of Tm7 cleavage at a few Er^{3+} concentrations. C) Cleavage rate as a function of Er^{3+} concentration. Inset: the same data plotted using the log scale.

Next, the cleavage kinetics was measured at various Er^{3+} concentrations (Figure 4.4B). With 0.7 μM DNAzyme, no cleavage was observed over 4 h in the presence of 0.5 μM Er^{3+}. On the other hand, the rate increased by 10-fold from 1 μM to 2 μM Er^{3+}. Since the rate did not increase linearly with the Er^{3+} concentration, the data indicated that multiple metal binding is required for activity. Figure 4.4C plots the cleavage rate as a function of Er^{3+} concentration and a sigmoidal curve was obtained with a Hill coefficient of 3.0. When the double log plot is presented (insert), the initial slope 2.7 suggested that three Er^{3+} ions are involved in catalysis. The highest rate was ~0.06 min^{-1} in the presence of 20 μM Er^{3+} at pH 6.0, which is similar to our last round of selection condition. However, this is much slower than the rate of the Lu12 DNAzyme which also presence in the sequenced library. The survival of this class of slower

DNAzyme is probably due to a long incubation time. From the sequences isolated after 6 rounds of selection, 16 Lu12 DNAzyme out of 60 (27%) were obtained. If the selection was continued with a shorter incubation time, the library is likely to be dominated by the Lu12 type of DNAzymes. Most of the sequences that were tested here showed very low activity with Lu^{3+}. This might be the reason that no Tm7 sequences were observed in the previous Lu^{3+}-dependent selection.[203] Although the selection was conducted in pH 6 environments, the rate of Tm7 increased significantly with the increasing pH and can reach higher than 1.6 min^{-1}.

To the best of our knowledge, this is the first time that metal cooperativity has been reported for RNA-cleaving DNAzymes. All the previously reported enzymes employ only a single metal ion.[78,87,125,146,167,203,210] While most small ribozymes use only one metal as well,[77,211] large ribozymes require multiple metal ions to perform more complex reactions such as RNA splicing.[212,213] For instance, it was demonstrated that lanthanides (especially Nd^{3+}) could accelerate the Pb^{2+}-dependent activity of the leadzyme, where a two-metal mechanism was proposed. However, the best rate was only ~0.01 min^{-1} when both metals were used.[177] In fact, those two metals did not show much cooperativity.

Komiyama was the first to report using multiple free lanthanide ions for RNA cleavage. [160] It is proposed that one lanthanide directly bonds with the leaving phosphate to decrease its negative charge density at the transition state. A bridging water (bridging two lanthanide ions) may acts as a general base to deprotonate the 2′-OH of the ribose to make it a better nucleophile.

4.2.5 The effect of pH

To gain further insights into Tm7, a pH-dependent study was performed, and the logarithm of cleavage rate was plotted in Figure 4.5A. While the selection was carried out at pH 6.0, the rate became progressively faster at higher pH.[125,191,210] When pH is higher than 7.0, the

rate improvement slowed down. By fitting the data in the pH range from 6.0 to 7.0, a slope of 0.97 was obtained (Figure 4.5B). This suggested that only a single deprotonation step occurs in the rate-limiting step of the hydrolysis. This is typical for RNA-cleaving DNAzymes and this deprotonation is happening at the 2′-OH group on the ribose.

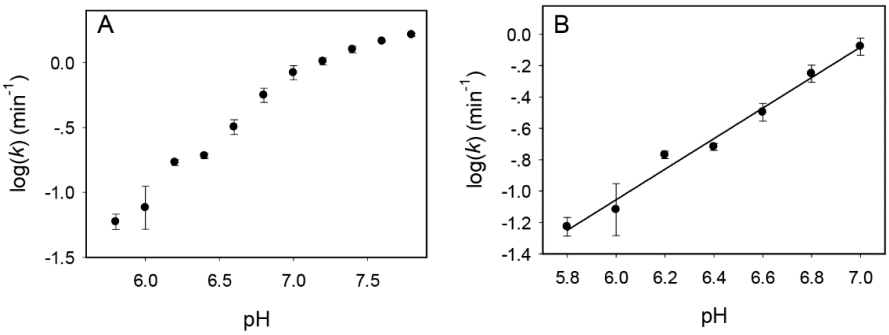

Figure 4.5 pH-dependentThe pH-rate profile of the Tm7 DNAzyme. Tm7 catalytic rate over (A) a wide pH range and (B) the initial linear range. A slope of 0.97 is obtained in (B), indicating a single deprotonation step.

4.2.6 Phosphorothioate modification

Since lanthanide ions are hard Lewis acids that prefer oxygen-based ligands, metal binding was exam by introducing a phosphorothioate (PS) modification at the cleavage junction, where one of the non-bridging oxygen atoms is replaced by a sulfur (Figure 4.6A).[214,215] Depending on the position of replacement, two diastereomers are possible. With the PS-modified substrate (a mixture of the two isomers), Tm7 barely showed cleavage with any metal, including thiophilic Cd^{2+} (Figure 4.6B), which is typically used to rescue the activity of PS-modified enzymes. Only Er^{3+} showed a trace amount of cleavage after 1 h. A quantitative kinetic measurement was performed (Figure 4.6D) and the initial kinetics is very similar to that of the PO substrate (within 10% difference) and no further cleavage occurred beyond ~5%. Therefore, this small fraction of cleavage is likely due to that the PS substrate is only ~95% pure. The remaining 5% are PO that caused the initial Er^{3+}-dependent cleavage kinetics.

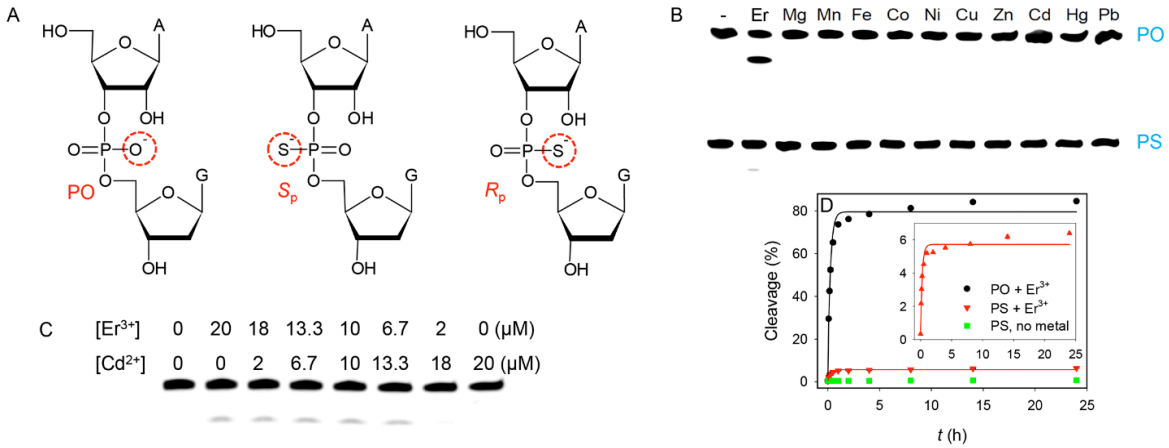

Figure 4.6 Kinetic study of the PS-Tm7 DNAzyme. A) Structures of the normal phosphate linkage (PO), and the two diastereomers of the PS modification. B) Cleavage of the Tm7 DNAzyme with the PS-modified substrate (racemic mixture) in the presence of various divalent metal ions and Er^{3+}. C) Cleavage of Tm7 with the PS substrate using a mixture of Er^{3+} and Cd^{2+}. D) Kinetics over 24 h for Tm7 cleaving the PO (black dots), and PS (red triangles) substrate in the presence of 10 μM Er^{3+}. The green squares are the Tm7/PS complex incubated without Er^{3+}. Inset is the re-plot of the PS sample magnifying the initial kinetics.

All the previously studies showed that ribozymes and DNAzymes such as the hammerhead ribozyme,[216] HDV ribozyme,[217] 10-23 DNAzyme,[218] and RNase P[219] use the pro-R_p oxygen for metal binding (mostly with Mg^{2+}). Replacing this particular oxygen atom with a sulfur atom usually completely inhibits the Mg^{2+}-dependent activity (by over 100-fold). However, the activity can be rescued by using thiophilic metals such as Mn^{2+} or Cd^{2+}. When the other PS isomer (S_p) was used, the activity is only slightly decreased (e.g. ~5-fold). This is because Mg^{2+} only coordinates to one of the non-bridging oxygen atoms (pro-R_p), and thus the pro-S_p substitution does not have much influence on activity. For the Tm7 experiment, a racemic mixture of R_p and S_p was used. Since no activity was observed with either Er^{3+} or Cd^{2+}, neither R_p nor S_p is active. The result indicated the metal(s) must interact with both phosphate oxygen atoms through inner sphere coordination. This is different from all the previously reported nucleic acid enzymes, including another lanthanide-dependent DNAzyme, Ce13d, whose activity was rescued by Cd^{2+}.[220]

If both non-bridging oxygen atoms are important, a mixture of Er^{3+} and Cd^{2+} might able to rescue the activity. However, this scenario will only work if these two metals do not need to interact with each other. By keeping the total concentration at 20 μM, the Er^{3+}/Cd^{2+} composition ratio was varied (Figure 4.6C). However, still only ~5% cleavage was observed when the Er^{3+} concentration was higher than 6.7 μM. This was again due to cleavage of the pre-existing PO substrate. This implies that the metals must act synergistically instead of independently. If one metal binds simply to one oxygen, the use of this mixture should have restored the activity with the PS substrate. The independent action of metal ions is best illustrated in the leadzyme, where a lanthanide was proposed to bind to the phosphate oxygen and the Pb^{2+} was used to deprotonate the 2′-OH group.[177] With the PS modification, Tm7 is the first RNA-cleaving nucleic acid enzyme that is completely inactivated with all the metal ions. More importantly, its catalysis seems to react in a new type of mechanism.

4.2.7 Cleavage mechanism

A substrate that contains seven consecutive RNA bases was used to test the Tm7 and 17E activity (Figure 4.7). The gel analysis showed that Tm7 is inactive for this substrate. Most DNAzymes selected with a chimeric substrate are not active with full RNA. However, they are still called RNA-cleaving DNAzymes because of the same reaction mechanism.

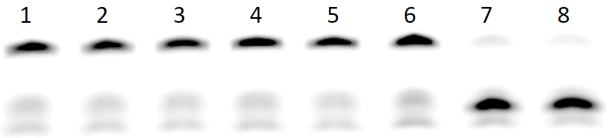

Figure 4.7 Tm7 and 17E cleavage of a RNA substrate (RNA-sub in Table 4.2 for sequence). Lane 1 is the substrate alone, and some degradation was observed. Lane 2 is the substrate with 10 μM Er^{3+}. Lane 3 is the Tm7 DNAzyme complex without metal. Lane 4 is the complex with 10 μM Er^{3+} for 30 min incubation. Lane 6 is the 17E DNAzyme complex without metal. Lane 7 and 8 are the 17E DNAzyme complex with 10 μM Pb^{2+} after 30 and 60 min incubation. The 17E DNAzyme is known to cleave full RNA, and it serves as a positive control. Cleavage was observed only with the 17E DNAzyme, but not Tm7.

With single ribonucleotide substrate, mass spectrometry studies were performed on the cleavage product (Figure 4.8). The spectrum showed that the fragment on the 5'-end contains a cyclic phosphate. This is a typical end product that was observed for most ribozymes and DNAzymes reaction.

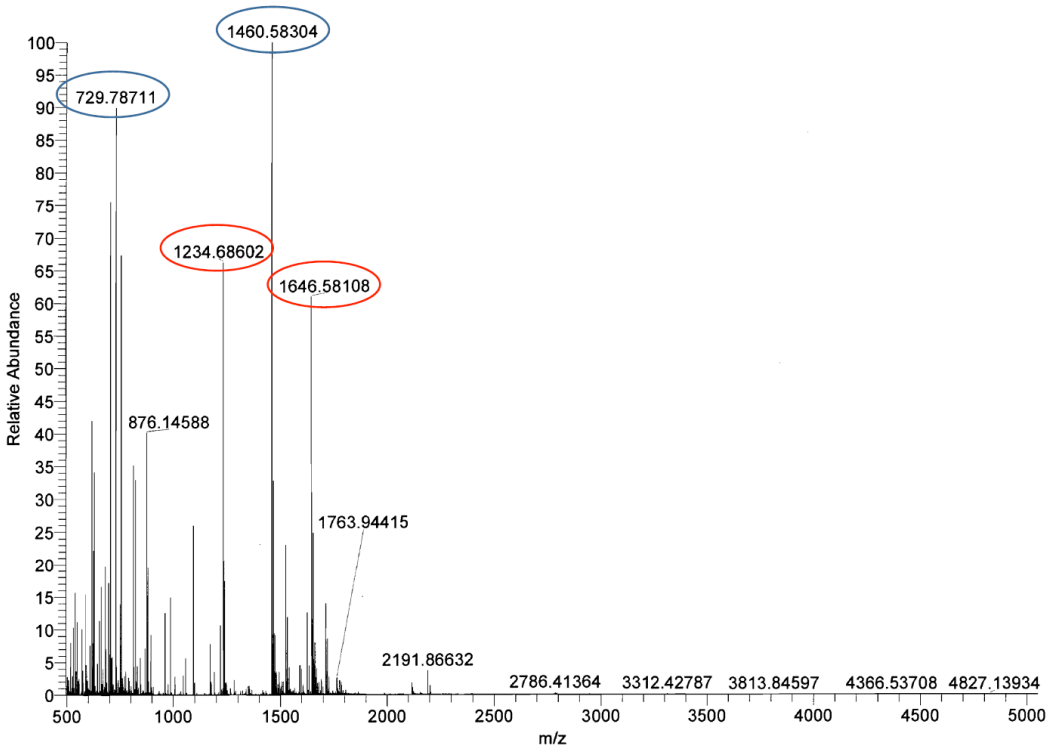

Figure 4.8 Mass spectrometry characterization of the Tm7 cleavage product. The peaks in red are the cyclic phosphate product from the 5′-fragment of the substrate (molecular weight = 4942.7, 3 and 4 charges for the two marked peaks), and the peaks in blue are from the 3′-fragment (molecular weight = 4384.7, 3 and 6 charges for the two marked peaks).

Cleaving RNA with dinuclear lanthanides complexes have been previously proposed. [160] However, this mechanism cannot explain the Tm7 results. Combined all the above studies, a new mechanism involving a trinuclear lanthanides center was proposed (Figure 4.9). From the PS studies, both non-bridging oxygen atoms are in direct inner sphere coordination with the lanthanide ions (Er^{3+} used as an example here). When the nucleophillic attack by the 2'-OH occurred, these two can stabilize the transition state via electrostatic interactions. The pH studies indicated that only a single deprotonation reaction was involved, so the 2'-OH was most likely to

be the source of the nucleophile. Since the lanthanide concentration-dependent studies indicated a total of three lanthanide ions are involved, the third ion is thus proposed to interact with the 2′-OH. The three ions could be linked together with hydroxyl bridges. Since heavy lanthanide ions have a lower pK_a value for the bound water, it is easier for them to form polynuclear hydrolyzed products. This could also explain the tendency of heavy lanthanide being much more effective. The role of the DNAzyme loop was likely to stabilize this trinuclear complex.

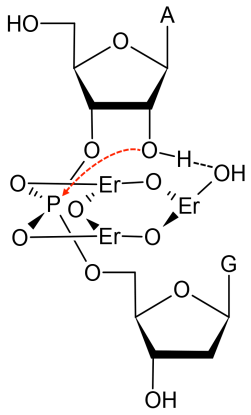

Figure 4.9 Proposed mechanism of the lanthanide-induced RNA cleavage for the Tm7 DNAzyme. The red arrow indicates nucleophilic attack of the phosphorus center. The bridging oxygen atoms linking the Er^{3+} ions are originated from deprotonated water.

4.2.8 Sensing heavy lanthanide ions

Apart from proposing a novel reaction mechanism, this study has provided a new probe for lanthanide detection. Rational design of small molecule ligands that selectively bind an individual lanthanide is quite difficult since these 15 elements have the same charge, similar sizes and comparable chemical properties.[221] DNA is a good candidate as a lanthanide ligand since the phosphate backbone provides high binding affinity through hard acid/base interactions and the nitrogen containing nucleobases may offer specificity to discriminate between different lanthanide ions.[222] With this in mind, DNA-based biosensors for lanthanides were developed. Although many sensor design methods are available,[138,139] a simple catalytic beacon design was

used.[193] The 3′-end of the substrate labeled was labeled with a FAM and the 5′-end of the enzyme labeled with a quencher (Figure 4.10).

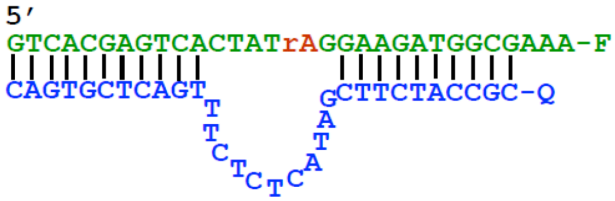

Figure 4.10 Catalytic beacon design of Tm7 DNAzyme. F = FAM. Q = Iowa Black® FQ dark quencher.

In the initial state, the beacon displayed low fluorescence. Once the substrate was cleaved and released, fluorescence was detected. Fluorescence enhancement was observed with Dy^{3+} and Y^{3+}, but the non-rare earth metals failed to produce signal (Figure 4.11A). Among all the lanthanide ions, only those seven heavy ones produce significant signals (Figure 4.11B). The result was also consistent with the gel-based assays, indicating that the signal generation was indeed due to cleavage. Interestingly, the Dy^{3+} produced the fastest signal. This might be attributed to the use of higher pH (7.5) in sensing as compared to pH 6.0 in the gel-based assay. In this case, Dy^{3+} was used as the target metal ion for metal concentration dependent study (Figure 4.11C). Barely any cleavage was observed with 5 nM Dy^{3+} and significant improvement was achieved when Dy^{3+} concentration was increased from 10 to 20 nM. This trend also verified the metal cooperativity proposed earlier. When the Dy^{3+}-concentration dependent rate was plotted in Figure 4.11D, the detection limit was calculated to be 14 nM Dy^{3+}.

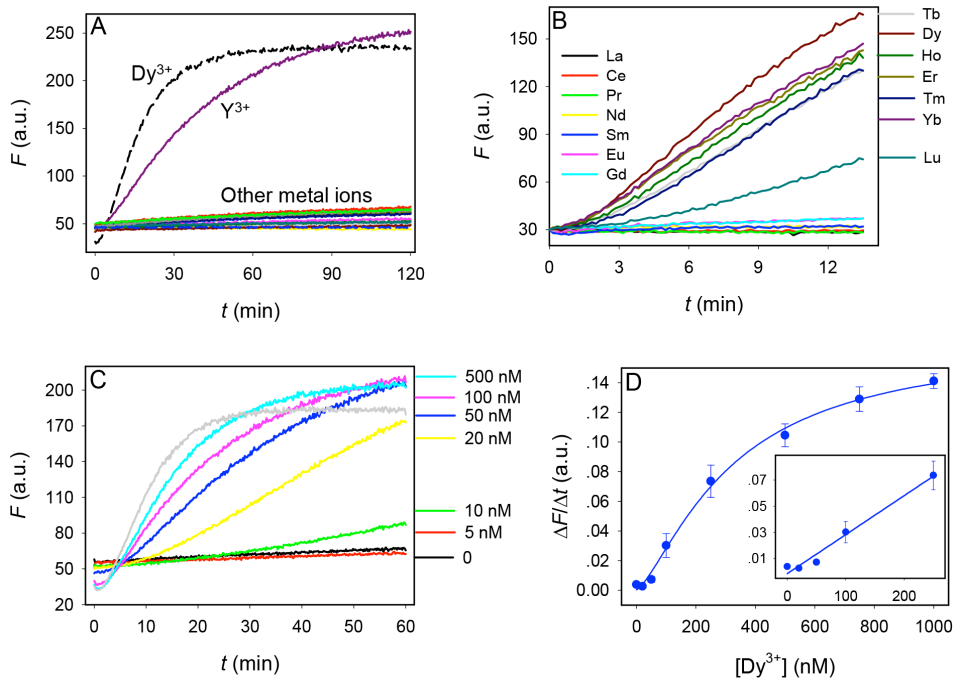

Figure 4.11 Kinetic studies of the Tm7 DNAzyme beacon. A) Sensor response to 0.5 μM of divalent and trivalent metal ions. The list of the other metal ions tested can be found in Figure 2B. B) Sensor response to 0.5 μM of various lanthanides. C) Sensor signaling kinetics in the presence of various concentrations of Dy^{3+}. DNAzyme sensor concentration = 50 nM. D) Quantification of Dy^{3+} based on the initial rate of sensor fluorescence enhancement. Inset: the initial linear response at low Dy^{3+} concentrations.

4.3 Summary

In summary, *in vitro* Ho^{3+}-, Er^{3+}-, and Tm^{3+}-dependent selections were carried out separately. Out of the 60 obtained sequences, half of them belong to a new family of DNAzyme that were only active with the seven heavy lanthanide ions. Based on the metal concentration dependency and the phosphorothioate replacement studies, this new DNAzyme shows metal cooperativity. Combined with the pH-rate profile, a new mechanism involving a trinuclear lanthanides complex was proposed. In this mechanism, two lanthanide ions interact with the non-bridging oxygen atoms while the third one interacts with the 2′-OH. This is the first RNA-cleaving DNAzyme showing such a metal binding property. To demonstrate its application, a catalytic DNA beacon was designed to showcase its 14 nM detection limit on heavy lanthanides.

4.4 Materials and Methods

4.4.1 Chemicals

The lists of chemicals used in this chapter can be found in Chapter 2 section 2.4.1. The sequences for the DNA used for *in vitro* selection and assays were listed in Table 4.2.

Table 4.2 Oligonucleotides used for *in vitro* selection and assays.

DNA Name	Sequence and modifications (from 5′ to 3′)
Lib-FAM-N_{35}	pGGCGAAACATCTT**N_{35}**TAGTGGGTAAGCTTGGCAC-**FAM**
Lib-rA	AATACGAGTCACTAT**rA**GGAAGAT
splint	AAGATGTTTCGCCATCTTCCTATAGTCCACCACCA
P1 primer	GTGCCAAGCTTACCG
P2 primer	CTGCAGAATTCTAATACGAGTCACTATAGGAAGATGGCGAAACA
P3 primer	**FAM**-AAATGATCCACTAATACGACTCACTAT**rA**GG
P4 primer	AACAACAACAAC-**iSp18**-GTGCCAAGCTTACCG
Tm4	TTTCGCCATCTTCAAAATTCAGTCTGACTCGTGAC
Tm7	TTTCGCCATCTTCGATACTCTCTTTGACTCGTGAC
Tm8	TTTCGCCATCTTCATACACGTTTTTTTA ACTCGTGAC
Er32	TTTCGCCATCTTTTGTACATTGATCTGACTCGTGAC
Er36	TTTCGCCATCTTCTAAACGTACATCATCTCTAACTCGTGAC
Ho11	TTTCGCCATCTTCTAAAATTCCCTCTAACTCGTGAC
Ho15	TTTCGCCATCTTCTAATAATTCTTTTAACTCGTGAC
RNA-sub	GTCACGAGTCAC**rUrArUrArGrGrA**AGATGGCGAAA-**FAM**
Sub-FAM	GTCACGAGTCACTAT**rA**GGAAGATGGCGAAA-**FAM**
Tm7-Q	**Iowa Black ® FQ**-CGCCATCTTCGATACTCTCTTTGACTCGTGAC

4.4.2 *In vitro* selection

The method of *in vitro* selection and PCR amplification conditions are similar to the one described in chapter 2 except that the initial library was obtained by ligating Lib-FAM-N_{35} and Lib-rA. For all the selections, the metal incubation time was maintained at 60 min. 50 μM lanthanides were used for the first four rounds. For the last three rounds, 10 μM lanthanides were used. The round 6 libraries for all the three selections were cloned and sequenced.

4.4.3 Activity assay

Gel-based activity assays were performed with a final concentration of 0.7 μM of the FAM-labeled substrate strand and 1.1 μM of the enzyme. The DNAzyme complexes were

prepared by annealing them in buffer A (50 mM MES, pH 6.0, 25 mM NaCl) and a final concentration of 10 μM lanthanides was added to initiate the cleavage reaction. The products were separated on a denaturing polyacrylamide gel and analyzed using a Bio-Rad ChemiDoc MP imaging system. For pH-dependent activity assay, the MES and MOPS buffers (50 mM with 25 mM NaCl) were used.

4.4.4 Mass spectrometry

The samples were prepared by reacting a non-labeled DNAzyme substrate with the Tm7 DNAzyme at 1 μM substrate and 1.5 μM enzyme concentration in buffer A. Then the samples were desalted using a Sep-Pak column and dried. After rehydration in water to ~20 μM substrate concentration, the samples were analyzed using an ESI mass spectrometer.

4.4.5 Sensing

The sensing kinetics studies were carried out using a microplate reader (SpectraMax M3). The sensor complex was formed by annealing the FAM-labeled substrate and the quencher-labeled enzyme (1:1.5 ratio) in buffer A. In each well, 100 μL of the complex containing 50 nM FAM-labeled substrate was diluted in 10 mM HEPES (pH 7.5). 1 μL of metal ion was added after 5 min of background reading and the signaling kinetics was monitored.

Chapter 5. Sensing Lanthanide Ions with a DNAzyme Array

5.1 Introduction

In the previous chapters, I reported three lanthanides-dependent RNA-cleaving DNAzymes. First, Ce13d DNAzyme was selected using Ce^{4+}/Ce^{3+} by using an N_{50} DNA library (a library with 50 random nucleotides).[87] Ce13d displayed similar activity cross the entire lanthanides (Ln^{3+}) series. Next, Lu12 was isolated using an N_{35} library in the presence of Lu^{3+}. Although Lu12 is also active with the whole Ln^{3+} series, it displayed higher activity with the light Ln^{3+} and showed descending activity with the last few heavy Ln^{3+}.[203] It also suggested the possibility of using a DNA-based sensor to discriminate different lanthanides. Finally, three separate selections using an N_{35} library in the presence of Ho^{3+}, Er^{3+} and Tm^{3+} were carried out, yielding the representative Tm7 DNAzyme. Unlike the previous two DNAzymes, Tm7 displayed almost no activity with the first seven light Ln^{3+} but is highly active with the heavy ones.[223] In fact, the studies revealed that Tm7 binds three metal ions cooperatively for catalysis, which has never been observed previously for DNAzymes.

So far, the N_{50} library was used only once with cerium. Since then, the N_{35} library was used to reduce the chance of re-selecting the general Ln^{3+}-dependent DNAzyme, Ce13d. In our continuous effort to search for new Ln^{3+}-dependent DNAzymes, the N_{50} library was used once again for the selection in the presence of lanthanides. In this chapter, dysprosium (Dy^{3+}) and gadolinium (Gd^{3+}) were used as intended targets for two separate selections. Both Dy and Gd absorb neutrons strongly and have high magnetic susceptibility, allowing applications in nuclear reactors and data storage.[221] In addition, Gd is commonly used as a contrast agent in magnetic resonance imaging (MRI).[188,224] Two new DNAzymes named Dy10 and Gd2b were isolated and

characterized in this work.

In the end, all five representative DNAzymes displayed different lanthanides recognition pattern. A sensor array was made based on the selected DNAzymes, which can separate lanthanides from other metals, light and heavy lanthanides, and for the most part, each lanthanide.

5.2 Results and Discussion

5.2.1 *In vitro* selection and sequence alignment of Dy^{3+}

With a DNA library containing 50 random nucleotides (N_{50}), *in vitro* selection of Dy^{3+} was carried out following the previously established method.[29] The incubation time and Dy^{3+} concentration used for each round are shown in Table 5.1. A total of six rounds of selection were carried out and 67% cleavage was observed in the last round (Figure 5.1A).

Table 5.1 *In vitro* selection conditions and progress for Dy^{3+}. In round 6, Dy^{3+} was added in two steps, each with 5 μM.

Round #	[Dy^{3+}] (μM)	Incubation time (min)	Cleavage (%)
1	50	60	0.2
2	50	60	0.3
3	50	60	5.1
4	10	60	8.5
5	10	60	10.0
6	5x2	30x2	64.7

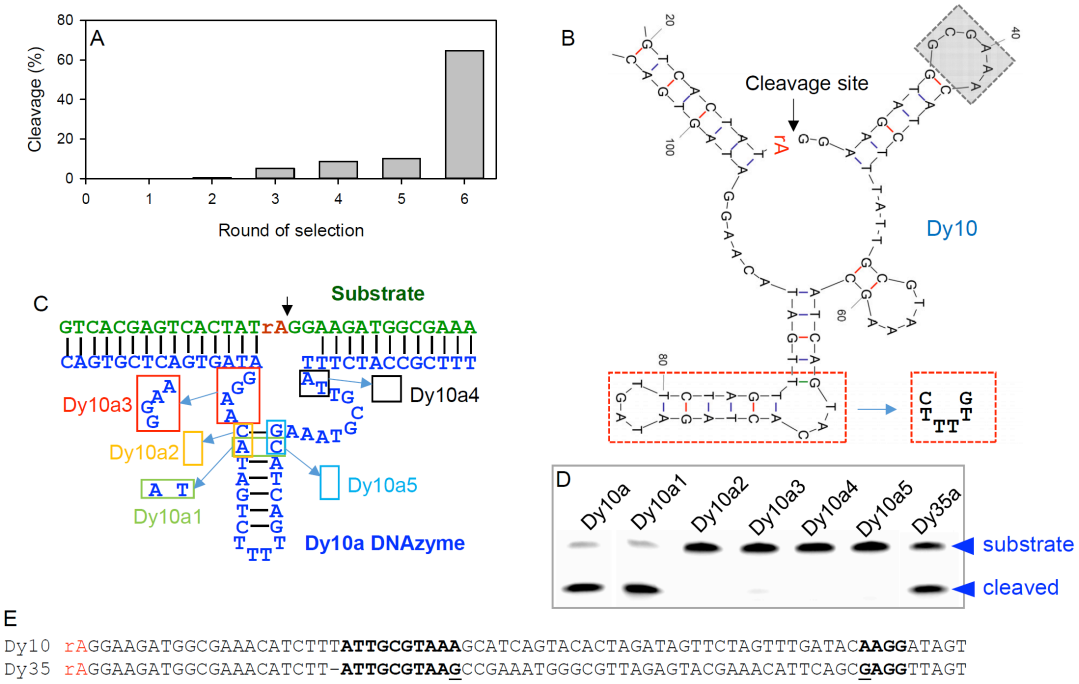

Figure 5.1 Activity analysis of the Dy10 DNAzyme and its mutants. A) Progress of the Dy^{3+}-dependent selection. B) The Mfold[7] predicted structure of cis-cleaving Dy10. To convert it to a trans-cleaving DNAzyme, the nucleotides in the shaded box were removed and the nucleotides in the red box were replaced by the six nucleotides next to it. C) The secondary structure of the trans-cleaving DNAzyme, named Dy10a. Various mutations are also shown, where the boxed nucleotides are replaced. D) A gel image showing activity of the various mutants of Dy10a after 1 h reaction with 0.5 μM Sm^{3+}. E) Sequence alignment of the two active sequences that do not belong to the Ce13 or Lu12 DNAzymes. Sequences start from the cleavage site rA (from the 5′) and the important nucleotides for Dy10 and Dy35 are in boldface (the two loop regions) and underlined parts show the differences.

The round 6 library was then sequenced. A total of 40 sequences were obtained and alignment is presented in Table 5.2. Unsurprisingly, 85% of the library was the previously reported Ce13 or Lu12 type DNAzymes since both are quite active with Dy^{3+}.[87,203] For the remaining four sequences, two of them (Dy10 and Dy35, Figure 5.1E) have very similar sequences. The other two (Dy1 and Dy17) are identical, but inactive (see Figure 5.2 for their characterization). The Mfold[190] predicted secondary structure of Dy10 is presented in Figure 5.1B and the cleavage site is marked by the arrowhead. This cis-cleaving structure can be easily converted to the trans-cleaving form by removing the nucleotides in the gray box. The nucleotides in the red box were suspected to be redundant. Thus, it was replaced with a smaller six nucleotides loop to generate a truncated DNAzyme named Dy10a (Figure 5.1C). In this

DNAzyme, two loops that connected the substrate binding regions were joined by the hairpin structure. The smaller loop has only an AAGG tetranucleotide. For Dy35 structure, this small loop contains a GAGG sequence (underlined in Figure 5.1E). Moreover, there is only one nucleotide difference in the larger loop between Dy10 and Dy35. To monitor cleavage, the substrate strand was labeled with a FAM (Figure 5.1C). Since Dy35 has similar structure as Dy10, it was also truncated and converted into a trans-cleaving form. Both Dy10a and Dy35a showed activity (lane 1 and 7 in Figure 5.1D). However, Dy10a appears to have much better activity. In fact, the Dy10a structure appears different from the three Ln^{3+}-dependent DNAzymes that were reported previously.[87,203,223] Therefore, Dy10a was used for detail studies.

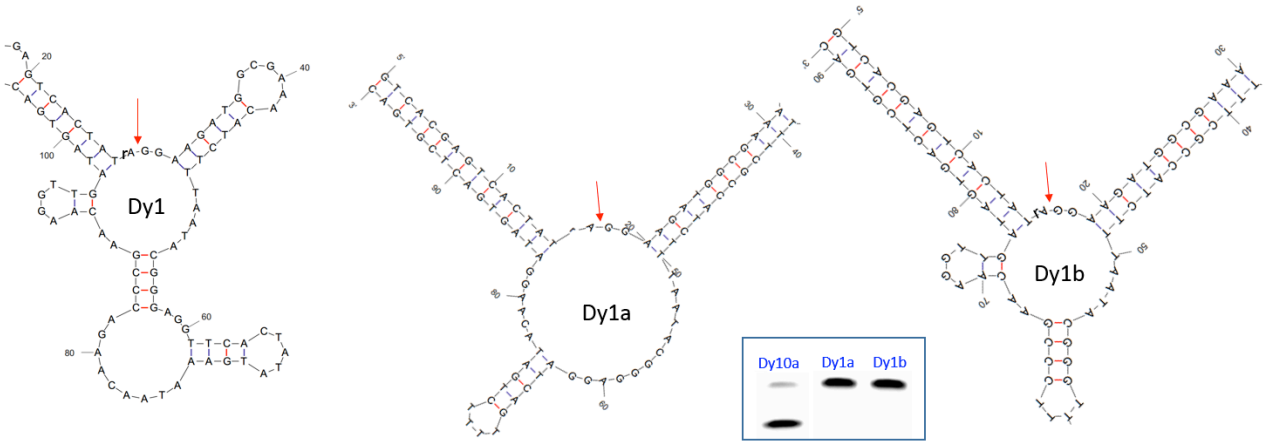

Figure 5.2 Mfold predicted secondary structure of Dy1 (cis-cleaving form). To make it into a trans-cleaving form, Dy1a and Dy1b were deigned. To test whether the folding is appropriate, these two enzymes were truncated at different positions. However, the gel-based assay using FAM-labeled substrate showed no cleavage with either enzyme. Therefore, we conclude that it is not a lanthanide-dependent DNAzyme. Reaction with 0.5 μM Sm^{3+} and 60 min incubation time.

Table 5.2 Sequence alignment of the Dy^{3+} selection. The sequences in green belong to the Lu12 family, and the sequences in blue belong to the Ce13 family. The ones in red are studied in this work and they are the new DNAzyme. The ones in black contain unreadable bases or cannot be classified into any of the families.

Clone #	Sequence (from 5'-end)	
Dy1	CTGCAGAATTCTAATACGAGTCACTATAGGAAGATGGCGAAACATCTTTAATACG---GG	57
Dy17	CTGCAGAATTCTAATACGAGTCACTATAGGAAGATGGCGAAACATCTTTAATACG---GG	57
Dy10	CTGCAGAATTCTAATACGAGTCACTATAGGAAGATGGCGAAACATCTTTATTGCGT--AA	58
Dy35	CTGCAGAATTCTAATACGAGTCACTATAGGAAGATGGCGAAACATCTT-ATTGCG---TA	56
Dy6	CTGCAGAATTCTAATACGAGTCACTATAGGAAGATGGCGAAACATCTTTACAAACG--AA	58
Dy27	CTGCAGAATTCTAATACGAGTCACTATAGGAAGATGGCGAAACATCTTTACSAACS--GT	58
Dy25	CTGCAGAATTCTAATACGAGTCACTATAGGAAGATGGCGAAACATCTTTACMATGG--AA	58
Dy16	CTGCAGAATTCTAATACGAGTCACTATAGGAAGATGGCGAAACATCTTTACGAGC---AT	57
Dy34	CTGCAGAATTCTAATACGA-TCACTATAGGAAGATGGCGAAACATCTTTACAAGC---AT	56
Dy12	CTGCAGAATTCTAATACGAGTCACTATAGGAAGATGGCGAAACATCTTTACGAGC---AT	57
Dy7	CTGCAGAATTCTAATACGAGTCACTATAGGAAGATGGCGAAACATCTTTACAAGAT--TA	58
Dy37	CTGCAGAATTCTAATACGAGTCACTATAGGAAGATGGCGAAACATCTTTACAGGCT--TA	58
Dy8	CTGCAGAATTCTAATACGAGTCACTATAGGAAGATGGCGAAACATCTTTACGAGGT--G-	57
Dy19	CTGCAGAATTCTAATACGAGTCACTATAGGAAGATGGCGAAACATCTTTACAAGCT--GA	58
Dy23	CTGCAGAATTCTAATACGAGTCACTATAGGAAGATGGCGAAACATCTTTACAAGGA--TA	58
Dy29	CTGCAGAATTCTAATACGAGTCACTATAGGAAGATGGCGAAACATCTTTACAAAG-----	55
Dy32	CTGCAGAATTCTAATACGAGTCACTATAGGAAGATGGCGAAACATCTTTACAAAG-----	55
Dy9	CTGCAGAATTCTAATACGAGTCACTATAGGAAGATGGCGAAACATCTTTACAAGGG----	56
Dy30	CTGCAGAATTCTAATACGAGTCACTATAGGAAGATGGCGAAACATCTTTACAAGC-----	55
Dy38	CTGCAGAATTCTAATACGAGTCACTATAGGAAGATGGCGAAACATCTTTACAAGC-----	55
Dy13	CTGCAGAATTCTAATACGAGTCACTATAGGAAGATGGCGAAACATCTTTACAAA-----T	55
Dy14	CTGCAGAATTCTAATACGAGTCACTATAGGAAGATGGCGAAACATCTTTACAAA-----T	55
Dy24	CTGCAGAATTCTAATACGAGTCACTATAGGAAGATGGCGAAACATCTTTACAAGGG--CC	58
Dy31	CTGCAG-ATTCTAATACGAGTCACTATAGGAAGATGGCGAAACATCTTTACAAGGG--CC	57
Dy40	CTGCAGAATTCTAATACGAGTCACTATAGGAAGATGGCGAAACATCTTTACAAG-C--AT	57
Dy11	CTGCAGAATTCTAATACGAGTCACTATAGGAAGATGGCGAAACATCTTTACGAGT---AA	57
Dy15	CTGCAGAATTCTAATACGAGTCACTATAGGAAGATGGCGAAACATCTTTACG------AA	54
Dy18	CTGCAGAATTCTAATACGAGTCACTATAGGAAGATGGCGAAACATTATGGAG-----CCA	55
Dy33	CTGCAGAATTCTAATACGAGTCACTATAGGAAGATGGCGAAACAAAATGGAG-----CCA	55
Dy28	CTGCAGAATTCTAATACGAGTCACTATAGGAAGATGGCGAAACATCATGGAG-----CCA	55
Dy20	CTGCAGAATTCTAATACGAGTCACTATAGGAAGATGGCGAAACATCATGGAG-----CCA	55
Dy26	CTGCAGAATTCTAATACGAGTCACTATAGGAAGATGGCGAAACATCATGGAG-----CCA	55
Dy3	CTGCAGAATTCTAATACGAGTCACTATAGGAAGATGGCGAAACAT-TTGGAG-----CCA	54
Dy4	CTGCAGAATTCTAATACGAGTCACTATAGGAAGATGGCGAAACATCTCGGAG-----CCA	55
Dy5	CTGCAGAATTCTAATACGAGTCACTATAGGAAGATGGCGAAACATCCGGGAG-----CCA	55
Dy36	CTGCAGAATTCTAATACGAGTCACTATAGGAAGATGGCGAAACATCTGGGAG-----CCA	55
Dy2	CTGCAGAATTCTAATACGAGTCACTATAGGAAGATGGCGAAACATCTTGGGGAGCGGCCA	60
Dy22	CTGCAGAATTCTAATACGAGTCACTATAGGAAGATGGCGAAACATCTTTACG-----AGA	55

Table 5.2 Sequence alignment of the Dy^{3+} selection. (Continued)

Clone #	Sequence (from 5'-end)	
Dy1	AGGTTCACTAT--ATGAAATA--ACAAGACCCGAA-CAAGGTTGATAGTGACGGTAAGCT	112
Dy17	AGGTTCACTAT--ATGAAATA--ACAAGACCCGAA-CAAGGTTGATAGTGACGGTAAGCT	112
Dy10	AGCATCAGTAC--ACTAGATAGTTCTAGTTTGATA-CAAG---GATAGTGACGGTAAGCT	112
Dy35	AGCCGAAATGG--GCGTTAGAGTACGAAACATTCAGCGAG---GTTAGTGACGGTAAGCT	111
Dy6	GTGGTTAGAG--TGACATATATAATGAGTAGATAAACAGG---GCTAGTGACGGTAAGCT	113
Dy27	TAAG-AAAAG--TGACTTATCCMGTGGTTATCTGACTAGT---GTTAGTGACGGTAAGCT	112
Dy25	CAGGTTATAGGAGGAGTTAACTGGCCATTAAC-AACCAG----ACTAGTGACGGTAAGCT	113
Dy16	ACGGTTATAGG-AGTCGGACTTACGGATTTAAAATACAAA---GCTA-TGACGGTAAGCT	112
Dy34	ACGGTTATAGG-GGTCGGACTTACGGATTTAAGATACAAA---GCTA-TGACGGTAAGCT	111
Dy12	GCGGTTATAGG-AGTCGGACTCACAGATTTAAGATACAAA---GCTA-TGACGGTAAGCT	112
Dy7	---AGTATTCG--ACTGGCAACAGGAGAGAGAATTACTACGGTTATAGTGACGGTAAGCT	113
Dy37	TACAGTAAAAG--ACGGTAAAGCGGTTATAGAGACAC-AC---ACTAGTGACGGTAAGCT	112
Dy8	--TTATAACACCGGTTGTAGTGAAT-TGTACGCCTGCCGGT---ATTAGGACGGTAAGCT	111
Dy19	AAACATGACAACGGTTATAGTGAAA-ACATAG--TGAGGGG---ATGGCGGCGGTAAGCT	112
Dy23	CACAAAGGATTTG--AATCCTACTC-ACTTCAGGTAACGGTT--ATAGTGACGGTAAGCT	113
Dy29	-ACCCCCGACAGAATAGAACTAATAGAAAGTTAGGGCCGGTT--GTAGTGACGGTAAGCT	112
Dy32	-ACCCCCGACAGAATAGAACTAATAGAAAGTTAGGGCCGGTT--GTAGTGACGGTAAGCT	112
Dy9	-GCCGCTACCAAAACACCAGTGCATGATAACGAGCTCCGGTT--CTAGTGACGGTAAGCT	113
Dy30	-ATGTCAAACAGTAATTCTGTAGGTGGTATTTGACAGCGGTT--TTAGTGACGGTAAGCT	112
Dy38	-ATGTCAAACAGTAATTCTGTAGGTGGTATTTGACAGCGGTT--TTAGTGACGGTAAGCT	112
Dy13	GAACTTGCCTACGATTCGACCGCAGGTAGACAGGTCCAGGTT--ATAGTGACGGTAAGCT	113
Dy14	GAACTTGCCTACGATTCGACCGCAGGTAGACAGGTCCAGGTT--ATAGTGACGGTAAGCT	113
Dy24	ATGCATATAATTATTAAGAGCACCCATATGCT---ACCGGTT--ATAGTGACGGTAAGCT	113
Dy31	ATGCATATAATTATTAAGAGCACCCATATGCT---ACCGGTT--ATAGTGACGGTAAGCT	112
Dy40	AAGCATGATTCGGCTAAAAGAACCAGAATGCTG--ATCGGTT--ATAGTGACGGTAAGCT	113
Dy11	TACATACCAGCACGTATGCGTTAGGGTTATAGCTACG-TAT----TAGTGACGGTAAGCT	112
Dy15	CACGAAGGCGCTAGCAGG-GAGTGGGTTATAGGACCGGTAAAGGCTAGTAACGGTAAGCT	113
Dy18	TAGGTCAAAGGTA-GGTGCGGGTCGTATCATATCGACCAG---TATAGTGACGGTAAGCT	111
Dy33	TAGGTCAAAGGTG-GGTGCTGGTCGTATCATATCGACTAGT--TATAGTGACGGTAAGCT	112
Dy28	TAGGTCAAAGGTA-GGTGCTGGTCGTACCTTATCGACCAGT--TATAGTGACGGTAAGCT	112
Dy20	TAGGTCAAAGGTG-GGTGCGGGTCGTATAATATCGACCAG---TATAGTGACGGTAAGCT	111
Dy26	TAGGTCAAAGGTG-GGTGCGGGTCGTATAATATCGACCAG---TATAGTGACGGTAAGCT	111
Dy3	TAGGTCAAAGGTG-GGCGCGGGTCGTATTATATCGACCAGT--TATAGTGACGGTAAGCT	111
Dy4	TAGGTCAAAGGTT-GGTGCGG-TCGTATCATATCGACCAGT--TATAGTGACGGTAAGCT	111
Dy5	TAGGTCAAAGGTG-GGTGCGGGTCGTA---TACCGACTAAGT-TATAGTGACGGTAAGCT	110
Dy36	TAGGTCAAAGGTG-GGTGCGGGTCGTA---TATCGACTAAGT-TATAGTGACGGTAAGCT	110
Dy2	ATGTTCACAAG-----CGAGGAACCTTAAAAATCTCGCGGT--TACAGTGACGGTAAGCT	113
Dy22	TAGGCGAAACGAGGAAAGCCGATCGGTT-ATAGAGAAAGTT--ATCAGTGACGGTAAGCT	112

5.2.2 Lanthanides selectivity of Dy10a

Besides sequences differences, another criterion to identify new Ln^{3+}-dependent DNAzymes is based on their activity pattern. This pattern is also important for discriminating individual Ln^{3+} for potential biosensor applications. For instant, Lu12 showed descending activity for the last few heavy Ln^{3+} and Tm7 is active only with the seven heavy lanthanides. With 1 μM Ln^{3+}, the Dy10a DNAzyme complex was incubated for 5 min with each Ln^{3+} and the gel is shown in Figure 5.3A. Although all the Ln^{3+} ions induced cleavage, the most active metals

appeared to be in the middle of the series (e.g. from Sm^{3+} to Dy^{3+}). When the cleavage at 1 min and 5 min were quantified (Figure 5.2B), the bell-shaped activity pattern observed is different from any known DNAzymes. In addition, Dy10a is also a quite efficient DNAzyme. Within a minute of incubation, >30% substrate cleavage was observed at pH 6 in the presence of Sm^{3+}.

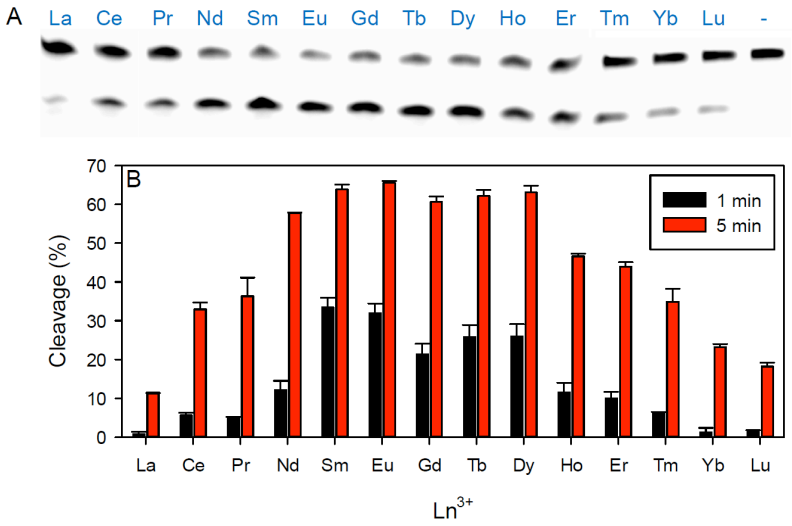

Figure 5.3 Lanthanides selectivity of the Dy10a DNAzyme. A) A gel image of Dy10a cleavage in the presence of 1 μM Ln^{3+} for 5 min at pH 6. The last lane is the negative control without added Ln^{3+}. (B) Fraction of substrate cleavage in the presence of 1 μM of each Ln^{3+} after 1 and 5 min reaction.

Interestingly, Dy10 DNAzyme sequence only appeared twice in the 40 sequences. Compared to Ce13 or Lu12 (85% of the library), Dy10 displayed much higher activity at low metal concentrations. The reason that Dy10 failed to dominate the library is attributed to it's smaller dynamic range. Under the same conditions, its activity is significantly suppressed with 10 μM Dy^{3+} (Figure 5.4). For comparison, Ce13 works optimally with 10 μM Ln^{3+}.[87] Since 50 to 10 μM of Dy^{3+} was used during the selection, Dy10 sequence failed to enrich. If the selection had been carried out with a lower concentration of the metal, more Dy10 sequences would appear in the final library.

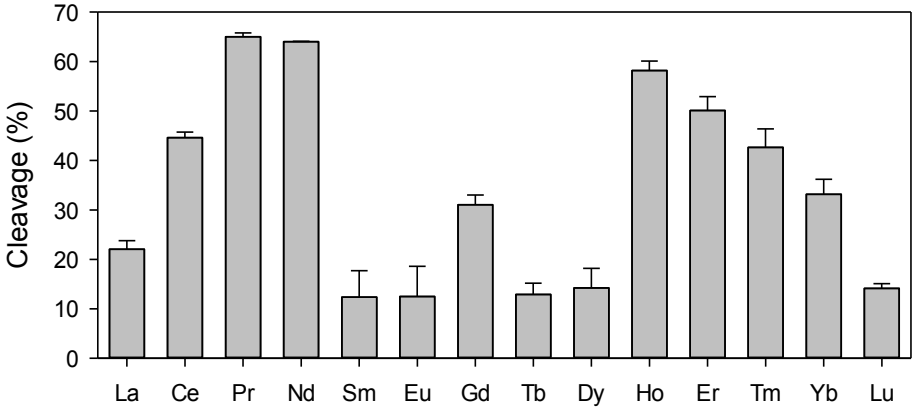

Figure 5.4 Cleavage yield of the Dy10a DNAzyme in the presence of 10 μM Ln^{3+}. The reaction was carried out at pH 6 for 5 min.

5.2.3 *In vitro* selection and sequence alignment of Gd^{3+}

The same N_{50} library was also used for *in vitro* selection of Gd^{3+}. The incubation time and the condition used for each round of Gd^{3+} selection are shown in Table 5.3. A total of six rounds of selection were carried out and 49% cleavage was observed in the last round (Figure 5.5A). In the end of round 6, the library was cloned and sequenced.

Table 5.3 *In vitro* selection conditions and progress for Gd^{3+}. In round 6, Gd^{3+} was added in two steps, each with 50 μM.

Round #	[Gd^{3+}] (uM)	Incubation time (min)	Cleavage (%)
1	100	60	0.1
2	100	60	0.2
3	100	60	5.5
4	100	60	29.2
5	100	60	45.0
6	50x2	60x2	49.1

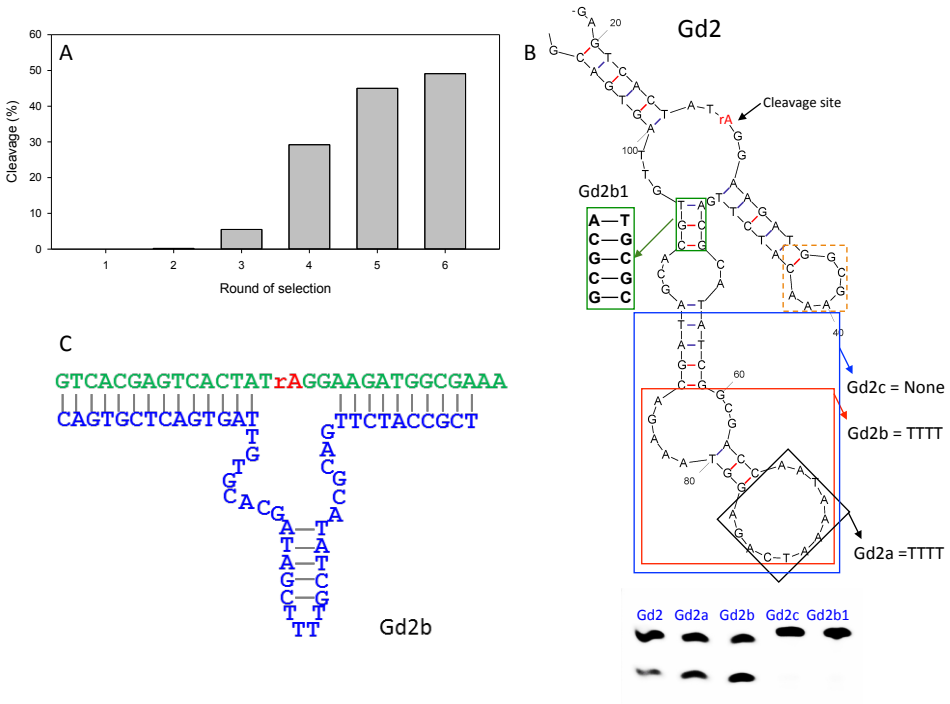

Figure 5.5 Activity analysis of the Gd2 DNAzyme and its mutants. A) Progress of the Gd^{3+}-dependent selection. B) The Mfold predicted structure of cis-cleaving Gd2. To convert it to a trans-cleaving DNAzyme, the nucleotides in the shaded orange box were removed. Various mutations are also shown, where the boxed nucleotides are replaced. A gel image showing activity of the various mutants of Gd2 after 1 h reaction with 10 μM Gd^{3+}. C) The secondary structure of the trans-cleaving DNAzyme, named Gd2b that was used for subsequent analysis.

A total of 42 sequences was obtained and alignment is presented in Table 5.4. 66% of the library was the previously reported Ce13 or Lu12 type DNAzymes. It was not surprising since both are quite active with Dy^{3+}.[87,203] For the sequences labeled in black, six of them have identical sequences but they were not able to fold into reasonable structures. On the other hand, the other two folded into a structure like Ce13 but they were inactive (Gd12 & Gd13). The six remaining clones (labeled in red) were only varied by one nucleotide. Based on the Mfold prediction, Gd2 also folded into a pre-designed structure and did not represent any of the Ln^{3+}-dependent DNAzymes we obtained so far. Thus, it was chosen for activity analysis. Since Gd2 contains a long stem loop, various truncated mutants were also tested (Figure 5.5B). Improved activity was observed by truncation into Gd2a and Gd2b, but Gd2c has no activity at all. On the basis of Gd2b, the putative base paired region in the green box was elongated to make it more

stable (Gd2b1). However, the changes also abolished the activity, suggesting that these bases might not be paired in the active enzyme. Based on the results, trans-cleaving Gd2b (Figure 5.5C) seems to be the optimal sequence to use for further studies.

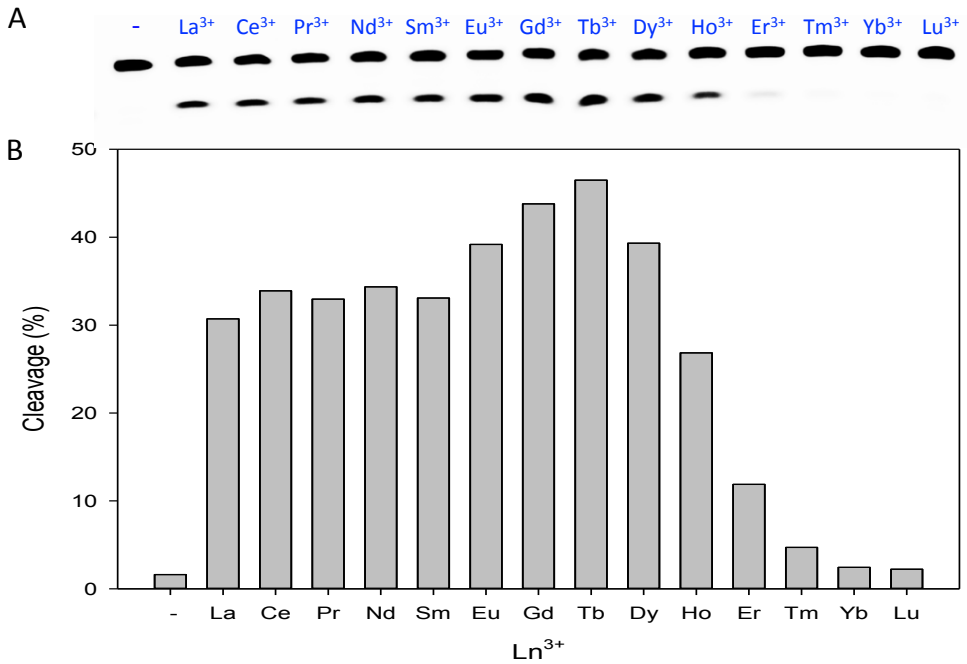

Figure 5.6 Lanthanides selectivity of the Gd2b DNAzyme. A) A gel image of Gd2b cleavage in the presence of 1 μM Ln^{3+} for 1h at pH 6. The first lane is the negative control without added Ln^{3+}. B) Fraction of substrate cleavage in the presence of 10 μM of each Ln^{3+} after 1h reaction.

When incubating with 10 μM lanthanides for 1 h (Figure 5.6), Gd2b had the best activity with Gd^{3+} and Tb^{3+} and was essentially inactive with the two heaviest lanthanides. The activity also dropped slightly for the lighter lanthanides.

Table 5.4 Sequence alignment of the Gd^{3+} selection. The sequences in blue belong to the Ce13 family, and the sequences in green belong to the Lu12 family. The ones in red are similar to Gd2 that was studied in this work. The ones in black are either unable to fold into proper structure or inactive.

Clone #	Sequence (from 5'-end)	
Gd20	CTGCAGAATTCTAATACGAGTCACTATAGGAAGATGGCGAAACA---TG-----GAGCCA	52
Gd25	CTGCAGAATTCTAATACGAGTCACTATAGGAAGATGGCGAAACA---TG-----GAGCCA	52
Gd42	CTGCAGAATTCTAATACGAGTCACTATAGGAAGATGGCGAAACA---TG-----GAGCCA	52
Gd41	CTGCAGAATTCTAATACGAGTCACTATAGGAAGATGGCGAAACA---TG-----GAGCCA	52
Gd39	CTGCAGAATTCTAATACGAGTCACTATAGGAAGATGGCGAAACA---TG-----GAGCCA	52
Gd5	CTGCAGAATTCTAATACGAGTCACTATAGGAAGATGGCGAAACACC-TT-----GAGCCA	54
Gd27	CTGCAGAATTCTAATACGAGTCACTATAGGAAGATGGCGAAACAT--TG-----GAGCCA	53
Gd18	CTGCAGAATTCTAATACGAGTCACTATAGGAAGATGGCGAAACA---TG-----GAGCCA	52
Gd38	CTGCAGAATTCTAATACGAGTCACTATAGGAAGATGGCGAAACA---TG-----GAGCCA	52
Gd22	CTGCAGAATTCTAATACGAGTCACTATAGGAAGATGGCGAAACA---TG-----GAGCCA	52
Gd29	CTGCAGAATTCTAATACGAGTCACTATAGGAAGATGGCGAAACATCCTG-----GAGCCA	55
Gd8	CTGCAGAATTCTAATACGAGTCACTATAGGAAGATGGCGAAACATCTGG-----GAGCCA	55
Gd35	CTGCAGAATTCTAATACGAGTCACTATAGGAAGATGGCGAAACATCTGG-----GAGCCA	55
Gd28	CTGCAGAATTCTAATACGAGTCACTATAGGAAGATGGCGAAACATC-CT-----GAGCCA	54
Gd16	CTGCAGAATTCTAATACGAGTCACTATAGGAAGATGGCGAAACATCTTG-----GAGCCA	55
Gd11	CTGCAGAATTCTAATACGAGTCACTATAGGAAGATGGCGAAACATCTTG-----GAGCCA	55
Gd37	CTGCAGAATTCTAATACGAGTCACTATAGGAAGATGGCGAAACATCTTG-----AAGCCG	55
Gd36	CTGCAGAATTCTAATACGAGTCACTATAGGAAGATGGCGAAACA---TG-----GTGCCA	52
Gd10	CTGCAGAATTCTAATACGAGTCACTATAGGAAGATGGCGAAACATCTAC-----AGGTC-	54
Gd40	CTGCAGAATTCTAATACGAGTCACTATAGGAAGATGGCGAAACATCTTC-----AGGTC-	54
Gd23	CTGCAGAATTCTAATACGAGTCACTATAGGAAGATGGCGAAACATCTTT-----ACG--A	53
Gd34	CTGCAGAATTCTAATACGAGTCACTATAGGAAGATGGCGAAACATCTTT-----ACG--A	53
Gd1	CTGCAGAATTCTAATACGAGTCACTATAGGAAGATGGCGAAACATCTTA-ACG-AG----	54
Gd24	CTGCAGAATTCTAATACGAGTCACTATAGGAAGATGGCGAAACATCTTA-ACG-AG----	54
Gd17	CTGCAGAATTCTAATACGAGTCACTATAGGAAGATGGCGAAACATCTTT-ACG-AG----	54
Gd31	CTGCAGAATTCTAATACGAGTCACTATAGGAAGATGGCGAAACATCTTA-ACG-AG----	54
Gd19	CTGCAGAATTCTAATACGAGTCACTATAGGAAGATGGCGAAACATCTTT-ACG-AGGTC-	57
Gd26	CTGCAGAATTCTAATACGAGTCACTATAGGAAGATGGCGAAACATCTTT-ACG-ACGTC-	57
Gd30	CTGCAGAATTCTAATACGAGTCACTATAGGAAGATGGCGAAACATCTTT-ACG-ACGTC-	57
Gd21	CTGCAGAATTCTAATACGAGTCACTATAGGAAGATGGCGAAACATCTTT-ACG-ACGTC-	57
Gd9	CTGCAGAATTCTAATACGAGTCACTATAGGAAGATGGCGAAACATCTTT-ACG-ACGTC-	57
Gd33	CTGCAGAATTCTAATACGAGTCACTATAGGAAGATGGCGAAACATCTTT-ACG-ACGTC-	57
Gd3	CTGCAGAATTCTAATACGAGTCACTATAGGAAGATGGCGAAACATCTTT-ACG-ACGTC-	57
Gd12	CTGCAGAATTCTAATACGAGTCACTATAGGAAGATGGCGAAACATCTTT-ACG-ACATCC	58
Gd13	CTGCAGAATTCTAATACGAGTCACTATAGGAAGATGGCGAAACATCTTT-ACG-ACATCC	58
Gd6	CTGCAGAATTCTAATACGAGTCACTATAGGAAGATGGCGAAACATCTTG-ACGCATATCG	59
Gd15	CTGCAGAATTCTAATACGAGTCACTATAGGAAGATGGCGAAACATCTTG-ACGCATATCG	59
Gd7	CTGCAGAATTCTAATACGAGTCACTATAGGAAGATGGCGAAACATCTTG-ACGCATATCG	59
Gd14	CTGCAGAATTCTAATACGAGTCACTATAGGAAGATGGCGAAACATCTTG-ACGCATATCG	59
Gd2	CTGCAGAATTCTAATACGAGTCACTATAGGAAGATGGCGAAACATCTTG-ACGCATATCG	59
Gd4	CTGCAGAATTCTAATACGAGTCACTATAGGAAGATGGCGAAACATCTTG-ACGCATATCG	59
Gd32	CTGCAGAATTCTAATACGAGTCACTATAGGAAGATGGCGAAACATCTTTTACAAAG----	56

Table 5.4 Sequence alignment of the Gd^{3+} selection. (Continued)

Clone #	Sequence (from 5'-end)	
Gd20	TAGGTCAAAGGTAGGTGCGGGTCGTATCAT-ATC-GACTAA----GTTATAGTGACGGTA	106
Gd25	TAGGTCAAAGGTAGGTGCGGGTCGTATCAT-ATC-GACTAA----GTTATAGTGACGGTA	106
Gd42	TAGGTCAAAGGTAGGTGCGGGTCGTATCAT-ATC-GACTAA----GTTATAGTGACGGTA	106
Gd41	TAGGTCAAAGGTAGGTGCGGGTCGTATCAT-ATC-GACTAA----GTTATAGTGACGGTA	106
Gd39	TAGGTCAAAGGTAGGTGCGGGTCGTATCAT-ATC-GACTAA----GTTATAGTGACGGTA	106
Gd5	TAGGTCAAAGGTAGGTGCGTGTCGTATCTT-ATC-GGCTAA----GTTATAGCGACGGTA	108
Gd27	TAGGTCAAAGGTAGGTGCGTGTCGTATCAT-ATC-GACTAA----GTTATAGTGACGGTA	107
Gd18	TAGGTCAAAGGTAGGTGCGAGTCGTATCAT-ATC-GACCAA----GTTATAGTGACGGTA	106
Gd38	TAGGTCAAAGGTAGGTGCGGGTCGTGTCTT-ATC-GACTAA----GTTATAGTGACGGTA	106
Gd22	TAGGTCAAAGGTGGGTGCGGGTCGTATCAT-ATC-GACTAA----GTTATAGTGACGGTA	106
Gd29	TAGGTCAAAGGTAGGTGCGGGTCGTATCAT-ATC-GACTAA----GT-ATAGTGACGGTA	108
Gd8	TAGGTCAAAGGTAGGTGCGGGTCGTAT----ATC-GACTAA----GTTATAGTGACGGTA	106
Gd35	TAGGTCAAAGGTGGGTGCGGGTCGTAT----ATC-GACTAA----GTTATAGTGACGGTA	106
Gd28	TAGGTCAAAGGTAGGTGCGGGTCGTATCAT-ATC-GACTA-----GTTATAGTGACGGTA	107
Gd16	TAGGTCAAAGGTAGGTGCG-GTCGTATCAT-ATC-GACTA-----GTTATAGTGACGGTA	107
Gd11	TAGGTCAAAGGTAGGTGCGGGTCGTATCAT-ATC-GACCAG------TATAGTGACGGTA	107
Gd37	TAGGTCAAAGGTGGGTGCGGGTCGTATCAT-ATC-GACCAG------TATAGTGACGGTA	107
Gd36	TAGGTCAAAGGTGGGTGCGAGTCGTATCAT-ATC-GACTA-----GTTATAGTGACGGTA	105
Gd10	TGGGTGCAGGG-AGTTCCGAATCTCTAGAT-GAT-GG-TAC----GAGATAGTGACGGTA	106
Gd40	TGGGTGCAGGG-AGTTCCGAATCTCTAGAT-GAT-GG-TAC----GAGGTAGTGACGGTA	106
Gd23	ACGGTTAAGAAAAGTGACTTATCCAGTGGTTATCTGACTA-----GTGTTAGTGACGGTA	108
Gd34	ACGGTTAAGAGAAGTGGCTTATCCAGTGGTTATCTGACTA-----GTGTTAGTGACGGTA	108
Gd1	----TGTAGAATCTCCCTGAAAGGCAGAATGCAAAGTACAC---GGTTATAGTGACGGTA	107
Gd24	----TGTGGAATCTCCCTGGAAGGCAGAATGCAAAGTACAC---GGTTATAGTGACGGTA	107
Gd17	----TGTAGAATCTCCCTGAAAGGCAGAATGCAAAGTACAC---GGTTATAGTGACGGTA	107
Gd31	----TGTAGAATCTCCCTTAAAGGCAGAATGCAAGGTACAC---GGTTATAGTGACGGTA	107
Gd19	---ATTTGGAGT-TCTGTAAGAAACTCCATGTATCA-AAAC---GGTTATAGTGACGGTA	109
Gd26	--ATCCTAAA----CA-----GGCCATTAAAAAAAGGATATAAGGGTTATAGTGACGGTA	106
Gd30	--ATCCTAAA----CA-----GGCCATTAAAAAAAGGATATAAGGGTTATAGTGACGGTA	106
Gd21	--ATCCTAAA----CA-----GGCCATTAAAAAAAGGATATAAGGGTTATAGTGACGGTA	106
Gd9	--ATCCTAAA----CA-----GGCCATTAAAAAAAGGATATAAGGGTTATAGTGACGGTA	106
Gd33	--ATCCCAAA----CA-----GGCCACTAAAAAAAGGATATAAGGGTTATAGTGACGGTA	106
Gd3	--ATCCTAAA----CA-----GGCCATTAGAAAAGGGATATAAGGGTTATAGTGACGGTA	106
Gd12	GGGGCATGAA----CCTCGATAGCCA-TATATAACGAAT----GGGTTATAGTGACGGTA	109
Gd13	GGGGCATGAA----CCACGATAGCCA-TATATAACGAAT----GGGTTATAGTGACGGTA	109
Gd6	GCGACTAACAAA-TCA----GAGGTGAAGACGATAGCAC------GTGTTAGTGACGGTA	108
Gd15	GCGACTAACAAA-TCA----GAGGTGAAGACGATAGCAC------GTGTTAGTGACGGTA	108
Gd7	GCGACCAACAAA-TCA----GAGGTAAAGACGATAGCAC------GTGTTAGTGACGGTA	108
Gd14	GCGACCAACGAA-ACA----GAGGTAAAGACGATAGCAC------GTGTTAGTGACGGTA	108
Gd2	GCGACCAATAAAATCA----GAGGTAAAGACGATAGCAC------GTGTTAGTGACGGTA	109
Gd4	GCTACCAATAAAACCA----GAGGT-AAGGCGATAGCAC------GTGTTAGTGACGGTA	108
Gd32	----TGCAAA---CCAGGCTGAGAAACAGCGTGGCA-ATACTACGGTTATAGTGACGGTA	108

5.2.4 Re-evaluating Ln^{3+}-specific DNAzyme sequences

Although only five Ln^{3+} selections were mentioned in detail in this thesis, a total of 14 independent selections were actually performed. For each selection, nearly 40 well-aligned sequences were obtained. While analyzing each of those sequences, we noticed sequence similarity across the different selections, prompting us to align them together. There are 336 sequences from the N_{50} library and 135 from the N_{35} library. These sequences are well mixed, which is a strong indication of chemical similarity across the lanthanides. In other words, the same DNAzymes are active with different lanthanides. Based on the alignment and extensive

activity tests, five types of enzymes with distinct structures, and more importantly, different activity patterns across the lanthanides (Figure 5.7A) were identified.

The occurrence of the DNAzymes was plotted in Figure 5.7B. Lu12 is a dominating sequence, representing more than 50% of the final selection libraries. It appears in both the N_{35} and N_{50} selections. Tm7 is featured by a long stretch of unpaired nucleotides in the substrate near the cleavage site. The enzyme has a very simple loop structure and it is only observed from the N_{35} selections. Gd2 was only selected from the N_{50} library, and Dy10 appeared only twice in the Dy^{3+} selection. A close examination reveals that Gd2 only appeared in the Tb^{3+} and Gd^{3+} selections; while Tm7 only appeared in the Ho^{3+}, Er^{3+} and Tm^{3+} selections. Ce13 is a very popular sequence in the N_{50} library selections, representing ~30% of the sequences. This enzyme has similar activity for all the lanthanides, explaining its widespread existence. Surprisingly, it did not show up even once in the five N_{35} selections, although the last five metals cleave Ce13 just as well. Therefore, the library design has a strong influence on the outcome of the selection result.

Their gel-based activities are in Figure 5.8B. Tm7 activity peaks with Ho^{3+} and Er^{3+}, descending on each side; while Gd2b peaks with Gd^{3+} and Tb^{3+}. Dy10a has a quite complex activity pattern with multiple peaks. We previously reported Ce13d based on a Ce^{4+} selection.[1] It has similar activity for all the lanthanides, which is less useful for distinction within this group but very important for separating lanthanides from other metals. It may also serve as a general calibration for quantification.

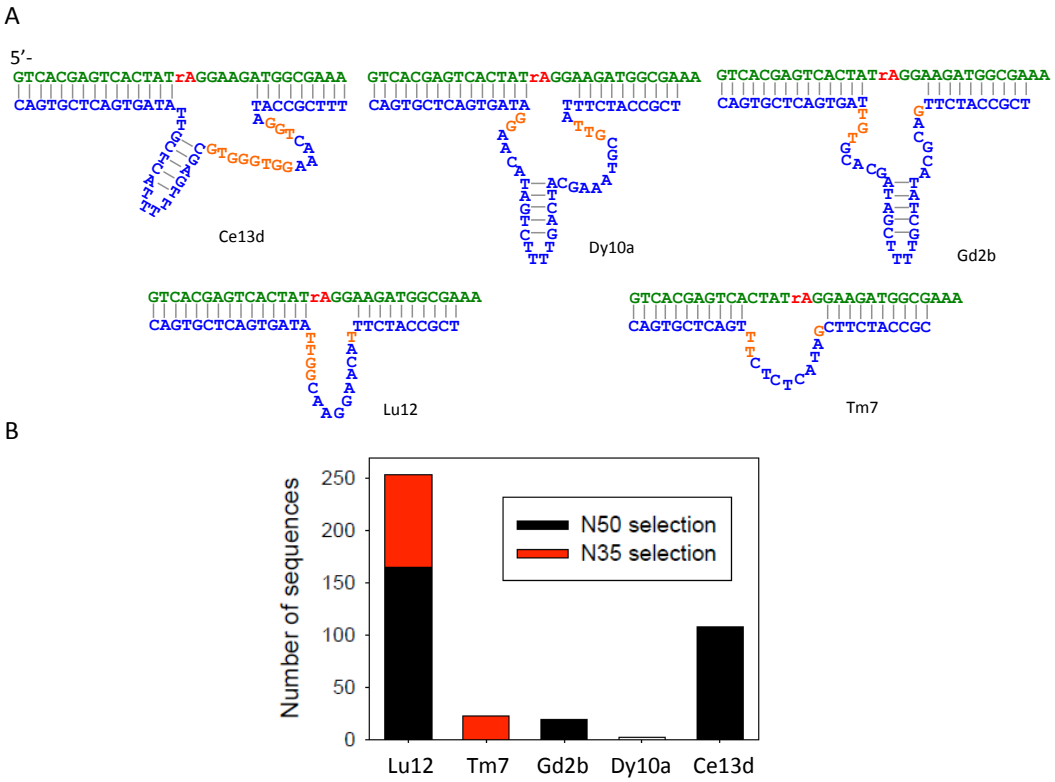

Figure 5.7 Secondary structure of the five representative Ln^{3+}-dependent DNAzymes. A) Optimized secondary structures of the five DNAzymes used in this work. (B) The number of DNA sequences belonging to each family from the selections.

5.2.5 Lanthanide sensor array

Since no enzyme showed absolute selectivity for any particular lanthanide, we aim to employ an alternative approach to develop a pattern-recognition-based array mimicking the human nose.[225] For batch analysis, the experiments were conducted based on an FRET design. The 3′-terminus of the substrate strand was labeled with a FAM fluorophore and the 5′-terminus of the enzyme strand was labeled with a dark quencher (Figure 5.8A).[193] In the absence of target metal ion, hybridization caused the fluorophore and quencher to come in close proximity and the fluorescence was quenched. Once the metal ion induced the cleavage of the substrate strand, the dissociation of substrate fragments and the enzyme strand led to fluorescence enhancement. First, we measured the sensor response to 16 divalent and trivalent metals with a positive

lanthanide control included in the assays (Figure 5.9A-E). Since Sc^{3+}, Y^{3+} and Ln^{3+} are collectively called rare earth metals, they share similar properties. It was not surprising that Y^{3+} is active since it has the same size as Ho^{3+}. On the other hand, Sc^{3+} has a much smaller size. Thus, this could explain why none of these DNAzymes was active with Sc^{3+}. Pb^{2+} is the next popular interfering ion that displayed activity with Lu12, Gd2b and Ce13d. In addition, Hg^{2+} showed moderate activity with Dy10a and its signal only appears in a narrow concentration range. Overall, all these DNAzymes have excellent selectivity for lanthanides.

Next, the sensor response to each lanthanide was studied (Figure 5.9F-J). The initial slope of the traces was extracted and the activity patterns (Figure 5.8C) are quite similar to those obtained using gel electrophoresis (Figure 5.8B). This indicates that the sensor signal is the direct result of the cleavage reaction. For each sensor, concentration-dependent response was measured with one of the most active lanthanides (Figure 5.9K-O). From these kinetic traces, the initial slope was plotted (Figure 5.9P-T). All the other sensors possess low nM sensitivity. It is interesting to note that Lu12 and Ce13d appear to bind to one metal, while Tm7, Gd2b and Dy10a show sigmoid responses. In particular, the Hill coefficient for Gd2b for Gd^{3+} binding reached ~4 and Dy10a for Ho^{3+} reached ~3, suggesting cooperative binding to multiple lanthanide ions for catalysis. This type of cooperative response has been seen in engineered aptazymes and riboswitches,[226,227] but is not common for metal-dependent DNAzymes. Polynuclear lanthanide complexes have been shown to facilitate nucleic acid hydrolysis,[160] and similar mechanisms might work in these DNAzymes. A close examination of the different DNAzymes suggests the importance of guanine and thymine in catalysis. The highly conserved *G* and *T* bases are highlighted in orange in Figure 5.7A. The different ways of arranging these nucleotides might be the reason for their unique activity patterns across the lanthanides.

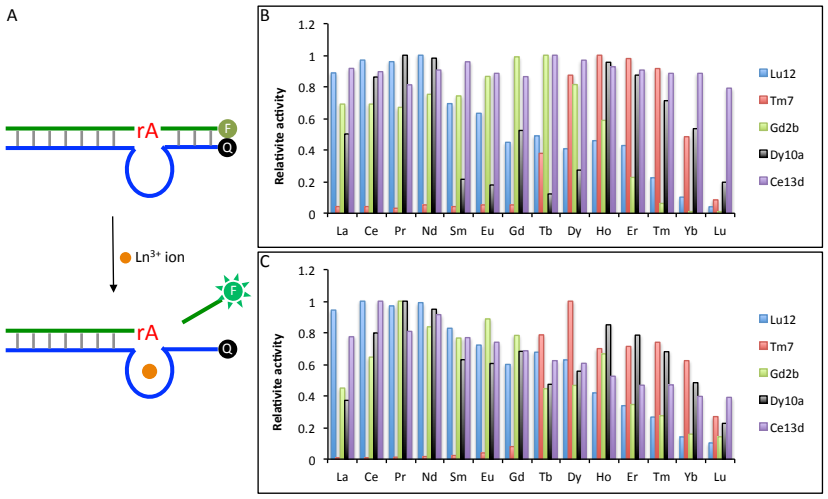

Figure 5.8 Lanthanides selectivity of the five DNAzymes. A) Schematics of DNAzyme beacon for Ln^{3+} detection. Relative activities of the five DNAzymes for different lanthanides using gel-based B) or sensor-based C) assay.

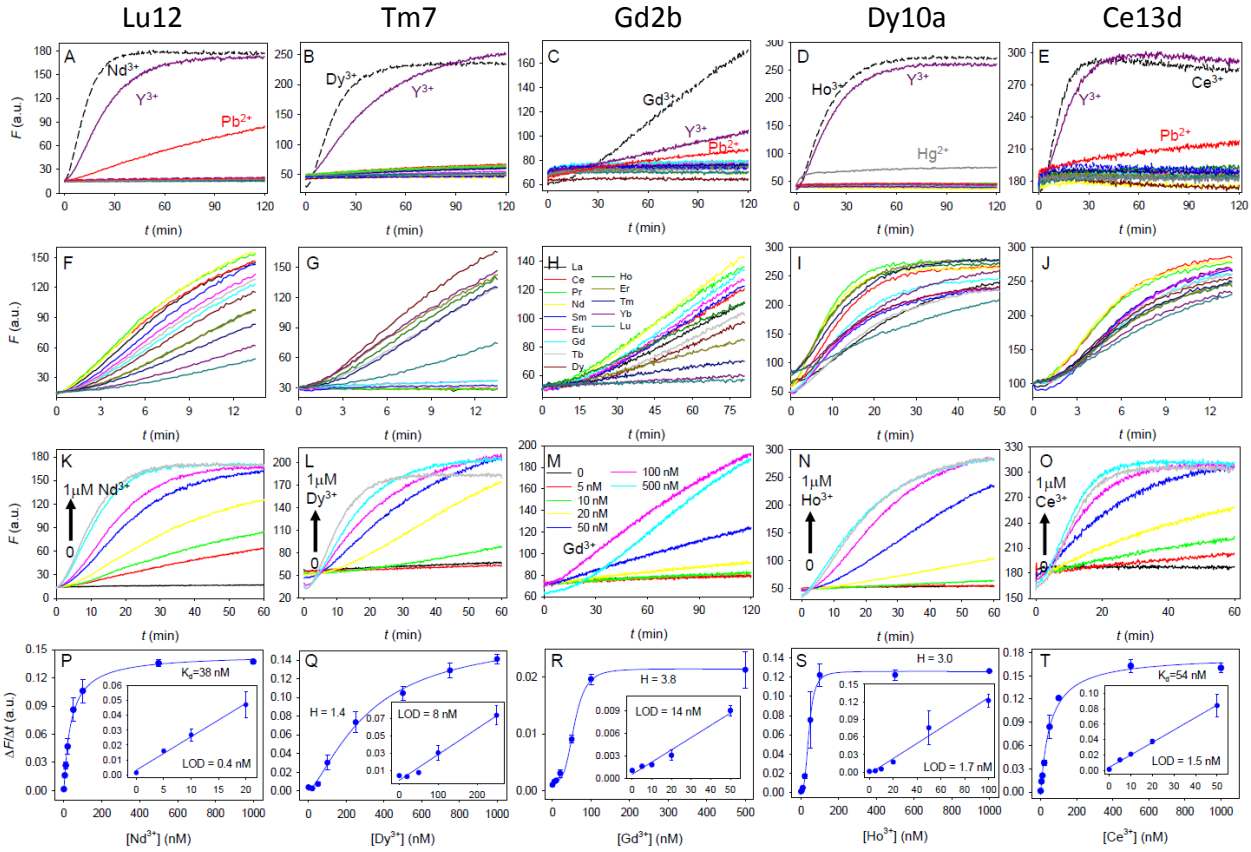

Figure 5.9 Complete metal selectivity and sensitivity characterization for the five sensors. The sensor names are on the top of each column. A-E) Sensor response to non-lanthanide metals; a positive control with an active lanthanide is also included. The tested competing metal ions (500 nM) include Mg^{2+}, Mn^{2+}, Co^{2+}, Cu^{2+}, Zn^{2+}, Sr^{2+}, Cd^{2+}, Hg^{2+}, Pb^{2+}, Al^{3+}, Sc^{3+}, Fe^{3+}, Ga^{3+}, Y^{3+}, In^{3+}, and Tl^{3+}. F-J) Sensor response to the 14 lanthanides; they share the same legend in (H). K-O) Sensor response to various concentrations of a particular lanthanide. P-T) Sensor calibration curves. Insets: the linear region at low lanthanide concentrations. The limit of detection (LOD), K_d or Hill-coefficient values are marked in the figures.

Based on the above assay, these DNAzymes can separate lanthanides from most other metals. It might even be possible to distinguish between different lanthanides. We picked the linear region within the first 10 min for the four faster enzymes to obtain the rate of fluorescence enhancement, while the slope of the slower Gd2b was calculated at around 40 min. We chose to use a metal ion concentration of 500 nM to achieve a fast and stable rate. The current data have five dimensions based on the sensors. To reduce dimension, linear discriminant analysis (LDA) was performed on the 14 lanthanides using 12 sets of training data. With this, a canonical score plot was obtained (Figure 5.10A). Remarkably, the lanthanides are separated into two groups: the first seven light lanthanides and the last seven heavy ones located on the each side of the dashed line, where the canonical variable 1 is zero. Using these LDA parameters, the positions of other metals were calculated (Figure 5.10B). Y^{3+} itself is sitting at the top right, while Pb^{2+} and other metals stand at the bottom left. Both are well separated from the lanthanides. However, separation for each lanthanide was not that obvious based on Figure 5.10A. This can be further improved by reducing the group size. A reasonable way to do this is to first determine whether the metal is a light or heavy lanthanide based on Figure 5.10A. Once it is identified, a second plot is used for its further identification. For example, a clear separation was achieved (except Dy^{3+} and Tb^{3+}, which are right next to each other) by using just the seven heavy lanthanides. It is interesting to note that those spots are arranged in a counter-clockwise order according to the atomic number of the lanthanides. The light lanthanides are also better separated within its own group after monitoring the signal of Tm7 for a longer time.

The next question is the distinction of mixed lanthanides. In principle, we may provide additional training data sets for the sensor array. On the other hand, it is difficult to experimentally prove generality. For example, a mixture of two lanthanides gives 91 possibilities

and a mixture of three lanthanides would be 364 possibilities. If the different concentrations are further considered, the possibility becomes infinite. For this initial work, our focus was on the feasibility of differentiating individual lanthanides.

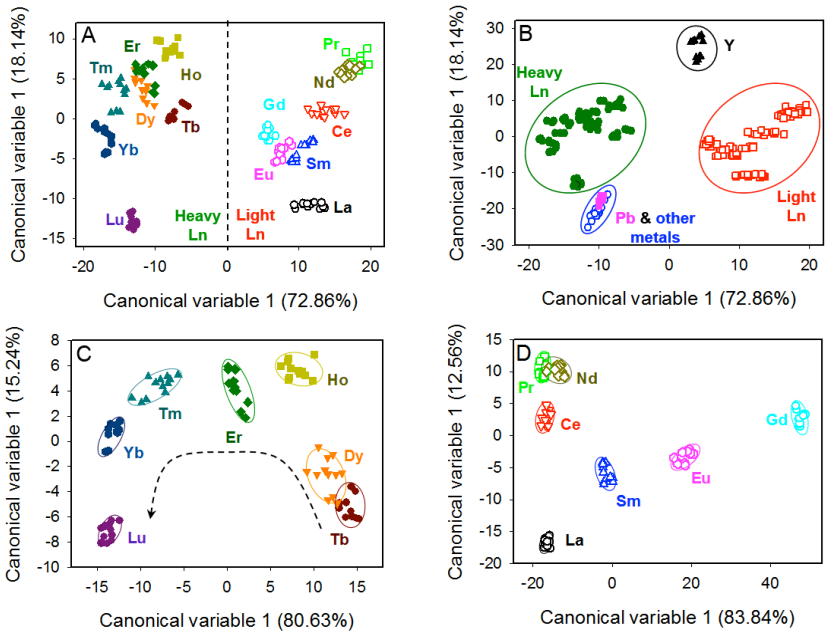

Figure 5.10 Linear discriminant analysis of the lanthanides based on the DNAzyme sensors. A) Canonical score plot based on the sensor array for the 14 lanthanides. Light and heavy lanthanides are separated by the dashed line. B) Using the parameters obtained in (A), the positions of other elements are calculated and plotted. Canonical plots of the seven heavy lanthanides C) and light lanthanides D). In (D) the data for Tm7 is from 40 min instead of 10 min to increase separation.

5.3 Summary

In summary, total of 14 *in vitro* selections with each trivalent lanthanide were conducted. Out of the 471 sequences, five DNAzymes with distinct activity patterns across the lanthanide series were obtained and characterized. A common fluorescent sensor design strategy was used, producing low nM sensitivity with excellent selectivity for lanthanides. Four of these enzymes have strong lanthanide-size dependent activity, allowing the production of an array-based sensor to distinguish each lanthanide. In addition, this study showed that DNA bases can detect the subtle differences of these very similar ions and suggesting a DNA-based separation method for

lanthanide purification and other applications is possible.

5.4 Materials and Methods

5.4.1 Chemicals

The lists of chemicals used in this chapter can be found in Chapter 2 section 2.4.1.

5.4.2 *In vitro* selection

The methods for *in vitro* selection, PCR, cloning and sequencing were previously described in Chapter 2. The only difference was that the metal ion used to induce cleavage was Dy^{3+} and Gd^{3+}. In the 6th round of Dy^{3+} selection, 5 μM of Dy^{3+} was added every 30 min for a total of 1 h incubation. For the last round of Gd^{3+} selection, 50 μM of Gd^{3+} was added twice with 1 h interval.

5.4.3 Gel-based assays

DNAzyme activity assays were performed with the FAM-labeled substrate (Sub-FAM, 0.7 μM) and Dy10a enzyme (1.1 μM). The DNAzyme complex was annealed in buffer A (50 mM MES, pH 6.0, 25 mM NaCl) before metal ions were added to initiate the cleavage reaction. For pH-dependent studies, the MES and MOPS buffers (50 mM with 25 mM NaCl) were used. The reaction products were separated on a denaturing polyacrylamide gel (dPAGE) and analyzed using a Bio-Rad ChemiDoc MP imaging system.

5.4.4 Sensor assay

For a typical gel-based activity assay, a final of 10 μM metal ions were incubated with 5 μL of 1 μM DNAzyme complex in buffer A for 1 h. The complex was formed by annealing the

FAM-labeled substrate and the enzyme in buffer A. The samples were quenched with 8 M urea and run in 15% dPAGE at 120 V for 80 min. The gel images were taken with Bio-Rad ChemiDoc MP imaging system. The kinetics studies were carried out using low binding half-area black 96 well plates using a microplate reader (SpectraMax M3). The stock complex was formed by annealing the FAM-labeled substrate and the quencher-labeled enzyme with molar ratio of 1:1.5 in buffer A. Each complex was further diluted with various concentrations of HEPES (pH 7.6). The buffer conditions were individually optimized for each sensor, and the following HEPES conditions were used for Lu12 (1 mM), Tm7 (10 mM), Gd2b (10 mM), Dy10a (10 mM), and Ce13d (50 mM). 100 μL of 50 nM DNAzyme complex was used for each well. 1 μL of target ions was added after 5 min of background reading. The samples were continuously monitored after addition for at least 30 min with 25 s intervals.

For each DNAzyme sensor, four replicates of detection were carried out using 500 nM of each lanthanide. The slope in the initial linear region was calculated for each kinetic trace. To account for the timing difference in the metal addition and reading, the slope was also calculated by offsetting for 25 sec. The data were analyzed using the Canonical Discriminant Analysis software from Origin. The results were validated by using the obtained parameters to predict the data set positions.

Chapter 6. Detecting Thiophilic Metal Ions Collectively and Individually with Phosphorothioate-Modified DNAzymes[d]

6.1 Introduction

Cadmium, mercury and lead are three heavy metal contaminants commonly found in the environment. Unlike some other essential metal ions, these metals have no useful functions in biological organisms. Bio-accumulation of these metal ions can cause many health issues such as neurological diseases and organ damage.[24,228] Because of their high toxicity, they were collectively banned by the European Union according to the Restriction of Hazardous Substances Directive set in 2006. Since then, many countries have also taken similar regulations. To enforce such regulations and to prevent their adverse environmental and health effects, an emphasis has been made on developing analytical strategies with higher sensitivity. The current standard method for element analysis relies heavily on inductive-coupled plasmon-mass spectrometry (ICP-MS). Even though the method is highly reliable, it is available only in centralized labs with a high cost and long turnaround time. In order to provide on-site analysis, a number of metal sensing platforms have been developed. [138,139,228-235]

DNAzymes are DNA-based catalysts obtained through *in vitro* selection and their catalytic activities usually require metal cofactors to function.[79,162-165] Owing to their high catalytic efficiency and versatility in sensor design, RNA-cleaving DNAzymes have emerged as a unique metal sensing platform.[43,163,191,236-238] By using specific metals during selection, RNA-

[d] This chapter is the basis for a published manuscript: Huang, P. J.; Liu, J. Sensing Parts-per-Trillion Cd2+, Hg2+, and Pb2+ Collectively and Individually Using Phosphorothioate DNAzymes. *Anal. Chem.* **2014**, *86*, 5999-6005.

cleaving DNAzymes selective for Mg^{2+},[79] Pb^{2+},[78,193] UO_2^{2+},[86] and trivalent lanthanide ions (Ln^{3+})[87] have been reported. However, all these metals are considered as hard or borderline Lewis acids.

High thiophilicity is a common feature of many toxic metals including cadmium and mercury. Since natural DNA does not contain sulfur, it has been difficult to use unmodified DNA to select DNAzymes with high specificity and selectivity for them. By incorporating modified bases with soft base ligands like imidazole, Zn^{2+} and Hg^{2+} dependent DNAzymes were also isolated.[79,239] However, their analytical applications have been limited due to the poor availability of these modified bases. In addition, using modified bases also complicates the *in vitro* selection since DNA polymerase may not incorporate such bases during the amplification steps. Phosphorothioate (PS) DNA refers to replacement of one of the non-bridging oxygen atoms in the phosphate backbone with a sulfur atom (Figure 6.1A). Traditionally, the PS modification is often used in the antisense technology to increase DNA stability against nuclease degradation.[240] It is also useful for studying the mechanism of (deoxy)ribozyme catalysis,[134,216,241,242] assembling nanoparticles,[243] and forming DNA structures.[244] However, PS-modified RNA-cleaving DNAzymes have not yet been systematically studied.

In the previous chapter, a highly sensitive Ln^{3+}-dependent DNAzyme named Ce13d was reported.[87] Because of the chemical similarity between trivalent Ln^{3+} and Y^{3+}, Ce13d also displayed similar activity in the presence of Y^{3+}. When incubating with other non-rare earth metal ions, only Pb^{2+} showed moderate activity. Since Ln^{3+} are hard Lewis acids that prefer oxygen-based ligands, it is feasible to convert to a thiophilic-metal-dependent enzyme by simple PS modification. In this chapter, the first PS-modified DNAzyme that can detect low nM concentration of Hg^{2+}, Cd^{2+} and Pb^{2+} as a group and individually is reported.

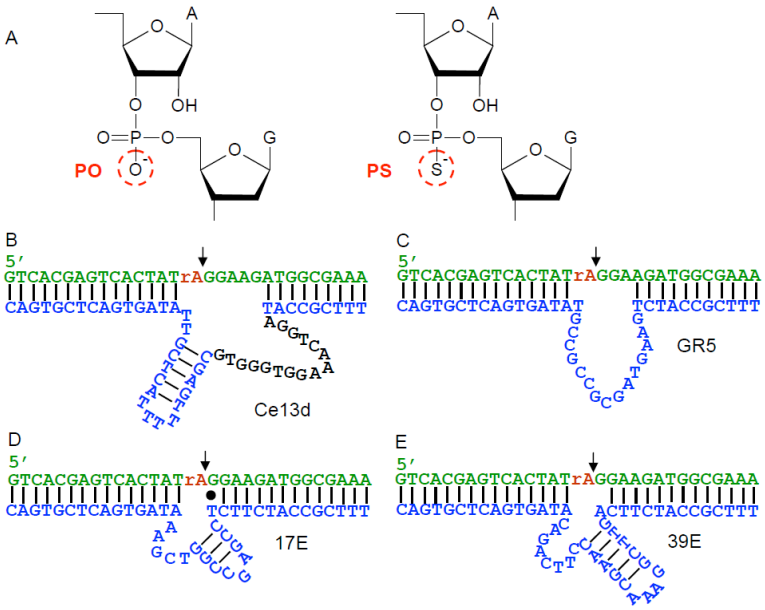

Figure 6.1 Secondary structure of the Ce13d, GR5, 17E, and 39E DNAzymes. A) Structure of the normal phosphodiester (PO) linkage and the phosphorothioate (PS) modification at the cleavage junction (rA-G). Secondary structures of the four DNAzymes used in this work: B) Ce13d; C) GR5; D) 17E; and E) 39E.

6.2 Results and Discussions

6.2.1 PS modification of substrate strand

In Figure 6.1B, the Ce13d DNAzyme complex contains a chimeric substrate strand with a single ribo-adenosine (rA) being the designated cleavage site (pointed with arrowhead). The bottom strand colored in blue/black is the enzyme. With a Ln^{3+}, the substrate is cleaved into two fragments. A FAM (carboxyfluorescein) was labeled at the 3'-end of the substrate for cleavage quantification. A gel-based assay was performed with the first row divalent transition metal, group 2B ions, Mg^{2+}, Pb^{2+} and Ce^{3+}. Ce^{3+} was included to represent Ln^{3+}. With the normal phosphate oxygen (PO) substrate, Ce13d only showed activity with Ce^{3+} and Pb^{2+}. When a single PS modification took place at the linkage between rA and G (Figure 6.1A), the Ce^{3+}-dependent activity was considerably suppressed. The cleavage went from ~70% down to ~5%. At the same time, significant amount of cleavages were observed with thiophilic metals such as Cu^{2+}, Cd^{2+},

Hg^{2+} and Pb^{2+}. Besides some noticeable cleavages that were observed with Fe^{2+} and Zn^{2+}, all other metals remained inactive. The influence of the PS modification on shifting the metal preference was clearly demonstrated.

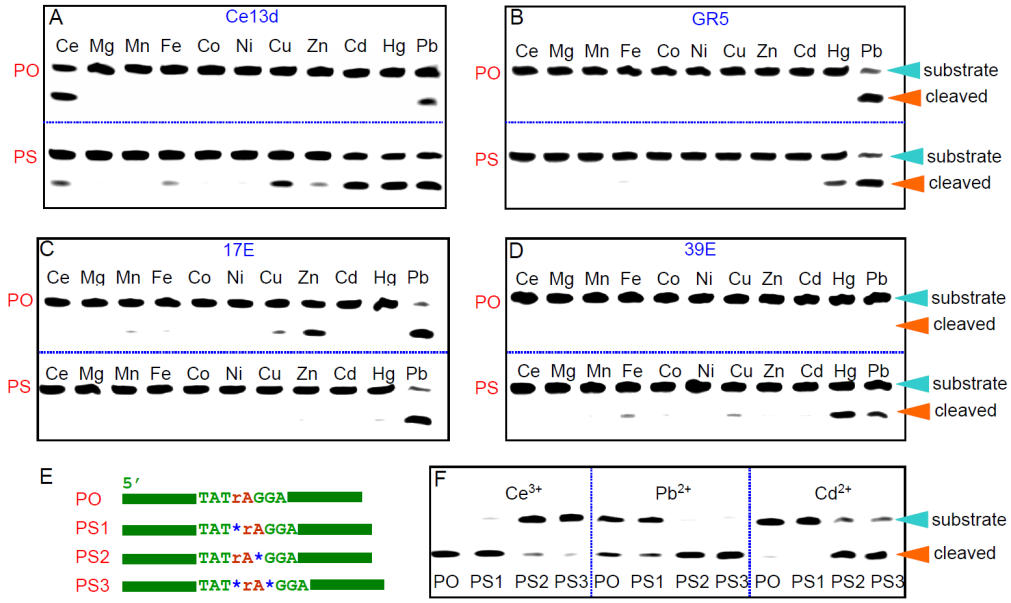

Figure 6.2 Enzymatic activity of the Ce13d, GR5, 17E, and 39E DNAzymes with PS-modified substrate in the presence of various metal ions. A-D) Gel images of the four DNAzymes with different metal ions and PO or PS (PS2 in (E)) substrate. E) Schemes of the substrate with different sites of the PS modification (denoted by the blue stars). F) Gel image of the four substrates with the Ce13d DNAzyme in the presence of different metal ions. For all the gels, the DNAzyme concentration was 1 μM and metal concentration was 10 μM. Reaction time was 30 min.

The PS modified substrate described above was named PS2. To further understand the effect of PS modification on the substrate strand, a few control substrates were also tested (Figure 6.2E). Thus, either a PS was placed on the neighboring linkage (PS1) or dual PS modifications were introduced on both sides of rA (PS3). Three metals were tested against the Ce13d for activity (Figure 6.2F). The results showed that PS1 behaved very similarly to the original PO substrate, indicating that the PS modification at this site has no effect. On the other hand, PS3 showed similar activity as PS2, therefore implying that metal coordination to the phosphate at the cleavage site (Figure 6.1A) is crucial. In this case, even though the Ce^{3+} activity was suppressed with the PS2 substrate, the DNAzyme activity can be restored with addition of

thiophilic metal ions. From the analytical standpoint, combination of Ce13d DNAzyme with PS2 substrate becomes a useful probe for detecting these toxic metals as a group.

6.2.2 PS modification of enzyme strand

In the previous chapter, the studies identified the loop region (Figure 6.1B, in black) in the Ce13d are highly conserved and crucial for activity.[87] To test whether any of these phosphates are involved in metal binding, each linkage was systematically modified (Figure 6.3A). Including the unmodified Ce13d, a total of 16 variants were tested. Interestingly, in all the cases, Ce^{3+} and Pb^{2+} showed similar activity (Figure 6.3B & D), while Cd^{2+} was completely inactive (Figure 6.3C).

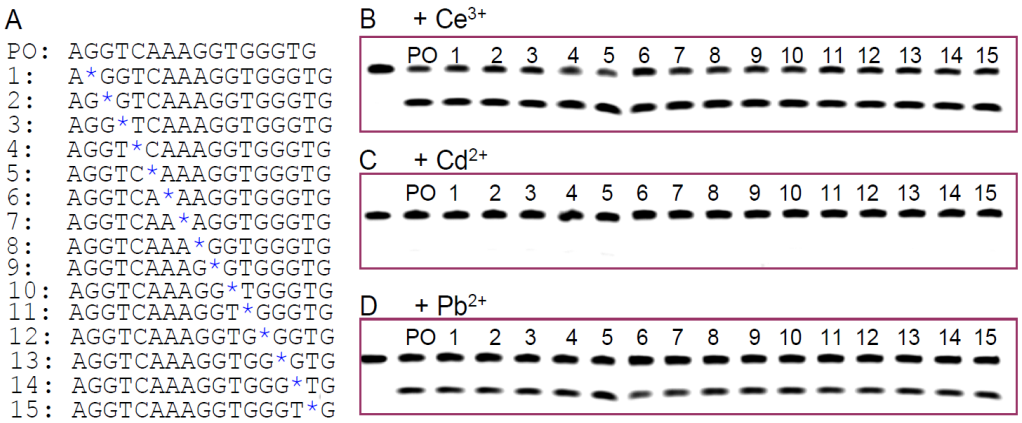

Figure 6.3 Enzymatic activity of the PS-modified Ce13d DNAzyme with PO substrate in the presence of Ce^{3+}, Cd^{2+}, or Pb^{2+}. A) The enzyme loop sequence of Ce13d (the nucleotides in black of Figure 1B) and the sites of PS modification (blue stars). In this assay, the normal PO substrate was used for reference. Gel images of the 16 Ce13d-based enzyme assays (the first lanes are the substrate alone, the second lanes are with the normal all PO enzyme and the rest are the PS modified) with B) Ce^{3+}, C) Cd^{2+} or D) Pb^{2+}. The reaction time was 1 h.

Based on the cleavage quantification shown in Figure 6.4, the metal is more likely to bind to the nucleobases than the phosphates backbone in the enzyme loop. In this particular DNAzyme, the loop is rich in guanine and adenine. Both nucleobases are known to be good ligands for lanthanides.[179,180] Overall, the PS modification at the cleavage junction has the largest effect in shifting metal preference.

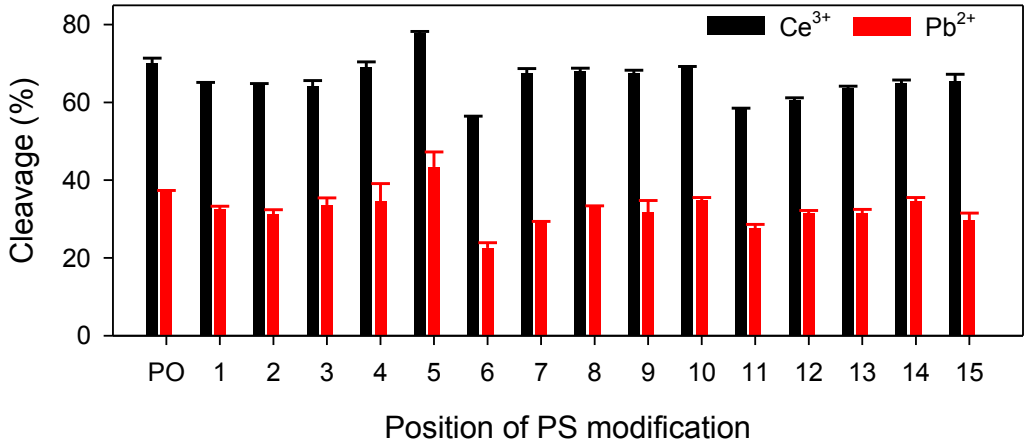

Figure 6.4 Quantification of the PS-modified cleavage activity at different positions of the enzyme loop. Data for Ce^{3+} and Pb^{2+} are shown while Cd^{2+} is completely inactive.

6.2.3 PS modification of existing DNAzymes

Although thiophilic metals as a group can be easily detected by PS-Ce13d DNAzyme complex, this analytical method would be even more valuable if selectivity within this group can be achieved. Cd13d was the latest example of the continuous expanding DNAzyme family. A few other metal-specific DNAzymes were already known and were well characterized. Based on the interesting results from Cd13d, PS modifications on these known DNAzymes may produce different metal binding patterns to improve selectivity. The first ever reported DNAzyme is called GR5 (Figure 6.1C).[78] This DNAzyme is only active with Pb^{2+}.[115] Then there are the famous 17E (Figure 6.1D) and 10-23 DNAzymes.[79] The 10-23 DNAzyme was recently suggested to be one of the 17E mutants.[126,245] The 17E DNAzyme has been selected by a number of different labs under different selection conditions and is active with many different metal ions including Pb^{2+}.[78,81,83,85,246] The 39E DNAzyme is highly specific for UO_2^{2+} (Figure 6.1E).[86,146,148] The four examples in Figure 6.1 represent the main independent and well characterized metal-specific DNAzymes reported so far.[247,248]

In Figure 6.2B, PO substrate with GR5 indeed only showed cleavage in the presence of Pb^{2+}. When the PS2 substrate was used instead, the enzyme also becomes slightly active with Hg^{2+}. With just this pair of DNAzymes, Pb^{2+} and Hg^{2+} can be easily identified. The 17E DNAzyme is the most active with low concentration of Pb^{2+}. However, Zn^{2+} and Cu^{2+} can also induce some cleavage (Figure 6.2C).[81,125,193] Interestingly, PS-17E becomes even more selective for Pb^{2+} then Zn^{2+}. Not surprisingly, none of the tested metal ions was active with the PO substrate since 39E is highly selective for UO_2^{2+}. However, the enzyme showed moderate activity with Hg^{2+} and Pb^{2+} when formed a complex with the PS substrate.

Therefore, Ce13d is a unique DNAzyme that can be activated by all thiophilic metal ions with the PS substrate. All the other DNAzymes are only active with Pb^{2+} and Hg^{2+} under the same conditions. It is likely that Ce13d has a general metal binding site that is not available in other DNAzyme.

6.2.4 Metal sensor array

With the above results, a sensor array was engineered (Figure 6.5A) to individually detect Cd^{2+}, Hg^{2+}, and Pb^{2+}. Based on the activity of Ce13d (Figure 6.5B), the metal ions can be first separated in three groups. If the enzyme displayed no activity with both the PO and the PS substrate, the sample might contain monovalent metals or only the first row transition metals. Noted that Cu^{2+} and Zn^{2+} were included in this group based on the subsequent biosensor assays (Figure 6.5B, *vide infra*). If the enzyme is more active with the PO substrate, the metal is likely to be Ln^{3+} or Y^{3+}. On the other hand, if the enzyme is more active with the PS substrate, the sample contains the three toxic metals (Cd^{2+}, Hg^{2+}, and Pb^{2+}). Subsequently, Pb^{2+} and Hg^{2+} can be identified based on the GR5 DNAzyme response. After ruling out these two, the only one left is Cd^{2+}. 17E and 39E were not included in the array because the information they provided was

redundant. The key component in this system is Ce13d; the activity pattern it provided can quickly separate the metals into three groups.

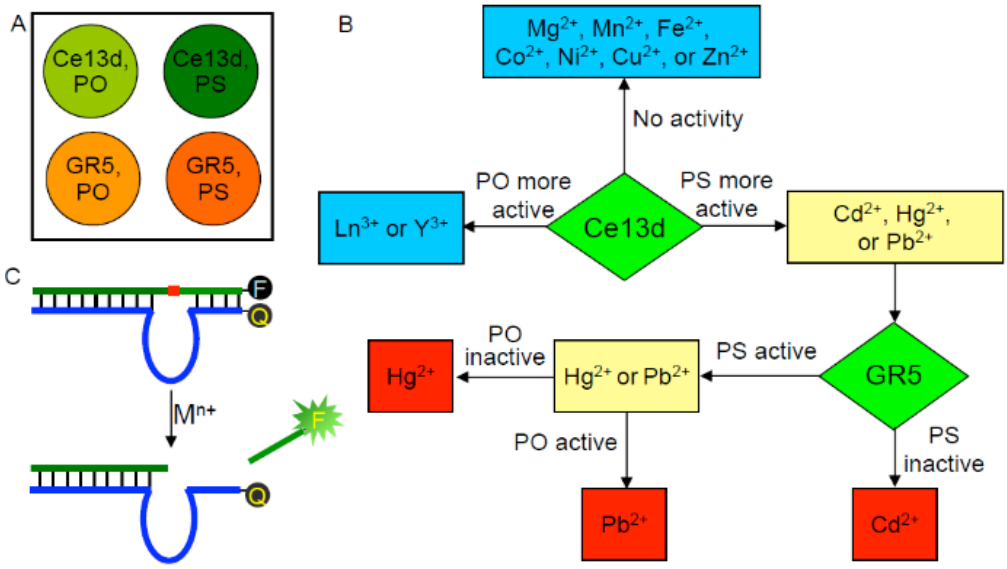

Figure 6.5 A design scheme of detecting thiophilic metal ions using PO- or PS-modified Ce13d and GR5. A) A scheme of the four-component sensor array. B) A flow chart of detecting Hg^{2+}, Pb^{2+} and Cd^{2+} based on the Ce13d and GR5 DNAzymes and the PO and PS substrates. The metal ions are categorized based on their sensor response. C) Schematics showing the DNAzyme beacon sensor design.

The above assays were based on gel electrophoresis using 10 μM metal ions. To expedite the analysis, these DNAzymes were converted to "turn-on" fluorescence biosensors. First, the beacon complex was formed by hybridizing a quencher labeled enzyme with a FAM-labeled substrate (Figure 6.5C). In the absence of metal ions, the beacon showed lower background signal due to fluorescence quenching. Fluorescence enhancement was observed over time after metal ions addition. With 500 nM metal, the response of the PO-Ce13d sensor is shown in Figure 6.6A. In this concentration, only Ce^{3+} and Pb^{2+} showed activity, which is consistent with the gel-based assay. The initial slope of the kinetic trace is plotted in Figure 6.6C. To evaluate this sensing array more closely, three metal concentrations from 50 nM to 5 μM were used. By using a rate of 0.05 unit as cut-off point, only Ce^{3+} showed response in all three concentration. With

the Ce13d/PS sensor, Cd^{2+}, Hg^{2+} and Pb^{2+} showed the highest response (Figure 6.6B), which is also consistent with the gel-based assay. Interestingly, Cu^{2+} was more active in the gel assay than Ce^{3+} but has the similar responses in sensor platform. This is likely due to the fluorescence quenching effect of Cu^{2+}. With PS-Ce13d, only Cd^{2+}, Hg^{2+} and Pb^{2+} were active with a cut-off value of 0.05. By subtracting the PO response from the PS data, a clear separation of the three groups can be observed: Ce^{3+} as one group, Cd^{2+}, Hg^{2+} and Pb^{2+} as the second group and the rest being the third (Figure 6.6E). This classification is consistent with the previous one illustrated in Figure 6.5B.

With the PO-GR5 sensor, only Pb^{2+} was active with 0.1 unit as the cut-off point (Figure 6.6F). With the PS-GR5 sensor and 0.02 as the cut-off point (Figure 6.6G), both Hg^{2+} and Pb^{2+} became active. It should be noted that Hg^{2+} induced significant quenching at 5 μM and appeared inactive from the sensors (Figure 6.7).

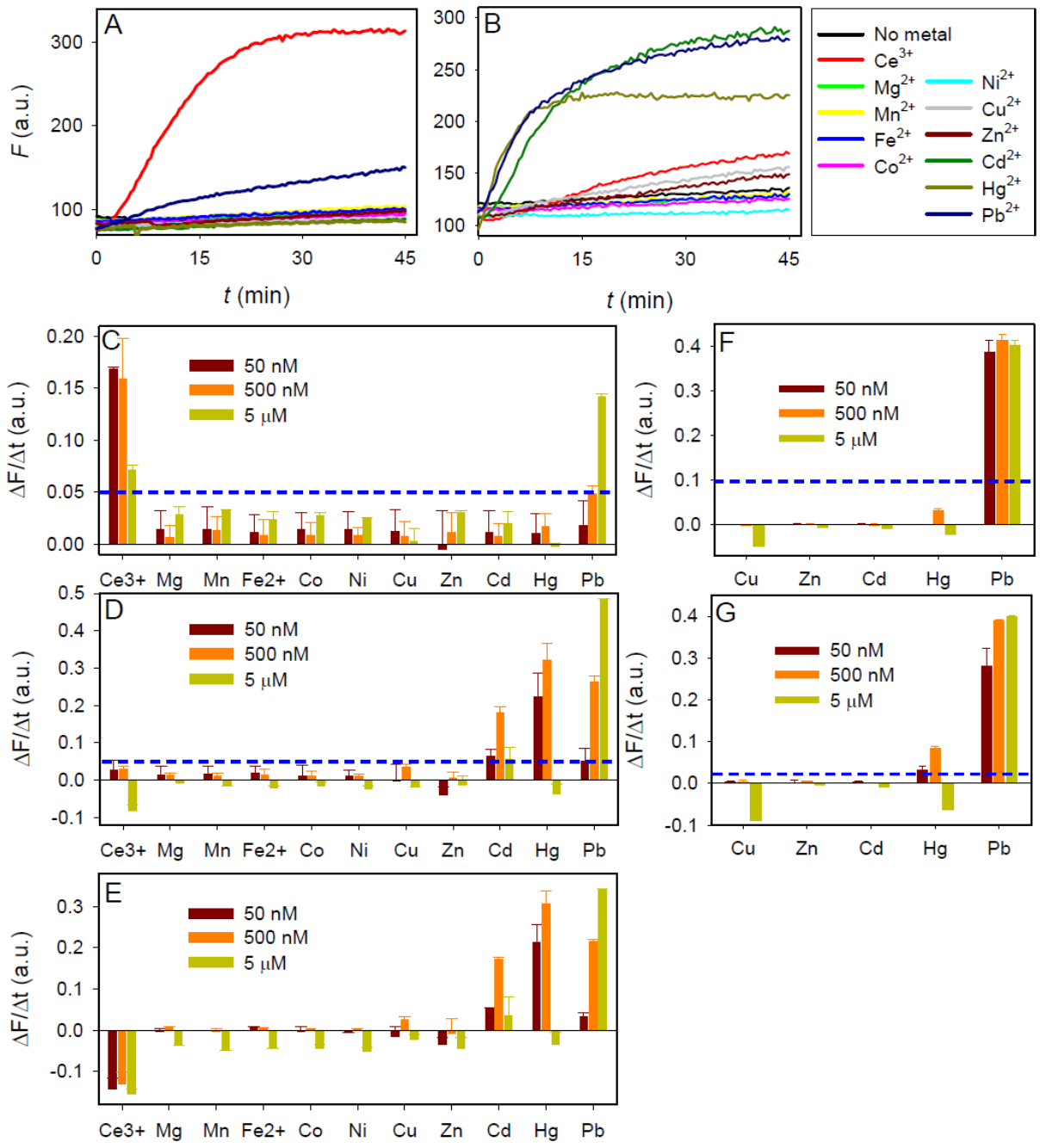

Figure 6.6 Sensor signaling kinetic traces with different metal ions using the PO-Ce13d A) or PS-Ce13d B) as sensor. Quantification of the rate of fluorescence increase with various concentrations of different metal ions with the PO-Ce13d sensor C) or PS-Ce13d sensor D), and their difference E). Rate of fluorescence increase with various concentrations of different metal ions with the PO-GR5 F) or PS-GR5 G) sensor.

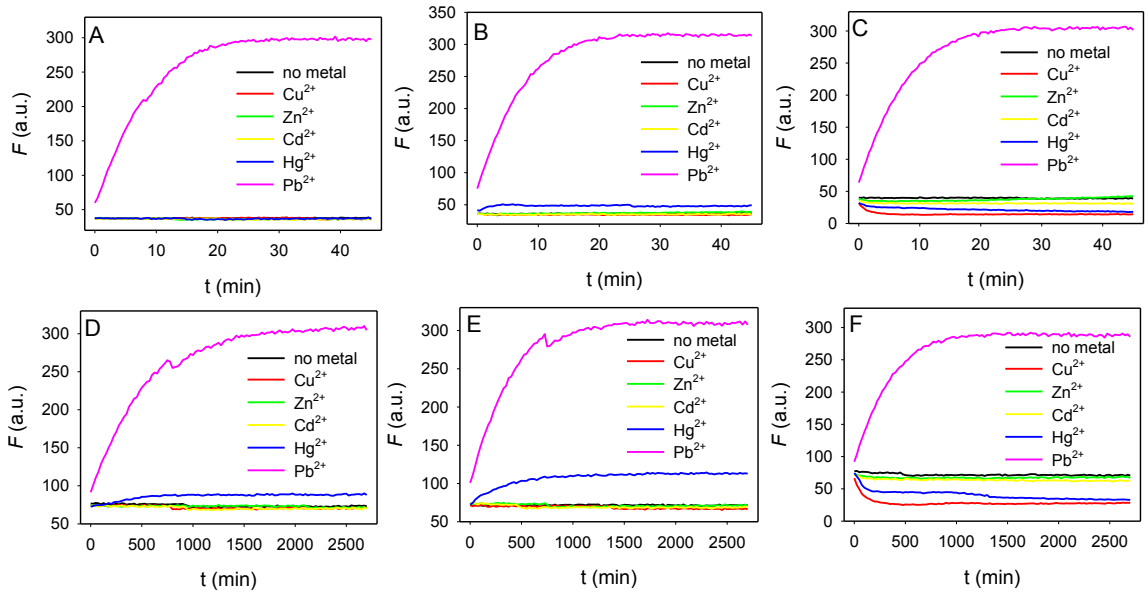

Figure 6.7 Selectivity of PO- or PS-modified GR5 DNAzyme beacons. Kinetic traces of GR5 DNAzyme to different metal ions at different concentrations with PO (A-C) or PS (D-F) substrate. The metal concentrations are 50 nM (A, D), 500 nM (B, E) or 5 μM (C, F).

6.2.5 Individual sensor performance

Once the metal was identified, the corresponding sensor can be used for quantification. By far, GR5 is the best sensor for Pb^{2+} with a reported detection limit of 3.7 nM (in pH 7.0 HEPES buffer).[36] A significant improvement of activity was observed at pH 7.6.[249] In Figure 6.8A, 0.2 nM Pb^{2+} can be clearly distinguished from the background. In the presence of 5 nM Pb^{2+}, full cleavage was observed within 30 min. Since our DNAzyme concentration was 50 nM, each Pb^{2+} turned over 10 sensor molecules in 30 min to amplify the signal. This impressive display of efficiency highlighted one of the advantages of using DNAzyme for metal detection. The calibration curve is shown in Figure 6.8B; an apparent dissociation constant (K_d) of 4.2 nM Pb^{2+} is obtained. To date, this is still the tightest metal binding DNAzyme ever reported. With this design, the detection limit was calculated to be 0.1 nM Pb^{2+} from 3σ/slope, where σ is the standard deviation of background variation.

Cd^{2+} detection was carried out using the PS-Ce13d sensor (Figure 6.8C & D). The K_d was estimated to be 154 nM for Cd^{2+}, and the detection limit was calculated to be 4.8 nM. At the same time, the PS-Ce13d sensor was also used for Hg^{2+} quantification (Figure 6.8E & F). The detection limit was determined to be as low as 2 nM. The US Environmental Protection Agency (EPA) set the maximal contamination limits at 15 ppb (72 nM) for Pb^{2+}, 5 ppb (45 nM) for Cd^{2+}, and 2 ppb (10 nM) for Hg^{2+}. Remarkably, all the three sensors can achieve these limits easily and detect the targets down to parts-per-trillion (ppt) level.

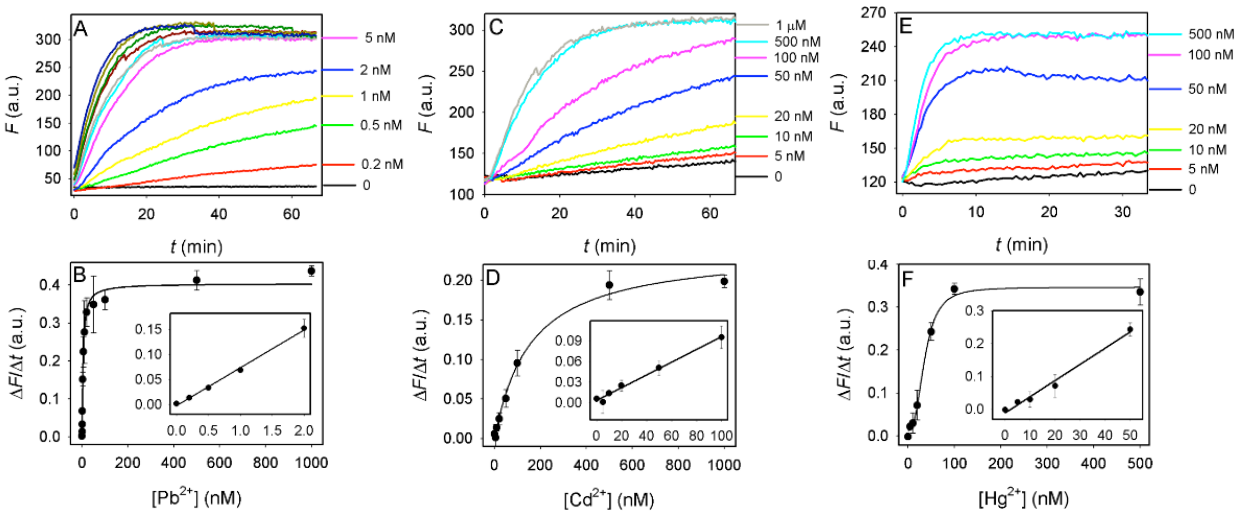

Figure 6.8 Sensitivity of PO-GR5, PS-Ce13d, and PO-Ce13d DNAzymes beacons. Kinetics of sensor fluorescence increase with the PO-GR5 DNAzyme for Pb^{2+} A), PS-Ce13d for Cd^{2+} C) and PS-Ce13d for Hg^{2+} E). The initial rates of fluorescence increase as a function of Pb^{2+} B), Cd^{2+} D) and Hg^{2+} F) concentration. Insets: the responses to low metal concentrations. For all the tests, the DNAzyme concentration was 50 nM in pH 7.6 HEPES buffer.

Modified DNAzymes have been extensively reported for various purposes. This work highlighted the advantages of the PS modification. First, the single O-to-S change at the cleavage junction in the substrate strand minimized the structure perturbation of the original DNAzyme. With this simple modification, DNAzyme with different metal ion preference was obtained without performing additional selection experiments. Second, it is cost effective to produce (e.g. less than $3 per PS modification), while modified bases cost much more and may not be

commercially available. Third, the chemical effects of such modifications are readily predictable. Last but not least, it provides the mechanistic insights for fundamental studies.

6.3 Summary

In summary, the effect of PS modification on the lanthanide-dependent Ce13d DNAzyme was systematically studied. The results indicated that the phosphate at the cleavage site determines its metal preference. This enzyme can be activated either using lanthanide or thiophilic metal ions based on a PO or PS substrate was used. The drastic change of enzyme characteristic was not observed in any other tested DNAzymes. This suggested a well-defined metal binding site that can tolerate a diverse range of metals. As a result, this could be a useful model system for studying DNAzyme bioinorganic chemistry.

Cd^{2+}, Hg^{2+}, and Pb^{2+} are the most popular toxic heavy metals that are banned by the European Union in electronic devices. Therefore, it is important to detect them as a group. The study showed that PS-Ce13d could detect Cd^{2+}, Hg^{2+}, and Pb^{2+} collectively. Combined with other DNAzymes, the concept of flow-chart-based metal analysis was demonstrated here. With the increasing collection of metal-specific DNAzymes, this method will find more applications in detecting multiple metals simultaneously. While the PS-modified Ce13d provides a method for detecting thiophilic metals as a group, a few enzymes need to be used together to identify each metal ion. In the next chapter, I will describe my effort in performing *in vitro* selection with a PS-modified library to obtain new enzymes with better metal specificity.

6.4 Materials and Methods

6.4.1 Chemicals

The fluorophore/quencher-modified DNAs were purchased from Integrated DNA Technologies (IDT, Coralville, IA). The unmodified and phosphorothioate (PS) modified enzyme strands were from Eurofins (Huntsville, AL). The DNA sequences used in this study are listed in Table 6.1. Cerium chloride heptahydrate, magnesium sulfate, manganese chloride tetrahydrate, iron chloride tetrahydrate, cobalt chloride hexahydrate, nickel chloride, copper chloride dehydrate, zinc chloride, cadmium chloride hydrate, mercury perchlorate, and lead acetate were purchased from Sigma-Aldrich except the iron salt was from Alfa Aesar. The solutions were made by directly dissolving their salts in water.

Table 6.1 DNAzyme and substrate sequences used in this work. rA = riboadenosine; Q = Iowa Black® FQ; FAM = carboxyfluorescein; *= PS modification.

DNA Name	Sequences and modifications (from 5'-end)
PO substrate	CGTTCGCCTCATGACGTTGAAGGATCCAGACT-FAM
PS1	GTCACGAGTCACTAT*rAGGAAGATGGCGAAA-FAM
PS2	GTCACGAGTCACTATrA*GGAAGATGGCGAAA-FAM
PS3	GTCACGAGTCACTAT*rA*GGAAGATGGCGAAA-FAM
Ce13d	TTTCGCCATAGGTCAAAGGTGGGTGCGAGTTTTTACTCGTTATAGTGACTCGTGAC
17E	CGCCATCTTCTCCGAGCCGGTCGAAATAGTGACTCGTGAC
GR5	TTTCGCCATCTGAAGTAGCGCCGCCGTATAGTGACTCGTGAC
39E	TTTCGCCATCTTCAGTTCGGAAACGAACCTTCAGACATAGTGACTCGTGAC
Ce13d-Q	Q-TTTCGCCATAGGTCAAAGGTGGGTGCGAGTTTTTACTCGTTATAGTGACTCGTGAC
GR5-Q	Q-TTTCGCCATCTGAAGTAGCGCCGCCGTATAGTGACTCGTGAC
Ce13d-A1*	TTTCGCCATA*GGTCAAAGGTGGGTGCGAGTTTTTACTCGTTATAGTGACTCGTGAC
Ce13d -G2*	TTTCGCCATAG*GTCAAAGGTGGGTGCGAGTTTTTACTCGTTATAGTGACTCGTGAC
Ce13d -G3*	TTTCGCCATAGG*TCAAAGGTGGGTGCGAGTTTTTACTCGTTATAGTGACTCGTGAC
Ce13d -T4*	TTTCGCCATAGGT*CAAAGGTGGGTGCGAGTTTTTACTCGTTATAGTGACTCGTGAC
Ce13d -C5*	TTTCGCCATAGGTC*AAAGGTGGGTGCGAGTTTTTACTCGTTATAGTGACTCGTGAC
Ce13d -A6*	TTTCGCCATAGGTCA*AAGGTGGGTGCGAGTTTTTACTCGTTATAGTGACTCGTGAC
Ce13d -A7*	TTTCGCCATAGGTCAA*AGGTGGGTGCGAGTTTTTACTCGTTATAGTGACTCGTGAC
Ce13d -A8*	TTTCGCCATAGGTCAAA*GGTGGGTGCGAGTTTTTACTCGTTATAGTGACTCGTGAC
Ce13d -G9*	TTTCGCCATAGGTCAAAG*GTGGGTGCGAGTTTTTACTCGTTATAGTGACTCGTGAC
Ce13d -G10*	TTTCGCCATAGGTCAAAGG*TGGGTGCGAGTTTTTACTCGTTATAGTGACTCGTGAC
Ce13d -T11*	TTTCGCCATAGGTCAAAGGT*GGGTGCGAGTTTTTACTCGTTATAGTGACTCGTGAC
Ce13d -G12*	TTTCGCCATAGGTCAAAGGTG*GGTGCGAGTTTTTACTCGTTATAGTGACTCGTGAC
Ce13d -G13*	TTTCGCCATAGGTCAAAGGTGG*GTGCGAGTTTTTACTCGTTATAGTGACTCGTGAC
Ce13d -G14*	TTTCGCCATAGGTCAAAGGTGGG*TGCGAGTTTTTACTCGTTATAGTGACTCGTGAC
Ce13d -G15*	TTTCGCCATAGGTCAAAGGTGGGT*GCGAGTTTTTACTCGTTATAGTGACTCGTGAC

6.4.2 Gel electrophoresis

The DNAzyme complexes were formed by annealing the FAM-labeled substrate and the enzyme at a molar ratio of 1:1.5 in buffer A (25 mM NaCl, 50 mM MES, pH 6). For a typical gel-based activity assay, a final of 10 μM metal ions were incubated with 5 μL of 1 μM DNAzyme complex in buffer A for 30 min to 1 h. The samples were then quenched with 1× loading dye with 8 M urea and 2 mM EDTA and run in 15% dPAGE at 120V for 80 min. The gel images were taken with a ChemiDoc MP imaging system (Bio-Rad).

6.4.3 DNAzyme beacon assay

The sensor kinetic studies were carried out with 96 well plates and monitored with a SpectraMax M3 microplate reader. The stock complex was formed by annealing the FAM-labeled substrate and the quencher-labeled enzyme with a molar ratio of 1:1.5 in buffer A. The stock complex was stored in -20 °C overnight before use. Each complex was further diluted with 25 mM HEPES buffer (pH 7.6). For each well, 100 μL of 50 nM FAM-Q DNAzyme was used. 1 μL of metal ion was added after 5 min of background reading to initiate cleavage. The samples were continuously monitored after addition for at least 30 min with 25 s intervals.

Chapter 7. *In Vitro* Selection of Single Phosphorothioate-Modified DNAzyme: Cadmium Specificity, Chiral Separation, and Detection in Rice

7.1 Introduction

In last chapter, I described that when a single PS modification was made on Ce13d at the cleavage site, the metal preference was switched from lanthanide ions to soft heavy metals. [220] Based on this observation, we made a sensor for detecting these heavy metals as a group. However, Ce13d does not have metal selectivity, and it is impossible to identify the species of the target metal.

To obtain metal-specific DNA, *in vitro* selection of RNA-cleaving DNAzymes is a powerful method.[138,139,162,163,246,250] For example, Pb^{2+}-,[78,125,193] UO_2^{2+}-,[86] and Ln^{3+}-dependent DNAzyme[87,203,223] have been selected and all of them displayed high sensitivity and selectivity. These metals are either hard or borderline Lewis acids and they tend to interact with the phosphate backbone of DNA. However, success is limited for selections against many other metals. This was possibly due to the lack of the chemical functionality in DNA. To overcome this intrinsic problem, replacing naturally occurring nucleobases with synthetic modified nucleobases were introduced.[239,251-253] However, two factors have limited their broader applications. First of all, these special modified bases are not commercially available. In fact, beyond those labs that synthesized the modified DNAzymes, not many others have studied them. Secondly, such selections require individually optimized PCR conditions to incorporate modified nucleotides. This actually makes it a technically demanding task.

Based on all previous results, we reason that it is possible that with a single modification near the substrate RNA cleavage site, sufficient affinity for metal binding can be generated. For

example, phosphorothiate (PS) modification might be a good choice for binding thiophilic metals. PS refers to replacing one of the non-bridging phosphate oxygen atoms by sulfur.[214,254] This type of modifications has been done previously on ribozymes. Many ribozymes (and some DNAzymes) that have Mg^{2+}-dependent activities have been selected. After the PS modification, these enzymes became less active with Mg^{2+} but can be re-activated by soft metals such as Mn^{2+} or Cd^{2+}.[220,241,242,245] By incorporating PS DNA into metal binding sites, the modification offers two advantages. First, PS is commercially available at a low cost (~$3 per modification). In fact, PS-modified DNA has been commonly used in chemical biology,[240] and materials sciences.[243,255-258] Second, the single PS modification is introduced in a fixed (instead of randomized) region of the DNA library so it does not complicate *in vitro* selection.

Cadmium is a highly toxic metal known for its carcinogenic effects on humans.[24] In the last century, discharge of Cd^{2+} has increased tremendously. This industrial byproduct led to contamination of water and agriculture products.[259] So far, most reported fluorescent sensors for Cd^{2+} are based on synthetic chelators.[228] However, they often require organic solvents and their performance can be strongly interfered by Zn^{2+}, Ca^{2+}, Hg^{2+}, or Pb^{2+}. This pointed out the challenges associated with rational ligand design. Other types of designs like nanoparticle-based colorimetric assays were also reported.[260-262] Even though the method is much simpler to operate, they often suffer from low sensitivity and interference. It is interesting to note that few biosensors are available for Cd^{2+}.[263,264] In this chapter, a Cd^{2+}-dependent DNAzyme selection using a PS modified library was conducted. To our knowledge, this is the first effort of strategically placing a PS in a selection library. Because each PS modification generated two diastereomers, a DNAzyme-based method for the chiral assignment and separation was demonstrated. In addition, a Cd^{2+} biosensor with ultrahigh sensitivity and specificity was

developed and tested.

7.2 Results and Discussions

7.2.1 Direct selections with a PS-modified library

To isolate Cd^{2+}-specific DNA, *in vitro* selection was carried out with a N50 library. With this library size, 50 random nucleotides can generate ~10^{14} possible sequences (Figure 6.1A). The cleavage site is indicated by the arrowhead at the single RNA (rA) position. This scissile bond is ~1-million-fold less stable compared to the rest DNA linkages.[52] In addtion, a PS modification was introduced at this cleavage junction (Figure 1B) to increase affinity towards thiophilic Cd^{2+}. So far, all the selections mentioned previously only used the normal phosphate (PO) linkage.[87,203,223]

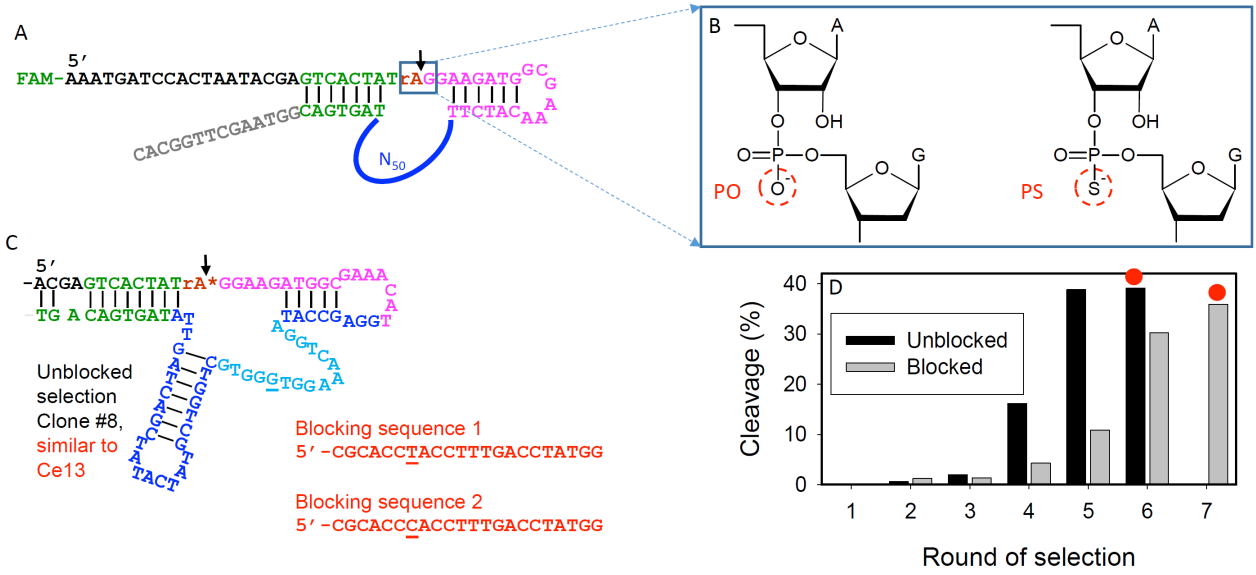

Figure 7.1 Library design for the Cd^{2+} DNAzyme selection. A) The library sequence for the PS DNAzyme selection. The structure of the cleavage junction (rAG) is shown in B), where rA denotes for ribo-adenosine. Instead of the normal PO, all the selections in this work used the PS linkage. C) A representative sequence from the direct selection, where the blue/cyan nucleotides are from the randomized N50 region. The star at the cleavage site represents the PS. This sequence is similar to Ce13, a previously reported DNAzyme. Two blocking sequences are complementary to the cyan region and they differ only by one base (underlined). D) Progress of the direct (unblocked) and blocked selections. The red dots indicate the rounds for DNA sequencing.

In each round of selection, Cd^{2+} was added to induce cleavage. The cleaved sequences were separated by gel electrophoresis. The isolated fragments were then amplified and extended by PCR to seed the next round of selection. After 5 rounds, ~35% cleavage was observed and the activity seemed to reach saturated (Figure 7.1D, black bars). The round 6 library was cloned and sequenced. Interestingly, 34 out of the 35 obtained sequences are similar to the Ce13 DNAzyme that was first isolated in a lanthanide-dependent selection (details characterization is presented in Chapter 2).[87] A representative sequence (Figure 7.1C) shows a hairpin (in blue) and a large loop (in cyan) that constitutes the catalytic core. Each individual clone may differ in the hairpin but the loop sequence is highly conserved. The alignment of the sequences are listed in Table 7.1.

Since Ce13 with a PS-modified substrate showed excellent activity in the presence of Cd^{2+} (detail studies are presented in Chapter 6),[220] it is not surprising that it was isolated again. This result also indicated that with the current library design, Ce13 is a preferred (or easy-to-obtain) solution for Cd^{2+}-dependent PS RNA cleavage. However, this DNAzyme is not specific for Cd^{2+}. PS-Ce13 also displayed activity with Pb^{2+}, Cu^{2+}, Hg^{2+} and Ce^{3+}. To obtain a new PS-modified Cd^{2+}-dependent DNAzyme, the selection protocol needed to be adjusted.

Table 7.1 Alignment of the Ce13 sequence with unblocked Cd^{2+} selection sequences. The Ce13 sequence is showed in green. The cleavage site adenine is marked in red, and the conserved loop sequence in blue. Only the last sequence (UNBlkCd39) cannot be aligned.

Clone#	Sequence (from 5'-end)	
UNBlkCd07	CTGCAGAATTCTAATACGAGTCACTATA-GGAAGATGGCGAAACATCTGGGAGCCATAGG	59
UNBlkCd34	CTGCAGAATTCTAATACGAGTCACTATA-GGAAGATGGCGAAACATCTGGGAGCCATAGG	59
UNBlkCd14	CTGCAGAATTCTAATACGAGTCACTATA-GGAAGTTGGCGAAACATTTCG-AGCCATAGG	58
UNBlkCd24	CTGCAGAATTCTAATACGAGTCACTATA-GGAAGATGGCGAAACAT---GGAGCCATAGG	56
Ce13	CTGCAGAATTCTAATACGAGTCACTATA-GGAAGATGGCGAAACAT---GGAGCCATAGG	56
UNBlkCd13	CTGCAGAATTCTAATACGAGTCACTATA-GGAAGATGGCGAAACAT---GGAGCCATAGG	56
UNBlkCd05	CTGCAGAATTCTAATACGAGTCACTATA-GGAAGATGGCGAAACAT---GGAGCCATAGG	56
UNBlkCd21	CTGCAGAATTCTAATACGAGTCACTATA-GGAAGATGGCGAAACAT---GGAGCCATAGG	56
UNBlkCd03	CTGCAGAATTCTAATACGAGTCACTATAAGGAAGATGGCGAAACAT---GGAGCCATAGG	57
UNBlkCd15	CTGCAGAATTCTAATACGAGTCACTATA-GGAAGATGGCGAAACAT---GGAGCCATAGG	56
UNBlkCd11	CTGCAGAATTCTAATACGAGTCACTATA-GGAAGATGGCGAAACAT---GGAGCCATAGG	56
UNBlkCd10	CTGCAGAATTCTAATACGAGTCACTATA-GGAAGATGGCGAAACAT---GGAGCCATAGG	56
UNBlkCd09	CTGCAGAATTCTAATACGAGTCACTATA-GGAAGATGGCGAAACAT---GGAGCCATAGG	56
UNBlkCd06	CTGCAGAATTCTAATACGAGTCACTATA-GGAAGATGGCGAAACAT---GGAGCCATAGG	56
UNBlkCd36	CTGCAGAATTCTAATACGAGTCACTATA-GGAAGATGGCGAAACAT---GGAGCCATAGG	56
UNBlkCd40	CTGCAGAATTCTAATACGAGTCACTATA-GGAAGATGGCGAAACAT---GGAGCCATAGG	56
UNBlkCd35	CTGCAGAATTCTAATACGAGTCACTATA-GGAAGATGGCGAAACAT---GGAGCCAGAGG	56
UNBlkCd38	CTGCAGAATTCTAATACGAGTCACTATA-GGAAGATGGCGAAACAT---GGAGCCATAGG	56
UNBlkCd02	CTGCAGAATTCTAATACGAGTCACTATA-GGAAGATGGCGAAACAT---GGAGCCATAGG	56
UNBlkCd17	CTGCAGAATTCTAATACGAGTCACTATA-GGAAGATGGCGAAACAT---GGAGCCATAGG	56
UNBlkCd37	CTGCAGAATTCTAATACGAGTCACTATA-GGAAGATGGCGAAACAT---GGAGCCATAGG	56
UNBlkCd26	CTGCAGAATTCTAATACGAGTCACTATA-GGAAGATGGCGAAACAT---GGAGCCATAGG	56
UNBlkCd25	CTGCAGAATTCTAATACGAGTCACTATA-GGAAGATGGCGAAACAT---GGAGCCATAGG	56
UNBlkCd19	CTGCAGAATTCTAATACGAGTCACTATA-GGAAGATGGCGAAACAT---GGAGCCATAGG	56
UNBlkCd12	CTGCAGAATTCTAATACGAGTCACTATA-GGAAGATGGCGAAACAT---GGAGCCATAGG	56
UNBlkCd28	CTGCAGAATTCTAATACGAGTCACTATA-GGAAGATGGCGAAACAT---GGAGCCATAGG	56
UNBlkCd29	CTGCAGAATTCTAATACGAGTCACTATA-GGAAGATGGCGAAACAT---G-AGCCATAGG	55
UNBlkCd23	CTGCAGAATTCTAATACGAGTCACTATA-GGAAGATGGCGAAACAT---GGAGCCATAGG	56
UNBlkCd30	CTGCAGAATTCTAATACGAGTCACTATA-GGAAGATGGCGAAACAT---GGAGCCATAGG	56
UNBlkCd22	CTGCAGAATTCTAATACGAGTCACTATA-GGAAGATGGCGAAACAT---TGAGCCATAGG	56
UNBlkCd33	CTGCAGAATTCTAATACGAGTCACTATA-GGAAGATGGCGAAACAT---GAAGCCATAGG	56
UNBlkCd27	CTGCAGAATTCTAATACGAGTCACTATA-GGAAGATGGCGAAACAT---GGAGCCATAGG	56
UNBlkCd04	CTGCAGAATTCTAATACGAGTCACTATA-GGAAGATGGCGAAACAT---GGAGCCATAGG	56
UNBlkCd08	CTGCAGAATTCTAATACGAGTCACTATA-GGAAGATGGCGAAACATCATGGAGCCATAGG	59
UNBlkCd20	CTGCAGAATTCTAATACGAGTCACTATA-GGAAGATGGCGAAACATCTTTACAAAAAAAC	59
UNBlkCd39	CTGCAGAATTCTAATACGAGTCACTATA-GGAAGATGGCGAAACATCTTT--ACTAAGGA	57

Table 7.1 Alignment of the Ce13 sequence with unblocked Cd^{2+} selection sequences. (Continued)

Clone#	Sequence (from 5′-end)	
UNBlkCd07	TCAAAGGTGGGTGCG-GTCGTTT---ATCGACTAGTT------ATAATGACGGTAAGCTT	109
UNBlkCd34	TCAAAGGTGGGTGCGTGTCGTAT---ATCGACTAAGT------ATAGTGACGGTAAGCTT	110
UNBlkCd14	TCAAAGGTGGGTGCGGGTCGTAT---ATCGACTAAGT-----TATAGTGACGGTAAGCTT	110
UNBlkCd24	TCAAAGGTGGGTGCGTGTCG-ATCTAATCGACTAAGT-----TATAGTGACGGTAAGCTT	110
Ce13	TCAAAGGTGGGTGCGGGTCGTATCATATCGACTAAGT-----TATAGTGACGGTAAGCTT	111
UNBlkCd13	TCAAAGGTGGGTGCGTGTCGTATCATATCGACTAAGT------ATAGTGACGGTAAGCTT	110
UNBlkCd05	TCAAAGGTGGGTGCGAGTCGTATCATATCGACGA-GT------ATAGTGACGGTAAGCTT	109
UNBlkCd21	TCAAAGGTGGGTGCGAGTCGTATCATATCGACGA-GT------ATAGTGACGGTAAGCTT	109
UNBlkCd03	TCAAAGGTGGGTGCGAGTCGTATCATATCGACGA-GT-----TATAGTGACGGTAAGCTT	111
UNBlkCd15	TCAAAGGTGGGTGCGAGTCGTATCATATCGACGA-GT-----TATAGTGACGGTAAGCTT	110
UNBlkCd11	TCAAAGGTGGGTGCGAGTCGTATCATATCGACGA-GT-----TATAGTGACGGTAAGCTT	110
UNBlkCd10	TCAAAGGTGGGTGCGAGTCGTATCATATCGACGA-GT-----TATAGTGACGGTAAGCTT	110
UNBlkCd09	TCAAAGGTGGGTGCGAGTCGTATCATATCGACGA-GT-----TATAGTGACGGTAAGCTT	110
UNBlkCd06	TCAAAGGTGGGTGCGAGTCGTATCATATCGACGA-GT-----TATAGTGACGGTAAGCTT	110
UNBlkCd36	TCAAAGGTGGGTGCGAGTCGTATCATATCGACGA-GT-----TATAGTGACGGTAAGCTT	110
UNBlkCd40	TCAAAGGTGGGTGCGAGTCGTATCATATCGGCGA-GT-----TATAGTGACGGTAAGCTT	110
UNBlkCd35	TCAAAGGTGGGTGCGAGTCGTATCATATCGACGA-GT-----TATAGTGACGGTAAGCTT	110
UNBlkCd38	TCAAAGGTGGGTGCGAGTCGTATCACATCGACGA-GT-----TATAGTGACGGTAAGCTT	110
UNBlkCd02	TCGAAGGTGGGCGCGAGTCGTATCATATCGACGA-GT-----TATAGTGACGGTAAGCTT	110
UNBlkCd17	TCAAAGGTGGGTGCGAGTCGTATCATACCGACGA-GT-----TATAGTGACGGTAAGCTT	110
UNBlkCd37	TCAAAGGTGGGTGCGAGTCGTATCATACCGACGA-GT-----TATAGTGACGGTAAGCTT	110
UNBlkCd26	TCAAAGGTGGGTGCGAGTCGTATCATATCGACGAAGT-----TATAGTGACGGTAAGCTT	111
UNBlkCd25	TCAAAGGTGGGTGCGAGTCGTATCATATCGACGAAGT-----TATAGTGACGGTAAGCTT	111
UNBlkCd19	TCAAAGGTGGGTGCGAGTCGAATCATGTCGACGAAGT-----TATAGTGACGGTAAGCTT	111
UNBlkCd12	TCAAAGGTGGGTGCGAGTCGTATCTTATCGACGAAGT-----TATAGTGGCGGTAAGCTT	111
UNBlkCd28	TCAAAGGTGGGTGCGAGTCGTATCTTATCGACGAAGT-----TATAGTGACGGTAAGCTT	111
UNBlkCd29	TCAAAGGTGGGTGCGAGTCGTATCATATCGACGAAGT-----AATAGTGACGGTAAGCTT	110
UNBlkCd23	TCAAAGGTGGGTGCTAGTCGTATCATATCGACTA-GT------ATAGTGACGGTAAGCTT	109
UNBlkCd30	TCAAAGGTGGGTGCTAGTCGTATCATATCGACTA-GT-----TATAGTGACGGTAAGCTT	110
UNBlkCd22	TCAAAGGTGGGTGCTAGTCGTATCATACCGACTA-GT-----TATAGTGACGGTAAGCTT	110
UNBlkCd33	TCAAAGGTGGGTGCGAGTCGTATCATATCAACTC-GT------ATAGTGACGGTAAGCTT	109
UNBlkCd27	TCAAAGGTGGGTGTG-GTCGTATCTTATCGACCA-GT-----AATAGTGACGGTAAGCTT	109
UNBlkCd04	TCAAAGGTTGGTGCTGGTCGCATTATATCGACTA-GT-----TATAGTGACGGTAAGCTT	110
UNBlkCd08	TCAAAGGTGGGTGCTG-TCGCATCATATCGACT--GT-----TATAGTAACGGTAAGCTT	111
UNBlkCd20	TCAAAAGTTGGCCCTTCCCGCATTTAAGTTTTCGGAA-----GATAGTGACGGTAAGCTT	114
UNBlkCd39	-GCAAA--TAGCGAGAAACCGGCGAAACTAGAGGCGATCTGGGTTAGTGACGGTAAGCTT	114

7.2.2 Blocked selections

It should be noted that the conserved sequence of Ce13 is quite long (e.g. the 15 nucleotides in cyan in Figure 7.1C). From the previous study, only one of the nucleotides (marked by underline) may change from G to A.[87] If the complementary DNA was used to block these conserved nucleotides, Ce13 sequences got supressed and the library might be able to evolve. Two blocking DNAs were designed for this purpose and the sequences is showed in Figure 7.1C. In the new selection scheme (Figure 7.2A), the blocking DNAs were first hybridized with the library to inactivate the Ce13 sequences (step 1). Cd^{2+} was then added (step

2) and the cleaved sequences were amplified (step 3). With this adjustment, the progress was slightly slower and it took 7 rounds to reach the similar amount of cleavage (Figure 7.1B, gray bars). The result implied that the suppression of the highly active Ce13 population was sucessful. The round 7 library was also sequenced and the Ce13 variants were indeed eliminated (see Table 7.2 for sequence alignment). However, the alignment showed that this enriched library contains a high sequence diversity. The results suggested that many solutions are available for Cd^{2+}-dependent cleavage. On top of that, the round 7 library displayed nearly 60% cleavage with a mixture of Pb^{2+}, Cu^{2+}, and Zn^{2+} (20 μM each) after 1 h incubation. This implied that the library still lacked specificity for Cd^{2+}.

Table 7.2 Sequence alignment of the second selection using the two blocking sequences. For sequences (07, 26, 18, 23) belong to the BN-Cd16 family in Table 7.3.

Clone#	Sequence (from 5′-end)	
BlkCd07	CTGCAGAATTCTAATACGAGTCACTATAGGAAGATGGCGAAACATCTTCATTCG------	54
BlkCd26	CTGCAGAATTCTAATACGAGTCACTATAGGAAGATGGCGAAACATCTTCATTCG------	54
BlkCd03	CTGCAGAATTCTAATACGAGTCACTATAGGAAGATGGCGAAACATCTTATCACG------	54
BlkCd10	CTGCAGAATTCTAATACGAGTCACTATAGGAAGATGGCGAAACATCTTAAGTCAT-----	55
BlkCd31	CTGCAGAATTCTAATACGAGTCACTATAGGAAGATGGCGAAACATCTTCACTAGT-----	55
BlkCd18	CTGCAGAATTCTAATACGAGTCACTATAGGAAGATGGCGAAACATCTTAGTCAGA-----	55
BlkCd23	CTGCAGAATTCTAATACGAGTCACTATAGGAAGATGGCGAAACATTTTT-AGAGC-----	54
BlkCd19	CTGCAGAATTCTAATACGAGTCACTATAGGAAGATGGCGAAACATCTTT---TAG-----	52
BlkCd16	CTGCAGAATTCTAATACGAGTCACTATAGGAAGATGGCGAAACATCTTT--ACGT-----	53
BlkCd01	CTGCAGAATTCTAATACGAGTCACTATAGGAAGATGGCGAAACATCTTTACTAGGCA---	57
BlkCd27	CTGCAGAATTCTAATACGAGTCACTATAGGAAGATGGCGAAACATCTTTACTAGCCT---	57
BlkCd15	CTGCAGAATTCTAATACGAGTCACTATAGGAAGATGGCGAAACATCTTTACTAGCAC---	57
BlkCd21	CTGCAGAATTCTAATACGAGTCACTATAGGAAGATGGCGAAACATCTTTACTAACG----	56
BlkCd02	CTGCAGAATTCTAATACGAGTCACTATAGGAAGATGGCGAAACATCTTTACTACGG----	56
BlkCd22	CTGCAGAATTCTAATACGAGTCACTATAGGAAGATGGCGAAACATCTTAATGGT-TT---	56
BlkCd30	CTGCAGAATTCTAATACGAGTCACTATAGGAAGATGGCGAAACATCTTTACTAG-GA---	56
BlkCd09	CTGCAGAATTCTAATACGAGTCACTATAGGAAGATGGCGAAACATCTTTACTAAGGC---	57
BlkCd24	CTGCAGAATTCTAATACGAGTCACTATAGGAAGATGGCGAAACATCTTTACTAAGGATAG	60
BlkCd36	CTGCAGAATTCTAATACGAGTCACTATAGGAAGATGGCGAAACATCTTTACTAATG----	56
BlkCd06	CTGCAGAATTCTAATACGAGTCACTATAGGAAGATGGCGAAACATCTTTACTAATAA---	57
BlkCd11	CTGCAGAATTCTAATACGAGTCACTATAGGAAGATGGCGAAACATCTTTACT--------	52
BlkCd14	CTGCAGAATTCTAATACGAGTCACTATAGGAAGATGGCGAAACATCTTTGCTG--A----	54
BlkCd39	CTGCAGAATTCTAATACGAGTCACTATAGGAAGATGGCGAAACATCTTTACAAGAA----	56
BlkCd12	CTGCAGAATTCTAATACGAGTCACTATAGGAAGATGGCGAAACATCTTTACTA-ACT---	56
BlkCd38	CTGCAGAATTCTAATACGAGTCACTATAGGAAGATGGCGAAACATCTTTAGTA-ACA---	56
BlkCd33	CTGCAGAATTCTAATACGAGTCACTATAGGAAGATGGCGAAACATCTTTACTA-TCC---	56
BlkCd40	CTGCAGAATTCTAATACGAGTCACTATAGGAAGATGGCGAAACATCTTTACTAGTAA---	57
BlkCd20	CTGCAGAATTCTAATACGAGTCACTATAGGAAGATGGCGAAACACCTTTAGTAGCAC---	57
BlkCd25	CTGCAGAATTCTAATACGAGTCACTATAGGAAGATGGCGAAACATCTTTACTAACA----	56
BlkCd32	CTGCAGAATTCTAATACGAGTCACTATAGGAAGATGGCGAAACATCTTTACTA-------	53
BlkCd35	CTGCAGAATTCTAATACGAGTCACTATAGGAAGATGGCGAAACATCTTTACTA-------	53
BlkCd28	CTGCAGAATTCTAATACGAGTCACTATAGGAAGATGGCGAAACACCTTTACTAGTTT---	57
BlkCd05	CTGCAGAATTCTAATACGAGTCACTATAGGAAGATGGCGAAACATCTTTACAAGAT----	56
BlkCd17	CTGCAGAATTCTAATACGAGTCACTATAGGAA-ATGGCGAAACATCTTTAGTAGTTGTAC	59
BlkCd04	CTGCAGAATTCTAATACGAGTCACTATAGGAAGATGGCGAAACATCTTTAGTAGTTT---	57
BlkCd13	CTGCAGAATTCTAATACGAGTCACTATAGGAAGATGGCGAAACATCTTTAGT--TAT---	55
BlkCd08	CTGCAGAATTCTAATACGAGTCACTATAGGAAGATGGCGAAACATCTTTAGTAGT-----	55
BlkCd34	CTGCAGAAT-----------TCGCCCTTGGAAGATGGCGAAACATCTTTAGTAATGG---	46

Table 7.2 Sequence alignment of the second selection using the two blocking sequences. (Continued)

Clone#	Sequence (from 5′-end)	
BlkCd07	----ATAGTTGAAATAGGTACAAGTATCACGGTGATATTG--TATCATG-TTAGTGTC-G	106
BlkCd26	----ATAGTTGAAATAGGTACGAGTATCACGGTGATATTG--TATCATG-TTAGTGAC-G	106
BlkCd03	----CGA-TAGAAATAGCGACAAGTCTAGGTGTGATTTATGCTCTCTT--CTAGTGAC-G	106
BlkCd10	----CTAATCACTCGAAGAAG---AGTGGCGAGGAGTAAGAATGTCGTG-ATGGTGAC-G	106
BlkCd31	----AAAGCAAAGCATAGAGCTCTACGGGTTAGGGGTACGAG-GTCGT---TGGTGAC-G	106
BlkCd18	----ATACGGACAAAGAGTGG-CAGACAGAAACCT-TCGATAGCTC-AA-ATAGTGAC-G	106
BlkCd23	----ATAAAACCAAAATTTGTTAAGACAGTGACCT-TCGATAGCAC-AA-ATAGTGAC-G	106
BlkCd19	----ATACTTATAAATGGTCAATGAGCAATGTTCAGTAGCTTGTGCGAC-TTAGTGAC-G	106
BlkCd16	----CCACTGATAGAGCTCATATTGGAAAGGAATA-TTGGTTATGAACC-CTAGTTAC-G	106
BlkCd01	---TTGAAATA-CTTTTGGATT--TATATTATCATATGGCCGGGAGAT----AGTGAC-G	106
BlkCd27	---GTGCCGCATCGTTAGGATT--ACGATAAGAACACCG-CGGGAAAT----AGTGAC-G	106
BlkCd15	---GTA--ATGCCTCATGCTCTGTATAATGAGGGGA-ACGTGAGGGTT----AGTGAC-G	106
BlkCd21	---GTAGCACGCCGAAAGTGCT--ATACAGAGGGGAGTAGTGTGGGTT----AGTGAC-G	106
BlkCd02	---AAACTACGTCGCGTGCATT--TAAAAGGCGAATAGAGAGGGGGTT----AGTGAC-G	106
BlkCd22	---ACATAGTCCATCTAAGACC-TTGTCACCTTCATCGCGAAG-AAAT----AGTGAC-G	106
BlkCd30	---GC-TAGGCCTCCTTATATT-TTATCACGAGTAGCTCACGGGAGAT----AGTGAC-G	106
BlkCd09	---TCAATGAGCCGCGAAGGCG-GCAT-GCATACAAGTCTGGG-AGAT----AGTGAC-G	106
BlkCd24	TTAGTTGTAGGTTGACAACGTG--TGGGACTAGACT-------GGGTT----AGTGAC-G	106
BlkCd36	--TGTAGGAGACTCCCATCGTT--ATGGACATGTCTCTA-CATGGGGT----AGTCAC-G	106
BlkCd06	---ATGGAGTGGTCAACCGAAT-TAGGAGCACGTAATG--CATGAGTT----AGTGAC-G	106
BlkCd11	--AGCAA-GTTTA-TTGCGGGT-TAATGACAGTTATAAAGCGTATCATTACTAGTGAC-G	106
BlkCd14	--AACATTGTTCAGTAGCCTTT-TATTAACACTAATAAAGAGCGACTT----AGTGAC-G	106
BlkCd39	--AGCAT-ATTCG-CAGCAGGG-GTATAGCGAAGATGAGTCGGAAGAT----AGTGACCG	107
BlkCd12	----AACGGAAAGCAAGTTGAAGAATCGA---TTGTCGATTG--TGGGAGATAGTAAC-G	106
BlkCd38	----AAC--ACACTAGGGTAAATATTGGG---ATTTCGAGTGGTTGCGCCTTAGTGAC-G	106
BlkCd33	----GACGAGGAGCCCTGGGCCAGGG-GG---ATATCAGTTG-GAGGGAGATAGTGAC-G	106
BlkCd40	----AAAGCCCAGCTATGGGTAGGTGTGG---GTATCCGTTT-ACGG--GATAGTGAC-G	106
BlkCd20	----ATCAGGAGAAACGTGGAAAAGATAG---CTACTG--AATGGCGGCT-TAGTGAC-G	106
BlkCd25	----ATCTGTATTATTGCTGTGGGGTGAG---TTACAG--AAGGTGGGAGGTAGTGAC-G	106
BlkCd32	----AGCAAT--AGCAAAGGATTGCAGAATTTTCTATGGCTATCGCTGGGTTAGTGAC-G	106
BlkCd35	----AGCAAT--AGCAAAGGATTGCAGAATTTTCTATGGCTATCGCTGGGTTAGTGAC-G	106
BlkCd28	----AACAATGACACCAAAGAATGGAGGG---ACATTG--TTTCGCGGGG-TAGTGAC-G	106
BlkCd05	-----CAGGGGCGATAAGTCATAGAACAAAGGATCTCCTGATCGGGTT----AGTGAC-G	106
BlkCd17	T-TAACCGGGGACAGAAGACATAG-----AGGGTATC---AACGCCTT----AGTGAC-G	105
BlkCd04	----AAACCGGAGTTGTCAATCAGA---CGTATGAAGGAAAAAC---GCCTTAGTGAC-G	106
BlkCd13	----AAACCGGA-TTCACTAATAGG---CTGATACAGAGAGGGCTATGGGTTAGTGAC-G	106
BlkCd08	----TCCAAGGGGATAAAAATGGAAGAGCGGGCCC-ATGGGAAC---GCCTTAGTGAC-G	106
BlkCd34	----TCTCCGACGTCTAAACTGGGT---CGGACTAGAAGTTAAT---GCCTTAGTGAC-G	95

7.2.3 Blocked negative selections

The activity observed can be rationalized with the thiophilicity of these metal ions. Aside from that, these metal ions may display different properties such as size, coordiation chemistry and the pK_a value of the bound water. These differences might be enough for DNA sequences to differentiate them. Under this assumption, the negative selection step was added in the each of next few rounds to further evolve the library. After incubating with a mixture of metal ions (Pb^{2+}, Zn^{2+}, and Cu^{2+}, step 4, Figure 7.2A), the cleaved sequences were discarded and the remaining

uncleaved library was harvested (step 5). The isolated library was then incubated with Cd^{2+} for the positive selection (step 2). Aiming for high specificity, stringent conditions were used for the negative selection by extending reaction time (Figure 7.2B, black bars). The activity of the competing metals went down from 58% cleavage in 1 h in round 8 to ~30% in 2 h in round 13. After that, we did a 12 h incubation followed by a 4 h incubation. At the end of round 15, only insignificant amount of cleavage was observed with the metal mixture. The progression indicated a significant improvement on selectivity.

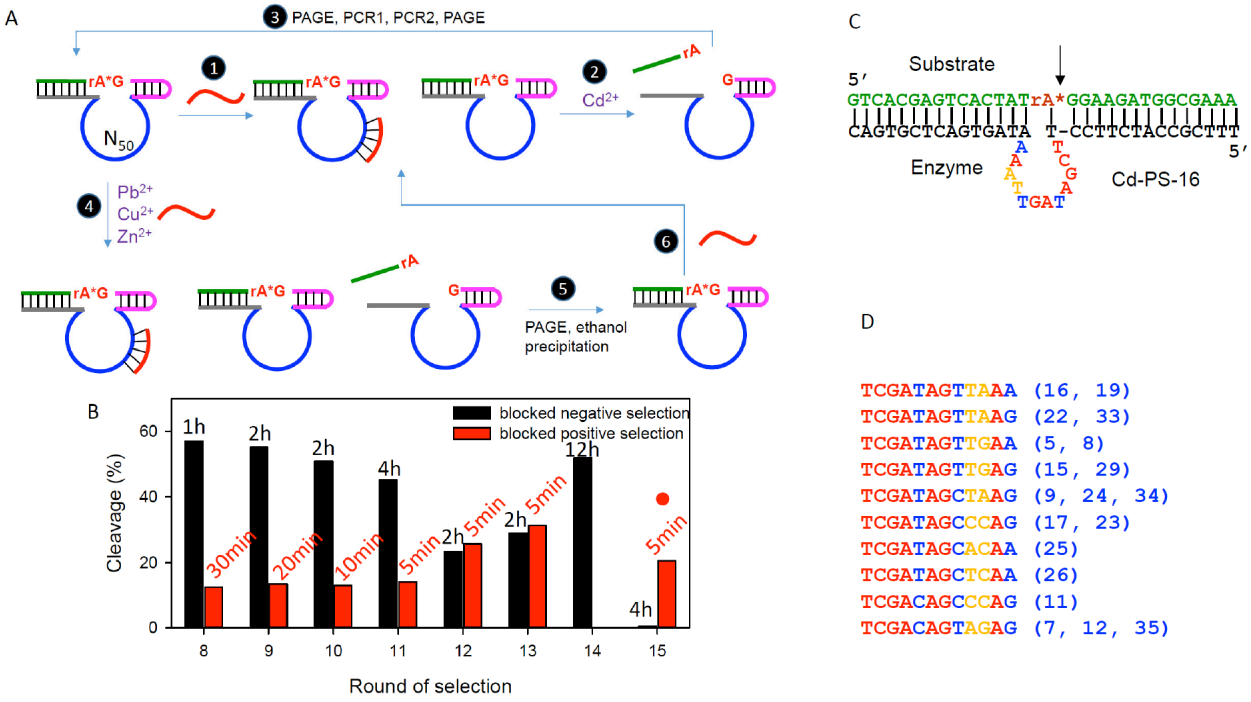

Figure 7.2 A design scheme for the modified Cd^{2+} selection. A) A scheme for the blocked selection and with negative selection. The blockers are intended to eliminate the Ce13 sequences. Steps 1, 2 and 3 consist of a completely blocked selection cycle. From round 8, negative selections were carried out with a metal soup. In this case, the uncleaved sequences were collected (steps 4, 5, 6) and then reacted with Cd^{2+} for the positive selection (steps 2, 3). B) Selection progress from round 8 of the blocked selection. For each round, both positive and negative selections were carried out. The round 15 library was sequenced. C) A trans-cleaving DNAzyme derived from BN-Cd16. D) Alignment of the enzyme loop for sequences similar to BN-Cd16. Nucleotides in red are absolutely conserved, in blue can be purine or pyrimidine substituted and in yellow are variable. The clone numbers are in the parenthesis. The color coding matches that in C).

At the same time of improving selectivity, the reaction time was shortened for the positive Cd^{2+}-dependent selections to enusre highly active DNAzyme was selected. In the last

four rounds, only 5-min was allowed and ~20% cleavage was consistently achieved (Figure 7.2B, red bars). At round 15, since both the negative and positive activities were optimized, this library was sequenced.

7.2.4 DNAzyme secondary structure analysis

From Table 7.3, 19 out of 37 sequences were aligned to a single family. One representative sequence, clone #16, was used for subsequent analysis. Its structure that was predicted by M-fold[190] is shown in Figure 7.3 and its simplified trans-cleaving structure is shown in Figure 7.2C. Interestingly, there are only 12 nucleotides in the enzyme loop. These loop sequences are well aligned (Figure 7.2D): the nucleotides in red are highly conserved, in yellow can be changed from purine to purine or from pyrimidine to pyrimidine, and the two blue nucleotides are more variable. Overall, this appears to be a well-defined new DNAzyme.

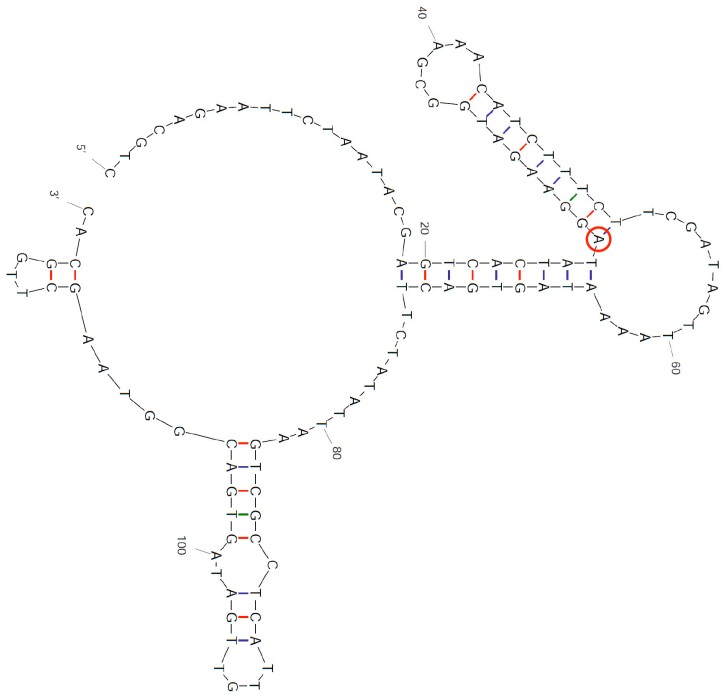

Figure 7.3 Mfold predicted secondary structure of Blk-N-Cd16. The cleavage site ribo-adenine is marked in the red circle.

Table 7.3 Sequence alignment for the third selection, where negative selections were carried out in the presence of the blocking DNAs.

Clone#	Sequence (from 5′-end)	
BN-Cd02	CTGCAGAATTCTAAT-ACGAGTCACTATAGGAAGATGGCGAAACA-TCTTA----GAGAT	54
BN-Cd20	CTGCAGAATTCTAAT-ACGAGTCACTATAGGAAGATGGCGAAACA-TCTTA----GCCAG	54
BN-Cd01	CTGCAGAATTCTAAT-ACGAGTCACTATAGGAAGATGGCGAAACA-TCTTTAATCGGTAA	58
BN-Cd10	CTGCAGAATTCTAAT-ACGAGTCACTATAGGAAGATGGCGAAACA-TCTTTAATCGGTAA	58
BN-Cd06	CTGCAGAATTCTAAT-ACGAGTCACTATAGGAAGATGGCGAAACA-CCTTTAATCGGTAA	58
BN-Cd30	CTGCAGAATTCTAAT-ACGAGTCACTATAGGAAGATGGCGAAACA-TCTTTAATCGGTAA	58
BN-Cd13	CTGCAGAATTCTAAT-ACGAGTCACTATAGGAAGATGGCGAAACA-CCTTG---CG-TAT	54
BN-Cd14	CTGCAGAATTCTAAT-ACGAGTCACTATAGGAAGATGGCGAAACA-CCTTG---CG-TAT	54
BN-Cd38	CTGCAGAATTCTAAT-ACGAGTCACTATAGGAAGATGGCGAAACA-TATTG---CT-CAT	54
BN-Cd04	CTGCAGAATTCTAAT-ACGAGTCACTATAGG-AGATGGCGAAACA-TTTAG---GGGTCC	54
BN-Cd21	CTGCAGAATTCTAAT-ACGAGTCACTATAGGAAGATGGCGAAACA-TCTTG---GGGTCT	55
BN-Cd40	CTGCAGAATTCTAAT-A-GAGTCACTATAGGAAGATGGCGAAACA-TCTTG---GGGCAC	54
BN-Cd07	CTGCAGAATTCTAAT-ACGAGTCACTATAGGAAGATGGCGAAACA-TCTTGCATAAATGT	58
BN-Cd35	CTGCAGAATTCTAAT-ACGAGTCACTATAGGAAGATGGCGAAACA-TCTTGCATAAATGT	58
BN-Cd12	CTGCAGAATTCTAAT-ACGAGTCACTATAGGAAGATGGCGAAACA-TCTTGCATAAATGT	58
BN-Cd09	CTGCAGAATTCTAAT-ACGAGTCACTATAGGAAGATGGCGAAACA-TCTTAG--ACGGCA	56
BN-Cd34	CTGCAGAATTCTAAT-ACGAGTCACTATAGGAAGATGGCGAAACA-TCTTAG--ACGGCA	56
BN-Cd24	CTGCAGAATTCTAAT-ACGAGTCACTATAGGAAGATGGCGAAACA-TCTTAG--ACGGCA	56
BN-Cd25	CTGCAGAATTCTAAT-ACSAGTCACTATAGGAAGATGGCGAAACA-TCTTAA--ACCAGG	56
BN-Cd36	CTGCAGAATTCTAAT-ACSAGTCACTATAGGAAGATGGCGAAACA-TCTTATG-AGCTAA	57
BN-Cd17	CTGCAGAATTCTAAT-ACGAGTCACTATAGGAAGATGGCGAAACA-TCTTTTTATTAAAA	58
BN-Cd23	CTGCAGAATTCTAAT-ACGAGTCACTATAGGAAGATGGCGAAACA-TCTTTTTATTAAAA	58
BN-Cd11	CTGCAGAATTCTAAT-ACGAGTCACTATAGGAAGATGGCGAAACA-TCTTTTTATTTAAA	58
BN-Cd03	CTGCAGAATTCTAAT-ACGAGTCACTATAGGAAGATGGCGAAACACCTTACACTCGAAGA	59
BN-Cd37	CTGCAGAATTCTAAT-ACGAGTCACTATAGGAAGATGGCGAAACACCTTACACTCGAAGA	59
BN-Cd05	CTGCAGAATTCTAAT-ACGAGTCACTATAGGAAGATGGCGAAACAATCTTCATTCGATAG	59
BN-Cd08	CTGCAGAATTCTAAT-ACGAGTCACTATAGGAAGATGGCGAAACA-TCTTCATTCGATAG	58
BN-Cd15	CTGCAGAATTCTAATAACGAGTCACTATAGGAAGATGGCGAAACA-TCTTCATTCGATAG	59
BN-Cd29	CTGCAGAATTCTAAT-ACGAGTCACTATAGGAAGATGGCGAAACA-CCTTCATTCGATAG	58
BN-Cd19	CTGCAGAATTCTAAT-ACGAGTCACTATAGGAAGATGGCGAAACA-CCTTCATTCGATAG	58
BN-Cd33	CTGCAGAATTCTAAT-ACGAGTCACTATAGGAAGATGGCGAAACA-CCTTCATTCGATAG	58
BN-Cd26	CTGCAGAATTCTAAT-ACGAGTCACTATAGGAAGATGGCGAAACA-TCTTCATTCGATAG	58
BN-Cd16	CTGCAGAATTCTAAT-ACGAGTCACTATAGGAAGATGGCGAAACA-TCTTTCTTCGATAG	58
BN-Cd22	CTGCAGAATTCTAAT-ACGAGTCACTATAGGAAGATGGCGAAACA-TCTTTCTTCGATAG	58
BN-Cd32	CTGCAGAATTCTAAT-ACGAGTCACTATAGGAAGATGGCGAAACA-TCTTTAC-CCAAAA	57
BN-Cd39	CTGCAGAATTCTAAT-ACGAGTCACTATAGGAAGATGGCGAAACA-CCTTTAATCCAAAC	58
BN-Cd18	CTGCAGAATTCTAAT-ACGAGTCACTATAGGAAGATGGCGAAACA-TCTTTACCCAAAAG	58

Table 7.3 Sequence alignment for the third selection, where negative selections were carried out in the presence of the blocking DNAs. (Continued)

Clone#	Sequence (from 5′-end)	
BN-Cd02	CTATTGAACGATAACTAATTAGCCATATTTATCCACCTACATCTTAGTGACGGTAAGCTT	114
BN-Cd20	CTGAAACAATCGAAGAGTTTTGCATATCGTGATGACGCAAAGAGTAGTGACGGTAAGCTT	114
BN-Cd01	CAGCAACAATAA-TAGGTTTCTACTGCTACG---TAGGGCCAATTAGTGACGGTAAGCTT	114
BN-Cd10	CAGCAACAATAA-TAGGTTTCTACTGCTACG---TAGGGCCAATTAGTGACGGTAAGCTT	114
BN-Cd06	CAGCGACAATAA-TAAGTTTGTACTGCTACG---TAGGGCCAATTAGTGACGGTAAGCTT	114
BN-Cd30	CAGCAACAATAA-TAAGTTTGTACTGCTACG---TAGGGCCAATTAGTGACGGTAAGCTT	114
BN-Cd13	CATCTTCAATTCGATAGAGTCCACGTCTACAGGAATGTGGGAAATAGTAACGGTAAGCTT	114
BN-Cd14	CATCTTCAATTCGATAGAGTCCACGTCTACAGGAATGTGGGAAATAGTAACGGTAAGCTT	114
BN-Cd38	YATCYTCAATTCGATAGAGTCCACGTTCACAAGAATGTGGGAAATAGTGACGGTAAGCTT	114
BN-Cd04	ATATTGCTCAAAGATAGT-TCGAACATCTGAAACGCACGAAGAATAGTGACGGTAAGCTT	113
BN-Cd21	ATATTGCTCAAAGATAGT-TCGTACAACTGAAACGCACGAAGAATAATGACGGTAAGCTT	114
BN-Cd40	GCTCTTAACCAAGATAATGTTAAGTATCTTACAGGAAC-CACTTTAGTGACGGTAAGCTT	113
BN-Cd07	CTACATGCAGAATATCCGCCA--TTTCATTCG--ACAGTAGAGATAGTGACGGTAAGCTT	114
BN-Cd35	CTACATGCAGAATATCCGCCA--TTTCATTCG--ACAGTAGAGATAGTGACGGTAAGCTT	114
BN-Cd12	CTACATGCAGAATATCCACCA--TTTCATTCG--ACAGTAGAGATAGTGACGGTAAGCTT	114
BN-Cd09	CCTGAGATGATTTAATCGCAGTTCTTCCTTCG--ATAGCTAAGATAGTGACGGTAAGCTT	114
BN-Cd34	CCTGAGATGATTTAATCGCAGTTCTTCCTTCG--ATAGCTAAGATAGTGACGGTAAGCTT	114
BN-Cd24	CCTGAGCTGATATAATCGCACTTCTTCCTTCG--ATAGCTAAGATAGTGACGGTAAGCTT	114
BN-Cd25	TGTCTTACTTTCTAAGCTGTCATCTTCATTCG--ATAGCACAAATAGTGACGGTAAGCTT	114
BN-Cd36	CGTAAAAGTTTCTAAAGCCAC-TGTTCCTTCS--ATAGTACAGATAGTGACGGTAAGCTT	114
BN-Cd17	CGTGTAAAAATGTGGGGGCAG--TTTCCTTCG--ATAGCCCAGATAGTGACGGTAAGCTT	114
BN-Cd23	CGTGTAAAAATGTAGGGGCAG--TTTCCTTCG--ATAGCCCAGATAGTGACGGTAAGCTT	114
BN-Cd11	CGTGTAAAAATGTAGGGGCAT--CTTCCTTCG--ACAGCCCAGATAGTGACGGTAAGCTT	114
BN-Cd03	GTCTCTTAAA--TTATACCTT--GTAGAATCCCCTG-GAGGAAATAGTGACGGTAAGCTT	114
BN-Cd37	GTCTCTTAAA--TTGTACCCG--GTACAATCCCCTG-GAGGAAATAGTGACGGTAAGCTT	114
BN-Cd05	TTGAAATAGG--TACGAGTAT--CACGGCGATGTTGTATCATGTTAGTAACGGTAAGCTT	115
BN-Cd08	TTGAAATAGG--TACAAGTAT--CACGGTGATATTGTATCACGTTAGTAACGGTAAGCTT	114
BN-Cd15	TTGAGATAGG--TACGAGTAT--CACGGTCATATTGTATCATGTTGGTGACGGTAAGCTT	115
BN-Cd29	TTGAGATAGG--TACAAGTAT--CACGGTGACATTGTATCATGTTAGTGTCGGTAAGCTT	114
BN-Cd19	TTAAAATAGG--TACGAGTAT--CACGGTGATATTGTACCATGTTAGTGACGGTAAGCTT	114
BN-Cd33	TTAAAATTGG--GAGGACATG--TAGTGGGACGATTCAACCCCCTAGTGACGGTAAGCTT	114
BN-Cd26	CTCAAATAGGACTATGTGTTT--AACTGGAATATG--AAAGGACTAGTGACGGTAAGCTT	114
BN-Cd16	TTAAAATAGT--GACTTCTAT--ATTAAGTCGCCTCATTGTTGATAGTGACGGTAAGCTT	114
BN-Cd22	TTAAGATAGT--GACTTCTAT--ATTAAGTCGTCTCATTGTTAATAATGACGGTAAGCTT	114
BN-Cd32	GGAG-TTCTTACGGATCCTAC--AATGAGGAAAAGTATGAGTTATAGTGACGGTAAGCTT	114
BN-Cd39	CACGGTGGTGACTGGCCTGAA--TAAGAGCATTAGACT--ATATTAGTGACGGTAAGCTT	114
BN-Cd18	GAAGGTTTTCTAATAACTGGC--TTTAGTAGAAACACA--GGAGTAGTGACGGTAAGCTT	114

7.2.5 Metal ions specificity

Some of the sequences shown in Figure 7.2D were tested for activity. As shown in Figure 7.4, they all displayed similar Cd^{2+}-dependent activity. BN-Cd16 sequence was chosen for further studies due to its sensitivity. 10 μM divalent metal ions were used first to test its metal specificity, and Cd^{2+} indeed shows the best cleavage (Figure 7.5A). Besides Cu^{2+}, Pb^{2+} and Hg^{2+} showed moderate activity, none of the other divalent metal ions produced any cleavage even when the concentration was increased up to 1 mM (Figure 7.5F). In particular, the Cd^{2+}

selectivity over Zn^{2+} was more than 100,000-fold based on their cleavage rates. Therefore, BN-Cd16 solves the challenging problem of separating Cd^{2+} and Zn^{2+}.

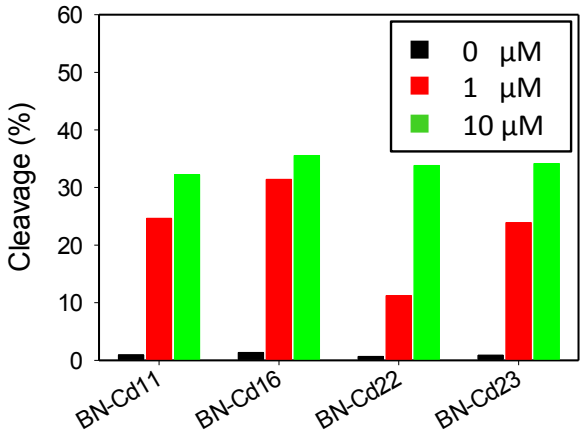

Figure 7.4 Cleavage of the PS-Sub by different enzymes with 1 and 10 µM Cd^{2+}. They all showed similar activity, which is consistent with their similar sequences in Figure 2D. BN-Cd16 was chosen for most of studies in this work. The reaction was in 50 mM MES, pH 6.0 with 25 mM NaCl.

Next, the kinetics of BN-Cd16 with the active metal ions was measured and a gel image with Cd^{2+} is shown in Figure 7.5B. With 10 µM Cd^{2+}, the cleavage rate is 0.12 min^{-1} that is 15 and 20-fold higher than the one with Cu^{2+} and Pb^{2+}, respectively. (Figure 7.5D, black bars). Hg^{2+} produced an interesting cleavage kinetic profile, as only ~8% cleavage was observed and it is all cleaved within the first half minute. It was reported that Hg^{2+} can cleave PS RNA even in the absence of any DNAzyme due to its extremely strong thiophilicity.[265]

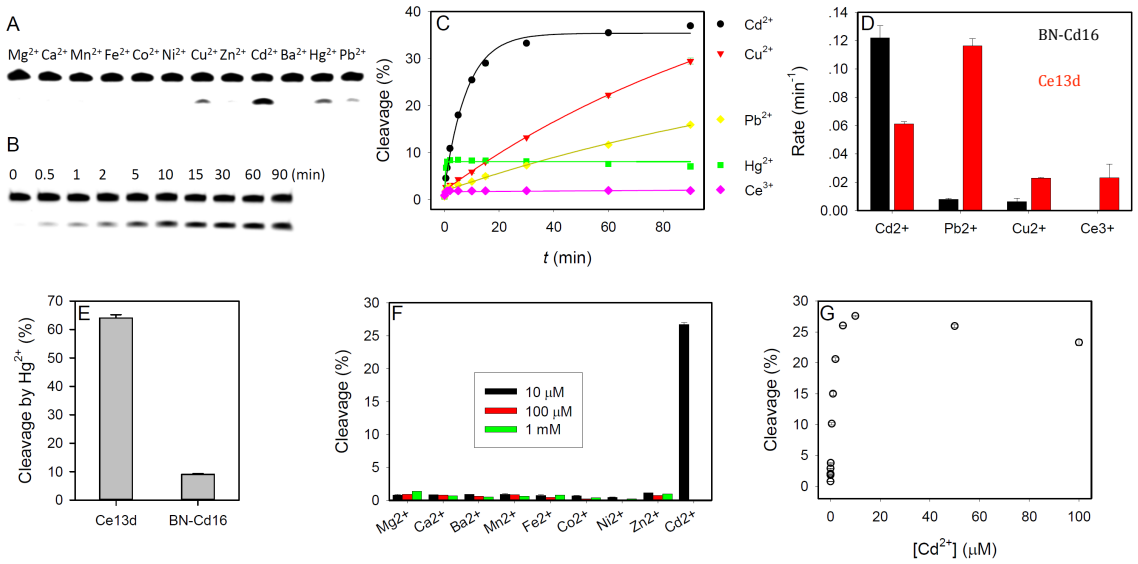

Figure 7.5 Biochemical characterization of the BN-Cd16 DNAzyme. Gel images of BN-Cd16 with the PS substrate reacting (A) in the presence of 10 µM various metals after 10 min incubation, and (B) with 10 µM Cd^{2+} as a function of time. (C) Kinetics of the PS substrate cleavage by BN-Cd16 with different metal ions (10 µM). (D) Comparison of rate of cleavage of BN-Cd16 and Ce13d with the PS substrate. (E) Comparison of the fraction of cleavage by Hg^{2+} (10 µM) with these two DNAzymes. (F) Cleavage percentage with three concentrations of various competing metals. (G) Fraction of cleavage after 15 min as a function of Cd^{2+} concentration. All the assays were run in 50 mM MES buffer (pH 6.0) with 25 mM NaCl.

Since Ce13d also active with Cd^{2+}, the cleavage rate of Ce13d (Figure 7.5D, red bars) was also measured for comparison. In this case, all four metals showed significant activity. Since the Hg^{2+} rate cannot be accurately measured, the final cleavage yield is compared (Figure 7.5E) and Ce13d produced ~8-fold more cleavage. Combined with all these results, BN-Cd16 is highly selective for Cd^{2+} and it represents a significant improvement over Ce13d. Since Cd^{2+} is the only active metal in low nM concentration (*vide infra*), it is probably more practical in real-life situations. Cd^{2+} concentration range was also tested and the highest activity was observed with 10 µM Cd^{2+} (Figure 7.5G). Any further increase of Cd^{2+} concentration reduced the activity slightly.

In addition to this most abundant family, a few other sequences were also tested. For example, BN-Cd13 (three similar sequences found in the library) is quite active (Figure 7.6A) but not selective (Figure 7.6B). BN-Cd04 displayed very low activity (Figure 7.6A). BN-Cd18

also showed poor selectivity (Figure 7.7). Even though BN-Cd40 displayed remarkable selectivity (Figure 7.7), it has very slow kinetics (Figure 7.8). Overall, BN-Cd16 is an optimal sequence both in terms of activity and specificity for Cd^{2+}.

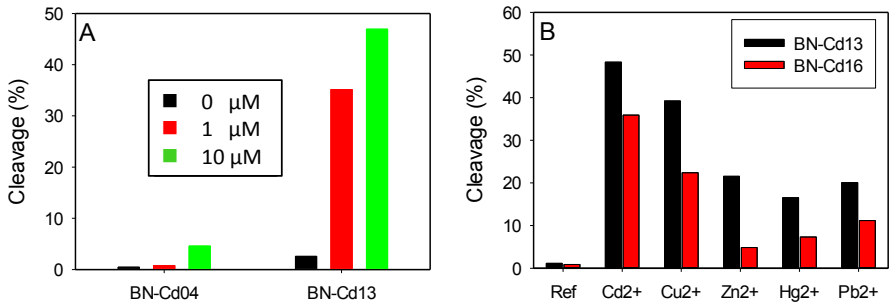

Figure 7.6 Additional gel-based assays on other Cd^{2+} DNAzymes using the PS-Substrate. There are other types of DNAzyme sequences in our blocked selection with negative selection. For example, BN-Cd13, BN-Cd14, and BN-Cd38 belong to the same family and we tested BN-Cd13 (A, the right side bars). It is quite active and cleaved nearly 50% with 10 µM Cd^{2+} in 1 h. Another DNAzyme, BN-Cd04 (and BN-Cd21) failed to show high activity and was not studied further. We next compared metal selectivity between BN-Cd13 and BN-Cd16 (B). It appears that BN-Cd16 has higher selectivity (1 h reaction with 10 µM various metal ions). Each metal ion was used at 10 µM concentration with 1 h incubation in 50 mM MES, pH 6.0 with 25 mM NaCl.

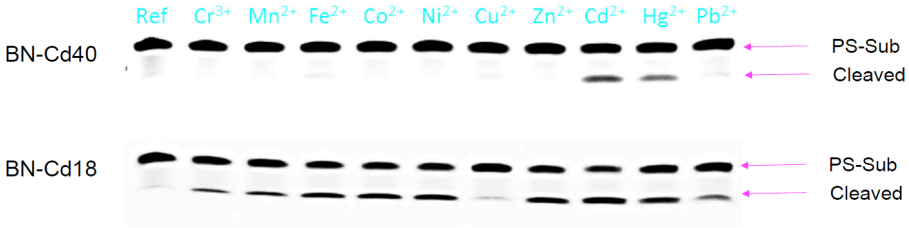

Figure 7.7 Metal specificity assay of BN-Cd40 and BN-Cd18 DNAzymes using PS-Substrate. BN-Cd40 has very good selectivity towards Cd^{2+} and this DNAzyme only appeared once in the blocked negative selection. BN-Cd18, on the other hand, has poor selectivity. Each metal ion was used at 10 µM concentration with 1 h incubation in 50 mM MES, pH 6.0 with 25 mM NaCl.

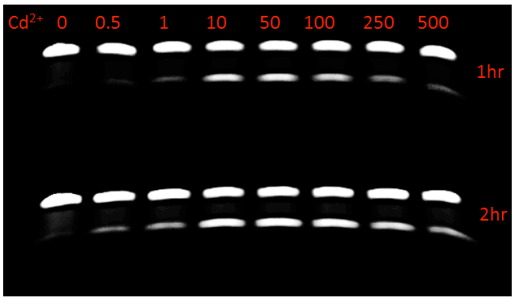

Cd^{2+} Concentration (uM)	% of Cleavage	
	1hr	2hr
0	0	0
0.5	2.3	4.9
1	2.9	7.6
10	21.9	28.0
50	23.9	30.4
100	17.5	26.0
250	8.9	15.4
500	5.0	9.9

Figure 7.8 Cd^{2+} concentration dependent study of the BN-Cd40 DNAzyme. Since the BN-Cd40 DNAzyme showed excellent metal specificity from the assay in Figure S5, it would be suitable to be developed into a cadmium sensor. A range of Cd^{2+} concentrations (0-500 µM) was tested for 1 and 2 h, and both gel images and quantifications are shown. With BN-Cd16, ~30% cleavage was achieved in 1 h, but BN-Cd40 only achieved ~3% cleavage under the same condition. Therefore, this is a much slower enzyme.

7.2.6 Stereo-specificity and DNAzyme-based chiral separation

For all these assays, Cd^{2+} cleaved no more than 35% of the PS substrate. Even after increasing enzyme concentration and reaction time, cleavage was still below 50% (Figure 7.9). This is much lower than most DNAzymes reported. In most cases, over 80% cleavage can be achieved under an hour.

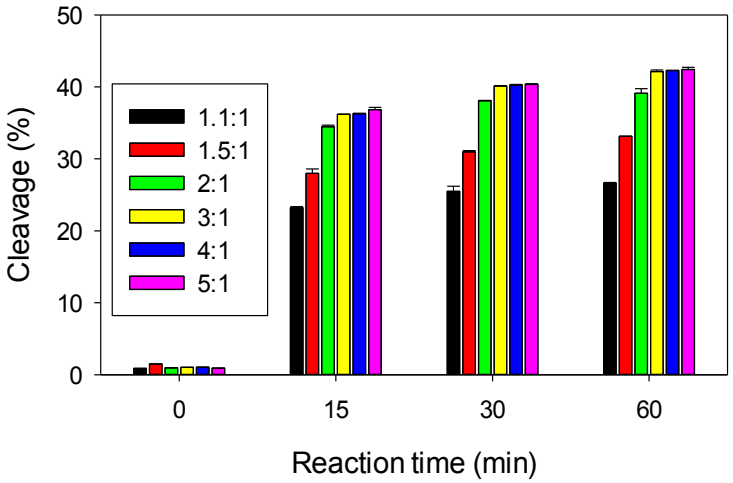

Figure 7.9 Quantification of PS-Sub cleavage as a function of BN-Cd16 enzyme concentration. At the high enzyme concentration (e.g. 5:1 ratio), and after 1 h reaction with 10 μM Cd^{2+}, the cleavage of the substrate reached ~45%. The improvement from 30 min to 1 h was minimal for these samples as well. This suggests that only about half of the substrate can be cleaved by Cd^{2+}.

Introducing a PS modification results in two diastereomers at the phosphorus center (R_p and S_p, Figure 7.10A). These two diastereomers were well studied in ribozymes,[216,217,219] and DNAzymes.[134,218] Most of these enzymes are active with Mg^{2+} , which has great affinity for oxygen-based ligands. When the pro-R_p oxygen was replaced by sulfur, the Mg^{2+}-dependent activity was nearly abolished (>100-fold slower). This activity can often be rescued by thiophilic metals such as Cd^{2+} or Mn^{2+}. When the pro-S_p oxygen was replaced, the adverse effect is much smaller (e.g. ~5-fold). This indicates that these enzymes use the pro-R_p oxygen to bind Mg^{2+}.

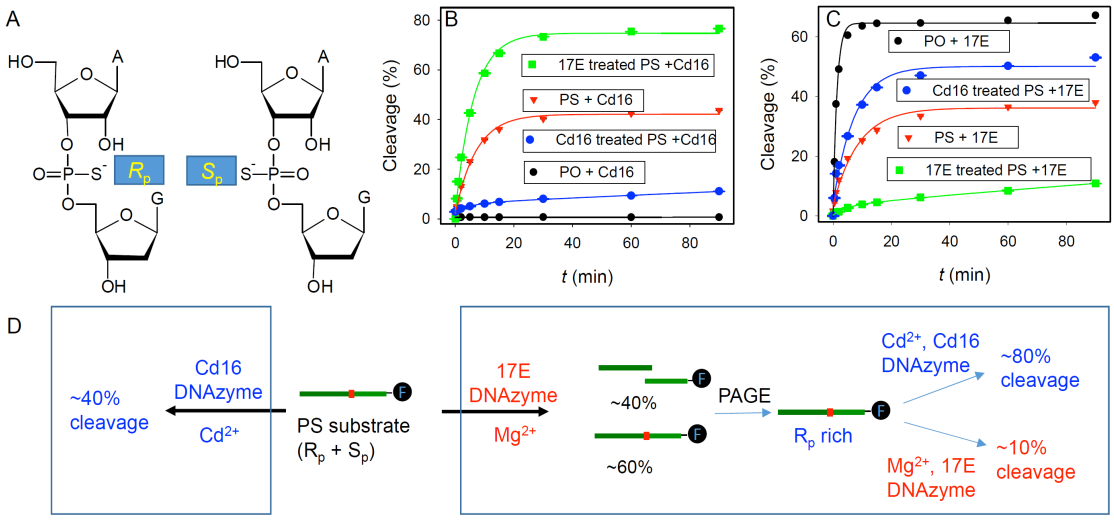

Figure 7.10 DNAzyme-based chiral separation. A) The structures of the two PS diastereomers at the cleavage junction. The BN-Cd16 DNAzyme is active only with the Rp isomer. Kinetics of PO, PS, and treated PS substrate cleavage by B) the BN-Cd16 DNAzyme in the presence of 10 μM Cd^{2+}, or by C) the 17E DNAzyme in the presence of 10 mM Mg^{2+}. D) The scheme of experiment design for treating the PS substrate to remove the Sp population by the 17E DNAzyme and to increase reaction yield.

It shoud be noted that these two isomers were not separated during the *in vitro* selection and assays. Thus, it is likely that only one of the diastereomers is active. To verify this, each isomer needed to be tested separately. However, the standard HPLC method failed the separation[25] due to the substrate length (30-mer) and the FAM modification. Therefore, an alternative method was needed for the confirmation.

17E is a well-characterized and Mg^{2+}-dependent DNAzyme.[125,126,162,250] Since 17E shares the same substrate sequence as the current BN-Cd16 DNAzyme, PS substrate was hybridized with 17E and incubated in presence of 10 mM Mg^{2+}. In 90 min, ~40% cleavage was achieved (Figure 7.10C, red dots, rate = 0.12 min^{-1}). For comparison, the normal PO substrate has a rate of 0.76 min^{-1} (Figure 7.10C, black dots). This ~6-fold rate difference reflects a typical thio effect.[217] The uncleaved PS substrate was isolated after gel electrophoresis and it was used to form a complex with BN-Cd16. Upon adding Cd^{2+}, ~80% cleavage was observed (Figure 7.10B, green dots). This is significantly higher than the untreated PS substrate (Figure 7.10B, red dots). The

rate of cleavage (0.16 min^{-1}) is similar to that of the untreated substrate (0.12 min^{-1}). Therefore, the same species is responsible for the cleavage before and after the 17E DNAzyme treatment. When the 17E treated substrate was reacted with 17E again, only ~10% cleavage was observed (Figure 7.10C, green dots). The data implies that the 17E treatment selectively removed one of the isomers. As a result, the signal generated by the remaining isomer with BN-Cd16/Cd^{2+} was significantly enhanced.

The 10-23 DNAzyme was selected together with 17E and displayed similar Mg^{2+}-dependent activity.[79] The 10-23 DNAzyme is known to use the pro-R_p oxygen to bind Mg^{2+}. Since the 10-23 DNAzyme is thought to be a variant of 17E,[79] these two enzymes should have the same steroselectivity.[134] In fact, all the known RNA-cleaving ribozymes use the pro-R_p oxygen to bind Mg^{2+}. Based on the results, it is suspected that BN-Cd16 uses the R_p sulfur to bind Cd^{2+}. Once the majority of S_p population is removed by 17E, the remaining R_p rich population is all active with BN-Cd16 (Figure 7.10D). This is the first time that a DNAzyme is utilized to achieve chiral separation. While preparing for the sensor (*vide infra*), 3 nmol substrate was purified in one run. It should be noted that this method can be readily scaled up.

To further verify the hypothesis, PS substrate with BN-Cd16 was treated with 10 μM Cd^{2+}. If the assumption is correct, this treatment should remove most of the R_p isomer. The remaining uncleaved S_p rich substrate with BN-Cd16 should show less activity in the presence of Cd^{2+}. Indeed, the complex only yielded ~10% cleavage (Figure 7.10B, blue dots). This kinetic data was a better fit to an equation with two rates (0.16 min^{-1} and 0.00019 min^{-1}; if fitting to a single exponential equation, $R^2 = 0.97$). The slower rate was assigned to the S_p isomer. This S_p isomer became the dominating species after the BN-Cd16 treatment and thus its rate became noticeable. This ~800-fold difference is typical for RNA cleavage.[217] In a separate experiment,

the activity of the PO substrate with BN-Cd16 in the presence of Cd^{2+} was also measured (black dots, Figure 7.10B). Not surprisingly, no cleavage was observed. The large difference in activity highlighted the importance of the PS modification. In fact, BN-Cd16 cannot cleave the PO substrate by any tested metals (Figure 7.11), which also explains its high metal specificity.

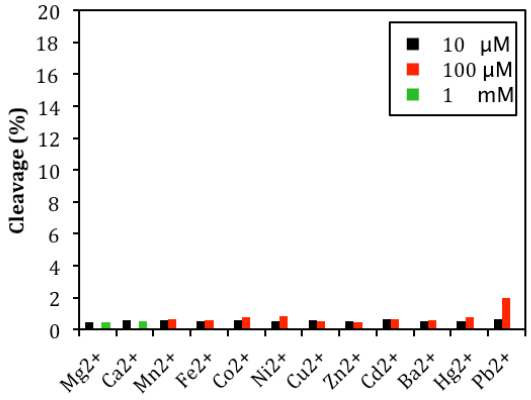

Figure 7.11 Cleavage of the PO substrate by BN-Cd16 in the presence of different metal ions. Only 2% cleavage was observed with a high concentration of Pb^{2+} in 1 h and others only showed only background signal. Therefore, this DNAzyme is highly specific for the PS substrate.

Since Cd^{2+} has relatively strong affinity with sulfur, one question is whether Cd^{2+} can be reused to activate multiple DNAzymes or it is sequestered after each reaction. To test this, 5 µM DNAzyme complex was incubated with 0.2 µM Cd^{2+}. The cleavage fraction was quantified in terms of turnover numbers (Figure 7.12), and multiple turnovers are indeed possible.

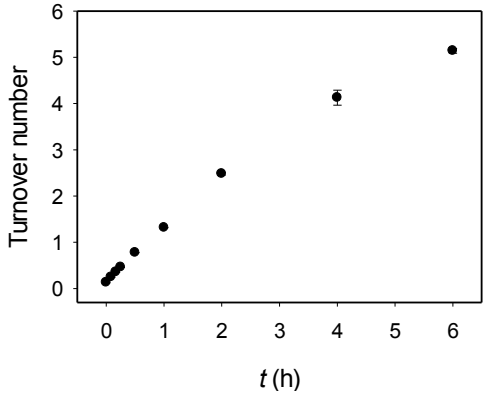

Figure 7.12 Multiple turnover analysis of the BN-Cd16 DNAzyme in the presence of 0.2 µM Cd^{2+}. The DNAzyme concentration was 5 µM.

7.2.7 A Cd^{2+} sensing beacon

A sensor based on this DNAzyme was developed for Cd^{2+} detection. While various methods of detection are available, [43,193,236,238] a simple catalytic beacon design was chosen.[193] In this design, the substrate was labeled with a FAM fluorophore at the 5'-end and the enzyme was labeled with a dark quencher at the 3'end (Figure 7.13A for detail sequences).

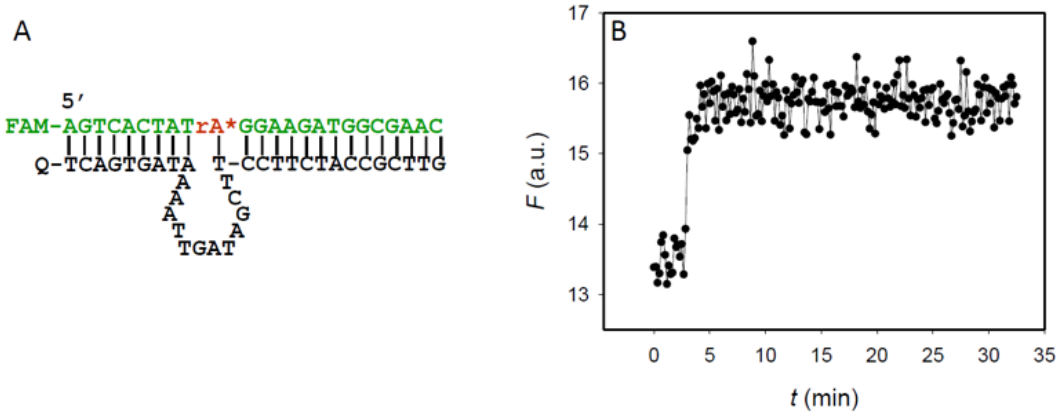

Figure 7.13 Design of the fluorescent BN-Cd16 DNAzyme beacon. A) Sensor sequence. B) Sensor response to 100 nM Hg^{2+} and only an initial increase was observed.

Initially the two strands were hybridized to form a complex and the fluorescence was quenched. When Cd^{2+} was added, a concentration dependent fluorescence enhancement was observed (Figure 7.14A). Significant fluorescence increase took place in the first 10 minutes at high Cd^{2+} concentrations. The slopes of these kinetic traces were measured for the first 10 minutes after adding Cd^{2+} (Figure 7.14B). The data in the first minute were discarded to eliminate potential Hg^{2+} interference (Figure 7.13B). This binding curve gave an apparent dissociation constant of 41 nM Cd^{2+}. This made it one of the tightest metal binding DNA. From the data, the detection limit for Cd^{2+} was calculated to be 1.1 nM based on 3σ/slope (Figure 7.14B inset). Since the EPA maximal contamination level in drinking water is 5 μg/L (45 nM) Cd^{2+}, this makes Cd16 DNAzyme a suitable sensor for aqueous contaminant detection. Sensor response to other metal ions was also tested for possible interference (Figure 7.14C & D), and

only Cd^{2+} showed an obvious signal increase at 100 nM. It should be noted that the substrate was first treated with 17E to remove the S_p population to improve sensitivity. Without the 17E treatment, the amount of fluorescence enhancement was ~40% lower (Figure 7.15).

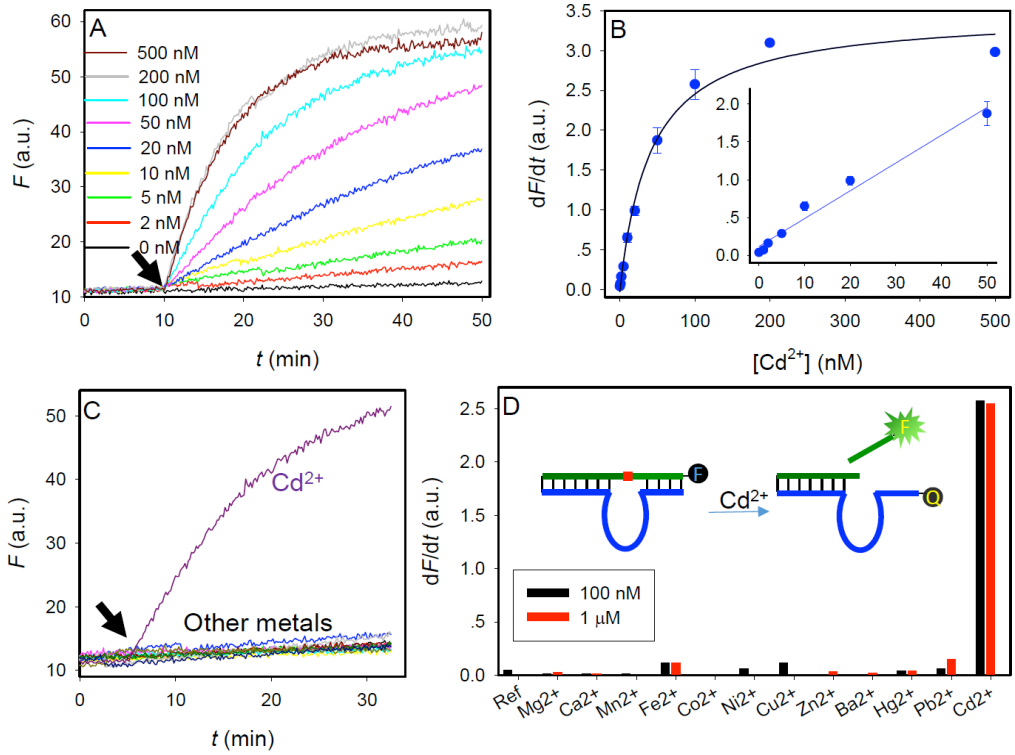

Figure 7.14 Sensitivity and selectivity analysis of BN-Cd16 DNAzyme beacon. A) Kinetics of sensor fluorescence enhancement with various concentrations of Cd^{2+}. The arrowhead points the time of Cd^{2+} addition. B) Initial rate of fluorescence enhancement (from 1 to 10 min after adding Cd^{2+}) as a function of Cd^{2+} concentration. Inset: the linear response at low Cd^{2+} concentrations. C) Sensor response to 100 nM of various metals. The list of other metals are in D). D) Sensor selectivity quantified at two metal concentrations. Inset: a scheme showing the sensor design.

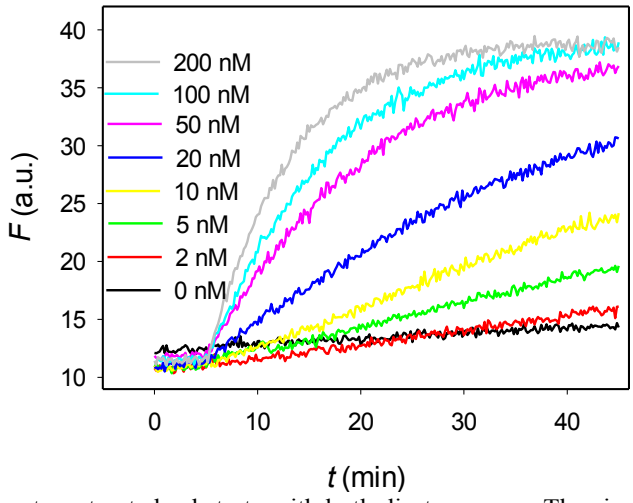

Figure 7.15 Sensor response to untreated substrate with both diastereomers. The signal increase was only ~3.5 fold as compared to the 6-fold for the 17E DNAzyme and Mg^{2+} treated.

7.2.8 Detecting Cd^{2+} in rice

Finally, the sensor was tested to see wheather it will also work in rice samples. The World Health Organization (WHO) has set the limit to be 0.4 mg/kg polished rice grain (i.e. 0.4 ppm). First, grinded rice powder was digested with acid under heating. The digested sample (Figure 7.16B inset) was then neutralized with base and then diluted 50 times into our sensor solution. After considering the dilution factor, the Cd^{2+} concentration is 17.8 nM at the toxic limit. The kinetics of the sensor response was monitored (Figure 7.16A). In this case, the detection limit was 1.6 nM Cd^{2+}, which is >10-fold lower than the WHO limit. This proof-of-concept showed the feasibility of using this sensor for rice samples analysis.

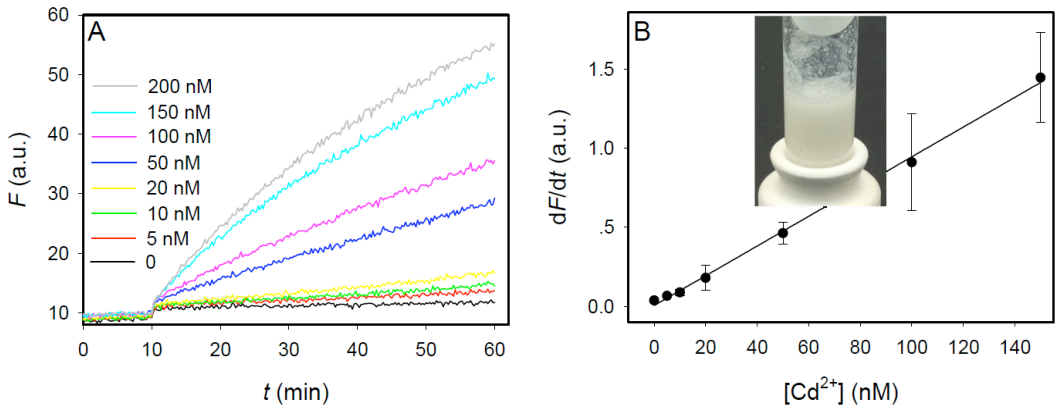

Figure 7.16 Sensing Cd^{2+} in rice. A) Sensor response kinetics to various concentrations of Cd^{2+} in rice extracts. The rice samples were added at 10 min. B) The slope of sensor signal increase as a function of Cd^{2+} concentration. Inset is a photograph showing grinded rice after heat digestion with acid.

7.3 Summary

In summary, a new library was constructed by strategically introducing a single PS modification at the RNA cleavage site. The library was then used for *in vitro* metal-dependent DNAzyme selection. With this design, three *in vitro* selections were performed to isolate DNA sequences specific for Cd^{2+}. The selection outcome was rationally guided by adding blocking DNA to avoid re-selecting known DNAzyme sequence. In addition, negative selections were

introduced to improve the selectivity. This was the first attempt on DNAzyme selection with the PS modification. Compared to selections using modified bases, this single PS did not complicate the typical selection protocol. Compared to the normal PO selections, the only minor difference is that one of the PCR primers containing the PS modification was used. The resulting DNAzyme is highly selective for Cd^{2+} with over 100,000-fold lower activity with Zn^{2+}. Since the PS modification introduces a chiral center, it was later identified that the R_p stereomer is the active one while the S_p one is essentially inactive. With this new discovery, a DNAzyme-based method was developed to remove the inactive S_p isomer. The separation led to double the cleavage yields. Combined with all these results, BN-Cd16 DNAzyme was engineered into a highly sensitive Cd^{2+} biosensor that displayed a detection limit of 1.1 nM in buffer and 1.6 nM in rice extract.

7.4 Materials and methods

7.4.1 Chemicals

The DNAs for selection (Table 7.4) and sensing were purchased from Integrated DNA Technologies (Coralville, IA). The other DNAs were from Eurofins (Huntsville, AL, Table 7.5). The metal salts were from Sigma-Aldrich at the highest available purity. Tris(hydroxymethyl)aminomethane (Tris), 2-(N-morpholino)ethanesulfonic acid (MES), 2-[4-(2-hydroxyethyl)piperazin-1-yl]ethanesulfonic acid (HEPES), EDTA, NaCl, and ammonium acetate were from Mandel Scientific (Guelph, Ontario, Canada). SsoFast EvaGreen supermix was from Bio-Rad. T4-DNA ligase, dNTP mix, Taq DNA polymerase, and DNA ladder were from New England Biolabs.

Table 7.4 DNA sequences related to *in vitro* Cd^{2+} DNAzyme selection. The cleavage site ribo-adenine is denoted by rA, FAM = carboxyfluorescein, iSp18 is an 18-atom hexa-ethyleneglycol spacer. The 5′ of the Lib-rA* DNA is phosphorylated (denoted by the p) for the ligation reaction. The star (*) denotes for phosphorothioate modification.

DNA Name	Sequence and modifications (from 5′-end)
Lib-FAM	GGCGAAACATCTT**N_{50}**TAGTGACGGTAAGCTTGGCAC-**FAM**
Lib-rA*	5'-pAATACGAGTCACTAT**rA***GGAAGAT
Splint DNA	5′-AAGATGTTTCGCCATCTTCCTATAGTCCACCACCA
P1 primer	5′-GTGCCAAGCTTACCG
P2 primer	5′-CTGCAGAATTCTAATACGAGTCACTATAGGAAGATGGCGAAACA
P3 primer	5′-**FAM**-AAATGATCCACTAATACGACTCACTAT**rA***GG
P4 primer	5′-AACAACAACAAC-**iSp18**-GTGCCAAGCTTACCG
Blocking DNA1	CGCACCTACCTTTGACCTATGG
Blocking DNA2	CGCACCCACCTTTGACCTATGG

Table 7.5 Cd^{2+} DNAzyme sequences used for the analysis. BHQ denotes for Black Hole Quencher® 1. Most of these sequences are the individual clones from the blocked negative selection for activity analysis.

DNA Name	Sequence and modifications (from 5′-end)
BN-Cd13	CGC CAT CTT CAA TTC GAT AGA GTC CAC GTC TAC AGG AAT GTG GGA AAT AGT GAC TCG TGA
BN-Cd11	TTT CGC CAT CTT CCT TCG ACA GCC CAG ATA GTG ACT CGT GAC
BN-Cd16	TTT CGC CAT CTT CCT TCG ATA GTT AAA ATA GTG ACT CGT GAC
BN-Cd23	TTT CGC CAT CTT CCT TCG ATA GCC CAG ATA GTG ACT CGT GAC
BN-Cd22	TTT CGC CAT CTT TCT TCG ATA GTT AAG ATA GTG ACT CGT GAC
BN-Cd04	TTT CGC CAT CTT GAA ACG CAC GAA GAA TAG TGA CTC GTG AC
BN-Cd40	TTT CGC CAT CTA ACA GGA AAC ACT TTA GTG ACT CGT GAC
BN-Cd18	CGC CAT CTT TAC CCA AAA GGA AGG TTT TCT ATT TTT AGA AAC ACA GGA GTA GTG ACT CGT
PS-Sub	GTC ACG AGT CAC TAT rA*GG AAG ATG GCG AAA-FAM
PO-Sub	GTC ACG AGT CAC TAT rAGG AAG ATG GCG AAA-FAM
Ce13d	TTTC GCC ATA GGT CAA AGG TGG GTG CGA GTT TTT ACT CGT TAT AGT GAC TCG T
17E	TTT CG CCA TCT TCT CCG AGC CGG TCG AAA TAG TGA CTC GTG AC
FAM-Sub	FAM-AGT CACTAT rA*GG AAG ATG GCG AAC
Q-BN-Cd16	GTT CGC CAT CTT CCT TCG ATA GTT AAA ATA GTG ACT-BHQ

7.4.2 *In vitro* selection

The initial library was prepared by ligating Lib-FAM (0.2 nmol) and Lib-rA* (0.3 nmol) with a splint DNA (0.3 nmol) using T4 ligase following the vendor's protocol. The ligated DNA was purified with 10% dPAGE and extracted from the gel with buffer A (1 mM EDTA, 10 mM Tris-HCl, pH 7.0). After ethanol precipitation, the library was re-suspended in 60 μL buffer B (50 mM MES, pH 6.0, 25 mM NaCl) and used for the first round of selection. For each subsequent round, the library was generated from PCR. For blocked selection, before each

selection step, the library was annealed with 150 pmol of each of the two blocking DNAs to inactivate the Ce13 related sequences. After incubating with Cd^{2+} (see Table 7.6 for incubation time and metal concentration), the reaction was quenched with 8 M urea and the cleaved product was purified by 10% dPAGE. The selected DNA was extracted from the gel, desalted with a Sep-Pak C18 column (Waters), and then suspended in 70 µL HEPES buffer (5 mM, pH 7.5). Two PCR steps were used to amplify the selected DNA. In PCR1, P1 and P2 primers were used and in PCR2, P3 and P4 were used as described previously.[18] For negative selections, the library was treated with a metal soup containing Zn^{2+}, Pb^{2+} and Cu^{2+} (20 µM each). The uncleaved sequences were harvested for a positive selection with Cd^{2+}.

Table 7.6 *In vitro* Cd^{2+} DNAzyme selection conditions. A total of 3 selections were carried out.

Selection 1. Direct selection		
Round	**[Cd^{2+}] (µM)**	**Incubation time (min)**
1	50	60
2	50	60
3	50	60
4	50	60
5	50	30
6	50	15
Selection 2. Blocked selection		
Round	**[Cd^{2+}] (µM)**	**Incubation time (min)**
1	50	60
2	50	60
3	50	60
4	50	60
5	50	60
6	50	40
7	50	40

Table 7.6 *In vitro* Cd^{2+} DNAzyme selection conditions. (Continued)

Selection 3. Blocked selection with negative selections		
Round	**[Zn^{2+}, Cu^{2+}, Pb^{2+}] (-) or [Cd^{2+}] (+) (μM)**	**Incubation time (min)**
8 (-)	50	60
8 (+)	50	30
9 (-)	50	120
9 (+)	50	20
10 (-)	20	120
10 (+)	50	10
11 (-)	20	240
11 (+)	50	5
12 (-)	10	120
12 (+)	50	5
13 (-)	10	120
13 (+)	50	5
14 (-)	10	1440
14 (+)	-	-
15 (-)	10	240
15 (+)	50	5

7.4.3 Sequencing

Three DNA sequencing experiments were performed. For each one, the PCR1 product was cloned using the TA-TOPO cloning kit and transformed into Efficiency DH5α competent cells following the vendor's protocol. The plasmid DNA was extracted and purified using DirectPrep 96 miniprep kit (QIAGEN). The extracted DNA was submitted to TCAG DNA Sequencing Facility (Toronto, ON).

7.4.4 Enzyme assays

Gel-based assays were performed with FAM-labeled PS substrate (0.7 μM) and enzyme (1.1 μM) annealed in buffer B. A final of 10 μM Cd^{2+} (or other metals/concentrations) was added to initiate the cleavage reaction. The products were separated on a dPAGE gel and analyzed using a ChemiDoc MP imaging system (Bio-Rad).

7.4.5 DNAzyme-based chiral separation

The FAM-labeled PS substrate (1 μM) was annealed with 17E or BN-Cd16 (3 μM) in

buffer C (50 mM MOPS, pH 7.5, 25 mM NaCl) or buffer B, respectively. $MgCl_2$ (10 mM) was added to the 17E sample (overnight), while $CdCl_2$ (10 μM) was added to the BN-Cd16 sample (1 h). Both samples were then desalted with Sep-Pak columns, and the uncleaved substrate was separated by 10% dPAGE. After another desalting step, the purified substrate was re-suspended in 5 mM HEPES (pH7.5) and the DNA concentration was determined by Nanodrop 1000 (Thermo).

7.4.6 Biosensor assays

The sensing kinetics were measured in a 96-well plate using a microplate reader (M3, SpectraMax). The sensor complex was formed by annealing the FAM-labeled PS substrate (after 17E treatment) and the quencher-labeled enzyme (molar ratio = 1:1.5) in buffer B. The final sensor concentration was 50 nM in 1 mM HEPES (pH 7.5, 100 μL each well). 1 μL metal ion was added to initiate cleavage and the signaling kinetics was monitored (Ex = 485 nm; Em = 520 nm).

7.4.7 Detecting Cd^{2+} in rice

White rice was purchased from a local supermarket and ground into fine powders. The rice powder (500 mg) was loaded in a Pyrex tube and HCl (100 mM, 1 mL) was added. After cooking at 95 °C for 3 h, NaOH (100 mM, 1 mL) was added to neutralize the sample. After centrifugation, the supernatant was collected. For detection, 2 μL of the extracted sample with various concentrations Cd^{2+} was added into 98 μL sensor.

References

1. Kruger, K.; Grabowski, P. J.; Zaug, A. J.; Sands, J.; Gottschling, D. E.; Cech, T. R. Self-Splicing RNA: Autoexcision and Autocyclization of the Ribosomal RNA Intervening Sequence of Tetrahymena. *Cell* **1982**, *31*, 147-157.
2. Guerrier-Takada, C.; Gardiner, K.; Marsh, T.; Pace, N.; Altman, S. The RNA Moiety of Ribonuclease P is the Catalytic Subunit of the Enzyme. *Cell* **1983**, *35*, 849-857.
3. Cech, T. R. Structural biology: The Ribosome is a Ribozyme. *Science* **2000**, *289*, 878-879.
4. Collins, C. A.; Guthrie, C. The question remains: Is the Spliceosome a Ribozyme? *Nat. Struct. Biol.* **2000**, *7*, 850-854.
5. Cech, T. R. Ribozymes, the First 20 Years. *Biochem. Soc. Trans.* **2002**, *30*, 1162-1166.
6. Ferre-D'Amare, A. R.; Scott, W. G. Small Self-Cleaving Ribozymes. *Cold Spring Harbor Perspectives in Biology* **2010**, *2*, a003574.
7. Cech, T. R. Self-Splicing of Group-I Introns. *Annu. Rev. Biochem.* **1990**, *59*, 543-568.
8. Michel, F.; Ferat, J. L. Structure and Activities of Group-II Introns. *Annu. Rev. Biochem.* **1995**, *64*, 435-461.
9. Evans, D.; Marquez, S. M.; Pace, N. R. RNase P: Interface of the RNA and Protein Worlds. *Trends Biochem. Sci.* **2006**, *31*, 333-341.
10. Johnson-Buck, A. E.; McDowell, S. E.; Walter, N. G. Metal ions: Supporting Actors in the Playbook of Small Ribozymes. *Metal Ions in Life Sciences* **2011**, *9*, 175-96.
11. Donghi, D.; Schnabl, J. Multiple Roles of Metal Ions in Large Ribozymes. *Metal Ions in Life Sciences* **2011**, *9*, 197-234.

12. Ohalloran, T. V. Transition Metals in Control of Gene Expression. *Science* **1993***, 261*, 715-725.

13. Izatt, R. M.; Christen.J. J.; Rytting, J. H. Sites and Thermodynamic Quantities Associated with Proton and Metal Ion Interaction with Ribonucleic Acid, Deoxyribonucleic Acid, and their Constituent Bases, Nucleosides, and Nucleotides. *Chem. Rev.* **1971***, 71*, 439-481.

14. Neidle, S. DNA Structure as Observed in Fibers and Crystals. In *Principles of Nucleic Acid Structure*; Neidle, S., Academic Press: New York, 2008; pp 38-80.

15. Luisi, B.; Orozco, M.; Sponer, J.; Luque, F. J.; Shakked, Z. On the Potential Role of the Amino Nitrogen Atom as a Hydrogen Bond Acceptor in Macromolecules. *J. Mol. Biol.* **1998***, 279*, 1123-1136.

16. Mueller, J. Functional Metal Ions in Nucleic Acids. *Metallomics* **2010***, 2*, 318-327.

17. Eichhorn, G. L.; Shin, Y. A. Interaction of Metal Ions with Polynucleotides and Related Compounds XII the Relative Effect of Various Metal Ions on DNA Helicity. *J. Am. Chem. Soc.* **1968***, 90*, 7323-7328.

18. Miyake, Y.; Togashi, H.; Tashiro, M.; Yamaguchi, H.; Oda, S.; Kudo, M.; Tanaka, Y.; Kondo, Y.; Sawa, R.; Fujimoto, T.; Machinami, T.; Ono, A. Mercury^{II}-Mediated Formation of Thymine-Hg^{II}-Thymine Base Pairs in DNA Duplexes. *J. Am. Chem. Soc.* **2006***, 128*, 2172-2173.

19. Ono, A.; Cao, S.; Togashi, H.; Tashiro, M.; Fujimoto, T.; Machinami, T.; Oda, S.; Miyake, Y.; Okamoto, I.; Tanaka, Y. Specific Interactions Between Silver(I) Ions and Cytosine-Cytosine Pairs in DNA Duplexes. *Chem. Commun.* **2008**, 4825-4827.

20. Ono, A.; Togashi, H. Highly Selective Oligonucleotide-Based Sensor for Mercury(II) in Aqueous Solutions. *Angew. Chem. Int. Ed.* **2004***, 43*, 4300-4302.

21. Ono, A.; Torigoe, H.; Tanaka, Y.; Okamoto, I. Binding of Metal Ions by Pyrimidine Base Pairs in DNA Duplexes. *Chem. Soc. Rev.* **2011***, 40*, 5855-5866.

22. Urata, H.; Yamaguchi, E.; Nakamura, Y.; Wada, S. Pyrimidine-Pyrimidine Base Pairs Stabilized by Silver(I) Ions. *Chem. Commun.* **2011***, 47*, 941-943.

23. Ihara, T.; Ishii, T.; Araki, N.; Wilson, A. W.; Jyo, A. Silver Ion Unusually Stabilizes the Structure of a Parallel-Motif DNA Triplex. *J. Am. Chem. Soc.* **2009***, 131*, 3826-3827.

24. Jarup, L. Hazards of Heavy Metal Contamination. *Br. Med. Bull.* **2003***, 68*, 167-182.

25. Sardans, J.; Montes, F.; Penuelas, J. Determination of As, Cd, Cu, Hg and Pb in Biological Samples by Modern Electrothermal Atomic Absorption Spectrometry. *Spectrochim. Acta, Part B* **2010***, 65*, 97-112.

26. Chen, J. R.; Teo, K. C. Determination of Cadmium, Copper, Lead and Zinc in Water Samples by Flame Atomic Absorption Spectrometry After Cloud Point Extraction. *Anal. Chim. Acta* **2001***, 450*, 215-222.

27. Pohl, P.; Stecka, H.; Sergiel, I.; Jamroz, P. Different Aspects of the Elemental Analysis of Honey by Flame Atomic Absorption and Emission Spectrometry: A Review. *Food Anal. Methods* **2012***, 5*, 737-751.

28. Pohl, F. M.; Jovin, T. M. Salt-Induced Cooperative Conformational Change of a Synthetic DNA: Equilibrium and Kinetic Studies with Poly(DG-DC). *J. Mol. Biol.* **1972***, 67*, 375-396.

29. Townsend, A. T.; Miller, K. A.; McLean, S.; Aldous, S. The Determination of Copper, Zinc, Cadmium and Lead in Urine by High Resolution ICP-MS. *J. Anal. At. Spectrom.* **1998***, 13*, 1213-1219.

30. Rao, R. N.; Talluri, M. V. N. K. An Overview of Recent Applications of Inductively Coupled Plasma-Mass Spectrometry (ICP-MS) in Determination of Inorganic Impurities in Drugs and Pharmaceuticals. *J. Pharm. Biomed. Anal.* **2007***, 43*, 1-13.

31. Arduini, F.; Calvo, J. Q.; Amine, A.; Palleschi, G.; Moscone, D. Bismuth-Modified Electrodes for Lead Detection. *Trends Anal. Chem.* **2010***, 29*, 1295-1304.

32. Cui, L.; Wu, J.; Ju, H. Electrochemical Sensing of Heavy Metal Ions with Inorganic, Organic and Bio-Materials. *Biosens. Bioelectron.* **2015***, 63*, 276-286.

33. Feeney, R.; Kounaves, S. P. Microfabricated Ultramicroelectrode Arrays: Developments, Advances, and Applications in Environmental Analysis. *Electroanalysis* **2000***, 12*, 677-684.

34. Fen, Y. W.; Yunus, W. M. M. Surface Plasmon Resonance Spectroscopy as an Alternative for Sensing Heavy Metal Ions: A Review. *Sens Rev* **2013***, 33*, 305-314.

35. West, M.; Ellis, A. T.; Potts, P. J.; Streli, C.; Vanhoof, C.; Wegrzynek, D.; Wobrauschek, P. Atomic Spectrometry Update: X-Ray Fluorescence Spectrometry. *J. Anal. At. Spectrom.* **2011***, 26*, 1919-1963.

36. West, M.; Ellis, A. T.; Potts, P. J.; Streli, C.; Vanhoof, C.; Wegrzynek, D.; Wobrauschek, P. 2013 Atomic Spectrometry Update: A Review of Advances in X-Ray Fluorescence Spectrometry. *J. Anal. At. Spectrom.* **2013***, 28*, 1544-1590.

37. McComb, J. Q.; Rogers, C.; Han, F. X.; Tchounwou, P. B. Rapid Screening of Heavy Metals and Trace Elements in Environmental Samples Using Portable X-Ray Fluorescence Spectrometer, A Comparative Study. *Water Air Soil Pollut.* **2014***, 225*, 2169.

38. Klockenkamper, R.; vonBohlen, A. Elemental Analysis of Environmental Samples by Total Reflection X-Ray Fluorescence: A Review. *X-Ray Spectrom.* **1996***, 25*, 156-162.

39. Das, A. K.; Chakraborty, R.; Cervera, M. L.; Delaguardia, M. Metal Speciation in Solid Matrices. *Talanta* **1995***, 42*, 1007-1030.

40. Cazes, J. *Ewing's analytical instrumentation handbook*, 3rd ed; New York : Marcel Dekker: New York, 2005; pp 57-126 .

41. Jiang, P. J.; Guo, Z. J. Fluorescent Detection of Zinc in Biological Systems: Recent Development on the Design of Chemosensors and Biosensors. *Coord. Chem. Rev.* **2004***, 248*, 205-229.

42. Russell, R. J.; Pishko, M. V.; Gefrides, C. C.; McShane, M. J.; Cote, G. L. A Fluorescence-Based Glucose Biosensor Using Concanavalin A and Dextran Encapsulated in a Poly(ethylene glycol) Hydrogel. *Anal. Chem.* **1999***, 71*, 3126-3132.

43. Liu, J. W.; Lu, Y. A Colorimetric Lead Biosensor Using DNAzyme-Directed Assembly of Gold Nanoparticles. *J. Am. Chem. Soc.* **2003***, 125*, 6642-6643.

44. Nath, N.; Chilkoti, A. A Colorimetric Gold Nanoparticle Sensor to Interrogate Biomolecular Interactions in Real Time on a Surface. *Anal. Chem.* **2002***, 74*, 504-509.

45. Haes, A. J.; Van Duyne, R. P. A Nanoscale Optical Biosensor: Sensitivity and Selectivity of an Approach Based on the Localized Surface Plasmon Resonance Spectroscopy of Triangular Silver Nanoparticles. *J. Am. Chem. Soc.* **2002***, 124*, 10596-10604.

46. Hrapovic, S.; Liu, Y. L.; Male, K. B.; Luong, J. H. T. Electrochemical Biosensing Platforms Using Platinum Nanoparticles and Carbon Nanotubes. *Anal. Chem.* **2004***, 76*, 1083-1088.

47. Wang, J.; Xu, D. K.; Kawde, A. N.; Polsky, R. Metal Nanoparticle-Based Electrochemical Stripping Potentiometric Detection of DNA Hybridization. *Anal. Chem.* **2001***, 73*, 5576-5581.

48. Katz, E.; Willner, I. Probing Biomolecular Interactions at Conductive and Semiconductive Surfaces by Impedance Spectroscopy: Routes to Impedimetric Immunosensors, DNA-Sensors, and Enzyme Biosensors. *Electroanalysis* **2003***, 15*, 913-947.

49. Gerard, M.; Chaubey, A.; Malhotra, B. D. Application of Conducting Polymers to Biosensors. *Biosens. Bioelectron.* **2002***, 17*, 345-359.

50. Nutiu, R.; Li, Y. F. Aptamers with Fluorescence-Signaling Properties. *Methods* **2005***, 37*, 16-25.

51. Jung, Y.; Jeong, J. Y.; Chung, B. H. Recent Advances in Immobilization Methods of Antibodies on Solid Supports. *Analyst* **2008***, 133*, 697-701.

52. Li, Y. F.; Breaker, R. R. Kinetics of RNA Degradation by Specific Base Catalysis of Transesterification Involving the 2 '-Hydroxyl Group. *J. Am. Chem. Soc.* **1999***, 121*, 5364-5372.

53. Smith, R.; Hansen, D. The pH-Rate Profile for the Hydrolysis of a Peptide Bond. *J. Am. Chem. Soc.* **1998***, 120*, 8910-8913.

54. Tuerk, C.; Gold, L. Systematic Evolution of Ligands by Exponential Enrichment: RNA Ligands to Bacteriophage T4 DNA Polymerase. *Science* **1990***, 249*, 505-510.

55. Ellington, A. D.; Szostak, J. W. *In Vitro* Selection of RNA Molecules that Bind Specific Ligands. *Nature* **1990***, 346*, 818-822.

56. Robertson, D. L.; Joyce, G. F. Selection *In Vitro* of an RNA Enzyme that Specifically Cleaves Single-Stranded DNA. *Nature* **1990***, 344*, 467-468.

57. Sen, D.; Gilbert, W. A Sodium-Potassium Switch in the Formation of Four-Stranded G4-DNA. *Nature* **1990***, 344*, 410-414.

58. He, F.; Tang, Y. L.; Wang, S.; Li, Y. L.; Zhu, D. B. Fluorescent Amplifying Recognition for DNA G-Quadruplex Folding with a Cationic Conjugated Polymer: A Platform for Homogeneous Potassium Detection. *J. Am. Chem. Soc.* **2005***, 127*, 12343-12346.

59. Kong, D.; Ma, Y.; Guo, J.; Yang, W.; Shen, H. Fluorescent Sensor for Monitoring Structural Changes of G-Quadruplexes and Detection of Potassium Ion. *Anal. Chem.* **2009***, 81*, 2678-2684.

60. Liu, Y.; Li, B.; Cheng, D.; Duan, X. Simple and Sensitive Fluorescence Sensor for Detection of Potassium Ion in the Presence of High Concentration of Sodium Ion Using Berberine-G-Quadruplex Complex as Sensing Element. *Microchem. J.* **2011***, 99*, 503-507.

61. Guo, Y.; Chen, Y.; Wei, Y.; Li, H.; Dong, C. Label-Free Fluorescent Aptasensor for Potassium Ion Using Structure-Switching Aptamers and Berberine. *Spectrochim. Acta, Part A* **2015***, 136*, 1635-1641.

62. Qin, H.; Ren, J.; Wang, J.; Luedtke, N. W.; Wang, E. G-Quadruplex-Modulated Fluorescence Detection of Potassium in the Presence of a 3500-Fold Excess of Sodium Ions. *Anal. Chem.* **2010***, 82*, 8356-8360.

63. Li, T.; Wang, E.; Dong, S. G-Quadruplex-Based DNAzyme as a Sensing Platform for Ultrasensitive Colorimetric Potassium Detection. *Chem. Commun.* **2009**, 580-582.

64. Yang, X.; Li, T.; Li, B.; Wang, E. Potassium-Sensitive G-Quadruplex DNA for Sensitive Visible Potassium Detection. *Analyst* **2010***, 135*, 71-75.

65. Zhou, X.; Kong, D.; Shen, H. G-Quadruplex-Hemin DNAzyme-Amplified Colorimetric Detection of Ag^+ Ion. *Anal. Chim. Acta* **2010***, 678*, 124-127.

66. Zhou, X.; Kong, D.; Shen, H. Ag^+ and Cysteine Quantitation Based on G-Quadruplex-Hemin DNAzymes Disruption by Ag^+. *Anal. Chem.* **2010***, 82*, 789-793.

67. Zhang, L.; Zhu, J.; Ai, J.; Zhou, Z.; Jia, X.; Wang, E. Label-Free G-Quadruplex-Specific Fluorescent Probe for Sensitive Detection of Copper(II) Ion. *Biosens. Bioelectron.* **2013***, 39*, 268-273.

68. Li, T.; Dong, S.; Wang, E. Label-Free Colorimetric Detection of Aqueous Mercury Ion (Hg^{2+}) Using Hg^{2+}-Modulated G-Quadruplex-Based DNAzymes. *Anal. Chem.* **2009***, 81*, 2144-2149.

69. Jia, S.; Liu, X.; Li, P.; Kong, D.; Shen, H. G-Quadruplex DNAzyme-Based Hg^{2+} and Cysteine Sensors Utilizing Hg^{2+}-Mediated Oligonucleotide Switching. *Biosens. Bioelectron.* **2011***, 27*, 148-152.

70. Li, T.; Wang, E.; Dong, S. Lead(II)-Induced Allosteric G-Quadruplex DNAzyme as a Colorimetric and Chemiluminescence Sensor for Highly Sensitive and Selective Pb^{2+} Detection. *Anal. Chem.* **2010***, 82*, 1515-1520.

71. Wang, J.; Liu, B. Highly Sensitive and Selective Detection of $Hg(^{2+})$ in aqueous solution with Mercury-Specific DNA and SYBR Green I. *Chem. Commun.* **2008**, 4759-4761.

72. Lee, J.; Han, M. S.; Mirkin, C. A. Colorimetric Detection of Mercuric ion (Hg^{2+}) in Aqueous Media AUsing DNA-Functionalized Gold Nanoparticles. *Angew. Chem. Int. Ed.* **2007***, 46*, 4093-4096.

73. Lin, Y.; Tseng, W. Highly Sensitive and Selective Detection of Silver Ions and Silver Nanoparticles in Aqueous Solution Using an Oligonucleotide-Based Fluorogenic Probe. *Chem. Commun.* **2009**, 6619-6621.

74. Li, B.; Du, Y.; Dong, S. DNA Based Gold Nanoparticles Colorimetric Sensors for Sensitive and Selective Detection of Ag(I) Ions. *Anal. Chim. Acta* **2009***, 644*, 78-82.

75. Pyle, A. M.; Barton, J. K. Probing Nucleic Acids with Transition Metal Complexes. *Prog. Inorg. Chem.* **1990***, 38*, 413-475.

76. Rajendran, M.; Ellington, A. D. Selection of Fluorescent Aptamer Beacons that Light Up in the Presence of Zinc. *Anal. Bioanal. Chem.* **2008***, 390*, 1067-1075.

77. Ward, W. L.; Plakos, K.; DeRose, V. J. Nucleic Acid Catalysis: Metals, Nucleobases, and Other Cofactors. *Chem. Rev.* **2014***, 114*, 4318-4342.

78. Breaker, R. R.; Joyce, G. F. A DNA Enzyme that Cleaves RNA. *Chem. Biol.* **1994***, 1*, 223-9.

79. Santoro, S. W.; Joyce, G. F. A General Purpose RNA-Cleaving DNA Enzyme. *Proc. Natl. Acad. Sci. U. S. A.* **1997***, 94*, 4262-4266.

80. Breaker, R. R.; Joyce, G. F. A DNA Enzyme with Mg^{2+}-Dependent RNA Phosphoesterase Activity. *Chem. Biol.* **1995***, 2*, 655-660.

81. Li, J.; Zheng, W. C.; Kwon, A. H.; Lu, Y. *In Vitro* Selection and Characterization of a Highly Efficient Zn(II)-Dependent RNA-Cleaving Deoxyribozyme. *Nucleic Acids Res.* **2000***, 28*, 481-488.

82. Geyer, C. R.; Sen, D. Evidence for the Metal-Cofactor Independence of an RNA Phosphodiester-Cleaving DNA Enzyme. *Chem. Biol.* **1997***, 4*, 579-593.

83. Faulhammer, D.; Famulok, M. The Ca^{2+} ion as a Cofactor for a Novel RNA-Cleaving Deoxyribozyme. *Angew. Chem. Int. Ed.* **1996***, 35*, 2837-2841.

84. Feldman, A. R.; Sen, D. A New and Efficient DNA Enzyme for the Sequence-Specific Cleavage of RNA. *J. Mol. Biol.* **2001***, 313*, 283-294.

85. Cruz, R. P. G.; Withers, J. B.; Li, Y. F. Dinucleotide Junction Cleavage Versatility of 8-17 Deoxyribozyme. *Chem. Biol.* **2004***, 11*, 57-67.

86. Liu, J.; Brown, A. K.; Meng, X.; Cropek, D. M.; Istok, J. D.; Watson, D. B.; Lu, Y. A Catalytic Beacon Sensor for Uranium with Parts-Per-Trillion Sensitivity and Millionfold Selectivity. *Proc. Natl. Acad. Sci. U. S. A.* **2007***, 104*, 2056-2061.

87. Huang, P. J.; Lin, J.; Cao, J.; Vazin, M.; Liu, J. Ultrasensitive DNAzyme Beacon for Lanthanides and Metal Speciation. *Anal. Chem.* **2014***, 86*, 1816-1821.

88. Carmi, N.; Balkhi, S. R.; Breaker, R. R. Cleaving DNA with DNA. *Proc. Natl. Acad. Sci. U. S. A.* **1998***, 95*, 2233-2237.

89. Carmi, N.; Breaker, R. R. Characterization of a DNA-cleaving Deoxyribozyme. *Bioorg. Med. Chem.* **2001***, 9*, 2589-2600.

90. Carmi, N.; Shultz, L. A.; Breaker, R. R. *In Vitro* Selection of Self-Cleaving DNAs. *Chem. Biol.* **1996***, 3*, 1039-1046.

91. Chandra, M.; Sachdeva, A.; Silverman, S. K. DNA-Catalyzed Sequence-Specific Hydrolysis of DNA. *Nat. Chem. Bio.* **2009***, 5*, 718-720.

92. Xiao, Y.; Chandra, M.; Silverman, S. K. Functional Compromises among pH Tolerance, Site Specificity, and Sequence Tolerance for a DNA-Hydrolyzing Deoxyribozyme. *Biochemistry* **2010***, 49*, 9630-9637.

93. Xiao, Y.; Allen, E. C.; Silverman, S. K. Merely Two Mutations Switch a DNA-Hydrolyzing Deoxyribozyme from Heterobimetallic (Zn^{2+}/Mn^{2+}) to Monometallic (Zn^{2+}-only) Behavior. *Chem. Commun.* **2011***, 47*, 1749-1751.

94. Burmeister, J.; vonKiedrowski, G.; Ellington, A. D. Cofactor-Assisted Self-Cleavage in DNA Libraries with a 3'-5'-Phosphoramidate Bond. *Angew. Chem. Int. Ed.* **1997***, 36*, 1321-1324.

95. Coppins, R. L.; Purtha, W. E.; Wang, Y. M.; Silverman, S. K. Synthesis of Native 3'-5' RNA Linkages by Deoxyribozymes. *Abstracts of Papers of the American Chemical Society* **2005**, *229*, U530-U530.

96. Purtha, W. E.; Coppins, R. L.; Smalley, M. K.; Silverman, S. K. General Deoxyribozyme Catalyzed Synthesis of Native 3'-5' RNA Linkages. *J. Am. Chem. Soc.* **2005**, *127*, 13124-13125.

97. Flynn-Charlebois, A.; Wang, Y. M.; Prior, T. K.; Rashid, I.; Hoadley, K. A.; Coppins, R. L.; Wolf, A. C.; Silverman, S. K. Deoxyribozymes with 2'-5' RNA Ligase Activity. *J. Am. Chem. Soc.* **2003**, *125*, 2444-2454.

98. Hoadley, K. A.; Purtha, W. E.; Wolf, A. C.; Flynn-Charlebois, A.; Silverman, S. K. Zn^{2+}-Dependent Deoxyribozymes that Form Natural and Unnatural RNA Linkages. *Biochemistry* **2005**, *44*, 9217-9231.

99. Wang, Y. M.; Silverman, S. K. Deoxyribozymes that Synthesize Branched and Lariat RNA. *J. Am. Chem. Soc.* **2003**, *125*, 6880-6881.

100. Wang, Y. M.; Silverman, S. K. Characterization of Deoxyribozymes that Synthesize Branched RNA. *Biochemistry* **2003**, *42*, 15252-15263.

101. Coppins, R. L.; Silverman, S. K. Mimicking the First Step of RNA Splicing: An Artificial DNA Enzyme can Synthesize Branched RNA Using an Oligonucleotide Leaving Group as a 5 '-Exon Analogue. *Biochemistry* **2005**, *44*, 13439-13446.

102. Coppins, R. L.; Silverman, S. K. A DNA Enzyme that Mimics the First Step of RNA Splicing. *Nat. Struct. Mol. Bio.* **2004**, *11*, 270-274.

103. Wang, Y. M.; Silverman, S. K. Efficient One-Step Synthesis of Biologically Related Lariat RNAs by a Deoxyribozyme. *Angew. Chem. Int. Ed.* **2005**, *44*, 5863-5866.

104. Pratico, E. D.; Wang, Y. M.; Silverman, S. K. A Deoxyribozyme that Synthesizes 2' 5'-Branched RNA with any Branch-Site Nucleotide. *Nucleic Acids Res.* **2005***, 33*, 3503-3512.

105. Cuenoud, B.; Szostak, J. W. A DNA Metalloenzyme with DNA-Ligase Activity. *Nature* **1995***, 375*, 611-614.

106. Sreedhara, A.; Li, Y. F.; Breaker, R. R. Ligating DNA with DNA. *J. Am. Chem. Soc.* **2004***, 126*, 3454-3460.

107. Pradeepkumar, P. I.; Hobartner, C.; Baum, D. A.; Silverman, S. K. DNA-Catalyzed Formation of Nucleopeptide Linkages. *Angew. Chem. Int. Ed.* **2008***, 47*, 1753-1757.

108. Wang, W.; Billen, L. P.; Li, Y. F. Sequence Diversity, Metal Specificity, and Catalytic Proficiency of Metal-Dependent Phosphorylating DNA Enzymes. *Chem. Biol.* **2002***, 9*, 507-517.

109. Li, Y. F.; Liu, Y.; Breaker, R. R. Capping DNA with DNA. *Biochemistry* **2000***, 39*, 3106-3114.

110. Sheppard, T. L.; Ordoukhanian, P.; Joyce, G. F. A DNA Enzyme with N-Glycosylase Activity. *Proc. Natl. Acad. Sci. U. S. A.* **2000***, 97*, 7802-7807.

111. Chandra, M.; Silverman, S. K. DNA and RNA Can be Equally Efficient Catalysts for Carbon-Carbon Bond Formation. *J. Am. Chem. Soc.* **2008***, 130*, 2936-2937.

112. Li, Y. F.; Sen, D. A Catalytic DNA for Porphyrin Metallation. *Nat. Struct. Biol.* **1996***, 3*, 743-747.

113. Li, Y. F.; Sen, D. Toward an Efficient DNAzyme. *Biochemistry* **1997***, 36*, 5589-5599.

114. Silverman, S. K. *In Vitro* Selection, Characterization, and Application of Deoxyribozymes that Cleave RNA. *Nucleic Acids Res.* **2005***, 33*, 6151-6163.

115. Lan, T.; Furuya, K.; Lu, Y. A Highly Selective Lead Sensor Based on a Classic Lead DNAzyme. *Chem. Commun.* **2010***, 46*, 3896-3898.

116. Zaborowska, Z.; Furste, J.; Erdmann, V.; Kurreck, J. Sequence Requirements in the Catalytic Core of the "10-23" DNA Enzyme. *J. Biol. Chem.* **2002***, 277*, 40617-40622.

117. Zaborowska, Z.; Schubert, S.; Kurreck, J.; Erdmann, V. Deletion Analysis in the Catalytic Region of the 10-23 DNA Enzyme. *FEBS Lett.* **2005***, 579*, 554-558.

118. Sugimoto, N.; Okumoto, Y.; Ohmichi, T. Effect of Metal Ions and Sequence of Deoxyribozymes on Their RNA Cleavage Activity. *J. Chem. Soc., Perkin Trans. 2* **1999**, 1381-1386.

119. Baum, D. A.; Silverman, S. K. Deoxyribozymes: Useful DNA Catalysts *In Vitro* and *In Vivo*. *Cell. Mol. Life Sci.* **2008***, 65*, 2156-2174.

120. Dass, C. R.; Choong, P. F. M.; Khachigian, L. M. DNAzyme Technology and Cancer Therapy: Cleave and Let Die. *Mol. Cancer Ther.* **2008***, 7*, 243-251.

121. Chakraborti, S.; Banerjea, A. C. Inhibition of HIV-1 Gene Expression by Novel DNA Enzymes Targeted to Cleave HIV-1 TAR RNA: Potential Effectiveness Against all HIV-1 Isolates. *Mol. Ther.* **2003***, 7*, 817-826.

122. Goila, R.; Banerjea, A. C. Inhibition of Hepatitis B Virus X Gene Expression by Novel DNA Enzymes. *Biochem. J.* **2001***, 353*, 701-708.

123. Toyoda, T.; Imamura, Y.; Takaku, H.; Kashiwagi, T.; Hara, K.; Iwahashi, J.; Ohtsu, Y.; Tsumura, N.; Kato, H.; Hamada, N. Inhibition of Influenza Virus Replication in Cultured Cells by RNA-Cleaving DNA Enzyme. *FEBS Lett.* **2000***, 481*, 113-116.

124. Peracchi, A.; Bonaccio, M.; Clerici, M. A Mutational Analysis of the 8-17 Deoxyribozyme Core. *J. Mol. Biol.* **2005***, 352*, 783-794.

125. Brown, A. K.; Li, J.; Pavot, C. M. B.; Lu, Y. A Lead-Dependent DNAzyme with a Two-Step Mechanism. *Biochemistry* **2003***, 42*, 7152-7161.

126. Schlosser, K.; Gu, J.; Sule, L.; Li, Y. Sequence-Function Relationships Provide New Insight Into the Cleavage Site Selectivity of the 8-17 RNA-Cleaving Deoxyribozyme. *Nucleic Acids Res.* **2008***, 36*, 1472-1481.

127. Peracchi, A. Preferential Activation of the 8-17 Deoxyribozyme by Ca^{2+} Ions: Evidence for the Identity of 8-17 with the Catalytic Domain of the MG5 Deoxyribozyme. *J. Biol. Chem.* **2000***, 275*, 11693-11697.

128. Schlosser, K.; Li, Y. F. Tracing Sequence Diversity Change of RNA-Cleaving Deoxyribozymes Under Increasing Selection Pressure During *In Vitro* Selection. *Biochemistry* **2004***, 43*, 9695-9707.

129. Bonaccio, M.; Credali, A.; Peracchi, A. Kinetic and Thermodynamic Characterization of the RNA-Cleaving 8-17 Deoxyribozyme. *Nucleic Acids Res.* **2004***, 32*, 916-925.

130. Kim, H.; Li, J.; Nagraj, N.; Lu, Y. Probing Metal Binding in the 8-17 DNAzyme by Tb^{III} Luminescence Spectroscopy. *Chem. –Eur. J.* **2008***, 14*, 8696-8703.

131. Liu, Y.; Sen, D. A Contact Photo-Cross-Linking Investigation of the Active Site of the 8-17 Deoxyribozyme. *J. Mol. Biol.* **2008***, 381*, 845-859.

132. Mazumdar, D.; Nagraj, N.; Kim, H.; Meng, X.; Brown, A. K.; Sun, Q.; Li, W.; Lu, Y. Activity, Folding and Z-DNA Formation of the 8-17 DNAzyme in the Presence of Monovalent Ions. *J. Am. Chem. Soc.* **2009***, 131*, 5506-5515.

133. Liu, Y.; Sen, D. Local Rather than Global Folding Enables the Lead-dependent Activity of the 8-17 Deoxyribozyme: Evidence from Contact Photo-Crosslinking. *J. Mol. Biol.* **2010***, 395*, 234-241.

134. Sekhon, G. S.; Sen, D. A Stereochemical Glimpse of the Active Site of the 8-17 Deoxyribozyme from Iodine-Mediated Cross-Links Formed with the Substrate's Scissile Site. *Biochemistry* **2010**, *49*, 9072-9077.

135. Sando, S.; Sasaki, T.; Kanatani, K.; Aoyama, Y. Amplified Nucleic Acid Sensing Using Programmed Self-Cleaving DNAzyme. *J. Am. Chem. Soc.* **2003**, *125*, 15720-15721.

136. Sando, S.; Narita, A.; Sasaki, T.; Aoyama, Y. Locked TASC Probes for Homogeneous Sensing of Nucleic Acids and Imaging of Fixed E Coli Cells. *Org. Biomol. Chem.* **2005**, *3*, 1002-1007.

137. Lu, Y.; Liu, J. W.; Li, J.; Bruesehoff, P. J.; Pavot, C. M. B.; Brown, A. K. New Highly Sensitive and Selective Catalytic DNA Biosensors for Metal Ions. *Biosens. Bioelectron.* **2003**, *18*, 529-540.

138. Liu, J. W.; Cao, Z. H.; Lu, Y. Functional Nucleic Acid Sensors. *Chem. Rev.* **2009**, *109*, 1948-1998.

139. Zhang, X.; Kong, R.; Lu, Y. Metal Ion Sensors Based on DNAzymes and Related DNA Molecules. *Annu. Rev. Anal. Chem.* **2011**, *4*, 105-128.

140. Willner, I.; Shlyahovsky, B.; Zayats, M.; Willner, B. DNAzymes for Sensing, Nanobiotechnology and Logic Gate Applications. *Chem. Soc. Rev.* **2008**, *37*, 1153-1165.

141. Stojanovic, M. N.; Mitchell, T. E.; Stefanovic, D. Deoxyribozyme-Based Logic Gates. *J. Am. Chem. Soc.* **2002**, *124*, 3555-3561.

142. Stojanovic, M. N.; Semova, S.; Kolpashchikov, D.; Macdonald, J.; Morgan, C.; Stefanovic, D. Deoxyribozyme-Based Ligase Logic Gates and Their Initial Circuits. *J. Am. Chem. Soc.* **2005**, *127*, 6914-6915.

143. Stojanovic, M. N.; Stefanovic, D. Deoxyribozyme-Based Half-Adder. *J. Am. Chem. Soc.* **2003***, 125*, 6673-6676.

144. Lederman, H.; Macdonald, J.; Stefanovic, D.; Stojanovic, M. N. Deoxyribozyme-Based Three-Input Logic Gates and Construction of a Molecular Full Adder. *Biochemistry* **2006***, 45*, 1194-1199.

145. Elbaz, J.; Lioubashevski, O.; Wang, F.; Remacle, F.; Levine, R. D.; Willner, I. DNA Computing Circuits Using Libraries of DNAzyme Subunits. *Nat. Nanotechnol.* **2010***, 5*, 417-422.

146. Brown, A. K.; Liu, J.; He, Y.; Lu, Y. Biochemical Study of Uranyl-Specific DNAzyme. *Abstracts of Papers of the American Chemical Society* **2010***, 239*.

147. He, Y.; Lu, Y. Metal-Ion-Dependent Folding of a Uranyl-Specific DNAzyme: Insight Into Function from Fluorescence Resonance Energy Transfer Studies. *Chem. –Eur. J.* **2011***, 17*, 13732-13742.

148. Cepeda-Plaza, M.; Null, E. L.; Lu, Y. Metal Ion as Both a Cofactor and a Probe of Metal-Binding Sites in a Uranyl-Specific DNAzyme: A Uranyl Photocleavage Study. *Nucleic Acids Res.* **2013***, 41*, 9361-9370.

149. Wu, P.; Hwang, K.; Lan, T.; Lu, Y. A DNAzyme-Gold Nanoparticle Probe for Uranyl Ion in Living Cells. *J. Am. Chem. Soc.* **2013***, 135*, 5254-5257.

150. He, Q. C.; Zhou, J. M.; Zhou, D. M.; Nakamatsu, Y.; Baba, T.; Taira, K. Comparison of Metal Ion-Dependent Cleavages of RNA by a DNA Enzyme and a Hammerhead Ribozyme. *Biomacromolecules* **2002***, 3*, 69-83.

151. Greenwood, N. N., Earnshaw, A., Eds.; *Chemistry of the Elements*, 2nd Ed.; Butterworth-Heinemann: Oxford, 1997; pp 1227-1249.

152. Hu, Z. Y.; Richter, H.; Sparovek, G.; Schnug, E. Physiological and Biochemical Effects of Rare Earth Elements on Plants and Their Agricultural Significance: A Review. *J. Plant Nutr.* **2004**, *27*, 183-220.

153. Liu, C.; Hong, F.; Tao, Y.; Liu, T.; Xie, Y.; Xu, J.; Li, Z. The Mechanism of the Molecular Interaction between Cerium(III) and Ribulose-1,5-Bisphosphate Carboxylase/Oxygenase (Rubisco). *Biol. Trace Elem. Res.* **2011**, *143*, 1110-1120.

154. Tyler, G. Rare Earth Elements in Soil and Plant Systems - A review. *Plant Soil* **2004**, *267*, 191-206.

155. Lim, S.; Franklin, S. J. Lanthanide-Binding Peptides and the Enzymes that Might Have Been. *Cell. Mol. Life Sci.* **2004**, *61*, 2184-2188.

156. Pol, A.; Barends, T. R. M.; Dietl, A.; Khadem, A. F.; Eygensteyn, J.; Jetten, M. S. M.; Op den Camp, H. J. M. Rare Earth Metals are Essential for Methanotrophic Life in Volcanic Mudpots. *Environ. Microbiol.* **2014**, *16*, 255-264.

157. Selvin, P. R. Principles and Biophysical Applications of Lanthanide-Based Probes. *Annu. Rev. Biophys. Biomol. Struct.* **2002**, *31*, 275-302.

158. Kobayashi, S.; Sugiura, M.; Kitagawa, H.; Lam, W. W. L. Rare-Earth Metal Triflates in Organic Synthesis. *Chem. Rev.* **2002**, *102*, 2227-2302.

159. Wang, F.; Han, Y.; Lim, C. S.; Lu, Y.; Wang, J.; Xu, J.; Chen, H.; Zhang, C.; Hong, M.; Liu, X. Simultaneous Phase and Size Control of Upconversion Nanocrystals Through Lanthanide Doping. *Nature* **2010**, *463*, 1061-1065.

160. Komiyama, M.; Takeda, N.; Shigekawa, H. Hydrolysis of DNA and RNA by Lanthanide Ions: Mechanistic Studies Leading to New Applications. *Chem. Commun.* **1999**, 1443-1451.

161. Komiyama, M.; Aiba, Y.; Yamamoto, Y.; Sumaoka, J. Artificial Restriction DNA Cutter for Site-Selective Scission of Double-Stranded DNA with Tunable Scission Site and Specificity. *Nat. Protoc.* **2008***, 3*, 655-662.

162. Breaker, R. DNA enzymes. *Nat. Biotechnol.* **1997***, 15*, 427-431.

163. Lu, Y. New Transition Metal-Dependent DNAzymes as Efficient Endonucleases and as Selective Metal Biosensors. *Chem. –Eur. J.* **2002***, 8*, 4589-4596.

164. Navani, N. K.; Li, Y. F. Nucleic Acid Aptamers and Enzymes as Sensors. *Curr. Opin. Chem. Biol.* **2006***, 10*, 272-281.

165. Silverman, S. K. DNA as a Versatile Chemical Component for Catalysis, Encoding, and Stereocontrol. *Angew. Chem. Int. Ed.* **2010***, 49*, 7180-7201.

166. Dokukin, V.; Silverman, S. K. Lanthanide Ions as Required Cofactors for DNA Catalysts. *Chem. Sci.* **2012***, 3*, 1707-1714.

167. Geyer, C.; Sen, D. Lanthanide Probes for a Phosphodiester-Cleaving, Lead-Dependent, DNAzyme. *J. Mol. Biol.* **1998***, 275*, 483-489.

168. Franklin, S. J. Lanthanide-Mediated DNA Hydrolysis. *Curr. Opin. Chem. Biol.* **2001***, 5*, 201-208.

169. Feig, A. L.; Panek, M.; Horrocks, W. D.; Uhlenbeck, O. C. Probing the Binding of Tb(III) and Eu(III) to the Hammerhead Ribozyme Using Luminescence Spectroscopy. *Chem. Biol.* **1999***, 6*, 801-810.

170. Zhang, M.; Le, H.; Jiang, X.; Yin, B.; Ye, B. Time-Resolved Probes Based on Guanine/Thymine-Rich DNA-Sensitized Luminescence of Terbium(III). *Anal. Chem.* **2013***, 85*, 11665-11674.

171. Fu, P. K. L.; Turro, C. Energy Transfer from Nucleic Acids to Tb(III): Selective Emission Enhancement by Single DNA Mismatches. *J. Am. Chem. Soc.* **1999***, 121*, 1-7.

172. Geraldes, C. F. G. C.; Luchinat, C. Lanthanides as Shift and Relaxation Agents in Elucidating the Structure of Proteins and Nucleic Acids. *Met. Ions Biol. Syst.* **2003***, 40*, 513-88.

173. Pintacuda, G.; John, M.; Su, X.; Otting, G. NMR Structure Determination of Protein-Ligand Complexes by Lanthanide Labeling. *Acc. Chem. Res.* **2007***, 40*, 206-212.

174. Morrow, J. R.; Andolina, C. M. Spectroscopic Investigations of Lanthanide Ion Binding to Nucleic Acids. *Metal ions in life sciences* **2012***, 10*, 171-99.

175. Walter, N.; Yang, N.; Burke, J. Probing Non-Selective Cation Binding in the Hairpin Ribozyme with Tb(III). *J. Mol. Biol.* **2000***, 298*, 539-555.

176. Sugimoto, N.; Ohmichi, T. Site-Specific Cleavage Reaction Catalyzed by Leadzyme is Enhanced by Combined Effect of Lead and Rare Earth Ions. *FEBS Lett.* **1996***, 393*, 97-100.

177. Ohmichi, T.; Sugimoto, N. Role of Nd^{3+} and Pb^{2+} on the RNA Cleavage Reaction by a Small Ribozyme. *Biochemistry* **1997***, 36*, 3514-3521.

178. Javadi-Zarnaghi, F.; Hoebartner, C. Lanthanide Cofactors Accelerate DNA-Catalyzed Synthesis of Branched RNA. *J. Am. Chem. Soc.* **2013***, 135*, 12839-12848.

179. Nishiyabu, R.; Hashimoto, N.; Cho, T.; Watanabe, K.; Yasunaga, T.; Endo, A.; Kaneko, K.; Niidome, T.; Murata, M.; Adachi, C.; Katayama, Y.; Hashizume, M.; Kimizuka, N. Nanoparticles of Adaptive Supramolecular Networks Self-Assembled from Nucleotides and Lanthanide Ions. *J. Am. Chem. Soc.* **2009***, 131*, 2151-2158.

180. Wang, F.; Liu, B.; Huang, P. J.; Liu, J. Rationally Designed Nucleobase and Nucleotide Coordinated Nanoparticles for Selective DNA Adsorption and Detection. *Anal. Chem.* **2013***, 85*, 12144-12151.

181. Liu, Y.; Tang, Z. Nanoscale Biocoordination Polymers: Novel Materials from an Old Topic. *Chem. –Eur. J.* **2012***, 18*, 1030-1037.

182. Pu, F.; Ju, E.; Ren, J.; Qu, X. Multiconfigurable Logic Gates Based on Fluorescence Switching in Adaptive Coordination Polymer Nanoparticles. *Adv Mater* **2014***, 26*, 1111-1117.

183. Roth, A.; Breaker, R. R. An Amino Acid as a Cofactor for a Catalytic Polynucleotide. *Proc. Natl. Acad. Sci. U. S. A.* **1998***, 95*, 6027-6031.

184. Massari, S.; Ruberti, M. Rare Earth Elements as Critical Raw Materials: Focus on International Markets and Future Strategies. *Resour. Policy* **2013***, 38*, 36-43.

185. Houk, R. S.; Fassel, V. A.; Flesch, G. D.; Svec, H. J.; Gray, A. L.; Taylor, C. E. Inductively Coupled Argon Plasma as an Ion-Source for Mass-Spectrometric Determination of Trace-Elements. *Anal. Chem.* **1980***, 52*, 2283-2289.

186. Das, P.; Ghosh, A.; Das, A. Unusual Specificity of a Receptor for Nd^{3+} Among Other Lanthanide Ions for Selective Colorimetric Recognition. *Inorg. Chem.* **2010***, 49*, 6909-6916.

187. Zapata, F.; Caballero, A.; Espinosa, A.; Tarraga, A.; Molina, P. A Selective Chromogenic and Fluorescent Molecular Probe for Yb^{III} Based on a Bichromophoric Azadiene. *Eur. J. Inorg. Chem.* **2010**, 697-703.

188. Buenzli, J. G. Lanthanide Luminescence for Biomedical Analyses and Imaging. *Chem. Rev.* **2010***, 110*, 2729-2755.

189. Mancin, F.; Scrimin, P.; Tecilla, P.; Tonellato, U. Artificial metallonucleases. *Chem. Commun.* **2005**, 2540-2548.

190. Zuker, M. Mfold Web Server for Nucleic Acid Folding and Hybridization Prediction. *Nucleic Acids Res.* **2003***, 31*, 3406-3415.

191. Liu, Z. J.; Mei, S. H. J.; Brennan, J. D.; Li, Y. F. Assemblage of Signaling DNA Enzymes with Intriguing Metal-Ion Specificities and pH Dependences. *J. Am. Chem. Soc.* **2003***, 125*, 7539-7545.

192. Shannon, R. D. Revised Effective Ionic-Radii and Systematic Studies of Interatomic Distances in Halides and Chalcogenides. *Acta Crystallogr. Sect. A: Fundam. Crystallogr.* **1976***, 32*, 751-767.

193. Li, J.; Lu, Y. A Highly Sensitive and Selective Catalytic DNA Biosensor for Lead Ions. *J. Am. Chem. Soc.* **2000***, 122*, 10466-10467.

194. Baun, D. L.; Christensen, T. H. Speciation of Heavy Metals in Landfill Leachate: A Review. *Waste Manage. Res.* **2004***, 22*, 3-23.

195. Feldmann, J.; Salaun, P.; Lombi, E. Critical Review Perspective: Elemental Speciation Analysis Methods in Environmental Chemistry - Moving Towards Methodological Integration. *Envir. Chem.* **2009***, 6*, 275-289.

196. Nutiu, R.; Yu, J. M. Y.; Li, Y. F. Signaling Aptamers for Monitoring Enzymatic Activity and for Inhibitor Screening. *Chembiochem* **2004***, 5*, 1139-1144.

197. Rupcich, N.; Nutiu, R.; Li, Y. F.; Brennan, J. D. Solid-Phase Enzyme Activity Assay Utilizing an Entrapped Fluorescence-Signaling DNA Aptamer. *Angew. Chem. Int. Ed.* **2006***, 45*, 3295-3299.

198. Wilson, D. S.; Szostak, J. W. *In Vitro* Selection of Functional Nucleic Acids. *Annu. Rev. Biochem.* **1999***, 68*, 611-647.

199. Silverman, S. K. Deoxyribozymes: Selection Design and Serendipity in the Development of DNA Catalysts. *Acc. Chem. Res.* **2009***, 42*, 1521-1531.

200. Matsumura, K.; Komiyama, M. Enormously Fast RNA Hydrolysis by Lanthanide(III) ions Under Physiological Conditions: Eminent Candidates for Novel Tools of Biotechnology. *J. Biochem.* **1997***, 122*, 387-394.

201. Marciniec, T.; Ciesiolka, J.; Wrzesinski, J.; Krzyzosiak, W. J. Identification of the Magnesiu, Europium and Lead Binding-Sites in *Escherichia Coli* and Lupine Transfer Rnaphe by Specific Metal Ion-Induced Cleavages. *FEBS Lett.* **1989***, 243*, 293-298.

202. Komiyama, M.; Sumaoka, J. Progress Towards Synthetic Enzymes for Phosphoester Hydrolysis. *Curr. Opin. Chem. Biol.* **1998***, 2*, 751-757.

203. Huang, P. J.; Vazin, M.; Liu, J. *In Vitro* Selection of a New Lanthanide-Dependent DNAzyme for Ratiometric Sensing Lanthanides. *Anal. Chem.* **2014***, 86*, 9993-9999.

204. Rakow, N.; Suslick, K. A Colorimetric Sensor Array for Odour Visualization. *Nature* **2000***, 406*, 710-713.

205. Pei, H.; Lu, N.; Wen, Y.; Song, S.; Liu, Y.; Yan, H.; Fan, C. A DNA Nanostructure-Based Biomolecular Probe Carrier Platform for Electrochemical Biosensing. *Adv Mater* **2010***, 22*, 4754-4758.

206. Yonuschot, G.; Helman, D.; Mushrush, G.; Vandewoude, G.; Robey, G. Terbium as a Solid-State Probe for RNA. *Bioinorg. Chem.* **1978***, 8*, 405-418.

207. Yonuschot, G.; Robey, G.; Mushrush, G.; Helman, D.; Vandewoude, G. Measurement of Binding of Terbium to DNA. *Bioinorg. Chem.* **1978***, 8*, 397-404.

208. Ringer, D.; Burchett, S.; Kizer, D. Use of Terbium(III) Fluorescence Enhancement to Selectively Monitor DNA and RNA Guanine Residues and Their Alteration by Chemical Modification. *Biochemistry* **1978***, 17*, 4818-4825.

209. Karraker, D. Coordination of Trivalent Lathanide Ions. *J. Chem. Educ.* **1970***, 47*, 424-&.

210. Santoro, S.; Joyce, G. Mechanism and Utility of an RNA-Cleaving DNA Enzyme. *Biochemistry* **1998***, 37*, 13330-13342.

211. Sigel, R. K. O.; Pyle, A. M. Alternative Roles for Metal Ions in Enzyme Catalysis and the Implications for Ribozyme Chemistry. *Chem. Rev.* **2007***, 107*, 97-113.

212. Stahley, M. R.; Adams, P. L.; Wang, J.; Strobel, S. A. Structural Metals in the Group I Intron: A Ribozyme with a Multiple Metal ion Core. *J. Mol. Biol.* **2007***, 372*, 89-102.

213. Weinstein, L.; Jones, B.; Cosstick, R.; Cech, T. A Second Catalytic Metal Ion in a Group I Ribozyme. *Nature* **1997***, 388*, 805-808.

214. Song, B.; Sigel, R.; Sigel, H. Acid-Base Properties of Adenosine 5'-O-Thiomonophosphate in Aqueous Solution. *Chem. –Eur. J.* **1997***, 3*, 29-33.

215. Frey, P.; Sammons, R. Bond Order and Charge Localization in Nucleoside Phosphorothioates. *Science* **1985***, 228*, 541-545.

216. Wang, S. L.; Karbstein, K.; Peracchi, A.; Beigelman, L.; Herschlag, D. Identification of the Hammerhead Ribozyme Metal Ion Binding Site Responsible for Rescue of the Deleterious Effect of a Cleavage Site Phosphorothioate. *Biochemistry* **1999***, 38*, 14363-14378.

217. Thaplyal, P.; Ganguly, A.; Golden, B. L.; Hammes-Schiffer, S.; Bevilacqua, P. C. Thio Effects and an Unconventional Metal Ion Rescue in the Genomic Hepatitis Delta Virus Ribozyme. *Biochemistry* **2013***, 52*, 6499-6514.

218. Nawrot, B.; Widera, K.; Sobczak, M.; Wojcik, M.; Stec, W. J. Effect of R(P) and S(P)phosphorothioate Substitution at the Scissile Site on the Cleavage Activity of Deoxyribozyme 10-23. *Curr. Org. Chem.* **2008***, 12*, 1004-1009.

219. Warnecke, J. M.; Furste, J. P.; Hardt, W. D.; Erdmann, V. A.; Hartmann, R. K. Ribonuclease P (RNase P) RNA is Converted to a Cd^{2+}-Ribozyme by a Single Rp-Phosphorothioate Modification in the Precursor tRNA at the RNase p Cleavage Site. *Proc. Natl. Acad. Sci. U. S. A.* **1996***, 93*, 8924-8928.

220. Huang, P. J.; Liu, J. Sensing Parts-per-Trillion Cd^{2+}, Hg^{2+}, and Pb^{2+} Collectively and Individually Using Phosphorothioate DNAzymes. *Anal. Chem.* **2014***, 86*, 5999-6005.

221. Platt, W. G. Group Trends. In *The Rare Earth Elements: Fundamentals and Applications*; Atwood, D. A., Ed.; John Wiley & Sons: Hoboken, 2012; pp43-55.

222. Kolarik, Z. Complexation and Separation of Lanthanides(III) and Actinides(III) by Heterocyclic N-Donors in Solutions. *Chem. Rev.* **2008***, 108*, 4208-4252.

223. Huang, P. J.; Vazin, M.; Matuszek, Z.; Liu, J. A New Heavy Lanthanide-Dependent DNAzyme Displaying Strong Metal Cooperativity and Unrescuable Phosphorothioate Effect. *Nucleic Acids Res.* **2015***, 43*, 461-9.

224. Zhang, J.; Li, Y.; Hao, X.; Zhang, Q.; Yang, K.; Li, L.; Ma, L.; Wang, S.; Li, X. Recent Progress in Therapeutic and Diagnostic Applications of Lanthanides. *Mini. Rev. Med. Chem.* **2011***, 11*, 678-694.

225. Lavigne, J. J.; Anslyn, E. V. Sensing a Paradigm Shift in the Field of Molecular Recognition: From Selective to Differential Receptors. *Angew. Chem. Int. Ed.* **2001***, 40*, 3119-3130.

226. Sudarsan, N.; Hammond, M. C.; Block, K. F.; Welz, R.; Barrick, J. E.; Roth, A.; Breaker, R. R. Tandem Riboswitch Architectures Exhibit Complex Gene Control Functions. *Science* **2006***, 314*, 300-304.

227. Liu, J.; Lu, Y. Rational Design of "Turn-On" Allosteric DNAzyme Catalytic Beacons for Aqueous Mercury Ions with Ultrahigh Sensitivity and Selectivity. *Angew. Chem. Int. Ed.* **2007***, 46*, 7587-7590.

228. Kim, H. N.; Ren, W. X.; Kim, J. S.; Yoon, J. Fluorescent and Colorimetric Sensors for Detection of Lead, Cadmium, and Mercury Ions. *Chem. Soc. Rev.* **2012***, 41*, 3210-3244.

229. Nolan, E. M.; Lippard, S. J. Tools and Tactics for the Optical Detection of Mercuric Ion. *Chem. Rev.* **2008***, 108*, 3443-3480.

230. Domaille, D. W.; Que, E. L.; Chang, C. J. Synthetic Fluorescent Sensors for Studying the Cell Biology of Metals. *Nat. Chem. Bio.* **2008***, 4*, 168-175.

231. Li, D.; Song, S.; Fan, C. Target-Responsive Structural Switching for Nucleic Acid-Based Sensors. *Acc. Chem. Res.* **2010***, 43*, 631-641.

232. Wang, H.; Yang, R.; Yang, L.; Tan, W. Nucleic Acid Conjugated Nanomaterials for Enhanced Molecular Recognition. *ACS Nano* **2009***, 3*, 2451-2460.

233. Lin, Y.; Huang, C.; Chang, H. Gold Nanoparticle Probes for the Detection of Mercury, Lead and Copper Ions. *Analyst* **2011***, 136*, 863-871.

234. Wegner, S. V.; Okesli, A.; Chen, P.; He, C. Design of an Emission Ratiometric Biosensor from MerR Family Proteins: A Sensitive and Selective Sensor for Hg^{2+}. *J. Am. Chem. Soc.* **2007***, 129*, 3474-3475.

235. Du, Y.; Li, B.; Wang, E. "Fitting" Makes "Sensing" Simple: Label-Free Detection Strategies Based on Nucleic Acid Aptamers. *Acc. Chem. Res.* **2013***, 46*, 203-213.

236. Xiao, Y.; Rowe, A. A.; Plaxco, K. W. Electrochemical Detection of Parts-per-Billion Lead via an Electrode-Bound DNAzyme Assembly. *J. Am. Chem. Soc.* **2007***, 129*, 262-263.

237. Lu, L.; Zhang, X.; Kong, R.; Yang, B.; Tan, W. A Ligation-Triggered DNAzyme Cascade for Amplified Fluorescence Detection of Biological Small Molecules with Zero-Background Signal. *J. Am. Chem. Soc.* **2011***, 133*, 11686-11691.

238. Wang, H.; Kim, Y.; Liu, H.; Zhu, Z.; Bamrungsap, S.; Tan, W. Engineering a Unimolecular DNA-Catalytic Probe for Single Lead Ion Monitoring. *J. Am. Chem. Soc.* **2009***, 131*, 8221-8226.

239. Hollenstein, M.; Hipolito, C.; Lam, C.; Dietrich, D.; Perrin, D. M. A Highly Selective DNAzyme Sensor for Mercuric Ions. *Angew. Chem. Int. Ed.* **2008***, 47*, 4346-4350.

240. Deleavey, G. F.; Damha, M. J. Designing Chemically Modified Oligonucleotides for Targeted Gene Silencing. *Chem. Biol.* **2012***, 19*, 937-954.

241. Nawrot, B.; Widera, K.; Wojcik, M.; Rebowska, B.; Nowak, G.; Stec, W. J. Mapping of the Functional Phosphate Groups in the Catalytic Core of Deoxyribozyme 10-23. *Febs J.* **2007***, 274*, 1062-1072.

242. Cunningham, L. A.; Li, J.; Lu, Y. Spectroscopic Evidence for Inner-Sphere Coordination of Metal Ions to the Active Site of a Hammerhead Ribozyme. *J. Am. Chem. Soc.* **1998***, 120*, 4518-4519.

243. Lee, J. H.; Wernette, D. P.; Yigit, M. V.; Liu, J.; Wang, Z.; Lu, Y. Site-Specific Control of Distances Between Gold Nanoparticles Using Phosphorothioate Anchors on DNA and a Short Bifunctional Molecular Fastener. *Angew. Chem. Int. Ed.* **2007***, 46*, 9006-9010.

244. Zhang, D.; Deng, M.; Xu, L.; Zhou, Y.; Yuwen, J.; Zhou, X. The Sensitive and Selective Optical Detection of Mercury(II) Ions by Using a Phosphorothioate DNAzyme Strategy. *Chem. –Eur. J.* **2009***, 15*, 8117-8120.

245. Wang, B.; Cao, L.; Chiuman, W.; Li, Y.; Xi, Z. Probing the Function of Nucleotides in the Catalytic Cores of the 8-17 and 10-23 DNAzymes by Abasic Nucleotide and C3 Spacer Substitutions. *Biochemistry* **2010***, 49*, 7553-7562.

246. Schlosser, K.; Li, Y. Biologically Inspired Synthetic Enzymes Made from DNA. *Chem. Biol.* **2009***, 16*, 311-322.

247. Schlosser, K.; Gu, J.; Lam, J. C. F.; Li, Y. *In Vitro* Selection of Small RNA-Cleaving Deoxyribozymes that Cleave Pyrimidine-Pyrimidine Junctions. *Nucleic Acids Res.* **2008***, 36*, 4768-4777.

248. Schlosser, K.; Li, Y. DNAzyme-Mediated Catalysis with Only Guanosine and Cytidine Nucleotides. *Nucleic Acids Res.* **2009***, 37*, 413-420.

249. Huang, P. J.; Liu, J. Two Pb^{2+}-Specific DNAzymes with Opposite Trends in Split-Site-Dependent Activity. *Chem. Commun.* **2014***, 50*, 4442-4444.

250. Schlosser, K.; Li, Y. A Versatile Endoribonuclease Mimic Made of DNA: Characteristics and Applications of the 8-17 RNA-Cleaving DNAzyme. *Chembiochem* **2010***, 11*, 866-879.

251. Santoro, S. W.; Joyce, G. F.; Sakthivel, K.; Gramatikova, S.; Barbas, C. F. RNA Cleavage by a DNA Enzyme with Extended Chemical Functionality. *J. Am. Chem. Soc.* **2000***, 122*, 2433-2439.

252. Lermer, L.; Roupioz, Y.; Ting, R.; Perrin, D. M. Toward an RNaseA Mimic: a DNAzyme with Imidazoles and Cationic Amines. *J. Am. Chem. Soc.* **2002***, 124*, 9960-9961.

253. Li, M.; Lin, N.; Huang, Z.; Du, L.; Altier, C.; Fang, H.; Wang, B. Selecting Aptamers for a Glycoprotein Through the Incorporation of the Boronic Acid Moiety. *J. Am. Chem. Soc.* **2008***, 130*, 12636-12637.

254. Frederiksen, J. K.; Piccirilli, J. A. Separation of RNA Phosphorothioate Oligonucleotides by HPLC. *Methods in Enzymol.* **2009***, 468*, 289-309.

255. Pal, S.; Sharma, J.; Yan, H.; Liu, Y. Stable Silver Nanoparticle-DNA Conjugates for Directed Self-Assembly of Core-Satellite Silver-Gold Nanoclusters. *Chem. Commun.* **2009**, 6059-6061.

256. Kumar, A.; Phadtare, S.; Pasricha, R.; Guga, P.; Ganesh, K. N.; Sastry, M. Assembling Gold Nanoparticles in Solution Using Phosphorothioate DNA as Structural Interconnects. *Curr. Sci.* **2003***, 84*, 71-74.

257. Farlow, J.; Seo, D.; Broaders, K. E.; Taylor, M. J.; Gartner, Z. J.; Jun, Y. Formation of Targeted Monovalent Quantum Dots by Steric Exclusion. *Nat. Methods* **2013***, 10*, 1203-1204.

258. Ma, N.; Sargent, E. H.; Kelley, S. O. One-Step DNA-Programmed Growth of Luminescent and Biofunctionalized Nanocrystals. *Nat. Nanotechnol.* **2009***, 4*, 121-125.

259. Zhuang, P.; McBride, M. B.; Xia, H.; Li, N.; Lia, Z. Health Risk From Heavy Metals via Consumption of Food Crops in the Vicinity of Dabaoshan Mine, South China. *Sci. Total Environ.* **2009***, 407*, 1551-1561.

260. Guo, Y.; Zhang, Y.; Shao, H.; Wang, Z.; Wang, X.; Jiang, X. Label-Free Colorimetric Detection of Cadmium Ions in Rice Samples Using Gold Nanoparticles. *Anal. Chem.* **2014***, 86*, 8530-8534.

261. Li, H.; Yao, Y.; Han, C.; Zhan, J. Triazole-Ester Modified Silver Nanoparticles: Click Synthesis and Cd^{2+} Colorimetric Sensing. *Chem. Commun.* **2009**, 4812-4814.

262. Zhang, M.; Liu, Y.; Ye, B. Colorimetric Assay for Parallel Detection of Cd^{2+}, Ni^{2+} and Co^{2+} Using Peptide-Modified Gold Nanoparticles. *Analyst* **2012***, 137*, 601-607.

263. Vallee, B. L.; Ulmer, D. D. Biochemical Effects of Mercury, Cadmium, and Lead. *Annu. Rev. Biochem.* **1972***, 41*, 91-&.

264. Chen, P. R.; He, C. Selective Recognition of Metal Ions by Metalloregulatory Proteins. *Curr. Opin. Chem. Biol.* **2008***, 12*, 214-221.

265. Ora, M.; Peltomaki, M.; Oivanen, M.; Lonnberg, H. Metal-Ion-Promoted Cleavage, Isomerization, and Desulfurization of the Diastereomeric Phosphoromonothioate Analogues of Uridylyl(3',5 ')uridine. *J. Org. Chem.* **1998***, 63*, 2939-2947.